Investigation of sensing membranes for QCM devices in gas sensing applications

HAMID, Amani Saghayer Sh.

INVESTIGATION OF SENSING MEMBRANES FOR QCM DEVICES IN GAS SENSING APPLICATIONS

AMANI SAGHAYER SH. HAMID

A thesis submitted to the ACES Faculty at Sheffield Hallam University

In Partial Fulfilments of Requirements for the degree of Doctor of Philosophy

2017

Declaration

I declare that this thesis has been composed solely by myself and that it has not been submitted, in whole or in part, in any previous application for a degree. Except where states otherwise by reference or acknowledgment, the work presented is entirely my own.

Signed

AMANI SAGHAYER SH. HAMID

ABSTRACT

The standard Quartz Crystal Resonator (QCR) and network analysis based methods in conjunction with curve fitting were used to investigate the sensing capability and characterize the properties of phthalocyanine films on vapour exposure. The measurement of frequency shift and resistance change (mass loading and film damping), caused by adsorption of organic vapour namely, Benzene, Hexane, Ethanol and Toluene were investigated. Confirmation of film properties using supplementary methods such as AFM, Ellipsometry and UV-visible spectrometer was also performed to provide a full characterization of the sensing membranes.

The extracted values of Δf and ΔR from subsequent fitting of the spectra to the BVD model are observed on vapour exposure. A frequency shift (Δf) and change in magnitude (as related to ΔR of the BVD equivalent circuit) indicate changes in the films viscoelastic properties for the increasing concentrations of tested vapours. The sensitivity of the coating has been estimated from the slope of fitted trend line and gives values below LEL thresholds (the *Lower explosive limit)* and IDLH thresholds (Immediately Dangerous to Life or Health) for the ZnPcs films.

The experimental results of the study demonstrate selected sensing membranes are easily applied through spin coating techniques evident from definitive shifts in resonance. Additionally when exposed to the target vapours tested, the film(s) exhibit fast and consistent responses, consequently giving significant potential for gas/vapour sensing applications. Changes in the film parameters have also been observed through the measurement of the admittance spectra. Shifts in both frequency and resistance are observed on exposures which indicate mass loading and changes in film viscosity caused by ad/absorption of the vapour. Response times appear to be quick and full recovery is observed. From the tested vapours, toluene gives the most significant frequency shift exhibiting the highest sensitivity for this compound; this can be attributed to relatively high saturated vapour pressure as compared to the other analytes. In addition, the film parameters extracted from this work were used to estimate the shear modulus parameters. It was found the shear modulus of viscous material (coating film) extracted electrical equivalent circuit parameters are dependent on film properties, thickness and analyte ad/absorption. Consequently, the QCR sensor can act

as a gravimetric and non gravimetric sensitive device for thin film depending on load and adsorption characteristics. In most instances the studied film behaviour demonstrates a rubbery regime that was indicated from increase in resistance for the coating film at series resonant frequency typically. Consequently the calculation of change in film mass from frequency shift (Sauerbrey equation) is inaccurate except for suitably thin rigid films.

A range of Phthalocyanine sensing membranes have been successfully evaluated; selected variants (mainly ZnPc) have given promising results to their viability as gas sensing membrane to detect a range of organic solvents at vapour concentrations below their lower explosive level, It was found suitably sensitive with detection limits in the low parts-per million ranges for the selected analytes. Furthermore, a comparison of gas sensor responses for the selected materials is included, and consequently a particular type of substituent is proposed as a suitable sensor coating for Quartz Crystal Resonator (QCR) gas sensor applications. Other phthalocyanine materials initially chosen proved less successful; demonstrating limited responsiveness to analytes ad/absorption and giving inconsistent results over the tested concentration range. Factors range from non-homogenous film surfaces to the structure and consequent suitability of the synthesised film(s).

Moreover, further research is suggested to fully characterize the complete adsorption process with wide range of phthalocyanine material and various organic analytes.

ACKNOWLEDGEMENTS

Because this maybe only opportunity to thank the support and guidance of various people, where this project would never have been possible without the support and guidance of them. Therefore, I may be verbose to express my sincere gratitude and appreciation to all those people who have shaping this PhD thesis.

Firstly and foremost, I am deeply indebted to my research guide Dr. Alan Holloway for his leading role in my thesis work. Alan provided me with every guidance, assistance and expertise I was needed during my work and at the same time he give me the freedom to do whatever I wanted with containing to contribute valuable feedback, advice, worm encouragement and thoughtful guidance, Thank you Alan for your patience in guiding me through this project. I quite simple cannot imagine a better supervisor.

Special thanks should also be given to Dr Aseel Hassan. Thanks for you to introducing me to study sensor subject in Sheffield Hallam University and for your continuous support and guidance in my study and giving me the necessary advice when I needed.

My heartfelt thanks to MERI staff for them kind support throughout my tenure at ACES faculty, I acknowledge Corrie Houton, Rachael Toogood and Gail Hallewell who were always ready to give their timely help whenever required.

Furthermore, I would like to thank colleagues who helped me out when I got any difficulties or quries regarding experiments work.

To my husband Hesham: I am far more grateful for you. I honestly say that without your help and support this dissertation would not exist. So thank you for being there for and with me.

To Ghalia Esklual: From the day we were met you have become one of my best friends. We have seen and helped each other through both good and bad times. I have always been able to turn to you when I have needed a listening ear, a dissenting opinion or someone to express his opinion about dress I could choose.

You also provide me with some references when I needed. I will always remember the great time we had

and I hope we will have more times to be together in future. Our friendship back to nine years ago it is strong and I hope it will continue to be as strong in future. You are a great friend. Thank you Ghalia.

As well I would like to thank my mother and my father. Your devotion unconditional love, support, optimism and device were more worthy than you could imagine.

To: my sister, my brother, and my friend Hajer. Thank you for the ongoing encouragement over the years.

To my University: (Tripoli University / formerly Al Fateh University) for providing scholarships to pursue doctoral studies and to Libyan cultural affairs in London who support me during my study.

Lastly the thanks must give to all the people who contribute in some way to the work described in this thesis.

Contents

6. BASELINE RESULT AND EXPERIMENTAL DISCUSSION

7. RESULT AND EXPERIMENTAL DISCUSSION

LIST OF PUBLICATIONS:

1. ***Investigation of Zinc phthalocyanine films for QCM sensing applications.***

   In: *SENSORS, 2015 IEEE.* IEEE.

   Paper from IEEE SENSORS 2015 conference, November 1-4, 2015, Busan, South Korea.

2. ***Investigation and Analysis of Zinc Phthalocyanine films for Resonant Gas Sensor Applications.*** Procedia engineering*, **168**, 259-263.* Part of the proceeding of the 30th anniversary Eurosensors Conference – Eurosensors 2016, 4-7. Sepember 2016, Budapest, Hungary

CHAPTER ONE

INTRODUCTION

The subject matter of this research will be briefly introduced in this chapter.

Introduction:

In recent years, there has been significant interest in chemical sensing devices to detect hazardous compounds such as Volatile Organic Compounds (VOCs) which could causes damage to human cells when exposed for long periods. From research studies, a range of gas sensors for VOC detection are become available examples include, photo ionization sensor, spectrophotometric, electrochemical cell and metal oxide based sensor devices.

As a result of technological developments, the sensor sensitivity has improved rapidly. However, there are still few sensor systems able to reach the ppb sensitivity levels achieved by photo ionization sensor devices for specific VOC gases [1, 2].The disadvantages of this type of detector is leaking selectivity, where it is necessary to ionize all gases using ionisation potential of the UV lamp beam [2].

Electrochemical sensors can be classified as either potentiometric or amperometric sensors depending on their respective output type for the chosen VOC measurement; these have been utilized widely for the measurement of ethylene oxide [2, 3, 4]. Furthermore, they have been applied to a range of inorganic and organic compounds [1, 2, 5]. Generally this type of sensor technology gives a similar sensitivity of between 1.9 and 2.8 μA/ppm; which when interfaced to suitably accurate measurement hardware can be considered to give a very low detection limit allowing measurement of VOC in the ppb range [1,2].

Other types of VOC sensor such as Metal Oxide (MOx) based devices include Metal Oxide Semiconductor (MOS) gas sensors which give the advantage of a high detection limit. However, a temperature cycled operation is used to achieve selectivity which needs complicated data processing, analysis and prior knowledge of specific parameters from the device datasheet [6].

Numerous sensor for VOC measurements are commercially available, figure (1-1) provides an overview the current state of the art with sensors categorized in their respective technology.

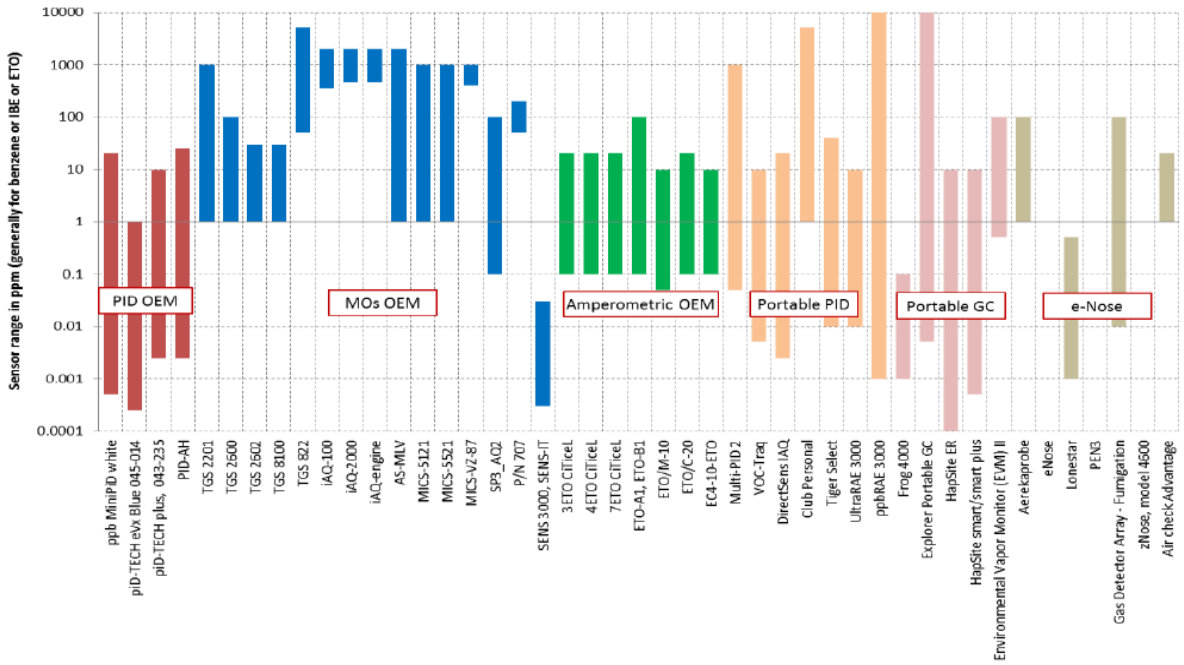

Figure (1-1). Commercially available sensor for VOC measurements.

A further more detailed comparison of typical selected devices from each technology is shown in figure xx with details of specific parameters (target analyte/size/ Detection limit/ Response time/ Sensitivity/ Selectivity/ Stability /cost provided. See table 1.

Table1.

Sensor type	Photo Ionization Detectors (PID) [2]	Electrochemical sensors (OEM) amperometric or potentiometric type, [2,3,5]	metal oxide sensors (MOx) [2,6]	Micro Gas Chromatographs (µGC) [2]	the Palm Portable Mass Spectrometer (PPMS) [2]	micro chromatographic systems the lab-on-a-chip sensor [2]

Target	benzene	Ethylene oxide	High concentrations of VOCs	benzene,	VOCs	VOCs
Size/Complexity	Compact/ portable hand held instrument	Compact /small	compact	Portable	Portable	Portable
Detection limit	0.00025 µmol/mol	Too high for air quality monitoring reaching 50nmol/mol	350µmol/mol	0.0005 µmol/mol	0.2 nmol/mol	2 µmol/mol
Response time (s)	a few seconds	<120s	15 min	1s	5 s	30 min
Sensitivity	1.125 V/µmol/mol	1.9 - 2.8 µA/µmol/mol	high sensitivity	According to the selectivity of the used columns. Generally this is not a problem for BETX and other VOCs	0.000017 (µmol/mol.min)	60 (µmol/mol.min)
Selectivity (interfering gaseous compounds)	All compounds with IP lower than the energy of the lamp are detected. Effect from humidity and temperature	VOCs in general	Alcohols, Aldehydes, Aliphatic hydrocarbons, Amines, Aromatic hydrocarbons, CO, CH 4 , LPG, Ketones, Organic acids		good separation performance	good separation performance
Stability (drift)	Frequent calibration, periodicity lower than a month	2% -15 % per year	No data	<1% over 24 hours	No data	No data
Cost		Low cost	Low cost			

The pursuit of suitable sensors to detect such VOC's with appropriate levels of selectivity and the capability of operating at low temperature (ambient) are of relevance[7].

Consequently the quartz crystal is commonly employed as the material for the sensing element due to its inherent physical properties and because of its commercial accessibility.

Quartz crystals have been widely used as sensing transducer elements with the most prominent example being the Quartz Crystal Resonator (QCR) which has until recently been utilized in the Quartz Crystal Microbalance (QCM) configuration [8, 9, 10, 11].

The technique allows small changes in mass to be detected and is fundamentally based on the piezoelectric phenomena.

The QCM technique is well established for analysing changes in mass on rigid surfaces/membranes and has been successfully used with high accuracy and efficiency in both air and vacuum environments. The Crystal forms the frequency determining element of an electrical oscillator circuit, the changes in frequency are related with the mass change on quartz (deposited film), which is described by the Sauerbrey equation (1 -1) [9, 12, 13, 14, 15, 16, 17, 18].

$$\Delta m\ (gcm^2) = \frac{\Delta f}{2.26 \times 10^{-6}\, f_0^2} \quad (1-1)$$

Where f_0 is the initial resonant frequency, Δm the added mass over active part of crystal, Δf frequency shift from the original resonant frequency, the constant 2.26×10^{-6} is a parameter of quartz crystal physical properties.

The frequency shift directly corresponds to the mass of coating when the film is purely rigid. However, In case of non rigid film when the dissipation occurs, the Sauerbery relationship becomes unveiled and further analysis are necessary.

For many years the QCM was primarily used a gas phase detector and metal deposition monitor. Applications in sensing and film characterisation have become an important area of investigation; it has become increasingly popular for measurements in liquids and for viscoelastic deposited materials [19, 20, 21, 22, 23,24].

In these applications if the characteristics of viscoelastic material change and/or mass loading occur, a considerable effect on the response may be observed.

This could lead to an over/under estimation in depositing mass and consequently concentration level in gas sensing applications. Under specific mass loading conditions, film resonance may lead to anomalies such as a positive frequency shift which under the Sauerbrey relationship would indicate mass loss.

In such cases it is important to extract additional parameters (film thickness and film dissipation) using advanced measurement techniques not solely the series resonant frequency traditionally measured in order to successfully characterize the film. Moreover, development of Quartz Crystal Resonator (QCR) in both gas and liquid phase could open many novel application fields.

The increase in using a sensor in different applications has resulted in part from the rapid progress in the development of sensing material/membranes. For gas detection, a wide range of materials have been utilized to build transducers ranging from polymers to a variety of organic materials such as phthalocyanines [26, 27, 28, 29, 30].

Phthalocyanines (Pcs) have become popular organic compounds in chemical gas sensors due to their capabilities as sensitive absorption layers. Many research works have proven that Phthalocyanines are highly compatible with QCR in gas sensing application [31, 32, 33, 34]. This can be attributed to the characteristics of the optimized thin films which have high stability, sensitivity, selectivity and can easily be produced as films through traditional coating methods [29, 31, 35, 36]. Additionally, different detection properties can be produced by variation of the phthalocyanine substituent. A property of phthalocyanine and viscous film has been addressed in the literature.

In this work, resonant measurements and the impedance analysis approach was implemented to investigate vapour adsorption of organic solvents by different types of

metallophthalocyanine. Previous literature work has shown a non gravimetric response may be expected due to the viscoelastic characteristics of proposed sensor membranes.[37, 38]

A range of complementary techniques including AFM, Ellipsometry and UV-visible spectroscopy were also used to fully characterize and validate the film properties. From the results obtained a model with corresponding film parameters are proposed with the aim to help predict sensor responses and the selection of suitable sensing membranes.

1.1 Aims:

The aim of the programme of study is to investigate the use of advanced QCR measurement techniques to extract information on sensing film parameters when exposed to target analytes (toxic chemicals) in gas.

1.2 Objectives:

- To characterise the film properties from parameters obtained from QCR measurements in conjunction with suitable data analysis and modelling techniques.
- Confirm/validate film properties (thickness and structure) using complementary existing methods such as AFM, SEM, XRD, FTIR, SIMS and Ellipsometry.
- Develop a model for the sensing membrane and use this to predict the response on ad/absorption of selected toxic chemicals.
- Develop/identify a suitable (high sensitivity, low cost, fast response, easily producible) range of membranes for sensing applications.

References:

1- Spinelle, L., Gerboles, M., Kok, G., & Sauerwald, T. (2015). Sensitivity of VOC sensors for air quality monitoring within the EURAMET key-VOC project. *Proceedings of the Fourth EuNetAir Scientific Meeting, Linköping, Sweden,* 3-5.

2- Spinelle, L., Gerboles, M., Kok, G., Persijn, S., & Sauerwald, T. (2017). Review of portable and low-cost sensors for the ambient air monitoring of benzene and other volatile organic compounds. *Sensors, 17*(7), 1520.

3- Gounder Thangamani, J., Deshmukh, K., Sadasivuni, K. K., Chidambaram, K., Ahamed, M. B., Ponnamma, D., . . . Pasha, S. K. (2017). Recent advances in electrochemical biosensor and gas sensors based on graphene and carbon nanotubes (CNT)-A.

4- Zhang, T., Nix, M. B., Yoo, B., Deshusses, M. A., & Myung, N. V. (2006). Electrochemically functionalized single-walled carbon nanotube gas sensor. *Electroanalysis, 18*(12), 1153-1158.

5- Swaminathan, N., Henning, A., Vaknin, Y., Shimanovich, K., Godkin, A., Shalev, G., & Rosenwaks, Y. (2016). Dynamic range enhancement using the electrostatically formed nanowire sensor. *ACS Sensors, 1*(6), 688-695.

6- Capone, S., Forleo, A., Francioso, L., Rella, R., Siciliano, P., Spadavecchia, J., . . . Taurino, A. (2003). Solid state gas sensors: State of the art and future activities. *Journal of Optoelectronics and Advanced Materials, 5*(5), 1335-1348.

7- National Research Council. (1995). *Expanding the vision of sensor materials* National Academies Press.

8- Benes, E., Groschl, M., Burger, W., & Schmid, M. (1995). Sensors based on piezoelectric resonators. *Sensors and Actuators-A-Physical Sensors, 48*(1), 1-22.

9- Buck, R. P., Lindner, E., Kutner, W., & Inzelt, G. (2004). Piezoelectric chemical sensors (IUPAC technical report). *Pure and Applied Chemistry, 76*(6), 1139-1160.

10- Meyer Jr, H. R. (1990). *Studies of Thin Film Chemical Sensors using the Quartz Crystal Microbalance,*

11- Steinem, C., & Janshoff, A. (2007). *Piezoelectric sensors* Springer Science & Business Media.

12- Bradshaw, L. (2000). Understanding piezoelectric quartz crystals. *RF Time and Frequency, 8*, 50-58.

13- Buttry, D. A., & Ward, M. D. (1992). Measurement of interfacial processes at electrode surfaces with the electrochemical quartz crystal microbalance. *Chemical Reviews, 92*(6), 1355-1379.

14- Dixon, M. C. (2008). Quartz crystal microbalance with dissipation monitoring: Enabling real-time characterization of biological materials and their interactions. *Journal of Biomolecular Techniques : JBT, 19*(3), 151-158.

15- Hierlemann, A., Weimar, U., Kraus, G., Schweizer-Berberich, M., & Göpel, W. (1995). Polymer-based sensor arrays and multicomponent analysis for the detection of hazardous oragnic vapours in the environment. *Sensors and Actuators B: Chemical, 26*(1-3), 126-134.

16- Holloway, A., Nabok, A., Thompson, M., Siddiqi, J., Ray, A., & Bliznyuk, V. (2004). Discriminative sensing of volatile organic solvents. comparative analysis using different QCM techniques. *Sensors, 2004. Proceedings of IEEE,* 1500-1503.

17- Nabok, A. (2005). *Organic and inorganic nanostructures (artech house mems and sensors library)* Artech House Publishers, Boston, MA, USA.

18- Arnau, A., Sogorb, T., & Jimenez, Y. (2000). QCM100-quartz crystal microbalance theory and calibration. *Rev.Sci.Instrum, 71*, 2563.

19- Auge, J., Hauptmann, P., Hartmann, J., Rösler, S., & Lucklum, R. (1995). New design for QCM sensors in liquids. *Sensors and Actuators B: Chemical, 24*(1-3), 43-48.

20- Kanazawa, K. K., & Gordon II, J. G. (1985). The oscillation frequency of a quartz resonator in contact with liquid. *Analytica Chimica Acta, 175*, 99-105.

21- Lu, C., & Czanderna, A. W. (2012). *Applications of piezoelectric quartz crystal microbalances* Elsevier.

22- Kanazawa, K. K., & Gordon, J. G. (1985). Frequency of a quartz microbalance in contact with liquid. *Analytical Chemistry, 57*(8), 1770-1771.

23- Martin, S. J., Frye, G. C., Ricco, A. J., & Senturia, S. D. (1993). Effect of surface roughness on the response of thickness-shear mode resonators in liquids. *Analytical Chemistry, 65*(20), 2910-2922.

24- White, C. C., & Schrag, J. L. (1999). Theoretical predictions for the mechanical response of a model quartz crystal microbalance to two viscoelastic media: A thin sample layer and surrounding bath medium. *The Journal of Chemical Physics, 111*(24), 11192-11206.

25- Martin, S. J. (1997). Closing remarks. *Faraday Discussions, 107*, 463-476.

26- Lucklum, R., & Hauptmann, P. (2000). The quartz crystal microbalance: Mass sensitivity, viscoelasticity and acoustic amplification. *Sensors and Actuators B: Chemical, 70*(1-3), 30-36.

27- Martin, S., Frye, G., & Wessendorf, K. (1994). Sensing liquid properties with thickness-shear mode resonators. *Sensors and Actuators A: Physical, 44*(3), 209-218.

28- Muramatsu, H., Tamiya, E., & Karube, I. (1988). Computation of equivalent circuit parameters of quartz crystals in contact with liquids and study of liquid properties. *Analytical Chemistry, 60*(19), 2142-2146.

29- Ogunsipe, A., Chen, J., & Nyokong, T. (2004). Photophysical and photochemical studies of zinc (II) phthalocyanine derivatives—effects of substituents and solvents. *New Journal of Chemistry, 28*(7), 822-827.

30- Reed, C., Kanazawa, K. K., & Kaufman, J. (1990). Physical description of a viscoelastically loaded AT-cut quartz resonator. *Journal of Applied Physics, 68*(5), 1993-2001.

31- Basova, T., Taşaltin, C., Gürek, A., Ebeoğlu, M., Öztürk, Z., & Ahsen, V. (2003). Mesomorphic phthalocyanine as chemically sensitive coatings for chemical sensors. *Sensors and Actuators B: Chemical, 96*(1-2), 70-75.

32- Kobayashi, N. (1999). Phthalocyanines. *Current Opinion in Solid State and Materials Science, 4*(4), 345-353.

33- Leznoff, C., & Lever, A.Phthalocyanines: Properties and applications (VCH, new york, 1989). *Google Scholar,*

34- Valli, L. (2005). Phthalocyanine-based Langmuir–Blodgett films as chemical sensors. *Advances in Colloid and Interface Science, 116*(1-3), 13-44.

35- Zhou, R., Josse, F., Göpel, W., Öztürk, Z., & Bekaroğlu, Ö. (1996). Phthalocyanines as sensitive materials for chemical sensors. *Applied Organometallic Chemistry, 10*(8), 557-577.

36- Zollinger, H. (2003). *Color chemistry: Syntheses, properties, and applications of organic dyes and pigments* John Wiley & Sons.

37- Lucklum, R., Behling, C., & Hauptmann, P. (2000). Gravimetric and non-gravimetric chemical quartz crystal resonators. *Sensors and Actuators B: Chemical, 65*(1-3), 277-283.

38- Lucklum, R., & Hauptmann, P. (2001). Thin film shear modulus determination with quartz crystal resonators: A review. *Frequency Control Symposium and PDA Exhibition, 2001. Proceedings of the 2001 IEEE International,* 408-418.

CHAPTER TWO

LITERATURE REVIEW

This chapter gives an overview of research related to proposed work and deep discussion on the piezoelectric effect. Phthalocyanines and significant properties related to work of this thesis are also discussed. Finally, a general overview of viscous films related to the sensing application is introduced.

2.1 Background:

Silicon dioxide (quartz) is a favoured material in a number of technological areas, due to its low cost and intrinsic properties including physical, chemical and electrical characteristics.

Of specific importance in this work is the piezoelectric effect which is exhibited by quartz. Piezoelectricity means electricity resulting from pressure and originally comes from the Greek language [1, 2].

The piezoelectric effect was first observed by Pierre and Jacqes in 1880; during the application of pressure to a small slice of quartz, an electrical potential was produced between the deformed surfaces. Therefore, the piezoelectric effect was discovered [2, 3].

Piezoelectric materials are used widely in various applications such as sensors, transducers, actuators and medical applications [2,4,5,6,7] that require thermal and mechanical stability and large piezoelectric coefficients. Although quartz has a small piezoelectric coefficient compared to other material, it is still extremely useful and popular, being heavily utilized in a range of frequency determining and oscillator applications and consequently as a mass sensor due to high stability (mechanical /thermal) and low cost.

Purely ionic crystalline solids possessing a structure that does not have a reflection centre will have piezoelectric property [45], this can be explained by "a hypothetical ionic solid a planar molecule", at equilibrium, that gives three dipoles have the same magnitude at 120˚ periods. Because of the symmetry of a planar molecule, the net moment of dipole vanishes [8].

Nevertheless, the changes could happen on a molecule along the orthogonal or parallel direction to one of the three tops such as compressed or extended. That will lead to deformation of each molecule; consequently the net moment will appear. Also crystal deformation or prolongation is parallel to the field direction followed by opposite sign in cross direction the length change.

Only symmetry of the crystal structure can lead to the piezoelectric effect. After eliminating crystals which structures have a centre of symmetry, there is only a remaining group of 20 which have piezoelectric properties [3, 8].

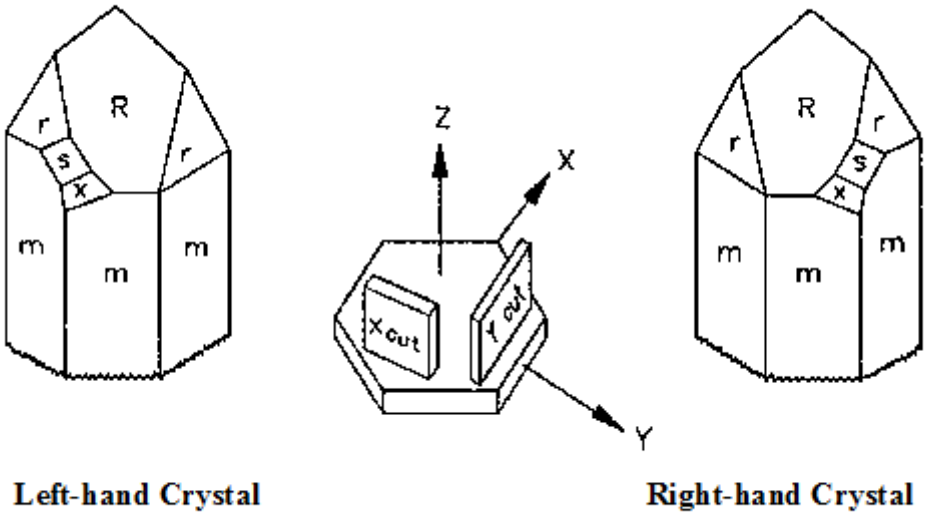

Figure (2-1) quartz crystal has a single axis of three-fold symmetry [8].

Using a quartz crystal as a microbalance can be credited to (Lord Rayleigh) who explained in his book (Theory of sound), that a perturbation added to the resonant frequency caused by a small change in inertia of mechanical system in vibration case [8].

The Quartz Crystal Microbalance (QCM) consists of a thin wafer of quartz crystal which has been cut at an angle of 35 degree with respect to the z- axis of single crystal to give high stability, low temperature coefficient and purely shear mode of oscillation. The quartz wafer is then sandwiched between two metal electrodes from which an external voltage can be applied [9,10,11,12].

Sauerbrey found that exposing a plate of quartz to deposited flux will lead to change in resonant frequency commensurate with deposited mass as described by equation (2-1) [13,14,15,16].

Accordingly, he suggested that the quartz crystal oscillator could be used as a sensor to measure the thickness of thin film [17,18,19].

$$\Delta f = -\frac{2f_0^2}{A\sqrt{\rho_q\,\mu_q}} \quad (2-1)$$

Where ρ_q is the density of quartz, μ_q the shear stiffness;

As a consequence, it has been used in determining the areal density of deposited films [20]. Subsequently, the developments of QCM based devices started and were successfully utilized by a number of researchers. In 1961, Stockbridge and Warner published results from their design of high pressure system and QCM control circuit. Which showed the crystal without electrodes can be tolerating vacuum to 300˚ at the active centre and the mass sensitivity agreed with frequency measurement posteriorly [21,22]. Stockbridge also found that there are linear relationships between rising frequency and pressure caused by quartz elasticity.

The quartz crystal microbalance is used to measure mass by acoustic waves generated from oscillating piezoelectric wafer of quartz crystal which known as nanogram sensitive technique [23]. The operation of the QCM is based on the piezoelectric effect. Resonance is produced when an AC voltage applied with frequency close to the crystals natural resonance and a standing wave condition is created. When the thickness of the quartz wafer is an odd integer number of the standing wave condition, resonance occurs as shown in figure (2-2) [22, 24].

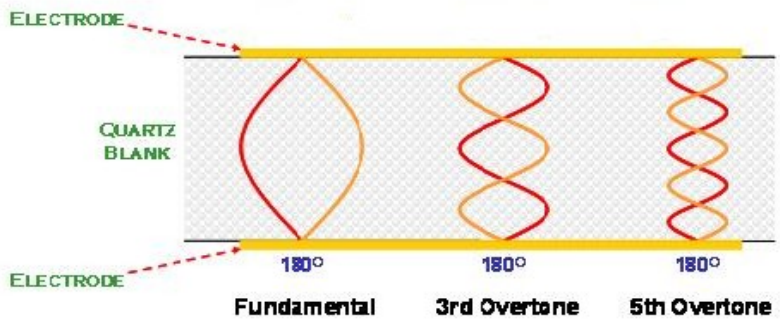

Figure (2-2) Only odd number waves can be excited in the crystal resonator. [1]

Shortly after the discovery of the Quartz Crystal Resonator (QCR), it was noted that the direction of quartz crystal chip with crystal axes has a significant impact on the QCR. This is called the crystal cut.

For quartz crystal resonators, there are different cuts which can be made and every one will give different properties. In this process, θ and φ are the two angles between crystallographic axes used to define crystal cuts.

The most common one is AT-Cut, which has a single rotation, where $\varphi = 0^{\circ}$ and $= 35^{\circ}$.

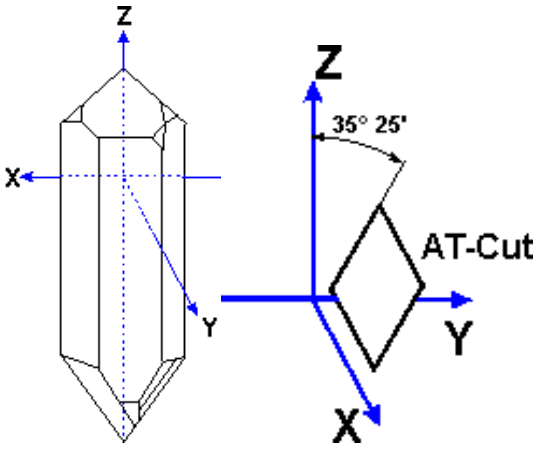

Figure (2-3) Quartz crystal diagram and AT crystal [59].

AT-cut has zero temperature coefficient of frequency at 25˚C and remarkable temperature stability around room temperature. It has two approximately equal and opposite temperature coefficients of elastic stiffness compensating each other where existence symmetrical of inflection temperature around as figure (2-4) shows [25,26,27].

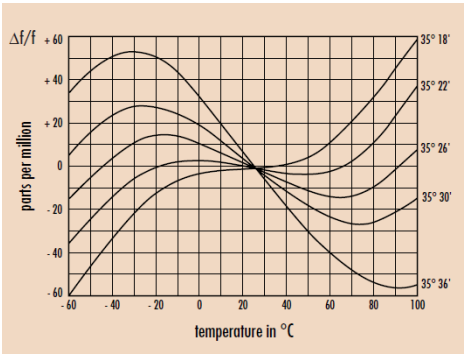

Figure (2-4) AT-cut temperature curve [4].

The velocity of the moving wave and dimensions of the confinement structure is both defined the frequency [24, 27]

When voltage is applied between two metal electrodes, internal and lateral movement will produce in AT crystal, which known as Thickness Shear Movement (TSM) [25, 28].

In the case of the QCR, the top and bottom limits of the quartz wafer give rise to a series of standing acoustic waves between two main surfaces and the frequencies of acoustic modes are given by equation (2-2)[28].

$$f_m = \frac{n\vartheta_m}{2d_q} \quad (2\text{-}2)$$

Where, m is index indicating to the mode, d_q is the thickness of chip ϑ_m is velocity of mode and n is a harmonic number and it is only odd, because the resonant frequency cannot be given in a closed form [23].

The quartz crystal can be considered as device for mechanical vibration. Therefore, it can be formulated by equivalent circuit.

For an unloaded quartz crystal, the motional impedance is an expression of Quartz Crystals (QC) mechanical properties and is described by a series Resistor, Inductor & and Capacitor arrangement (RLC).

In order to complete the equivalent circuit of QC, a capacitance in parallel with the motional impedance (the series RLC) should added, the resultant circuit is commonly referred to as the Butterworth-Van Dyke (BVD) shown in figure (2-5). In this case, every element in BVD equivalent circuit has specific physical meaning [29, 30,31,32,33,34, 35].

R_s (resistor), corresponds to energy loss caused by composition of structure and by contact between crystal and surrounding medium. i.e. losses arising from the viscosity of the solution.

L_s (inductor), the inertial related to the inertial element of the oscillation which is linked to the changing mass while the vibration.

C_s (capacitor), corresponds to the elasticity of the quartz and stored energy in oscillation [35,36, 37,38, 39, 40,41,42].

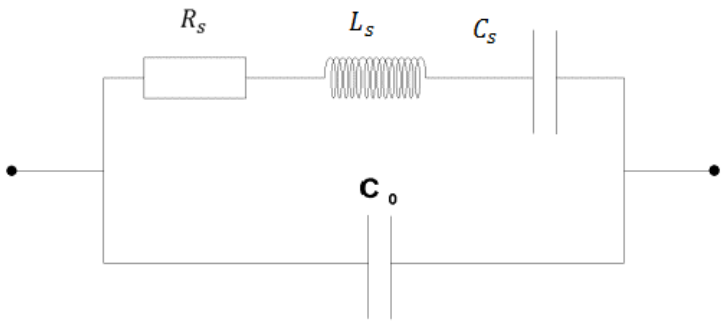

Figure (2-5) BVD equivalent circuit.

The impedance (Z) for circuit is consists of real and imaginary parts

$$Z = R + jX \quad (2-3)$$

Where:

$$R = R_s \qquad x = j\left(wL_s - \frac{1}{wc_s}\right) \quad (2-4)$$

The resonant frequencies can be found as follows:

$$\left(f_s^{el} = \frac{1}{2\pi\sqrt{L_s c_s}}\right) \qquad (2-5)$$

$$f_p^{el} = \left(\frac{1}{2\pi\sqrt{L_s\, c^*}}\right) \qquad (2-6)$$

$$c^* = \frac{c_s\, c_0}{c_s + c_0} \qquad (2-7)$$

The series and parallel resonances occur at the frequencies where the impedance spectra has solely real (resistive) parts.

Where C_0 is the static capacitor dominates the admittance spectra away from quartz resonance.

$$C_0 = \varepsilon_q \frac{A}{h_q} \qquad (2-8)$$

*(*A*)* the active area of the electrodes on the crystal.

The QCM is highly sensitive and responds to small mass changes and consequently has been used as a mass sensor. Initially, it was used in dry phase (vacuum and gas phase); however it has now become widely used in applications where viscoelastic changes are observed and with advances in drive circuitry and measurement techniques become applicable in liquid environments [43,44]. Details of the oscillator drive circuit used in this work will be described in chapter 5.

Therefore, the Sauerbrey equation is no longer sufficient to fully model and characterize non rigid films and must be extended to add the effects caused by viscoelastic coatings.

One of the first who researched in ultrasonic using quartz was Mason with other co-worker, where the shear viscosity and elasticity of liquid was measured [45, 46, 47]

Since the behaviour of QCR has been discovered in gas and liquid phase a huge number of potential application areas has been opened.

Examples from viscous and liquid phase applications in general show large values of dissipation (acoustic energy loss) compared to that observed in vacuum or gaseous media.

Contact with a non-rigid film (Viscoelastic and/or liquid) will therefore lead to energy lost from electrical equivalent circuit [45, 48, 49].

To improve the accuracy of the QCM it must be adapted for liquid and gas phase, the added viscoelastic contribution must be considered, the models and respective equations should be modified.

2.2 Quartz Crystal Microbalance with Dissipation (QCM-D):

As stated previously, in the case of non rigid adsorbed film, the Sauerbrey equation becomes invalid because the film is viscoelastic and thus will under estimate surface mass.

Accordingly, over one thousand reviewed publications have addressed this aspect [50,51,52,53]. Where energy losses occur during crystal oscillation as a result of viscoelastic properties of the adsorbed film and bulk liquid coupling to crystal surface motion in case of liquid environment application. This crystal damping is often referred to as dissipation and it is described as the inverse of the quality factor Q [51]. Regarding to this, a quartz crystal microbalance with dissipation (QCM-D) technique was developed for surface analysis. Where the dissipation value (D) gives a new parameter about structural properties of adsorbed layers (viscoelastic layers), where frequency and dissipation of the QCM-D are measures and D defined as:

$$D = \frac{1}{Q} = \frac{E_{lost}}{2\pi\, E_{stored}} \qquad (2-9)$$

Where E_{lost} indicate to energy lost during one oscillation cycle and E_{stored} is energy stored in the oscillator [50,51,54].

2.3 Viscous films:

In the case of rigid coating or very thin film where phase shift of the acoustic wave across the film is $\ll \frac{\pi}{2}$ the Sauerbrey equation can be used and gives a linear relation between change of the QCM resonant frequency and mass of thin film [25]. In non-rigid films (viscoelastic film) employing impedance measurement around the resonance frequency of quartz crystal combined with additional analysis and feature extraction can be used to fully characterise the film.

The studies of crystal resonator and it's impedance with or without contacting media can lead to the discovery of significant information about the crystal and contacting media. The frequency at maximum conducting f_s (real part of the admittance) is the resonant frequency of the motional branch of the circuit, and is what is traditionally linked with standard microbalance measurements. In terms of conductance, the higher value of Q factor of the crystal the sharper conductance peak, and this indicates the film is rigid [25,39,55, 53, 56].

A broad peak refers to viscous losses in film or contacting solution.

The zero phase frequency f_r occurs when the applied voltage is in same phase with current flowing through crystal.

The admittance Y , resistance R and phase angle are $\theta°$ measured while frequency is swept and f_s determined using equation (2-10).

$$f_s = \frac{1}{2\pi\sqrt{L_1 C_1}} \qquad (2-10)$$

Figure (2-8) Shows conductance spectra of AT cut crystal in air and with contacting water in one side [27, 57, 58, 59].

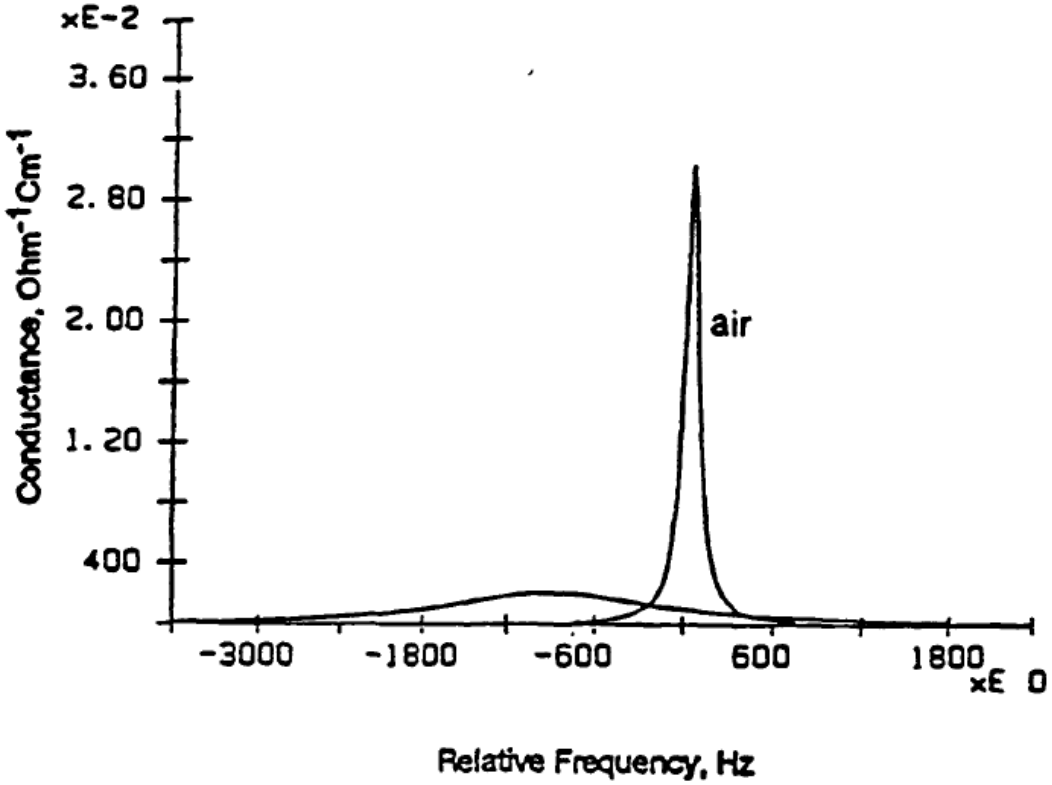

Figure (2-8) conductance spectra of AT cut crystal in air and with contacting water on one side [27].

A large shift in frequency Δf and expanding in peak is observed. Δf Nominally indicates mass loading. A broadening or the peak indicates a decrease in film rigidity/an increase in viscosity.

2.4 Viscous (Liquid) film:

The applications of the QCM were limited to vapour environments until Glassfords noted the acoustic losses in liquid after examining the distribution of silicon oil droplets by measuring the shear wave velocity of the films on QCM surface. From this work the equations for QCM response of liquids relative to solids were derived [27].

Different studies found that crystal oscillations are only maintained when it is exposed to liquid on one face. The liquid ad/absorption and its effects could be then detected.

One face in full contact with solution was analysed theoretically by Kanazawa and Gordon and the developed technique [37, 60, 61].

$$\Delta f = -f_0^{\frac{3}{2}} \sqrt{\frac{d_f \eta_f}{\pi d_q \mu_q}} \qquad (2-11)$$

Where d_f , η_f density and viscosity of liquid, d_q, μ_q are the density and shear modules of quartz.

The solution of the problem of acoustic losses in viscoelastic media was first addressed by Kanazawa [59, 62]. He derived a complex equation for the observed frequency where the shear modulus, quartz density, viscosity and thickness of viscoelastic layer are considered.

The general solution of the wave equation, for shear waves was used in viscoelastic media.

This equation has been simplified to Lu and Lewis's [8,27] and resulted in the limit of purely elastic and Kenawaza and Gordon's equation for behaviour of purely viscous limit. More information and discussion about viscous film will be addressed in chapter five.

Also they defines quality factor Q, complex function of the viscosity, shear modulus, density and film thickness, which is used to study change of frequency in viscoelastic films as function of film thickness [63, 64].

2.5 Phthalocyanine:

In 1907, after Brawn and Tcherniac's involvement in the research of heated o-cyanobenzamide at high temperature, the first synthesise of phthalocyanine was recorded [65].

A quarter of a century later, the extensive research of Linstead and the X-ray diffraction analyses undertaken by Robertson led to the identification of the structure - metal-free un-substituted phthalocyanine. During this investigation both (a) metallophthalocyanine and (b) metal-free phthalocyanine (Fig 2- 6 a and 2-6 b) were classified [22, 65, 66,67]

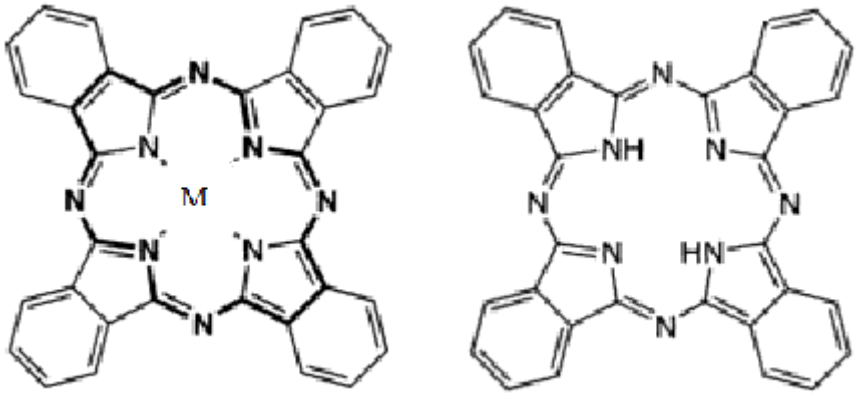

Figure (2-6) a) metallophthalocyanine. **b)** metal-free phthalocyanine.

Over recent years, Phthalocyanine's has become an important field for many particular areas of study such as dyes, electrochemistry, batteries, photodynamic therapy and chemical sensors [22, 68,69,70,71, 72, 73, 74].

The important property of phthalocyanine which was of significant interest is its specific spectral properties; it has an isolated and single band (Q-band) in the visible spectrum. The Q-band is the strongest and intensive band in major number of phthalocyanine where it sits in

visible range at wavelengths between $650\ to\ 670\ nm$ [75]. That gives it deep and pure colour with molar absorptivity.

Generally, metalphthalocyanine exhibit a single Q-band but ordinarily a split of Q-band has been observed which can be attributed to their less symmetry. Once the phthalocyanine scaffold become unsymmetrical substituted, the split of the Q-band increase. Moreover, there are different impact cause shift of the Q-band.

This opened the door for many areas of research and applications. Additionally because it its inherent gas adsorption and semiconducting properties there have been a significant number of works utilizing Phthalocyanine's in chemical sensors [70,71,28,77, 78].

Also other characteristics such as chemical and thermal stability in many environments make it suitable for sensor applications. In addition, they can easily be produced as films through traditional coating methods.

One could describe a phthalocyanine sensor simply as a thin film of phthalocyanine coated over a flat surface or interdigitated electrode. The interaction (gas absorption) between the phthalocyanine film with a particular vapour may be detected as a change in the physical properties of the film. For instance, mass, conductivity and optical properties.

However, there are several research groups investigating the phthalocyanine in sensor applications and various aspects such as chemical interaction with gases and the performance of sensing devices [22, 28,79, 81, 87].

In general form, a micro sensor consists of two main parts.

* sensing chemical coating.

* Microelectronic substrate.

Where, the coating has the characteristics of responding to the existence or absence of a particular gas.

In the case of phthalocyanine, if the film absorbs or forms a weak bond with a specific gas, that lead to change in conductivity as a result of this interaction. The donor- acceptor complex formation with the equilibrium which resulting from the partial pressure by components of gaseous [22]. Phthalocyanine has been known as p-type semiconductors, which is based on its response to gases (donor- acceptor).

There are different deposition techniques to prepare phthalocyanine films, which are based on different coating techniques. These include spin coating and Langmuir- Blodgett (L-B) which is very compatible because it offers a high level of control over film thickness and reproducibility [68, 82, 83]. Both techniques will be discussed later in this thesis.

Numerous studies have been performed on various metals Phthalocyanine such as (Co, Ni, Cu and Zn) and clearly indicate that the film morphology has significant role in electrical response for exposure to gases [22, 84, 85, 86, 87].

Several studies of functional properties of phthalocyanine material have recently been performed regarding in both basic and application aspects. Phthalocyanines are a promising organic compound for thin film and sensor applications. It's suitable for use in sensor since it is easily synthesized and produced as a thin film through traditional coating methods.

Wide ranges of metallophthalocyanine have been synthesized and are capable for sensor applications. Among these Zinc phthalocyanines (ZnPcs) are an increasingly popularity organic compound that due to their unique prosperities, high solubility in most common solvent and it is non toxic to the environment.

Although numerous of research studies have been investigated on different type of phthalocyanine, due to the large number of potentially synthesizable films only a limited subset have been investigated and characterized. Consequently, their use in sensing applications has not been fully evaluated and from the available literature, the basic studies

on phthalocyanine thin films, and more investigations in detailed are needed before going in organic gas sensor [22, 89].

Hence, this research will present our particular work made on a selection of specific phthalocyanines thin films. In total nine different substituted metallophthalocyanine were prepared and characterized in order to study their performance as a gas sensor. The list of compound material and empirical formula with molecular weight are given it table (2-1).

	Chemical name	**Code**	**Empirical formula (Hill Notation)**	**Molecular weigh g/mol**
1	Zinc2,3,9,10,16,17,23,24octakis(octyloxy)-29H,31H phthalocyanine	Zn-oct-oct-Pc	$C_{96}H_{144}N_8O_8Zn$	1603.61
2	Zinc 1,2,3,4,8,9,10,11,15,16,17,18,22,23,24,25-hexadecafluoro 29H,31H-phthalocyanine	Zn-hexa-Pc	$C_{32}F_{16}N_8Zn$	865.76
3	Zinc 1,4,8,11,15,18,22,25-octabutoxy-29H,31H-phthalocyanine	Zn-octa-Pc	$C_{64}H_{80}N_8O_8Zn$	1154.76
4	Zinc 2,9,16,23-tetra-*tert*-butyl-29*H*,31*H*-phthalocyanine	Zn-tp-tb-Pc	$C_{48}H_{48}N_8Zn$	802.34
5	Zinc 2,11,20,29-tetra-*tert*-butyl-2,3-naphthalocyanine	Zn-tp-tb-nPc	$C_{64}H_{56}N_8Zn$	1002.57
6	Nickel(II) 1,4,8,11,15,18,22,25-octabutoxy-29*H*,31*H*-phthalocyanine	Ni(II)-oct-Pc	$C_{64}H_{80}N_8NiO_8$	1148.06
7	Nickel(II) phthalocyanine	Ni(II)-Pc	$C_{32}H_{16}N_8Ni$	571.22
8	Cobalt(II) phthalocyanine	Co(II)-Pc	$C_{32}H_{16}CoN_8$	571.46
9	Copper(II) phthalocyanine	Cu(II)-Pc	$C_{32}H_{16}CuN_8$	576.07

Table (2-1) the list of compound material used in this study.

All Chemical Structure for material used in this work are depicted in figure (2-7) (a-i).

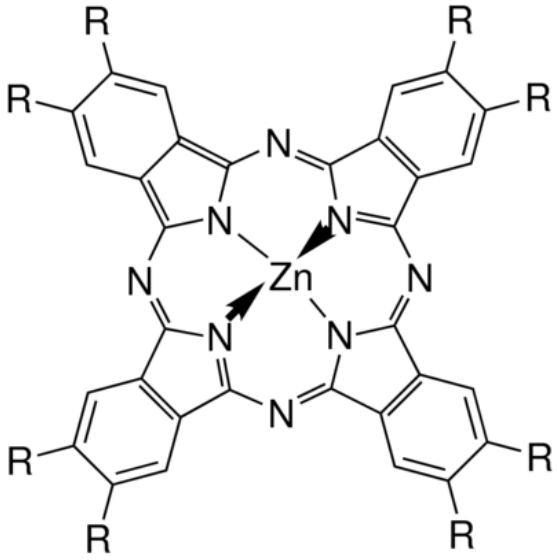

(a)

Zinc2,3,9,10,16,17,23,24 octakis(octyloxy) − 29H, 31H − phthalocyanine

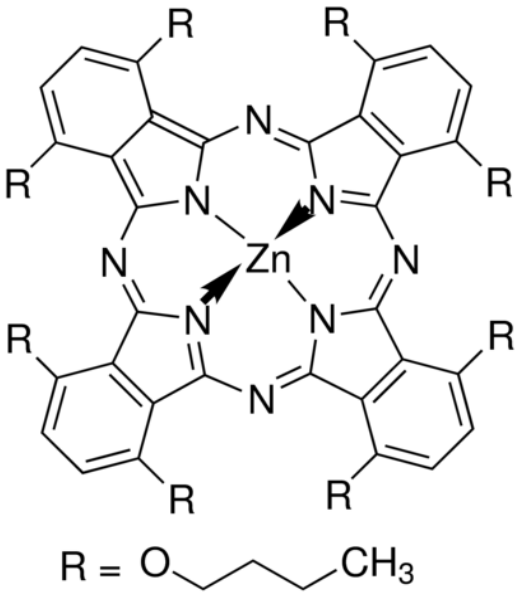

(b)

Zinc 1,4,8,11,15,18,22,25 octabutoxy − 29H, 31H − phthalocyanine

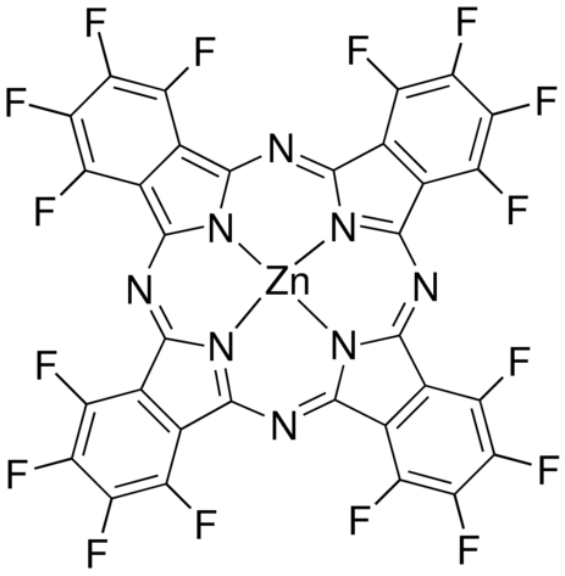

(c)

Zinc 1,2,3,4,8,9,10,11,15,16,17,18,22,23,24,25, −hexadecafluoro 29H, 31H − phthalocyanine

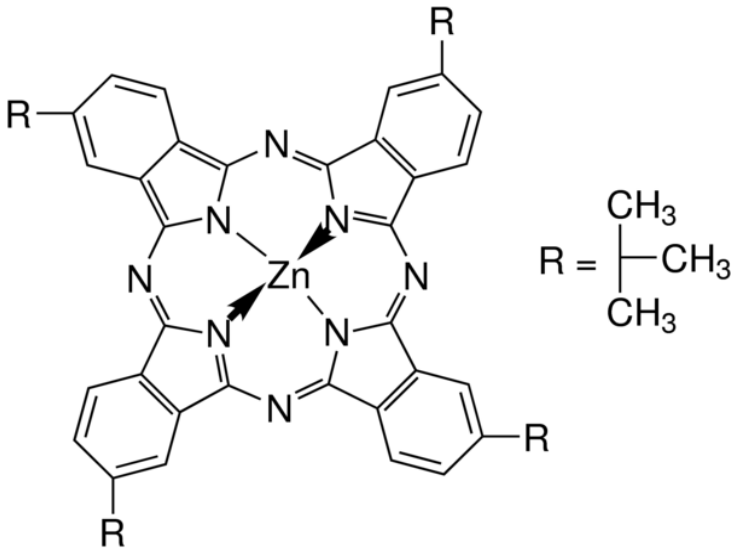

(d)

Zinc 2,9,16,23 − tetra − tert − butyl − 29H, 31H − phthalocyanine

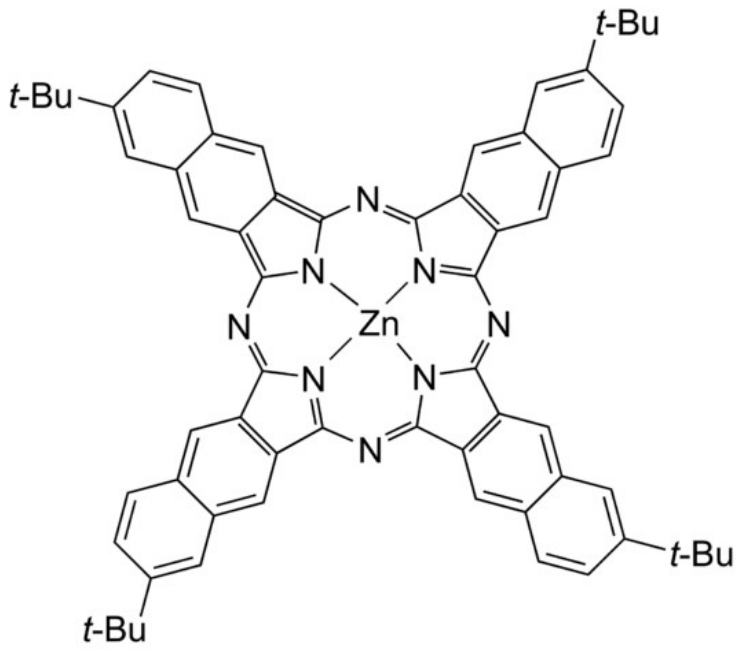

(e)

Zinc 2,11,20,29 − tetra − tert − butyl − 2,3 − naphthalocyanine

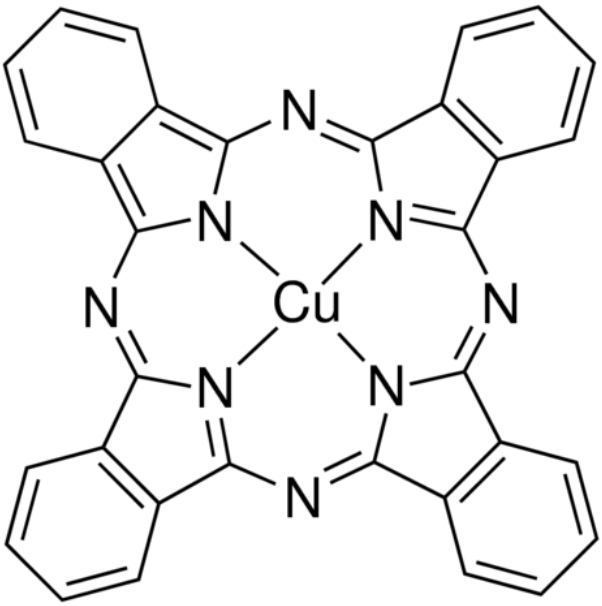

(f)

Copper(II) − phthalocyanine

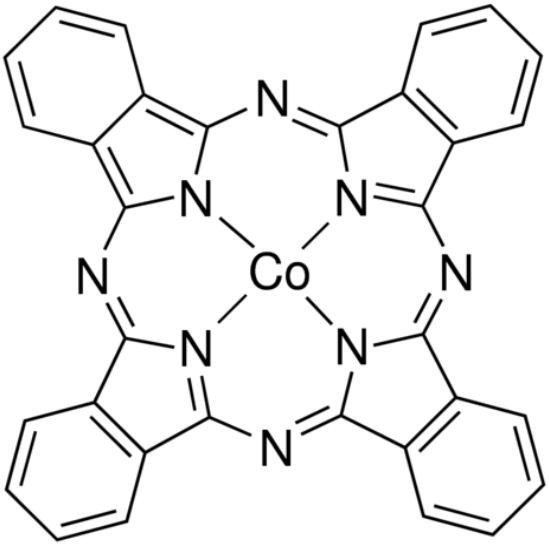

(g)

Cobalt(II) – phthalocyanine

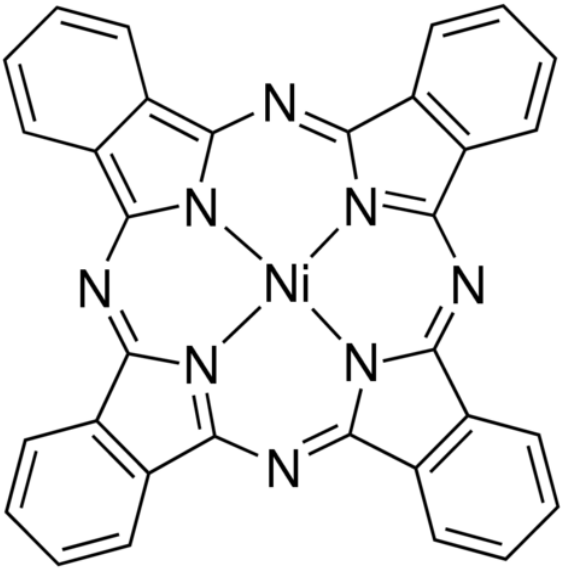

(h)

Nickel(II) – phthalocyanine

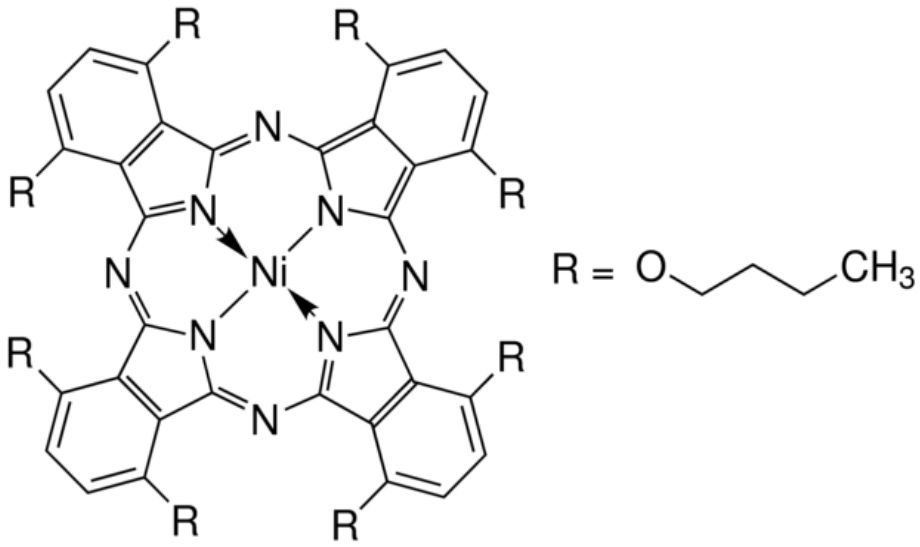

(i)

Nickel(II) 1,4,8,11,15,18,22,25 – octabutoxy − 29H, 31H − phthalocyanine

Figure (2-7) Chemical Structure for material used.

References:

1- *Basics of a quartz crystal microbalance.* [online]. Last accessed 8/2 2013 at: http://www.gamry.com/application-notes/basics-of-a-quartz-crystal-microbalance/.

2- BUCK, Richard P., et al. (2004). Piezoelectric chemical sensors (IUPAC technical report). *Pure and applied chemistry,* 76 (6), 1139-1160.

3- BRADSHAW, Louis (2000). Understanding piezoelectric quartz crystals. *RF time and frequency,* 8 , 50-58.

4- ARNAU, Antonio, et al. (2004). Interface electronic systems for AT quartz crystal microbalance sensors. In: *Piezoelectric Transducers and Applications.* Springer, 111-140.

5- BENES, E., et al. (1995). Sensors based on piezoelectric resonators. *Sensors and actuators-A-physical sensors,* 48 (1), 1-22.

6- HIERLEMANN, Andreas, et al. (1995). Polymer-based sensor arrays and multicomponent analysis for the detection of hazardous oragnic vapours in the environment. *Sensors and actuators B: Chemical,* 26 (1-3), 126-134.

7- PRICE, Gareth J., et al. (2002). Piezoelectric chemical sensors based on morpholine containing polymers. *Sensors and actuators B: Chemical,* 84 (2-3), 208-213.

8- LU, Chao and CZANDERNA, Alvin Warren (2012). *Applications of piezoelectric quartz crystal microbalances.* Elsevier.

9- FERREIRA, Guilherme NM, DA-SILVA, Ana-Carina and TOMÉ, Brigitte (2009). Acoustic wave biosensors: physical models and biological applications of quartz crystal microbalance. *Trends in biotechnology,* 27 (12), 689-697.

10- JANSHOFF, Andreas, GALLA, Hans-Joachim and STEINEM, Claudia (2000). Piezoelectric Mass-Sensing Devices as Biosensors—An Alternative to Optical Biosensors? *Angewandte chemie international edition,* 39 (22), 4004-4032.

11- KALANTAR-ZADEH, Kourosh (2013). *Sensors: an introductory course.* Springer Science & Business Media.

12- MARX, Kenneth A. (2003). Quartz crystal microbalance: a useful tool for studying thin polymer films and complex biomolecular systems at the solution− surface interface. *Biomacromolecules,* 4 (5), 1099-1120.

13- ARNAU, Antonio, et al. (2009). A different point of view on the sensitivity of quartz crystal microbalance sensors. *Measurement science and technology,* 20 (12), 124004.

14- BEHLING, Carsten, LUCKLUM, Ralf and HAUPTMANN, Peter (1998). Response of quartz-crystal resonators to gas and liquid analyte exposure. *Sensors and actuators A: Physical,* 68 (1-3), 388-398.

15- GALLAGHER, Patrick K. (1998). *Handbook of Thermal Analysis and Calorimetry, Vol. 1*. Elsevier, Amsterdam.

16- NABOK, Alexei, et al. (2007). Specific binding of large aggregates of amphiphilic molecules to the respective antibodies. *Langmuir,* 23 (16), 8485-8490.

17- Nabok, A. V., Hassan, A. K., & Ray, A. K. (2000). Condensation of organic vapours within nanoporous calixarene thin films. *Journal of Materials Chemistry, 10*(1), 189-194.

18- MARXER, C. Galli, et al. (2003). Simultaneous measurement of the maximum oscillation amplitude and the transient decay time constant of the QCM reveals stiffness changes of the adlayer. *Analytical and bioanalytical chemistry,* 377 (3), 570-577.

19- ZHOU, XC, et al. (1997). Organic vapour sensors based on quartz crystal microbalance coated with self-assembled monolayers. *Sensors and actuators B: Chemical,* 42 (1), 59-65.

20- NABOK, Alexei (2005). *Organic And Inorganic Nanostructures (Artech House Mems and Sensors Library).* Artech House Publishers, Boston, MA, USA.

21- LUCKLUM, Ralf and HAUPTMANN, Peter (2000). The quartz crystal microbalance: mass sensitivity, viscoelasticity and acoustic amplification. *Sensors and actuators B: Chemical,* 70 (1-3), 30-36.

22- LEZNOFF, Clifford C., et al. (1996). *Phthalocyanines: properties and applications.* VCH publishers

23- LUCKLUM, Ralf, BEHLING, Carsten and HAUPTMANN, Peter (2000). Gravimetric and non-gravimetric chemical quartz crystal resonators. *Sensors and actuators B: Chemical,* 65 (1-3), 277-283.

24- LUCKLUM, Ralf and HAUPTMANN, Peter (2003). Transduction mechanism of acoustic-wave based chemical and biochemical sensors. *Measurement science and technology,* 14 (11), 1854.

25- STEINEM, Claudia and JANSHOFF, Andreas (2007). *Piezoelectric sensors.* Springer Science & Business Media. , 5.

26- VAN QUY, Nguyen, et al. (2011). Gas sensing properties at room temperature of a quartz crystal microbalance coated with ZnO nanorods. *Sensors and actuators B: Chemical,* 153 (1), 188-193.

27- HOLLOWAY, AF, et al. (2003). New method of vapour discrimination using the thickness shear mode (TSM) resonator. *Sensors,* 3 (6), 187-191.

28- HAUPTMANN, PR, LUCKLUM, R. and SCHRÖDER, J. (2005). QCR-SENSORS–MODELS AND APPLICATIONS.

29- .. WAJID, Abdul (1991). Improving the accuracy of a quartz crystal microbalance with automatic determination of acoustic impedance ratio. *Review of scientific instruments,* 62 (8), 2026-2033.

30- BANDEY, HELEN L., et al. (1999). *Equivalent-circuit model for the thickness-shear mode resonator with a viscoelastic film near film resonance,* .

31- HOLLOWAY, AF, et al. (2004). Discriminative sensing of volatile organic solvents. Comparative analysis using different QCM techniques. In: *Sensors, 2004. proceedings of IEEE,* IEEE, 1500-1503.

32- LUCKLUM, Ralf and HAUPTMANN, Peter (2000). The Δf–ΔR QCM technique: an approach to an advanced sensor signal interpretation. *Electrochimica acta,* 45 (22-23), 3907-3916.

33- MATTHYS, Robert J. (1983). Crystal oscillator circuits. *New york, wiley-interscience, 1983, 244 p.,* .

34- VIG, John R. (1992). *Introduction to quartz frequency standards.revision,* .

35- XIE, Qingji, et al. (2000). An electrochemical quartz crystal impedance study on cystine precipitation onto an Au electrode surface during cysteine oxidation in aqueous solution. *Journal of electroanalytical chemistry,* 484 (1), 41-54

36- ARNAU, A., SOGORB, T. and JIMÉNEZ, Y. (2002). Circuit for continuous motional series resonant frequency and motional resistance monitoring of quartz crystal resonators by parallel capacitance compensation. *Review of scientific instruments,* 73 (7), 2724-2737.

37- EICHELBAUM, Frank, et al. (1999). Interface circuits for quartz-crystal-microbalance sensors. *Review of scientific instruments,* 70 (5), 2537-2545.

38- HOLLOWAY, AF, et al. (2004). Impedance analysis of the thickness shear mode resonator for organic vapour sensing. *Sensors and actuators B: Chemical,* 99 (2-3), 355-360.

39- MARTIN, Stephen J. (1997). Closing remarks. *Faraday discussions,* 107 , 463-476.

40- MARTIN, Stephen J., et al. (2000). Equivalent-circuit model for the thickness-shear mode resonator with a viscoelastic film near film resonance. *Analytical chemistry,* 72 (1), 141-149.

41- Arnau, A., Sogorb, T., & Jimenez, Y. (2000). QCM100-quartz crystal microbalance theory and calibration. *Rev.Sci.Instrum, 71*, 2563.

42- ROBERT, Matthys J. (1983). Crystal oscillator circuit.

43- ETCHENIQUE, R. and BRUDNY, VL (1999). Characterization of porous polyaniline–polystyrenesulfonate composite films using EQCM. *Electrochemistry communications,* 1 (10), 441-444.

44- HOSSENLOPP, Jeanne, et al. (2004). Characterization of epoxy resin (SU-8) film using thickness-shear mode (TSM) resonator under various conditions. *Journal of polymer science part B: Polymer physics,* 42 (12), 2373-2384.

45- MEYER JR, Howard R. (1990). *Studies of thin film chemical sensors using the quartz crystal microbalance, .*

46- Nakamoto, T., Nakamura, K., & Moriizumi, T. (1996). Study of oscillator-circuit behavior for QCM gas sensor. *Ultrasonics Symposium, 1996. Proceedings., 1996 IEEE, , 1* 351-354.

47- RODAHL, Michael and KASEMO, Bengt (1996). A simple setup to simultaneously measure the resonant frequency and the absolute dissipation factor of a quartz crystal microbalance. *Review of scientific instruments,* 67 (9), 3238-3241.

48- ARNAU, Antonio, JIMÉNEZ, Yolanda and SOGORB, Tomás (2000). Thickness-shear mode quartz crystal resonators in viscoelastic fluid media. *Journal of applied physics,* 88 (8), 4498-4506.

49- MARTIN, Stephen J., FRYE, Gregory C. and SENTURIA, Stephen D. (1994). Dynamics and response of polymer-coated surface acoustic wave devices: effect of viscoelastic properties and film resonance. *Analytical chemistry,* 66 (14), 2201-2219.

50- DIXON, Matthew C. (2008). Quartz crystal microbalance with dissipation monitoring: enabling real-time characterization of biological materials and their interactions. *Journal of biomolecular techniques: JBT,* 19 (3), 151.

51- HOOK, F., et al. (1999). The dissipative QCM-D technique: interfacial phenomena and sensor applications for proteins, biomembranes, living cells and polymers. In: *Frequency and time forum, 1999 and the IEEE international frequency control symposium, 1999., proceedings of the 1999 joint meeting of the european,* IEEE, 966-972.

52- LUCKLUM, Ralf and HAUPTMANN, Peter (1997). Determination of polymer shear modulus with quartz crystal resonators. *Faraday discussions,* 107 , 123-140.

53- VIKINGE, Trine P., et al. (2000). Comparison of surface plasmon resonance and quartz crystal microbalance in the study of whole blood and plasma coagulation. *Biosensors and bioelectronics,* 15 (11-12), 605-613.

54- RODAHL, Michael, et al. (1995). Quartz crystal microbalance setup for frequency and Q-factor measurements in gaseous and liquid environments. *Review*

55- CALVO, EJ, et al. (1997). Quartz crystal impedance studies at 10 MHz of viscoelastic liquids and films. *Faraday discussions,* 107 , 141-157.

56- SABOT, Andrea and KRAUSE, Steffi (2002). Simultaneous quartz crystal microbalance impedance and electrochemical impedance measurements. Investigation into the degradation of thin polymer films. *Analytical chemistry,* 74 (14), 3304-3311.

57- KANAZAWA, K. Keiji and GORDON II, Joseph G. (1985). The oscillation frequency of a quartz resonator in contact with liquid. *Analytica chimica acta,* 175 , 99-105.

58- MARTIN, Stephen J., GRANSTAFF, Victoria Edwards and FRYE, Gregory C. (1991). Characterization of a quartz crystal microbalance with simultaneous mass and liquid loading. *Analytical chemistry,* 63 (20), 2272-2281.

59- REED, CE, KANAZAWA, K. Keiji and KAUFMAN, JH (1990). Physical description of a viscoelastically loaded AT-cut quartz resonator. *Journal of applied physics,* 68 (5), 1993-2001.

60- Ferreira, G. N., Da-Silva, A., & Tomé, B. (2009). Acoustic wave biosensors: Physical models and biological applications of quartz crystal microbalance. *Trends in Biotechnology, 27*(12), 689-697.

61- KANAZAWA, K. Keiji and GORDON, Joseph G. (1985). Frequency of a quartz microbalance in contact with liquid. *Analytical chemistry,* 57 (8), 1770-1771.

62- MURAMATSU, Hiroshi, TAMIYA, Eiichi and KARUBE, Isao (1988). Computation of equivalent circuit parameters of quartz crystals in contact with liquids and study of liquid properties. *Analytical chemistry,* 60 (19), 2142-2146.

63- BENES, E. (1984). Improved quartz crystal microbalance technique. *Journal of applied physics,* 56 (3), 608-626.

64- BRUSCHI, L., DELFITTO, G. and MISTURA, G. (1999). Inexpensive but accurate driving circuits for quartz crystal microbalances. *Review of scientific instruments,* 70 (1), 153-157.

65- ZOLLINGER, Heinrich (2003). *Color chemistry: syntheses, properties, and applications of organic dyes and pigments.* John Wiley & Sons.

66- NEMYKIN, Victor N. and LUKYANETS, Evgeny A. (2010). Synthesis of substituted phthalocyanines. *ARKIVOC: Online journal of organic chemistry,* .

67- OGUNSIPE, Abimbola, CHEN, Ji-Yao and NYOKONG, Tebello (2004). Photophysical and photochemical studies of zinc (II) phthalocyanine derivatives—effects of substituents and solvents. *New journal of chemistry,* 28 (7), 822-827.

68- BASOVA, TV, et al. (2003). Mesomorphic phthalocyanine as chemically sensitive coatings for chemical sensors. *Sensors and actuators B: Chemical,* 96 (1-2), 70-75

69- EGGINGER, Martin and Neugebauer, Ass Prof Dr Helmut Zn-Phthalocyanine/C60 Solar Cells.

70- ERBAHAR, Dilek D., et al. (2012). Pesticide sensing in water with phthalocyanine based QCM sensors. *Sensors and actuators B: Chemical,* 173 , 562-568.

71- HARBECK, Mika, et al. (2010). Phthalocyanines as sensitive coatings for QCM sensors operating in liquids for the detection of organic compounds. *Sensors and actuators B: Chemical,* 150 (1), 346-354.

72- Kobayashi, N. (1999). Phthalocyanines. *Current Opinion in Solid State and Materials Science, 4*(4), 345-353.

73- OGUNSIPE, Abimbola and NYOKONG, Tebello (2004). Effects of substituents and solvents on the photochemical properties of zinc phthalocyanine complexes and their protonated derivatives. *Journal of molecular structure,* 689 (1-2), 89-97

74- WRÓBEL, Danuta and BOGUTA, Andrzej (2002). Study of the influence of substituents on spectroscopic and photoelectric properties of zinc phthalocyanines. *Journal of photochemistry and photobiology A: Chemistry,* 150 (1-3), 67-76

75- CLAESSENS, Christian G., HAHN, Uwe and TORRES, Tomás (2008). Phthalocyanines: From outstanding electronic properties to emerging applications. *The chemical record,* 8 (2), 75-97.

76- HARBECK, Mika, et al. (2010). Preferential sorption of polar compounds by fluoroalkyloxy substituted phthalocyanines for the use in sorption based gas sensors. *Sensors and actuators B: Chemical,* 150 (2), 616-624.

77- KUMAR, A., et al. (2015). Tetra-tert-butyl copper phthalocyanine-based QCM sensor for toluene detection in air at room temperature. *Sensors and actuators B: Chemical,* 210 , 398-407.

78- SBERVEGLIERI, Giorgio (2012). *Gas sensors: principles, operation and developments.* Springer Science & Business Media.

79- CALVETE, Mario, YANG, Guo Ying and HANACK, Michael (2004). Porphyrins and phthalocyanines as materials for optical limiting. *Synthetic metals,* 141 (3), 231-243.

80- HARBECK, Mika, et al. (2011). Phthalocyanines as sensitive coatings for QCM sensors: Comparison of gas and liquid sensing properties. *Sensors and actuators B: Chemical,* 155 (1), 298-303.

81- ZHOU, R., et al. (1996). Phthalocyanines as sensitive materials for chemical sensors. *Applied organometallic chemistry,* 10 (8), 557-577.

82- GIANCANE, G., et al. (2012). Investigations and application in piezoelectric phenol sensor of Langmuir–Schäfer films of a copper phthalocyanine derivative functionalized with bulky substituents. *Journal of colloid and interface science,* 377 (1), 176-183.

83- VALLI, Ludovico (2005). Phthalocyanine-based Langmuir–Blodgett films as chemical sensors. *Advances in colloid and interface science,* 116 (1-3), 13-44.

84- BASOVA, T., et al. (2009). Investigation of gas-sensing properties of copper phthalocyanine films. *Materials science and engineering: C,* 29 (3), 814-818.

85- CUI, Li-Ying, et al. (2007). Synthesis, crystal structure and characterization of a new zinc phthalocyanine complex. *Journal of molecular structure,* 827 (1), 149-154.

86- MOSER, Frank H. and THOMAS, Arthur L. (1964). Phthalocyanine compounds. *Journal of chemical education,* 41 (5), 245.

87- MUKHERJEE, Debdyuti, et al. (2017). Phthalocyanines as Sensitive Materials for Chemical Sensors. In: *Materials for Chemical Sensing.* Springer, 165-226.

88- *QCM100- quartz crystal microbalance theory and calibration* . [online]. Last accessed 22/05 2017 at: http://www.thinksrs.com/downloads/PDFs/ApplicationNotes/QCMTheoryapp.pdf.

89- SAKAMOTO, Keiichi and OHNO-OKUMURA, Eiko (2009). Syntheses and functional properties of phthalocyanines. *Materials,* 2 (3), 1127-1179.

CHAPTER THREE

METHODOLOGIES

This chapter is presented in order to convey a basic knowledge about measurement techniques used in this project including:

- **Spectroscopic Ellipsometry.**
- **Atomic Force Microscope.**
- **UV- Visible absorption Spectrophotometer.**

3.1 Spectroscopic Ellipsometry:

Ellipsometry is an optical measurement technique which is used to determine the dielectric properties and thickness of thin transparent films. Ellipsometry does not measure thickness or optical constants directly; it actually measures changes in polarisation state of light after reflection from the surface of the sample. [1,2, 3]

The significant features of the method which give it merit are: accuracy, short measurement time (approximately a few seconds), high thickness sensitivity $(\approx 0.01\ nm)$ and it is inherently non $-$ destructive. Therefore, ellipsometry is a typical measurement technique used in fundamental research and also in industry [3,4, 5, 6].

The experimental data are usually expressed as two parameters that are related to the Fresnel reflection coefficient r_p and r_S by:

$$\rho = \frac{r_p}{r_s} = \tan\psi\, e^{i\Delta} \qquad (3-1)$$

These two coefficients contain information related to material optical properties and physical dimension. This complex ratio is measured as function of wave length, where (p, s) indicate to the polarization states in system of two orthogonal basis vectors.

s-direction stands perpendicular to the plane of incidence, ψ and Δ determine the differential change in amplitude and phase. Ellipsometry produces the material optical constant (n, k) directly.

The complex refraction index can be defined from n and k by $N = n - ik$ and the complex dielectric constant $\varepsilon = \varepsilon_1 - i\varepsilon_2$ and absorption coefficient α can also be obtained from:

$$\varepsilon_1 = n^2 - k^2, \quad \varepsilon_2 = 2nk, \qquad \alpha = \frac{n\pi k}{\lambda} \qquad (3-2)$$

Where λ is the light wave length [3, 5].

For thin films, the thickness can be evaluated then both, Transmittance and Reflectance ($T$and R), can be calculated.

To analyse data from ellipsometry requires an optical model defined by an optical constant and the sample layer thickness.

Figure (3-1) diagram for ellipsometry measuring process.

One of the disadvantages of the ellipsometry technique is the analysis can become complicated.

Fundamentally, when an electric field of light is referred to as

Polarized light, as an important fact of light polarization superimposing two light waves propagation in orthogonal. By that way all states of polarization can be expressed. [3, 5]

3.1.1 Ellipsometry measurement:

Light waves consist of perpendicular electrical and magnetic fields oscillating in all possible directions there are orthogonal with the wave direction. Linearly, polarized light is defined as light which has an oscillating wave in one perpendicular direction. When light is reflected from a reflective sample, it will classified into the p and s polarized light wave. This depends on the direction of the electric field oscillations. [1, 3, 5]

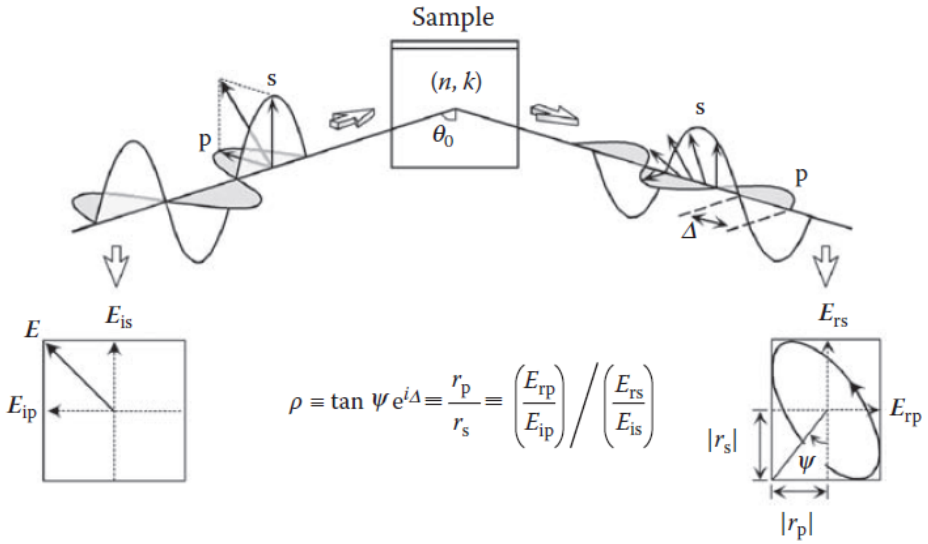

Figure (3-2) Measurement principle of ellipsometry [3].

(i) And (r) indicate to incidence and reflected light wave for the s and p polarization.

The polarizations, E_{ip} and E_{rp} oscillate within the same plane, which called the incidence plane. In ellipsometry measurement, the polarization states of incident and reflected light wave are defined by the coordinates of p and s polarization. When $= +45^{\circ}$, the incident light is the linear polarization oriented relative to the E_{ip} axis.

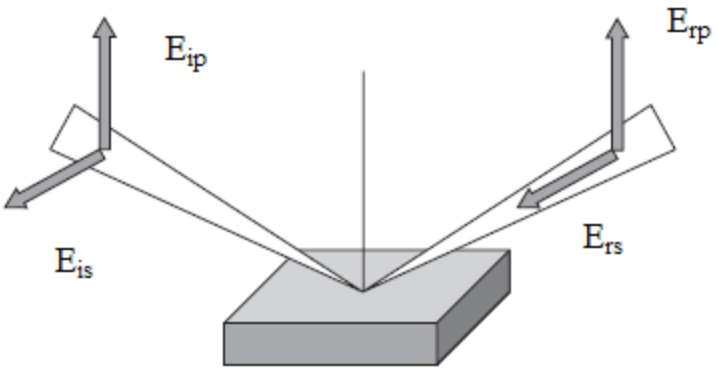

Figure (3-3) Polarization of reflected Light [3].

In general, the light is reflected from a sample p and s polarization display change in both phase and amplitude. The two values (ψ, Δ) given by different ratios between p and s polarization are the parameters measured by the ellipsometry technique. The ratio of reflected to incident light, known as the amplitude reflection coefficient r equation (3-3) and (3-4) are given by [3].

$$r_p \equiv \frac{E_{rp}}{E_{ip}} = \left|r_p\right| exp(i\delta_p) \qquad (3-3)$$

$$r_s \equiv \frac{E_{rs}}{E_{is}} = |r_s| \exp(i\delta_s) \qquad (3-4)$$

Both (ψ, Δ) are given by ratios of the amplitude reflection coefficients for p and s – polarization.

$$\rho = \frac{r_p}{r_s} = \tan\psi \, e^{i\Delta} \qquad (3-5)$$

$$\tan\psi = \frac{\left|r_p\right|}{|r_s|} \qquad (0° \leq \psi \leq 90°) \qquad (3-6)$$

$$\Delta = \delta_p - \delta_s \quad (-180° \leq \Delta \leq 180°) \qquad (3-7)$$

In this work, the phthalocyanine film samples were deposited on a silicon substrate at $2000rpm$ after cleaning the substrate surface with acetone or chloroform then subsequently rinsed with ultra pure water to ensure that it is free of dust or any contamination. The Thicknesses were obtained in accordance with ellipsometry fitting procedures, measurement result are included in chapter six.

3.2 Atomic Force Microscope:

The Atomic Force Microscope (AFM) was invented in 1986 by Binnig, Quate and Gerber. [7,8, 9] It was a major event for nanotechnology and considered as an ancestor of all scanning probe. [7, 10, 11]

However, the Scanning Tunnelling Microscope (STM) had been presented a few years earlier and achieved atomic resolution but only for conductive surfaces. The principle of (STM) operation is based on detection of the force acting between tip and sample.

The (AFM) technique is also based on this principle of operation however it does not have this restriction (conductive surfaces only). Therefore, for all surface types in all environments (AFM) has rapidly become a standard tool for nanometre scale imaging. (AFM) is used to measure surface morphology and properties through an interaction between the tip and surface. The tip is attached to the free end of a cantilever and is brought very close to a surface. The repulsion or attraction force resulting from interaction between the tip and the surface will cause a positive or negative bending of the cantilever.

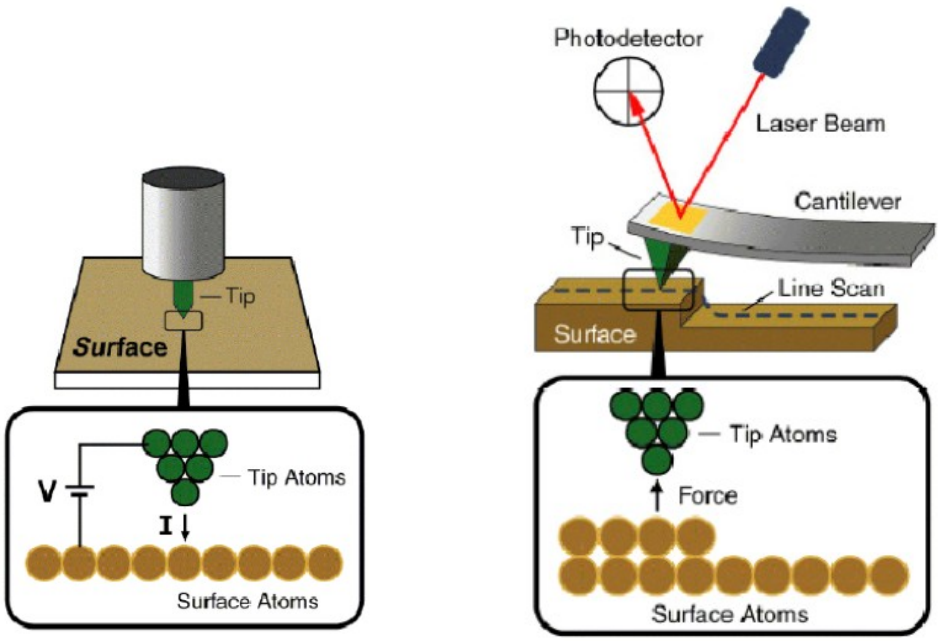

Figure (3-4) Principle of STM (left) and AFM (right). [10]

The bending is detected by means of a laser beam, which is reflected from the back side of the cantilever.

One can think of it as a spring and the amount of force between the probe and sample is dependent on the spring constant, which is stiffness of the cantilever and distance between the probe and the sample surface.

It can be described by Hooke's Law. [7,10, 11,12]

$$F = -kx \qquad (3-8)$$

Figure (3-6) Spring depiction of a cantilever.[10]

In order to be sensitive to small forces, the spring constant has to be selected as small as possible $(0.01 - 100\ N/m)$. On the other hand, the influence of acoustic waves and building vibrations should be minimized and the resonance frequency has to be kept high $(\approx 10 - 100\ KHz)$. [7, 10, 12]

There are modes of imaging, two force operations are prominent.

- Contact mode.
- Non-contact mode.

In the non-contact regime, the cantilever is held (10-100) angstrom from the sample surface and the force between the cantilever and the sample is attractive**.**

Force can be sensed and gives information about surface topography, distributions of charge magnetic domain wall structure or liquid film distribution.

The advantage of this mode is fast scanning and is suited to rough samples and used in friction analysis but the force could damage deform soft samples.

In the contact regime, the cantilever is held as less than a few angstroms from the sample surface and the inter atomic force between the cantilever and the sample is repulsive Ionic repulsion forces allow the surface topography to be traced with high resolution.

Under the best conditions, atomic resolution is achieved. Also frictional forces and elastic or plastic deformation can be detected under appropriate condition. The repulsive forces in the AFM tend to cause the cantilever to bend up. Repulsive force increase as the probe begins to contact the surface.

In Contact mode: The force between the tip and the sample is repulsive and the force drives the cantilever to oscillate up and down around it's resonance frequency where the frequency and amplitude of driving force are maintained constant which results in that the amplitude of cantilever oscillation kept constant. On condition when there is no interaction with the surface [11, 13].

The interaction between the surface and force on cantilever, when the tip approaching to tested sample, will lead to change in amplitude of cantilever oscillation. In most case it is decreasing when the tip becomes close to the surface where the AFM tapping image created by imaging the intermittent contacts force of the tip with the surface of sample [13].

For experimental work in this thesis, the same samples were used in Ellipsometry measurement which described in chapter six they were also used to investigate tested films morphology using AFM measurements in tapping mode.

3.3 UV- Visible absorption Spectrophotometer:

Absorption spectroscopy is widely used to get absorbance spectra of certain molecule in solutions and solids. This expression is used for different spectroscopic techniques description such as UV-visible [14, 15].

The absorption of electromagnetic spectrum has been studied in ranging from near ultraviolet to the very near infrared, between $180 - 1100\,nm$ because it gives some structural information and it is very helpful for quantative measurements and it known as UV-visible.

However, UV-visible spectrum region has been divided in to three sub-domains which are near UV $(185 - 400\,nm)$, visible $(400 - 700\,nm)$ and very near infrared $(700 - 1100\,nm)$. Figure (3-6) are explained UV- visible region in electromagnetic spectrum [6, 10, 14].

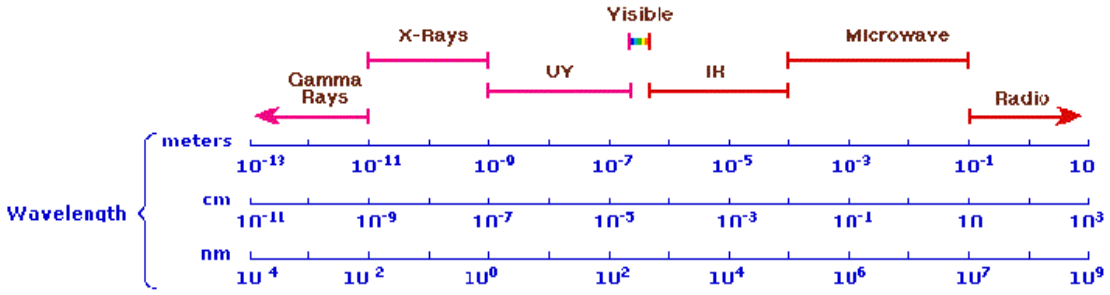

Figure(3-6) The electromagnetic spectrum. [8]

The interaction between photon from source and sample molecules or ions is the essence of absorption. When a molecule absorbs UV-visible photon by one or more of its farther electron it will capture the corresponding energy. Therefore, a modification occurs on their electronic energy E_{ele} , vibration energy E_{vib} and component of the total mechanical energy with its energy of rotation E_{rot} -equation (3 - 9).

$$\Delta E_{tot} = \Delta E_{rot} + \Delta E_{vib} + \Delta E_{ele} \qquad (3-9)$$

The majority of the studies in the UV-visible are represented by electronic transition of organic compounds. The observed transitions involve electrons participate in σ or π or non-bounding n electron orbital's of light atom as illustrated in figure (3-7).

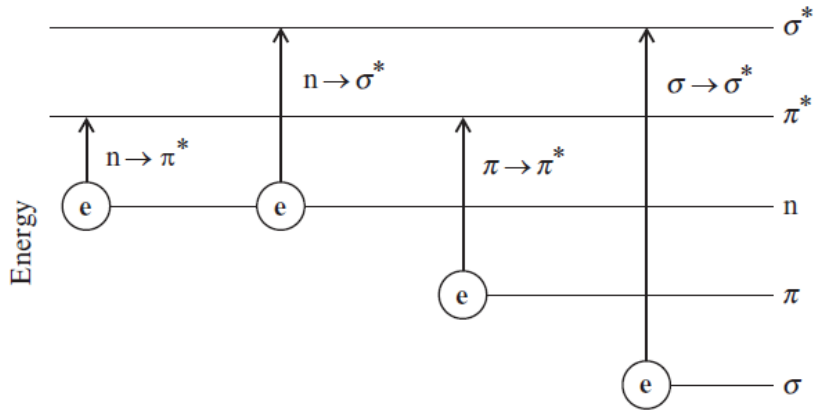

Figure (3-7) Electronic transition of σ, π, and n electrons.

The UV-visible spectrometer represents the transmittance as a function of wavelength along x-axis given in nanometres. It collects the data over the specific range and generates the spectrum of the compound under analysis as a graph. However, UV–visible spectrophotometers illustrated in figure (3-8) have five main components: Source of light, monochromator, sample holder, detector, and interpreter [3, 16].

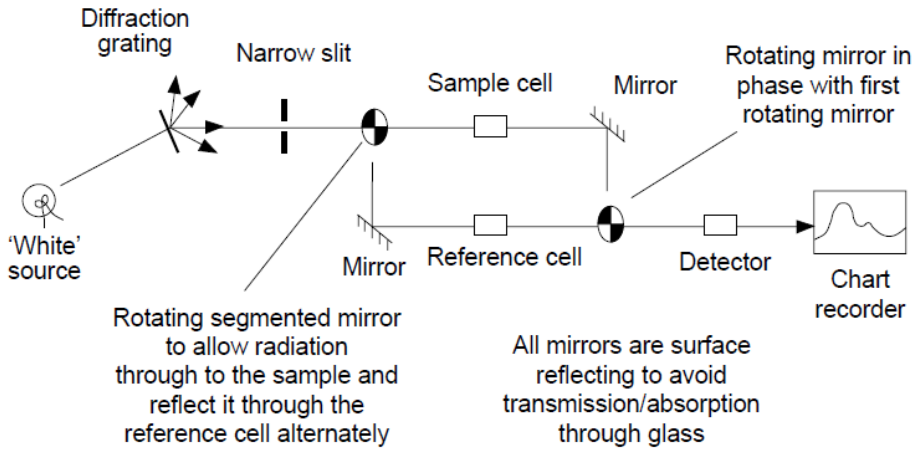

Figure (3-8) Diagram showing how the ultraviolet/visible spectrometer works [16].

The Transmittance (T) is expressed as percentage of the intensities of the beam before passing the sample or solution (I_0) and intensities of transmitted beam (I).

$$T = \frac{I}{I_0} \qquad (3-10)$$

The Beer-Lambert law defined as :

$$\log \frac{I_0}{I} = \varepsilon l c \qquad (3-11)$$

Where ε is a molar absorption coefficient (it is constant for each absorbing material), l is sample thickness or path of solution, and c is the concentration of the absorbing species in mol dm^{-3}.

In the following chapter, these techniques have been used to identify the fundamental properties of absorbed film. Spectroscopic ellipsometry will be used to determine film thickness and identify any change to it before and after exposed to gas.

The atomic force microscopic (AFM) will be used to give the information about film morphology before and after gas exposing, to future indicate if the gas has an effect on it or not.

Also UV-visible absorption spectrophotometer will be used to get absorbance spectra for films used in this research .

References:

1- Azzam, R. M., & Bashara, N. M. (1987). *Ellipsometry and polarized light* North-Holland. sole distributors for the USA and Canada, Elsevier Science Publishing Co., Inc.

2- UT, Full Automatic Spectroscopic Ellipsometer.Part 2: Basic principles of spctroscopic ellipsometry and photo-elastic modulator.

3- Yoshizawa, T. (2009). *Handbook of optical metrology: Principles and applications* CRC Press.

4- *Ellipsometry*. [online]. Last accessed 11/10 2013 at: http://www.tf.uni-kiel.de/servicezentrum/neutral/praktika/anleitungen/copy_of_b508.pdf.

5- Goldstein, D. (2003). Polarized light, revised and expanded (optical science and engineering). *Crc, 10*, 9780203911587.

6- Jellison Jr, G. (1993). Data analysis for spectroscopic ellipsometry. *Thin Solid Films, 234*(1-2), 416-422.

7- Binnig, G., Quate, C. F., & Gerber, C. (1986). Atomic force microscope. *Physical Review Letters, 56*(9), 930.

8- Meyer, E. (1992). Atomic force microscopy. *Progress in Surface Science, 41*(1), 3-49.

9- Heinzelmann, H., Meyer, E., Brodbeck, D., Overney, G., & Güntherodt, H. (1992). Atomic-scale contrast mechanism in atomic force microscopy. *Zeitschrift Für Physik B Condensed Matter, 88*(3), 321-326.

10- Wilson, R. A., & Bullen, H. A. (2006). Introduction to scanning probe microscopy (SPM): Basic theory atomic force microscopy (AFM). *Creative Commons Attribution-Noncommercial-Share Alike, 2*

11- Glatzel, T., Holscher, H., Schimmel, T., Baykara, M. Z., Schwarz, U. D., & Garcia, R. (2012). Advanced atomic force microscopy techniques. *Beilstein Journal of Nanotechnology, 3*, 893-894. 10.3762/bjnano.3.99 [doi]

12- Phillips, R. W. (1994). Atomic force microscopy for thin film analysis. *Surface and Coatings Technology, 68*, 770-775.

13- Nabok, A. (2005). *Organic and inorganic nanostructures (artech house mems and sensors library)* Artech House Publishers, Boston, MA, USA.

14- Everett, D. R. (1998). Modern chemical techniques (royal society of chemistry). *The Chemical Educator, 3*(1), 1-2.

15- Owen, A. (1996). Fundamentals of UV-visible spectroscopy.

16- Rouessac, F., & Rouessac, A. (2013). *Chemical analysis: Modern instrumentation methods and techniques* John Wiley & Sons.

CHAPTER FOUR

THE THEORETICAL BACKGROUND OF QCR MODELLING

- This chapter focuses towards studying the theoretical background of QCR modelling

4.0 Introduction:

This chapter provides an overview of techniques used for modelling the behaviour QCR and contacting media. Firstly, an overview of the QCR transformation between mechanical and electrical domains is given defined as the Transmission Line Model (TLM). The Acoustic Load Concept (ALC) for modelling the acoustic sensor response is also discussed. Furthermore, the effects of different loads (rigid, vicoelastic and liquid) on QCR parameters are introduced in the section Characterization of Viscoelastic film using Thickness Shear mode (TSM) resonator. Finally, the piezoelectric quartz crystal microbalance and Thickness monitors using Z-match technique are addressed.

4.1 The Transmission Line Model (TLM):

The Transmission Line Model (TLM) illustrates the piezoelectric transformation between mechanical and electrical vibration and the propagation of acoustic wave in system [1, 2, 3, 4, 5].

The basic of principle of the TLM is to model a QCR with consideration of how the acoustic wave propagates into a composite sensor that consists of one piezoelectric resonator layer with several non-piezoelectric layers (sensor membrane). The piezoelectric substrate is used to generate and detect the acoustic wave. The geometric and varied material parameters of all layers make changes to the wave propagation characteristics through the multilayer configuration. Differences in physical properties occurring at the nonpiezoelectric layers surface including changes in film modulus; refer to changes in wave properties (velocity, amplitude, phase and frequency). Hence, different values of shear parameter may be obtained for every small change in coating thickness in particular if film resonance is observed. This increases the ambiguity of several solutions from impedance analysis performed that are made using some approximations to extract value of shear parameters are inevitable.

Therefore, the one dimensional wave equation model was widely used to derive quartz resonator behaviour [5, 6, 7, 8].

Assume two acoustic waves (A,B) are travelling into a composite sensor in opposite directions. From the superposition principle and boundary condition on wave function at quartz face and all external interface. Also similarity and consistency field.

Mechanical tension	T	electrical voltage	u
Particle velocity	ϑ	electrical current	I
Acoustic impedance	$Z^a = \frac{T}{\vartheta}$	electrical impedance	$Z^e = \frac{u}{I}$

The acoustic voltage $u(z)$ and current $i(z)$ can be defined as following equation.

$$u_i(z) = (A_i\, e^{-\gamma Z} + B_i\, e^{\gamma Z})\, e^{i\omega t} \qquad (4-1)$$

$$i_i(z) = \frac{1}{Z_i}\,(A_i\, e^{-\gamma Z} - B_i\, e^{\gamma Z})\, e^{i\omega t} \qquad (4-2)$$

Where Z is the acoustic impedance $Z = (\rho G)^{\frac{1}{2}}$, G is the complex shear modulus.

$$\gamma = jk = j\frac{\omega}{(G/\rho)^{\frac{1}{2}}} \qquad (4-3)$$

And ω angular frequency, γ complex wave propagation and ρ layer density.

A chain matrix technique is used for impedance concept in propagation problem where transfer matrix $\boldsymbol{T}$ and propagation matrix $\boldsymbol{P}$ for each layer (q) of thickness (h_q) are.

$$\boldsymbol{T} = \begin{bmatrix} \frac{1}{Z_q} & 1 \\ \frac{1}{Z_q} & -1 \end{bmatrix} \qquad (5-4a) \quad , \quad \boldsymbol{P} = \begin{bmatrix} e^{-\gamma h_q} & 0 \\ 0 & e^{\gamma h_q} \end{bmatrix} \qquad (4-4b)$$

The transformation matrix $\boldsymbol{M_q}$ is:

$$\boldsymbol{M_q} = \begin{bmatrix} \cosh(\gamma h) & Z\sinh(\gamma h) \\ \frac{1}{Z}\sinh(\gamma h) & \cosh(\gamma h) \end{bmatrix} \qquad (4-5)$$

A chain matrix technique of (TSM) was used to characteristic of system from electric port to acoustic port. In QCM case, the equivalent circuit is consists of three port as figure (5-1) shows [5, 6, 9, 10, 11, 12, 13, 14, 15, 16, 17].

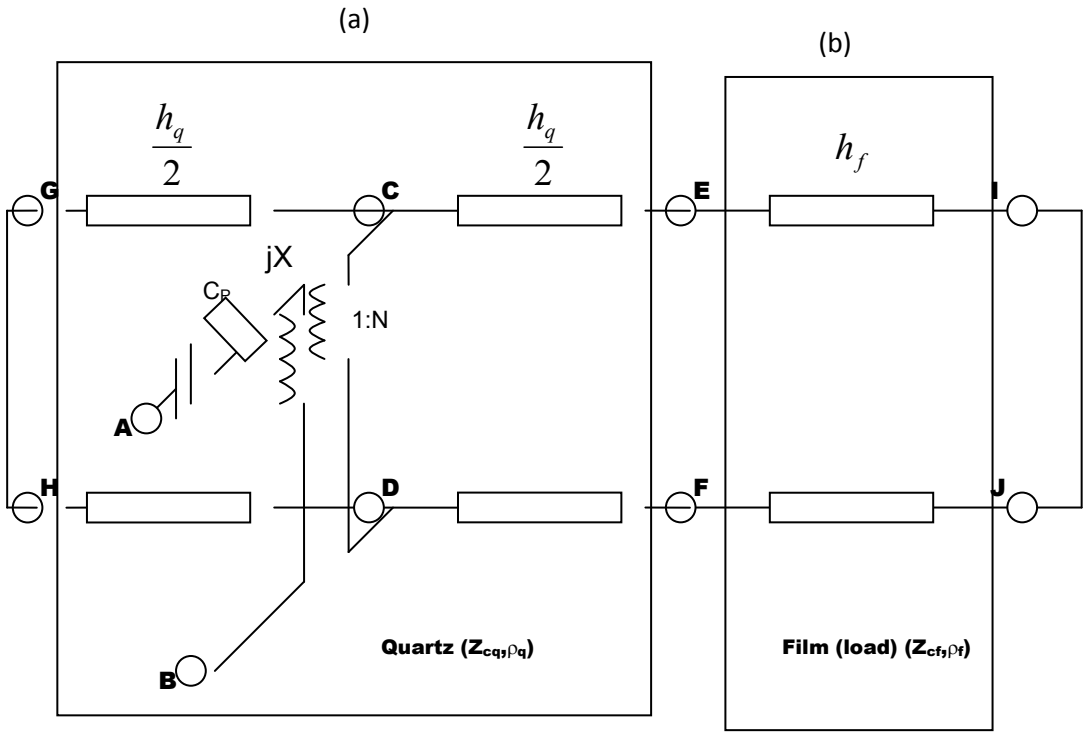

Figure (4-1) the transmission line Model (TLM). Section (a) identifies the uncoated quartz crystal with two acoustic ports and one electrical port representing the piezoelectric properties of the quartz. Section (b) identifies the additional non piezoelectric layer.

From piezoelectric transformer element jX with turn's ratio $1:\mathrm{N}$ composite electrical impedance can be deduced.

$$Z = Z_{AB} = \frac{1}{j\omega C_0} + jX + \frac{1}{N^2} Z_{cp} \qquad (4-6)$$

$$Z = \frac{1}{j\omega C_0}\left(1 - \frac{k^2}{\alpha}\frac{2\tan\frac{\alpha}{2} - j\frac{Z_L}{Z_q}}{1 - j\frac{Z_L}{Z_q}\cot\alpha}\right) \qquad (4-7)$$

Where

$$\frac{1}{N^2} = \frac{1}{A}\left(\frac{2e_q}{\varepsilon_q \omega Z_{cq}} sin\left(k_q \frac{h_q}{2}\right)\right) \qquad (4-8a)$$

$$X = \frac{e_q^2}{A\varepsilon_q^2\,\omega^2 Z_{cq}} \sin(\,k_q h_q\,) \qquad (4-8b)$$

e_q Piezoelectric constant

ε_q Permittivity

$C_0 = \varepsilon_q \frac{A}{h_q}$ Static capacitance of quartz crystal

$\alpha = \frac{\omega h_q}{\vartheta_q}$ Wave phase shift in quartz

k_0^2 $\frac{e_q^2}{\varepsilon_q C_q}$Electromechanical coupling

$Z_{cq} = \sqrt{\rho_q C_q}$ Specific quartz impedance

It is more useful to convert the electrical impedance into tow part (motional Z_m and parallel circuit) where parallel is a static capacitanceC_0.

Moreover, motional impedance often split to represent two parts, unload quartz Z_{mq} and the other part is the acoustic load Z_{mL} [5, 9, 18, 20, 21, 22].

$$Z_m = Z_{mq} + Z_{mL} \qquad (4-9)$$

$$Z_{mq} = \frac{1}{j\omega C_0}\left(\frac{{}^{\alpha}/_{k^2}}{2\tan({}^{\alpha}/_{2})} - 1\right) \qquad (4-10)$$

$$Z_{mL} = \frac{1}{\omega C_0}\frac{\alpha}{4k^2}\frac{Z_L}{Z_q}\frac{1}{1-\left[{}^{j\left(\frac{Z_L}{Z_q}\right)}/_{2\tan({}^{\alpha}/_{2})}\right]} \qquad (4-11)$$

To simplify this expression a few approximation can be made.

Around resonance of unloaded quartz.

$$\tan\frac{\alpha}{2} = \frac{4\alpha}{(N\pi)^2 - \alpha^2} \qquad (4-12)$$

$$Z_{mq} = \frac{1}{j\omega C_0}\left(\frac{(N\pi)^2 - \alpha^2}{8k^2} - 1\right) \qquad (4-13)$$

Where

$$\alpha = \omega h_q \left({}^{\rho_q}/_{\mu_q} \right)^{1/2} \qquad (4-14)$$

$$\mu_q = \mu_{q_0} + j\omega\eta_q\mu_{q_0} \qquad (4-15)$$

$$Z_{mq} = \left(\frac{\omega^2 h_q^2 \rho_q \eta_q}{8k^2 C_0 \left|\mu_q\right|^2} \right) + j\omega \left(\frac{h_q^2 \rho_q \mu_{q_0}}{8k^2 C_0 \left|\mu_q\right|^2} \right) + \frac{1}{j\omega} \left(\frac{(N\pi)^2 - 8k^2}{8k^2 C_0} \right) \qquad (4-16)$$

$$Z_{mq} = R_q + j\omega L_q + \frac{1}{j\omega C_0} \qquad (4-17)$$

By assuming a quartz loss is a small $\omega = \omega_s = 2\mu f_s$, the equation (4-17) can be formulated into motional arm of BVD circuit and the definition of each elements are.

$$R = \left(\frac{\omega^2 h_q^2 \rho_q \eta_q}{8k^2 C_0 \left|\mu_q\right|^2} \right) \qquad (4-18)$$

$$L = \left(\frac{h_q^2 \rho_q \mu_{q_0}}{8k^2 C_0 \left|\mu_q\right|^2} \right) \qquad (4-19)$$

$$C = \left(\frac{8k^2 C_0}{(N\pi)^2 - 8k^2 C_0} \right) \qquad (4-20)$$

Where $\omega\eta_q \ll \mu_{q_0}$ so $\left|\mu_q\right| \cong \mu_{q_0}$.

The basic of all acoustic sensors is the dependence on acoustic wave propagation in the multilayer structure where the change in acoustic properties at interface of resonator appear as result of change in material properties such as mass and thickness [5, 23, 24, 25].

In the case of a coated QCM, the acoustic wave travels into the platform (substrate) and film and consequently deform it, as result of that it is possible to investigate it is mechanical and acoustic properties. Therefore, the surface acoustic load is a dominant function in the acoustic analysis of the coating.

The acoustic load impedance of viscoelastic can be found only by film density, shear modulus and film thickness, where it is the total acoustic load at the interface between platform and film. This holds all information related to any change in the sensitive coating (film); whether mass accumulation or material properties change (including softening) by chemical or physical effect [4, 5, 23, 24, 25, 26, 27, 28, 29, 30].

By applying a simple approximation, the frequency shift of the in-phase admittance magnitude $\Delta f(r)$ is corresponds to imaginary part of Z_L [31].

While the dissipation of acoustic energy represented by change of motional BVD circuit resistance is related to real part as equation (4-21) and (4-22) shows respectively.

$$\frac{\Delta f}{f_0} = \frac{\mathrm{Im}\,(Z_L)}{\pi Z_{cq}} \qquad (4-21)$$

$$\frac{\Delta R}{2\omega_0 L_q} = \frac{Re\,(Z_L)}{\pi Z_q} \qquad (4-22)$$

Where Z_L is the acoustic load.

4.2 Characterization of Viscoelastic film using Thickness Shear mode (TSM) resonator:

Numerous film coatings exhibit viscoelastic properties which lead to substantial differences in sensor responses in comparison to that of a rigid mass layer.

When applying shear stress on viscoelastic material part of the energy is stored and other part dissipated. These two quantities determine as real and imaginary components of complex shear modulus.

$$G = G' + jG'' \qquad (4-23)$$

Where G is defined as the ratio between shear stress and shear strain. The stress in phase with strain (energy storage) represented by real part of shear modulus while the imaginary part act for stress 90° out of phase with the strain (energy dissipation). Accordingly G', G'' are indicated to storage and loss shear modulus respectively. If the film behaves as a rigid layer when excited by a probing acoustic wave it is often referred to as a glassy state. Conversely it is referred to as a rubbery regime when the film or coatings act as viscolelastic layer even at the high probing frequency.[5, 32, 33, 34, 35, 36, 37].

In the rubbery state the material takes more time for deformation than relaxation where the inter chain motion accommodate the strain. It is described by G' around $10^6\ Pa$ and $G'' < G'$. While in the glassy regime G' is typically around $10^9\ Pa$ and the relaxation time τ is much longer than the period of the oscillation [6, 11, 35, 37].

As previously mentioned the modified BVD model can be used to characterize the surface loaded TSM resonator.

From equation (4-24) the complex impedance is:

$$Z_m = R + j\omega L + \frac{1}{j\omega c} + Z_m^L \qquad (4-24)$$

Where the electrical impedance is:

$$Z_m^L = R + j\omega L_2 = \frac{N\pi}{4k\omega c}\left(\frac{Z_L}{Z_q}\right) \qquad (4-25)$$

For viscoelastic film the shear mechanical impedance Z_L is derived from (TLM) are given by equation (4-26)

$$Z_L = j\sqrt{\rho_f G}\ \tan\left(\omega\sqrt{\frac{\rho_f}{G}}\ h\right) \qquad (4-26)$$

G' , G'' Shear modulus can be obtained in terms of film properties (thickness, density) and frequency shift from impedance / admittance analysis of BVD circuit by expanded tangent function in Taylor series around zero.

Than the electric impedance Z_{mL} become:

$$Z_{mL} = R_2 + j\omega L_2$$

$$= \frac{N\pi}{4k_2^2\omega c}\frac{1}{\sqrt{\mu_q\rho_q}}\left[\left(\frac{\omega^3 h^3 \rho_f^2 G''}{3|G|^2}\right)\right.$$

$$\left. + j\omega\left(\frac{\rho_f h + \omega^3 h^3 \rho_f^2 G'}{3|G|^2}\right)\right] \qquad (4-27)$$

By setting :

$$A = \frac{G''}{|G|^2} \qquad (4-28a) \qquad , \qquad B = \frac{G'}{|G|^2} \qquad (4-28b)$$

The storage and loss shear modulus respectively are:

$$G' = \frac{B}{A^2 + B^2} \qquad (4-29a) \qquad , \qquad G'' = \frac{A}{A^2 + B^2} \qquad (4-29b)$$

Where

$$A = \left(\frac{\left(\frac{19\rho_f h}{24} - \frac{L_2}{A_0}\right) + \left[\left(\frac{L_2}{A_0} - \frac{19\rho_f h}{24}\right)^2 + \frac{R_2^2}{\omega^2 A_0^2}\right]^{\frac{1}{2}}}{\frac{4\omega^4 \rho_f^3 h^5}{15}} \right)^{1/2} \qquad (4-30)$$

$$B = \frac{15R_2}{4\,\omega^5 \rho_f^3 h^5 A_0} \frac{1}{A} - \frac{5}{4\omega^2 h^2 \rho_f} \qquad (4-31)$$

With

$$A_0 = \frac{N\pi}{4k^2 \omega\, C_0} \frac{1}{\sqrt{\mu_q \rho_q}} \qquad (4-32)$$

4.3 The piezoelectric quartz crystal microbalance:

For the ideal physics model in the figure (2-4) the basis of QCM as Sauerbrey assume can be described as following equations [4, 5, 8, 39, 40, 41, 42].

$$h_q = \frac{\lambda_q}{2} \qquad (4-33a)$$

Where $\lambda_q f_q = \vartheta_q \qquad (-33b)$, $f_q h_q = \frac{\vartheta_q}{2} \qquad (4-33c)$

h_q quartz plate thickness, λ_q wavelength of shear mode resonant frequency.

The change in resonant frequency caused by thickness change is:

$$\frac{\Delta f_q}{f_q} = \frac{-\Delta h_q}{h_q} = \frac{-\Delta M_q}{M_q} \qquad (4-34)$$

Where the negative indicate to, reverse relation between resonance frequency and the added mass.

The change in mass can be equivalent mass change such as the mass of thin film M_f than equation (4-34) can be written in approximation form of

$$\frac{(f_c - f_q)}{f_q} = \frac{-M_f}{M_q} \qquad (4-35)$$

Where f_c is resonant frequency of quartz crystal with dissipation film from definition of areal density $M_f = h_f \rho_f$, $M_q = h_q \rho_q$ where ρ_f , ρ_q is the density of film and quartz and h_f , h_q the thickness of film and quartz.

$$\rho_f h_f = \frac{-(f_c - f_q)\,\rho_q \vartheta_q}{2 f_q^2} \qquad (4-36)$$

This can be written as

$$\Delta f = -C_f M_f \qquad (4-37)$$

This equation can only be used for a small mass load where$M_f \ll M_q$. The accuracy is around 2% [5]. The use of the QCM as a film thickness monitor for vacuum deposition processes has been popular and employed in a wide range of deposition applications [4]. However, increases in deposited mass onto crystal lead to expect significant errors in density determination, because of that Behrndt and Love suggest using equation (4-38) instead of equation (4-37)

$$\Delta f_c = -C_f' M_f \qquad (4-38)$$

Where Δf_c is the frequency shift caused by added material and $C_f' = \frac{2f_c^2}{\rho_q \vartheta_q}$.

Taking integration of equation (4-38) following equation is obtained:

$$M_f = \frac{\rho_q \vartheta_q}{2}\left[\frac{1}{f_c} - \frac{1}{f_q}\right] \qquad (4-39)$$

Which that the period τ of oscillator crystal crystal is proportional to mass loading as equation (4-40) illustrate

$$\frac{M_f}{m_q} = \frac{\tau_c - \tau_q}{\tau_q} \qquad (4-40)$$

The equation (4-40) could give more accuracy than 10% in frequency shift of compered to that given by equation (4-37).

In addition more attention paid to crystal design (edge mounting, crystal contour, electrodes) increase mass loading capability to over 15% [5].

A different approach were used by Miller and Bolef to treated a combination of quartz film as composite acoustic resonator in a small loss acoustic system as equation (4-41)

$$2\,r\left[\cos\left(2\pi f_c/f_f\right)-\cos\left(2\pi f_c/f_q\right)\right]+\ (1+r^2)\left[1-\cos\left(2\pi f_c/f_q\right)\cos\left(2\pi f_c/f_f\right)\right]$$
$$+\ (1-r^2)\sin\left(2\pi f_c/f_q\right)\sin\left(2\pi f_c/f_f\right)\ =0 \qquad (4-41)$$

Where r is the acoustic wave reflection coefficient at film interface,

And

$$f_f=\frac{\vartheta_f}{2h_f} \qquad (5-42)$$

Subsequently, simplification of complicated equation were showed by Lu and Lewis

$$\tan\left(\pi f_c/f_q\right)=-\left(\rho_f\vartheta_f/\rho_q\vartheta_q\right)\ \tan\left(\pi f_c/f_f\right) \qquad (4-43)$$

4.4 Thickness monitors using Z-match technique:

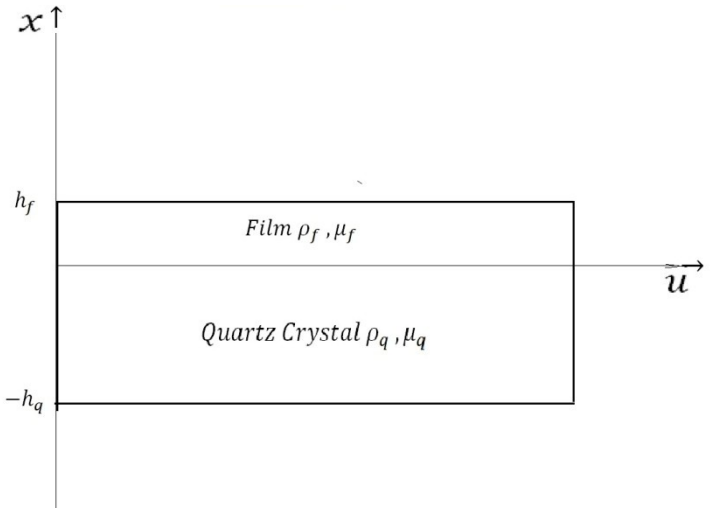

Figure (4-2) The one-dimensional composite resonator model.

If a shear wave $u_q(x,h)$ is generated along thickness direction and assuming no losses in both media [5, 30, 39, 40, 43, 44].

The wave travelling in both quartz and film can be described by the general wave equation.

$$\psi_q(x,h) = A\ exp\left[i\omega\left(\frac{\rho_q}{G_q}\right)^{1/2} x\right] + B\ exp\left[-i\omega\left(\frac{\rho_q}{G_q}\right)^{1/2} x\right] \qquad (4-44)$$

And

$$\psi_f(x,h) = C\ exp\left[i\omega\left(\frac{\rho_f}{G_f}\right)^{1/2} x\right] + D\ exp\left[-i\omega\left(\frac{\rho_f}{G_f}\right)^{1/2} x\right] \qquad (4-45)$$

From continuity condition at film/quartz interface

$\psi_q = \psi_f$ At $x = 0$ $(4-46a)$

And

$G_q\left(\frac{d\psi_q}{dx}\right) = G_f\left(\frac{d\psi_f}{dx}\right)$ At $x = 0$ $(4-46b)$

From standing wave system the two free surface antinodes

$\frac{d\psi_q}{dx} = 0$ At $x = -h_a$ $(4-47a)$

$$\frac{d\psi_f}{dx} = 0 \qquad \text{At} \qquad x = h_f \qquad (4-47b)$$

From boundary conditions

$$A - B - \left(\frac{G_f\rho_f}{G_q\rho_q}\right)^{1/2} C + \left(\frac{G_f\rho_f}{G_q\rho_q}\right)^{1/2} D = 0 \qquad (4-48)$$

$$A - B - C - D = 0 \qquad (4-49)$$

$$A - B\exp\left[2i\omega\left(\frac{\rho_q}{G_q}\right)^{1/2} h_q\right] = 0 \qquad (4-50)$$

$$C - D\exp\left[-2i\omega\left(\frac{\rho_f}{G_f}\right)^{1/2} h_f\right] = 0 \qquad (4-51)$$

These equations have non zero solution only if:

$$\begin{vmatrix} 1 & -\left(\frac{G_f\rho_f}{G_q\rho_q}\right)^{1/2} & \left(\frac{G_f\rho_f}{G_q\rho_q}\right)^{1/2} \\ 1 & -1 & 1 \\ 1 & -exp\left(2i\omega\left(\frac{\rho_f}{G_f}\right)^{1/2} h_q\right) & 0 \\ 0 & 1 & -exp\left(-2i\omega\left(\frac{\rho_f}{G_f}\right)^{1/2} h_f\right) \end{vmatrix} = 0 \qquad (4-52)$$

$$\frac{exp\left(\ 2i\omega\ \left(\frac{\rho_f}{G_f}\right)^{1/2}\ h_q\right)-1}{exp\left(\ 2i\omega\ \left(\frac{\rho_f}{G_f}\right)^{1/2}\ h_q\right)+1}$$

$$= \frac{\left(\frac{G_f\rho_f}{G_q\rho_q}\right)^{1/2}\left\{exp\left(-2i\omega\ \left(\frac{\rho_f}{G_f}\right)^{1/2}\ h_f\right)\ -1\right\}}{exp\left(-2i\omega\ \left(\frac{\rho_f}{G_f}\right)^{1/2}\ h_f\right)+1} \qquad (4-53)$$

$$\tan\left(\omega\ \left(\frac{\rho_f}{G_f}\right)^{1/2}\ h_q\right) = \left(\frac{\rho_f}{G_f}\right)^{1/2}\tan\left(\omega\ \left(\frac{\rho_f}{G_f}\right)^{1/2}\ h_f\right) \qquad (4-54)$$

Where, $\vartheta_q$velocity of shear is wave in quartz and ϑ_f velocity of shear wave in film.

As well $\omega = 2\pi f_c$

$$\tan\left[\left(\frac{\pi f_c}{f_q}\right)\left(\frac{\rho_q}{G_q}\right)^{1/2}\ \vartheta_q\right] = -\left(\frac{G_f\rho_f}{G_q\rho_q}\right)^{1/2}\ \tan\left[\left(\frac{\pi f_c}{f_f}\right)\left(\frac{\rho_f}{G_f}\right)^{1/2}\ \vartheta_f\right] \qquad (4-55)$$

By Replace

$$\vartheta_q = \left(\frac{G_q}{\rho_q}\right)^{1/2} \qquad (4-56)$$

$$Z = \sqrt{\rho G}$$

$$Z_q = \sqrt{\rho_q \, G_q} \qquad (5-57a) \quad , \qquad Z_f = \sqrt{\rho_f \, G_f} \qquad (4-57b)$$

$$\tan\left(\frac{\pi \, f_c}{f_q}\right) = \frac{-\, Z_f}{Z_q} \tan\left(\frac{\pi \, f_c}{f_f}\right) \qquad (4-58)$$

$$Z = \frac{Z_q}{Z_f} \qquad (4-59)$$

$$\tan\left(\frac{f_c}{f_q}\right)\pi = \frac{-1}{Z} \tan\left(\frac{f_c}{f_f}\right)\pi \qquad (4-60)$$

Where:

Z_q Is acoustic impedance of quartz, Z_f acoustic impedance of film, f_c composite resonance frequency, f_q , f_f mechanical resonant frequency for quartz and film [5, 30, 39, 40, 43, 44].

To define deposited film density the last equation can be written as follows:

$$\rho_f t_f = \left(\frac{\rho_q \vartheta_q}{2\pi Z f_c}\right) tan^{-1}\left[Z \tan\left(\frac{f_q - \, f_c}{f_q}\right)\right] \qquad (4-61)$$

Where, it shows that the elastic properties and acoustic impedance of film lead to different mass frequency relation.

This equation is only valid for very small mass load where $\frac{\Delta f}{f_q} \ll 1$

Experimentally it is substantiated up to 70 % of mass loading [5, 30].

4.5 Summary:

This chapter has summarized several techniques which are used for modelling the QCR behaviour and contacting media which will be used in the coming result chapters. These techniques included the Transmission Line Model (TLM), the Acoustic Load Concept (ALC), the piezoelectric quartz crystal microbalance and thickness monitors using Z-match technique. The QCR modelling techniques detailed in this chapter have been used and verified.

In this research, the transmission line model (TLM) were used to present unloaded crystal and the acoustic film load as described in equations (4-10) (4-11) respectively. As the Thickness Shear Mode (TSM) measurement technique has been applied to study viscoelastic properties of tested film extracting the electrical BVD parameters as described in equations (4-18) to (4-20). Moreover, in order to calculate film shear model equations (4-29a) to (4-32) have been employed by Matlab program as will describe in result chapter.

Reference:

1- Ferreira, G. N., Da-Silva, A., & Tomé, B. (2009). Acoustic wave biosensors: Physical models and biological applications of quartz crystal microbalance. *Trends in Biotechnology, 27*(12), 689-697.

2- Filiâtre, C., Bardèche, G., & Valentin, M. (1994). Transmission-line model for immersed quartz-crystal sensors. *Sensors and Actuators A: Physical, 44*(2), 137-144.

3- Granstaff, V. E., & Martin, S. J. (1994). Characterization of a thickness-shear mode quartz resonator with multiple nonpiezoelectric layers. *Journal of Applied Physics, 75*(3), 1319-1329.

4- Homola, J. (2006). *Springer series on chemical sensors and biosensors* Sl.

5- Lu, C., & Czanderna, A. W. (2012). *Applications of piezoelectric quartz crystal microbalances* Elsevier.

6- Lucklum, R., Behling, C., Cernosek, R. W., & Martin, S. J. (1997). Determination of complex shear modulus with thickness shear mode resonators. *Journal of Physics D: Applied Physics, 30*(3), 346.

7- Lucklum, R., Schranz, S., Behling, C., Eichelbaum, F., & Hauptmann, P. (1997). Analysis of compressional-wave influence on thickness-shear-mode resonators in liquids. *Sensors and Actuators A: Physical, 60*(1-3), 40-48.

8- Miller, J., & Bolef, D. (1968). Sensitivity enhancement by the use of acoustic resonators in cw ultrasonic spectroscopy. *Journal of Applied Physics, 39*(10), 4589-4593.

9- Bandey, H. L., Martin, S. J., Cernosek, R. W., & Hillman, A. R. (1999). Modeling the responses of thickness-shear mode resonators under various loading conditions. *Analytical Chemistry, 71*(11), 2205-2214.

10- Hauptmann, P., Lucklum, R., & Schröder, J. (2005). Qcr-sensors–models and applications.

11- Lucklum, R., & Hauptmann, P. (1997). Determination of polymer shear modulus with quartz crystal resonators. *Faraday Discussions, 107*, 123-140.

12- Lucklum, R., & Hauptmann, P. (2000). The Δf–ΔR QCM technique: An approach to an advanced sensor signal interpretation. *Electrochimica Acta, 45*(22-23), 3907-3916.

13- Lucklum, R., & Hauptmann, P. (2003). Transduction mechanism of acoustic-wave based chemical and biochemical sensors. *Measurement Science and Technology, 14*(11), 1854.

14- Lucklum, R., Behling, C., Hauptmann, P., Cernosek, R., & Martin, S. (1998). Error analysis of material parameter determination with quartz-crystal resonators. *Sensors and Actuators A: Physical, 66*(1-3), 184-192.

15- Lucklum, R., Behling, C., & Hauptmann, P. (1999). Thin film shear modulus determination with quartz crystal resonators. *Sensors and Materials, 11*(2), 111-130.

16- Lucklum, R., & Hauptmann, P. (2001). Thin film shear modulus determination with quartz crystal resonators: A review. *Frequency Control Symposium and PDA Exhibition, 2001. Proceedings of the 2001 IEEE International,* 408-418.

17- Lucklum, R., & Hauptmann, P. (2002). Generalized acoustic parameters of non-homogeneous thin films. *Frequency Control Symposium and PDA Exhibition, 2002. IEEE International,* 234-241.

18- BANDEY, H. L., CERNOSEK, R. W., Hillman, A., & MARTIN, S. J. (1999). *Equivalent-Circuit Model for the TSM Resonator with a Viscoelastic Layer,*

19- Bandey, H., Martin, S., Cemosek, R., & Hillman, A. (1999). Equivalent-circuit model for the tsm resonator with a viscoelastic film near film resonance. *Chemical Sensors IV: Proceedings of the Symposium, , 4* 320.

20- Cernosek, R. W., Martin, S. J., Hillman, A. R., & Bandey, H. L. (1998). Comparison of lumped-element and transmission-line models for thickness-shear-mode quartz resonator sensors. *IEEE Transactions on Ultrasonics, Ferroelectrics, and Frequency Control, 45*(5), 1399-1407.

21- Auge, J., Hauptmann, P., Hartmann, J., Rösler, S., & Lucklum, R. (1995). New design for QCM sensors in liquids. *Sensors and Actuators B: Chemical, 24*(1-3), 43-48.

22- Martin, S. J., Bandey, H. L., Cernosek, R. W., Hillman, A. R., & Brown, M. J. (2000). Equivalent-circuit model for the thickness-shear mode resonator with a viscoelastic film near film resonance. *Analytical Chemistry, 72*(1), 141-149.

23- Behling, C., Lucklum, R., & Hauptmann, P. (1998). Response of quartz-crystal resonators to gas and liquid analyte exposure. *Sensors and Actuators A: Physical, 68*(1-3), 388-398.

24- Gallagher, P. K., Brown, M. E., & Kemp, R. (1998). *Handbook of thermal analysis and calorimetry* Elsevier.

25- Richardson, A. J. (2009). Determination of nanogram mass and measurement of polymer solution free volume using thickness-shear mode (tsm) quartz resonators.

26- Lucklum, R., Behling, C., & Hauptmann, P. (2000). Gravimetric and non-gravimetric chemical quartz crystal resonators. *Sensors and Actuators B: Chemical, 65*(1-3), 277-283.

27- Lucklum, R., Behling, C., & Hauptmann, P. (1999). Role of mass accumulation and viscoelastic film properties for the response of acoustic-wave-based chemical sensors. *Analytical Chemistry, 71*(13), 2488-2496.

28- Lucklum, R., Behling, C., & Hauptmann, P. (2000). Signal amplification with multilayer arrangements on chemical quartz-crystal-resonator sensors. *IEEE*

Transactions on Ultrasonics, Ferroelectrics, and Frequency Control, 47(5), 1246-1252.

29- Lucklum, R., & McHale, G. (2000). Treatment of slip in a generalized acoustic load concept. *Frequency Control Symposium and Exhibition, 2000. Proceedings of the 2000 IEEE/EIA International,* 40-46.

30- Steinem, C., & Janshoff, A. (2007). *Piezoelectric sensors* Springer Science & Business Media.

31- Behling, C., Lucklum, R., & Hauptmann, P. (1997). Possibilities and limitations in quantitative determination of polymer shear parameters by TSM resonators. *Sensors and Actuators A: Physical, 61*(1-3), 260-266.

32- Arnau, A., Montagut, Y., García, J. V., & Jiménez, Y. (2009). A different point of view on the sensitivity of quartz crystal microbalance sensors. *Measurement Science and Technology, 20*(12), 124004.

33- Holt, R. C., Gouws, G. J., & Zhen, J. Z. (2006). Measurement of polymer shear modulus using thickness shear acoustic waves. *Current Applied Physics, 6*(3), 334-339.

34- Hossenlopp, J., Jiang, L., Cernosek, R., & Josse, F. (2004). Characterization of epoxy resin (SU-8) film using thickness-shear mode (TSM) resonator under various conditions. *Journal of Polymer Science Part B: Polymer Physics, 42*(12), 2373-2384.

35- Jiang, L., Hossenlopp, J., Cernosek, R., & Josse, F. (2003). Characterization of epoxy resin su-8 film using thickness-shear mode (tsm) resonator. *Frequency Control Symposium and PDA Exhibition Jointly with the 17th European Frequency and Time Forum, 2003. Proceedings of the 2003 IEEE International,* 986-992.

36- Martin, S. J. (1997). Closing remarks. *Faraday Discussions, 107*, 463-476.

37- Morray, B., Li, S., Hossenlopp, J., Cernosek, R., & Josse, F. (2002). PMMA polymer film characterization using thickness-shear mode (TSM) quartz resonator. *Frequency Control Symposium and PDA Exhibition, 2002. IEEE International,* 294-300.

38- Lucklum, R., & Hauptmann, P. (2000). The quartz crystal microbalance: Mass sensitivity, viscoelasticity and acoustic amplification. *Sensors and Actuators B: Chemical, 70*(1-3), 30-36.

39- Benes, E. (1984). Improved quartz crystal microbalance technique. *Journal of Applied Physics, 56*(3), 608-626.

40- Benes, E., Schmid, M., & Thorn, G. (1989). Progress in monitoring thin film thickness by use of quartz crystals. *Thin Solid Films, 174*, 307-314.

41- Benes, E., Groschl, M., Burger, W., & Schmid, M. (1995). Sensors based on piezoelectric resonators. *Sensors and Actuators-A-Physical Sensors, 48*(1), 1-22.

42- Lu, C., & Lewis, O. (1972). Investigation of film-thickness determination by oscillating quartz resonators with large mass load. *Journal of Applied Physics, 43*(11), 4385-4390.

43- Wajid, A. (1991). Improving the accuracy of a quartz crystal microbalance with automatic determination of acoustic impedance ratio. *Review of Scientific Instruments, 62*(8), 2026-2033.

44- Wajid, A. (1997). On the accuracy of the quartz-crystal microbalance (QCM) in thin-film depositions. *Sensors and Actuators a: Physical, 63*(1), 41-46.

CHAPTER FIVE

DEPOSITION AND MEASUREMENT TECHNIQUES OF EXPERIMENTAL PROCEDURE

This chapter describes how the sensing members are deposited onto QCR and also gives a brief discussion on the measurement techniques used.

5.0 Introduction:

An organic thin film can be deposited on a substrate by different techniques such as thermal evaporation, sputtering, electro deposition, molecular beam epitaxy, adsorption from solution, spin coating, Langmuir-Blodgett (LB) technique, self-assembly, etc.

To produce high quality films there are two main factors. The coating solution and substrate surface cleanliness. Therefore, the standard procedure before coating is to ensure a contaminant free surface by thorough cleaning using acetone to rinse the crystal and minimizing any contact through the careful use of gloves and tweezers during the work.

5.1 Spin Coating:

The method of spin coating materials was the adopted approach for the deposition of high quality thin films. Spin coating allows easy and rapid deposition of thin coatings onto relatively flat substrates.

To illustrate the process simply, the substrate is held in place on a rotating fixture where a vacuum is usually used to securely hold the fixture, the resulting centrifugal force used to distribute the coating solution onto the surface.

As a result of spinning, the solution will spread out and leave behind a very uniform coating of the chosen material on the surface of the substrate [1, 2]. The rapid drying of solution caused by the rotating substrate is the fundamental principle of this method.

In this project, we used QCR as the substrate (secured on a glass slide fixture), held firmly in position by a vacuum to clamp the sample and accelerated to a speed of $2000rpm$.

A micropipette was then used to drop calculated amount of solution onto the rotating substrate surface. Note that, micro pipette should be very close to the substrate surface.

When the solution drops and makes contact with the substrate and spreads out across the substrate under the influence of centrifugal force. The solvent subsequently evaporates leaving the desired film. The advantages of this technique are: fast, low cost, and relatively simple.

5.2 Resonant Frequency Measurements:

The resonant oscillator circuit is the simplest measurement technique for QCR, where the crystal is the component used to determine the frequency in an electronic oscillator circuit. The high stability of frequency and low thermal drift is the important properties of the quartz crystal. There are various oscillator circuit configurations used for different loading applications (gas/liquid phase); these been developed to provide suitable drive characteristics for the particular application with different phase measurements [3, 4, 5]. For the specified application a bespoke QCR sensor has been developed at SHU. The system is able to simultaneously measure the resonant frequency three QCM sensors with a resolution and sample rate of 1 Hz. The unit consists of two stackable circuit boards. The top board containing three independent oscillator driver circuits; these are interfaced to the lower board which houses the data question and processing components. A Programmable Logic Device (PLD) is utilized to provide accurate and real time (1Hz) frequency measurements. The PLD subsequently outputs the obtained frequencies via serial protocol to a microcontroller mounted on the same circuit board for further processing to enable communication and data logging with a standard PC via RS232. The complete unit measures 124mm × 77mm and is powered from a 5V supply.

Figure (5-1) shows functional block diagram of SN74LVC1GX04 Crystal Oscillator Driver has been used in this study, more information about features, description and application can be found in Texas instruments company website [6].

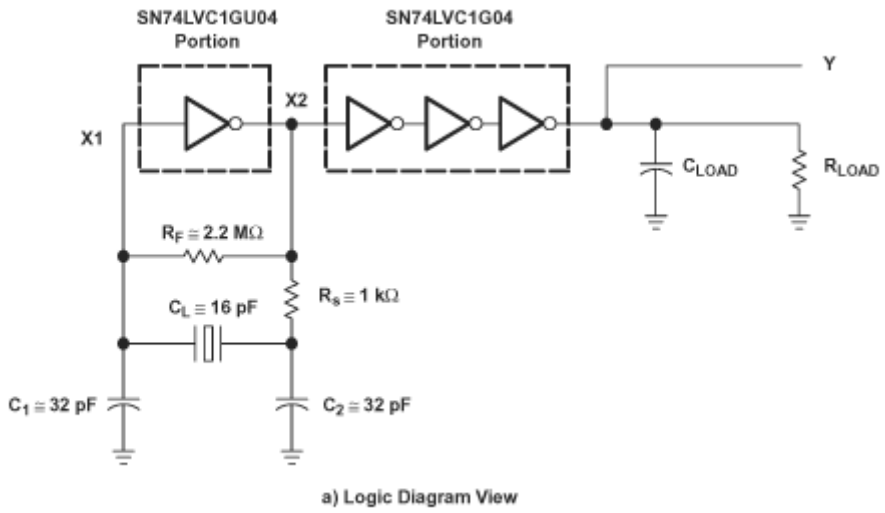

Figure (5-1) Crystal Oscillator Driver [6].

5.3 Impendence Measurements:

The measurement of impendence/admittance at a range of frequencies around crystal resonance is the technique predominantly used technique for complete analysis of crystal and contacting media. All crystal resonances can be observed by this method. [3, 5]

As described in the previous chapter, the mechanical properties of quartz crystal resonator can be described by equivalent circuit (BVD). Accordingly, the sensor impedance is a complex $Z = R + iX$ quantity and dependant on the frequency of the applied signal. Where imaginary part (X) represent energy storage, while R is the resistance which represent energy dissipation. [4,7, 8, 9]

Physically, the impedance is defined as the ratio of applied voltage a cross the crystal and the current flowing through it.

The impedance analysis of QCR is performed by measuring the incident voltage versus the reflected sinusoidal voltage from quartz crystal around the resonant frequencies, also impedance magnitude and phase angel are calculated.

The signal attenuation measured gives the impedance magnitude$|Z|$, while the delay between applied field and the resulting displacement is measured by the phase [7]. The information may also be expressed in terms of admittance (the reciprocal of impedance), which is represented using the complex equation (3-3), where G is the conductance and B is the susceptance.

$$Y = G + jB \quad (5-1)$$

This technique has high accuracy but is relatively complex. However, with appropriate test equipment or suitably designed circuitry lab and field based measurements can be made providing an effective and comprehensive measurement and analysis tool. For instance, the impedance measurements have been successfully used to display variation of viscoelastic properties in the course of electro deposition of conducting polymer films. [10,11,12,13,14]

5.4 Measurement Procedure:

A typical measurement protocol was carried out as follows:

5.4.1 Substrate Preparation:

The essential processes that must be performed before any initial measurements or deposition onto crystal is to clean surface to be sure it is free from any defects/ contaminants as described in section 5.1.

5.4.2 Gas Chamber:

The measurements were carried out in a Teflon chamber in order to avoid vapour condensation; the internal volume was about $63.6cm^3$ where the depth is 4cm, diameter 4.5cm and the inlet pipe was located on the top of the chamber. Sealing the chamber was achieved by using a Nitrile O-ring between the lid and base sections which was clamped and compressed securely by bolts on the stainless steel outer fixture. The cell is shown in figure (5-2)

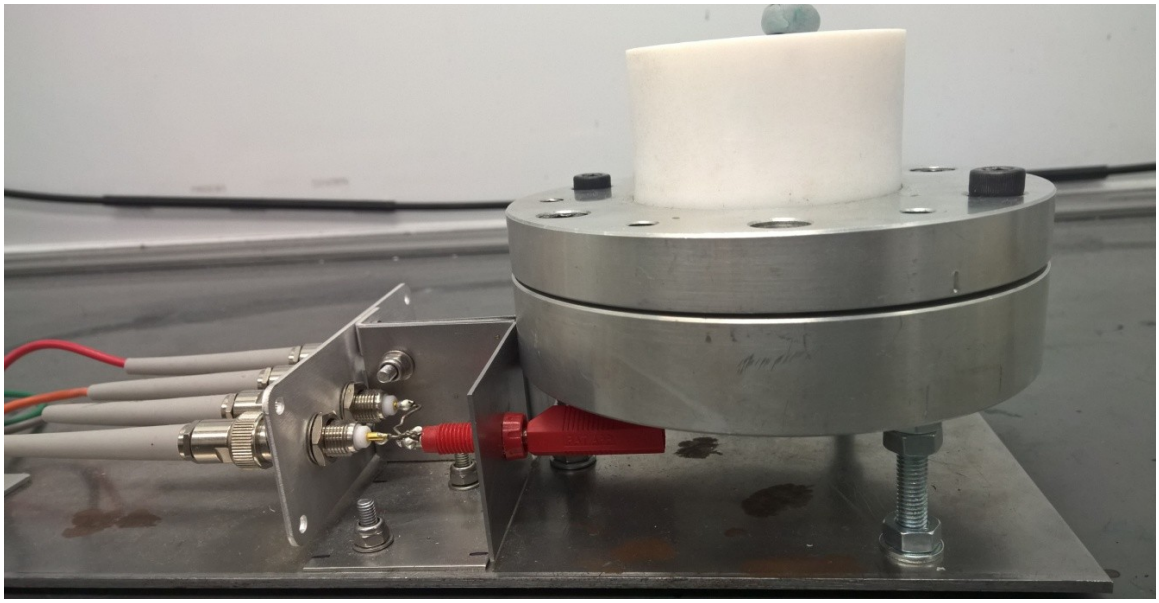

Figure (4-2). Gas cell and test fixture electrical connections.

5.4.3 Vapour injection:

The target analytes was inserted by a needle through inlet pipes was located on the top of the chamber. A small amount of liquid solvent in the volume range between $1\mu l$ to $70\mu l$ was injected into chamber with a micro syringe and allowed to evaporate. The chamber was flushed with air after every exposure.

5.4.4 Concentration and saturated vapour pressure:

In order to work out the vapour concentration of liquid solvent we have been used for injection into the chamber the equation (5-2) was employed.

$$Concentration\ (ppm) = \frac{D \times Q_s \times 22.4 \times 1000}{m.w \times V_{Cell}} \qquad (5-2)$$

Where $D, m.w, Q_s$ are density, molecular weight and quantity of liquid solvent in micro litres respectively, 22.4 molar mass gas constant and V_{Cell} is the internal volume of chamber.

To calculate saturated vapour pressure which will be used for result analysis later on this thesis the equation (5-3) used.

$$w\left({}^{g}/_{l}\right) = \frac{P \times m.w \times V}{R \times (T + 273.15)} \qquad (5-3)$$

Where w is, concentration in grams per litre, V is the volume $= 1$ litre. Is pressure of vapour in atmosphere at T temperature in degrees Celsius, R_{gas} is ideal gas constant($8.206\ e^{-2}$L atm K^{-1} mol^{-1}), P vapour pressure in atm $= \frac{kPa}{101.325}$.

To calculate the concentration in ppm from g/l the equation (5-5) was used.

$$ppm = \frac{w\left(\frac{mg}{m^3}\right) \times R_{gas} \times (T = 273.15)}{m.w} \qquad (5-5)$$

The concentration of injected liquid solvent was chosen dependant on Saturated Vapour Pressure (SVP), where the range was used in this study for each vapour was between 0 to 100% SVP (relative vapour pressure units), it is the concentration in unit of relative vapour pressure in respect to saturated vapour pressure (p/p_s)

The analytes solvent with their molecular weight and vapour pressure and concentration in ppm are listed in table (5-1).

Compound	**molecular weight**	**Vapour pressure (KPa)**	**vapour pressure (atm)**	**Concentration (mg/m^3)**	**Concentration (ppm)**
Benzene	78.11	10	0.0986923	320456.152	98692
Hexane	86.2	17	0.1677769	601198.881	167776
Ethanol	46.06	5.95	0.058722	789000000	58228
Toluene	92.1	2.9	0.0286207	109577.050	28620.

Table (5-1) the list of target organic solvents with their parameters at saturated vapour pressures.

5.5 Measurement data fitting:

The E4990A impedance analyzer provides 0.045% accuracy over range of 20 Hz to 120 MHz In this work, the original sampling frequency range of initial crystal measurement was chosen to be around 20 kHz above and below both parallel and series resonant frequency. If the initial measurement suitably covers the full crystal spectra then the start and stop frequency point can be adjusted to provide more accuracy.

Typical measurement spectra consisted of a frequency range from 9.96 MHz to 10.02 MHz). In order to raise the accuracy of measurements, additional data fitting was utilized which in turn provide an extra point over sampling frequency. The fourth order polynomial is used to fit the result data. The peak of admittance spectra is fitted to polynomial curve, while the zero phase is fitted to linear equation.

Around frequency of maximum admittance, nine data point are taken and fitted to polynomial than the best fit coefficients are saved.

The next admittance spectra peak is plotted using the saved best fit at sampling frequency of 1Hz increased. As same as the zero phase fitting.

5.6 Nulling Procedure:

From the definition of the impedance expression: the impedance is the opposition to alternating direct electric current for any electrical system or circuit , the opposition will be offered by each elements or component , where the impedance is a two dimension vector quantity.

The principle above applies to all components in the signal path not only the sensing element. Additional stray impedances (capacitance/inductance) will be introduced by cables, connectors and test fixture. Although considerable effort was made to minimize these effects including the use of high quality cable assemblies, minimized (short) signal paths and optimized test fixture further calibration is still required.

In order to eliminate and/or reduce the error, a suitable the nulling procedure has been applied before each set of measurements. The nulling procedure basis is to perform an open and short circuit test to find the impedance of test setup and then deduct this value at each measurement from resulting experimental data.

References:

1- Critchley, S. M., Willis, M. R., Cook, M. J., McMurdo, J., & Maruyama, Y. (1992). Deposition of ordered phthalocyanine films by spin coating. *Journal of Materials Chemistry, 2*(2), 157-159.

2- Taylor, J. F. (2001). Spin coating: An overview. *Metal Finishing, 99*(1), 16-21.

3- Calvo, E., Etchenique, R., Bartlett, P., Singhal, K., & Santamaria, C. (1997). Quartz crystal impedance studies at 10 MHz of viscoelastic liquids and films. *Faraday Discussions, 107*, 141-157.

4- Eichelbaum, F., Borngräber, R., Schröder, J., Lucklum, R., & Hauptmann, P. (1999). Interface circuits for quartz-crystal-microbalance sensors. *Review of Scientific Instruments, 70*(5), 2537-2545.

5- Steinem, C., & Janshoff, A. (2007). *Piezoelectric sensors* Springer Science & Business Media.

6- *SN74LVC1GX04 Crystal Oscillator Driver.* http://www.ti.com/product/SN74LVC1GX04/datasheet/abstract#SCES5815526

7- Etchenique, R., & Brudny, V. (1999). Characterization of porous polyaniline–polystyrenesulfonate composite films using EQCM. *Electrochemistry Communications, 1*(10), 441-444.

8- Ferreira, G. N., Da-Silva, A., & Tomé, B. (2009). Acoustic wave biosensors: Physical models and biological applications of quartz crystal microbalance. *Trends in Biotechnology, 27*(12), 689-697.

9- Rodahl, M., & Kasemo, B. (1996). A simple setup to simultaneously measure the resonant frequency and the absolute dissipation factor of a quartz crystal microbalance. *Review of Scientific Instruments, 67*(9), 3238-3241.

10- Holloway, A., Nabok, A., Thompson, M., Ray, A., Crowther, D., & Siddiqi, J. (2003). New method of vapour discrimination using the thickness shear mode (TSM) resonator. *Sensors, 3*(6), 187-191.

11- Holloway, A., Nabok, A., Thompson, M., Ray, A., & Wilkop, T. (2004). Impedance analysis of the thickness shear mode resonator for organic vapour sensing. *Sensors and Actuators B: Chemical, 99*(2-3), 355-360.

12- Holloway, A., Nabok, A., Thompson, M., Siddiqi, J., Ray, A., & Bliznyuk, V. (2004). Discriminative sensing of volatile organic solvents. comparative analysis using different QCM techniques. *Sensors, 2004. Proceedings of IEEE,* 1500-1503.

13- Nabok, A. (2005). *Organic and inorganic nanostructures (artech house mems and sensors library)* Artech House Publishers, Boston, MA, USA.

14- Sabot, A., & Krause, S. (2002). Simultaneous quartz crystal microbalance impedance and electrochemical impedance measurements. investigation into the degradation of thin polymer films. *Analytical Chemistry, 74*(14), 3304-3311.

15- Xie, Q., Zhang, Y., Yuan, Y., Guo, Y., Wang, X., & Yao, S. (2000). An electrochemical quartz crystal impedance study on cystine precipitation onto an au electrode surface during cysteine oxidation in aqueous solution. *Journal of Electroanalytical Chemistry, 484*(1), 41-54.

CHAPTER SIX

BASELINE RESULT AND EXPERIMENTAL DISCUSSION

This chapter reports the results from measurements taken on the crystal coating process, QCR sensor(s) and characterization of the resultant film(s).

Baseline measurements:

- Crystal Coating:
- Preliminary exposure.
    - Oscillator measurements:
    - Impedance measurements:

Main Results:

- Impedance analysis:
- Crystal coating:
- Film characterization:
    - UV–Vis absorption spectra
    - Ellipsometry measurements
    - AFM measurements

6.0 Chapter overview:

The chapter is divided into several sections. The first part of this chapter gives the results obtained from preliminary feasibility/viability measurements. This continues with the investigation of the selected thin film sensing materials (Pcs) by UV- visible absorption spectroscopy. Moreover, film properties such as thickness and homogeneity are characterised. The second part of this chapter will address the measurements taken using QCR sensor(s), the crystal coating process and characterization of the resultant film(s).

6.1 Preliminary measurements:

Considerable previous literature suggests that phthalocyanine materials produce good organic thin films through appropriate coating methods and they can subsequently be employed as a sensing material in gas environments [1, 2, 3, 4, 5, 6, 7, 8]. To assess the viability and practicability of the proposed films preliminary tests were however undertaken to warrant that the direction of work would lead to effective films as sensing membranes.

Two different substituted metallophthalocyanine were selected to achieve this objective. Namely;

1- Zinc 2,9,16,23-tetra-*tert*-butyl-29*H*,31*H*-phthalocyanine.
2- Zinc 2,11,20,29-tetra-*tert*-butyl-2,3-naphthalocyanine.

These were all purchased from the supplier Sigma-Aldrich. In total three AT-cut quartz crystals were used as a sensing element(s) for each compound all with a fundamental resonant frequency of 10MHz. Prior coating with sensitive films, the bare crystals were measured using the impedance analysis technique and the spectrum fitted to the BVD equivalent circuit.

A typical plot of the experimental admittance spectra is shown in figure (6-1). Maximum admittance magnitude and both *R* and *f* were extracted for all six crystals.

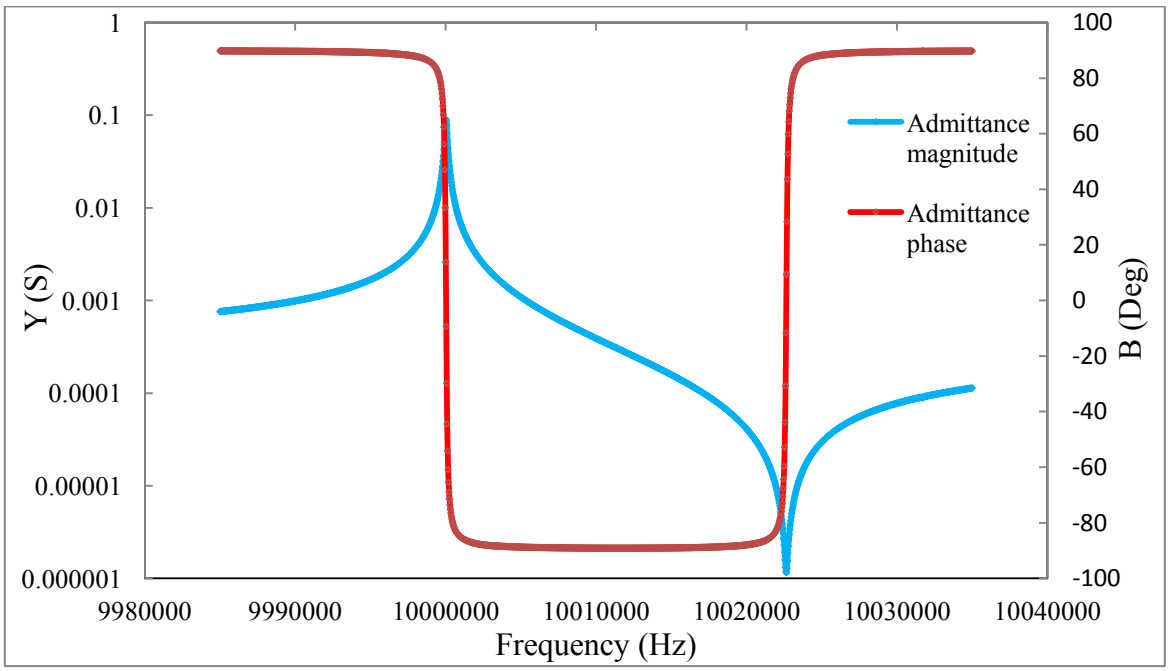

Figure (6 -1). Admittance spectra of an uncoated QCR.

Plots of magnitude and phase spectra for all QCRs can be found in the Appendix.

Statistically, based on frequency measurements, the mean frequency and Standard Deviation (SD) for using QCR's they were 10001483.33Hz, 4147.9 Hz respectively

The Solatron 1260 impedance gain/phase analyser was used to measure the admittance spectra of the crystal. This was interfaced to a PC via the GPIB interface and the measurement process was controlled by a custom LabVIEW program.

The measured resonant frequencies and maximum admittance values of the six uncoated crystals are listed in table (6-1).

QCR	*f* resonance (Hz)	Y max (S)
1	10005100	0.003380
2	10005500	0.005390
3	9997600	0.03410
4	10005200	0.005790
5	9997900	0.004360
6	9997600	0.02270

Table (6 -1) Value of crystal resonant frequencies and maximum admittance.

6.2 Crystal Coating:

Prior to coating, the crystal surface was cleaned by dipping the crystal in acetone then subsequently rinsed with ultra pure water. The sensitive films of the different Pcs on the transducer surface were deposited using the spin coating technique. Solution of sensitive material was prepared by dissolving the Zinc-tetra butyl-phthalocyanine (Zn-tb-pc) or Zinc-tetra-butyl- naphthalocyanine (Zn-nph-pc) in analytical grade chloroform with a concentration of 10mg/ml at room temperature. A micropipette was used to drop a known amount of solution onto both side of rotating substrate surface (QCR) at 2000rpm. The solvent subsequently evaporates leaving the desired film. No further chemical or physical treatment of sample was performed after deposition.

The coating process was all completed inside a fume cupboard to create a dust free environment and suitable safe environment for the solvent (chloroform) to evaporate.

Impedance/Admittance measurements were then taken and resultant spectra fitted to the BVD equivalent circuit.

Figures (6-2) and (6-3) shows plots magnitude and phase of uncoated and coated QCR for with (Zn-tb-pc) film respectively.

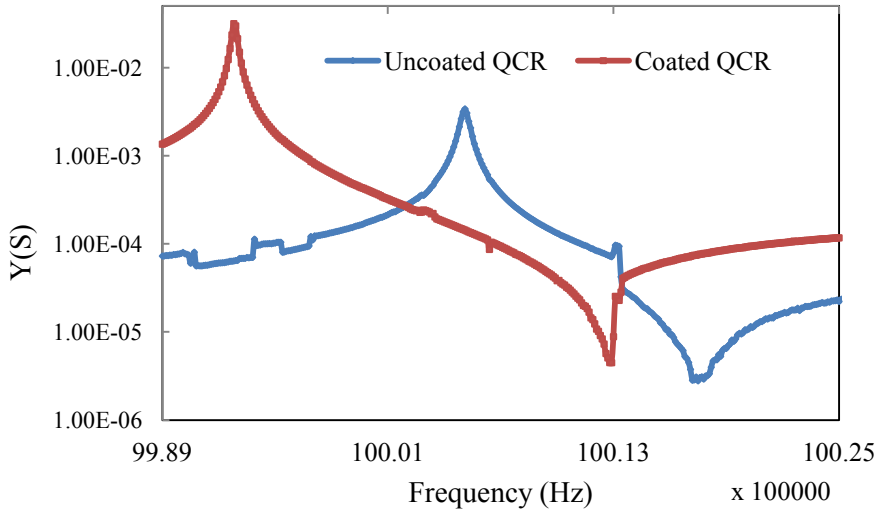

Figure (6-2) Admittance magnitude for QCR before and after coating with Zn-tb-pc film.

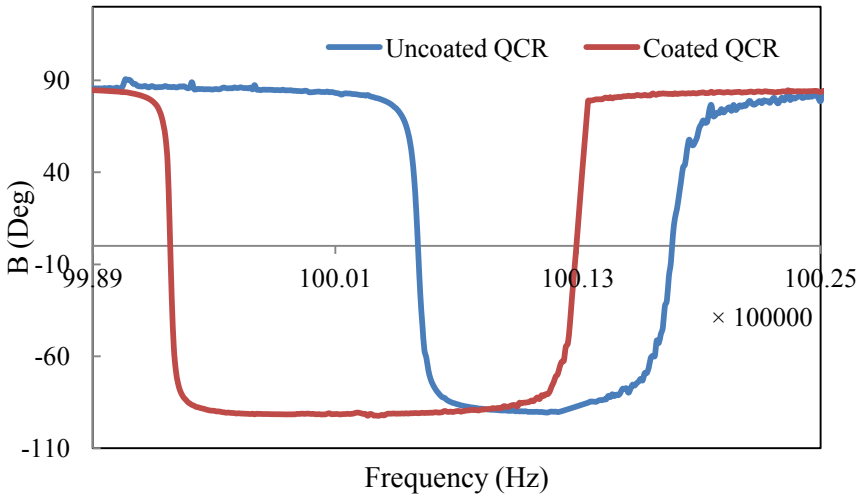

Figure (6-3) Phase for QCR before and after coating with Zn-tb-pc film.

Table 6-2 summarises the changes in frequency and admittance magnitude observed after coating for all six crystals.

QCR	Coating film	f $Resonance$ (Hz) Uncoated QCR	Y_{max} (S) Uncoated QCR	f $Resonance$ (Hz) Coated QCR	Y_{max} (S) Coated QCR	Δf(Hz)	ΔY_{max} (S)
1	Zn-tb-pc	10005100	0.003380	9999800	0.03140	5300	0.02802
2	Zn-tb-pc	10005500	0.005390	9993900	0.04280	11600	0.03741
3	Zn-tb-pc	9997600	0.03410	9993700	0.03160	3900	-0.0025
4	Zn-nph-pc	10005200	0.005790	9994900	0.00566	10300	-0.00013
5	Zn-nph-pc	9997900	0.004360	9994800	0.01520	3100	0.14764
6	Zn-nph-pc	9997600	0.02270	9993900	0.01790	3700	-0.0048

Table (6-2) Changes in frequency and admittance magnitude for the 6 used crystal.

6.3 Film thickness:

From the data of coated and uncoated QCRs the film thickness was calculated. Initially, the Sauerebey equation has been used to give an approximate value of film thickness; extracting Δf from the resonant frequency of QCR before and after coating with the film and applying equation (2-1) was used.

Table 6-3 shows the calculated film thickness and shows that there are some differences between thickness obtained from the ellipsometry measurements and the thickness calculated from the QCR data. This can be expected as the film is non rigid film and the change in frequency should be interpreted not purely as mass loading only. i.e; the viscoelastic effect also occurs and will therefore contribute to the observed frequency shift.

Compound	Calculated Film Thickness nm
$Zn-tb-pc$	23
	51
	15
$Zn-nph-pc$	46
	14
	16

Table (6-3) calculated film thickness for six crystals using the Sauerebey equation.

6.4 Vapour exposure:

In this experiment four types of solution were used as target analytes, specifically (Hexane, Benzene, Ethanol and Toluene). All of which are considered as rapid volatilization Volatile Organic Compounds (VOCs), highly flammable and also present potential toxicity hazards , caused by repeated or long exposure to these analytes has been shown to damage organs [9]. While the cancer or genetic defects could be a result of exposure to benzene gas, as well hexane and benzene are both classified as harmful and toxic to aquatic life [9, 10]. Moreover, toluene could be a reason of damaging fertility [10, 11]. Additionally, (VOCs) are in the main considered as dangerous for the environment. Therefore, methods of organic vapour detection have become very important for human health, environmental protection, safety supervision, food production and quality control in many industries, etc. [10, 11]. Additionally the chosen analytes provide a varied chemical structure and physical properties which potentially could show significant variation in the viscoelastic properties of the coating on ad/absorption.

A specifically designed Teflon chamber with volume of $0.0636\ m^3$ was used as the exposure cell with the inlet/extraction pipe located on the top of the chamber.

As detailed in chapter 4 calculated amounts liquid solvent to produce known vapour concentrations were injected into chamber with a micro syringe and allowed to evaporate. The chamber was flushed with air after every exposure in order to observe the recovery response time and if any sensor poisoning/degradation occurs.

6.4.1 Vapour exposure & Oscillator measurements:

Initially frequency only measurements were conducted to establish the suitability of the membranes for further investigation. The oscillator only measurements have significant time saving advantage compared to full impedance/admittance measurements using the high precision Solartron impedance analyser, and also allow simultaneous measurement of multiple sensor elements within the same cell. Figure (6-4a) and (6-4b) shows a block diagram of oscillator based array and impedance analysis test set up respectively, full details of experimental set up can be found in chapter four.

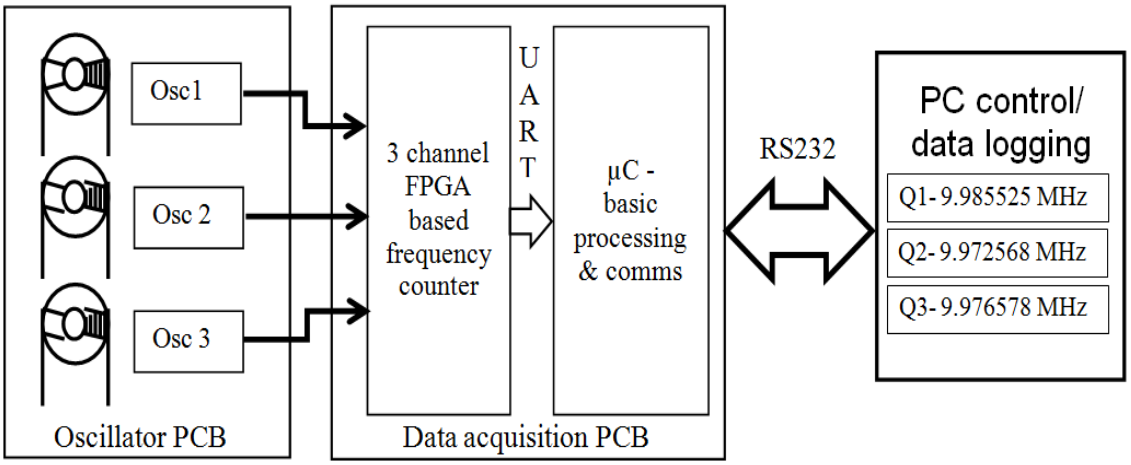

Figure (6-4a) Block diagram of resonant oscillator QCR array

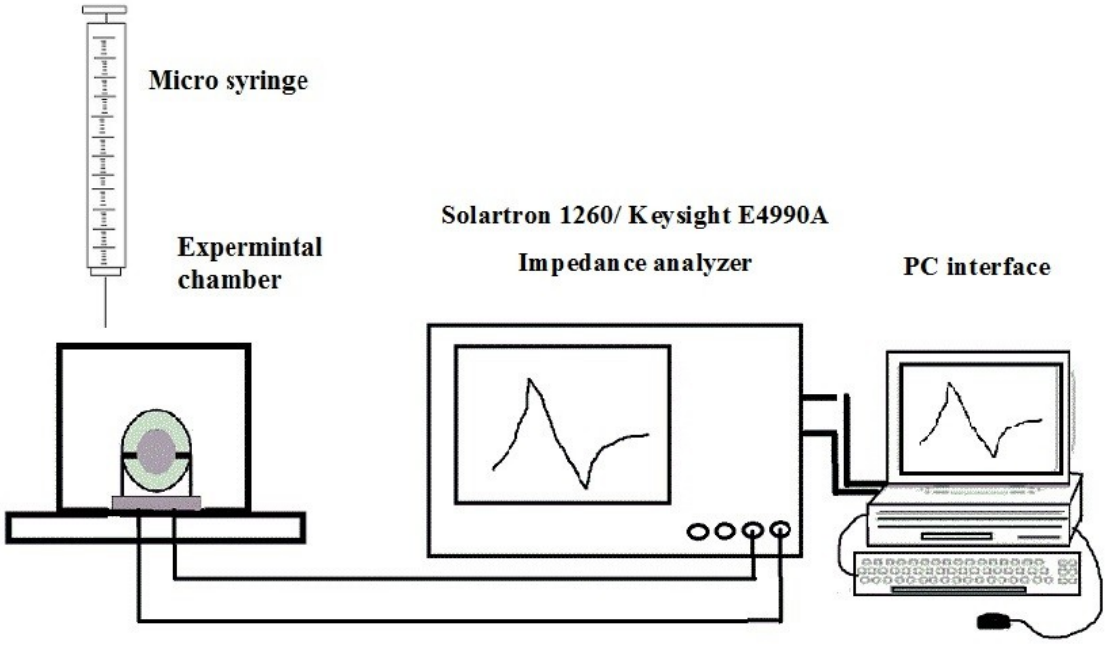

Figure (6-4b) Diagram of the basic impedance analysis experimental set-up.

Figures (6-5) and (6-6) shows plot of data collected from vapour exposure.

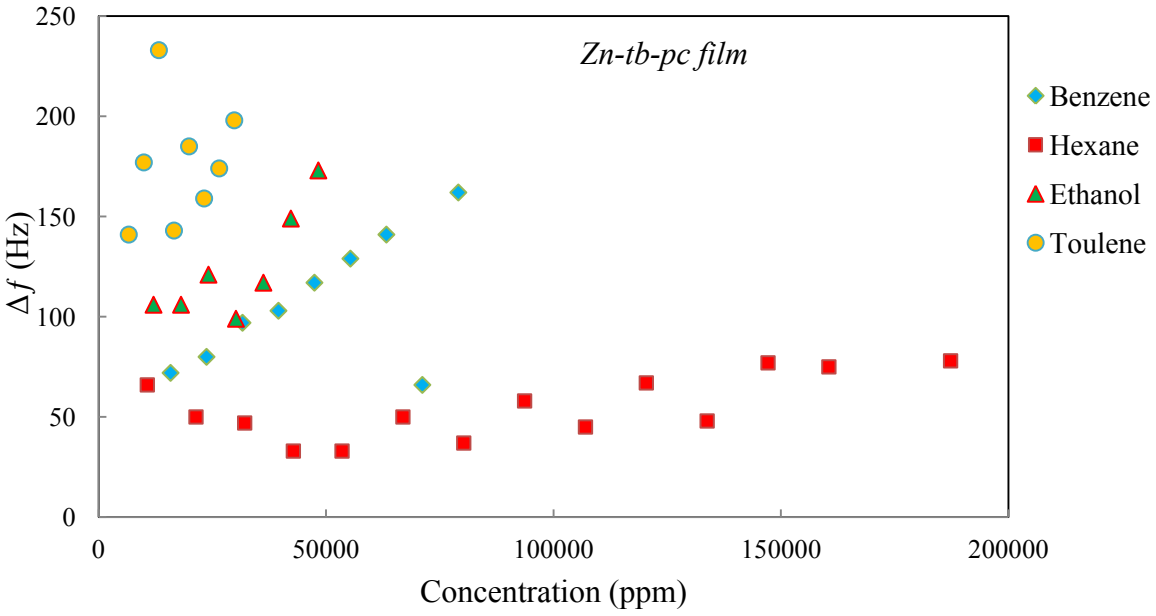

Figure (6-5) Frequency response of coated QCR (Zn-tb-pc film) exposed to a selected set concentrations for the target vapours.

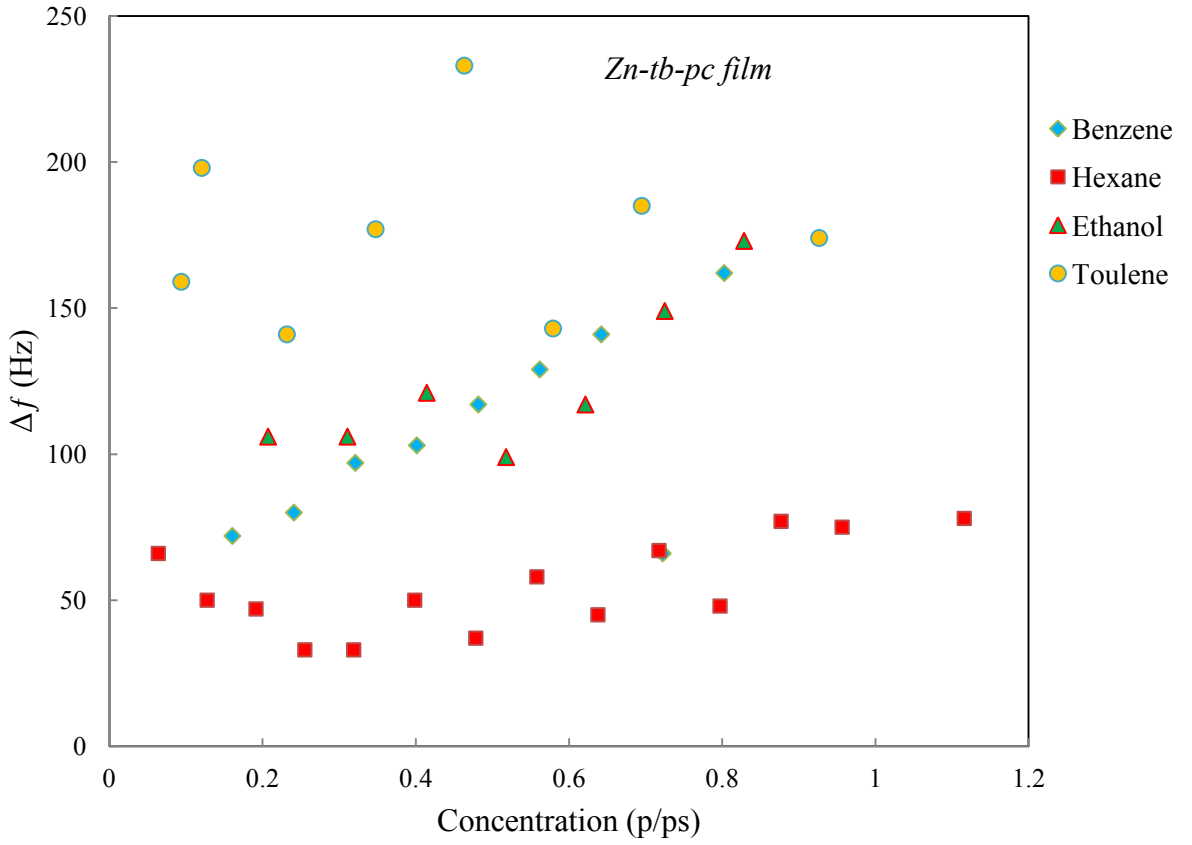

Figure (6-6) Frequency response of coated QCR (Zn-tb-pc film) exposed to a selected set concentrations p/p_s for the target vapours.

The change in the resonant frequency (Δf) is extracted from the data captured during vapour exposure the change between the frequencies before the vapour is injected and subsequently after injection when the frequency stabilizes is used, as shown figure (6-7). The time axis is given in arbitrary units (a.u) representing each sample time of approximately one second. A Matlab program was used to automate the process and extract Δf from the experimental data.

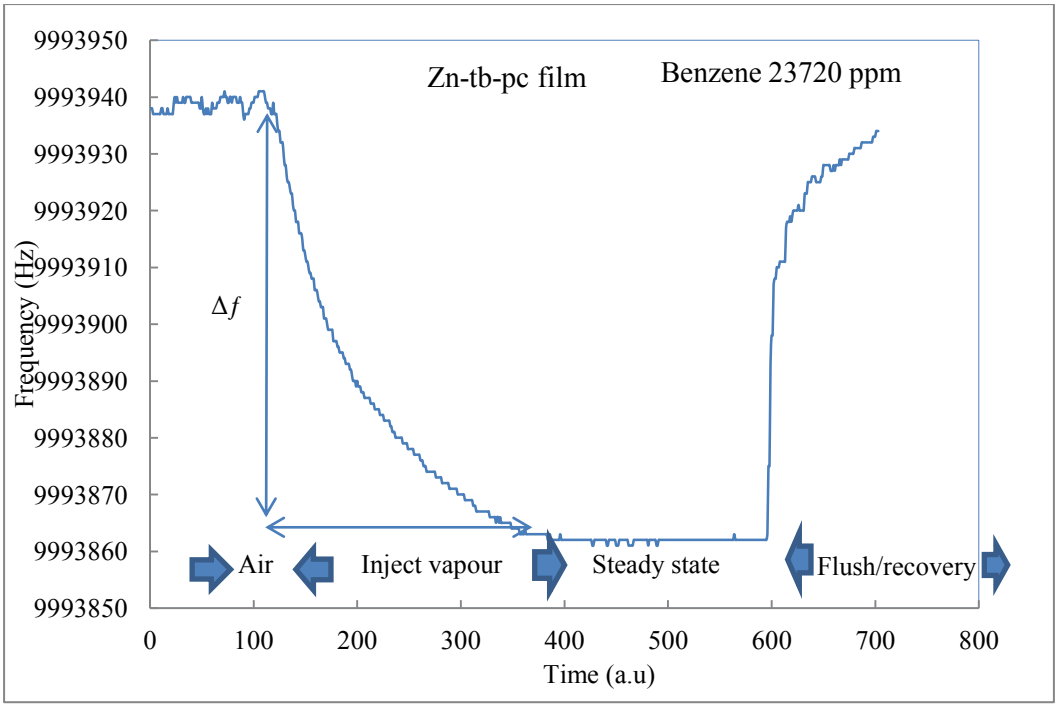

Figure (6-7) The change in frequency during a typical vapour exposure with Δf indicated.

6.4.2 Vapour exposure & Impedance Analysis:

After successful measurements using oscillator only techniques the films were tested using the impedance analysis setup for six coated QCR for both films. Each sweep has 100 points and gives the frequency against the conductance and susceptance; the maximum value of Y centred in each sweep. Each measurement took around two minutes.

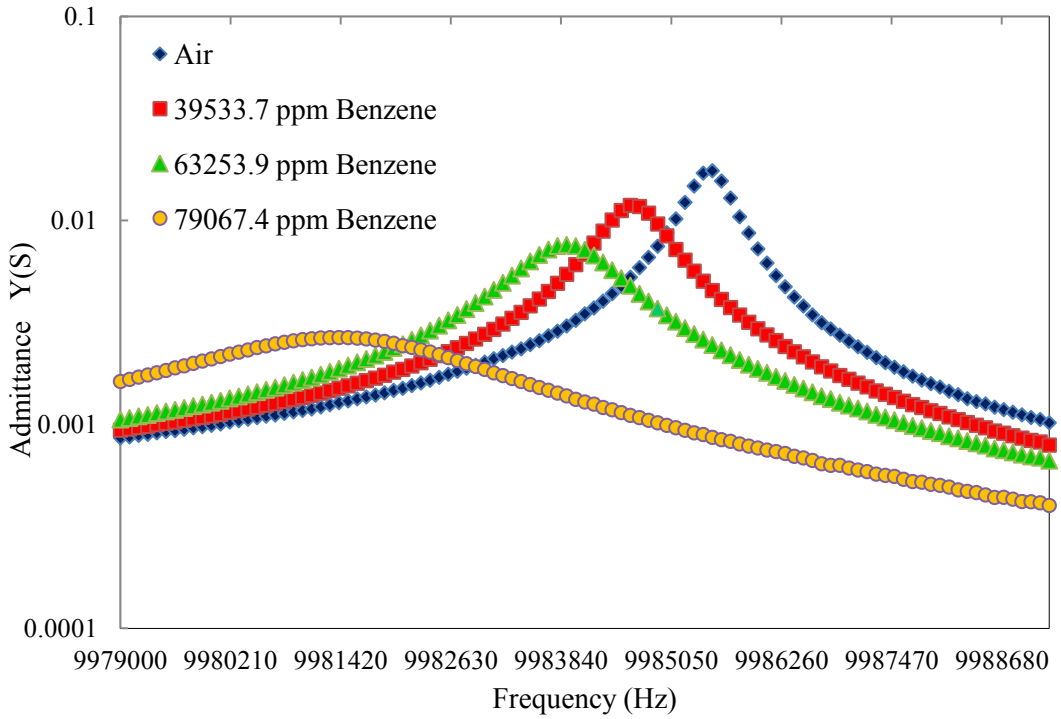

Figure (6-8) Frequency against admittance magnitude for different values concentrations of benzene vapours of *Zn-tb-pc* film.

The spectra obtained by measurement were then fitted to the BVD equivalent circuit by using LabVIEW program and circuit parameters extracted. Figure (6-9) shows a typical plot of admittance for an unexposed and exposed sensor with the distinct changes in both magnitude and resonant frequency highlighted. Table 6- 4 summarises the changes in frequency and admittance magnitude (related to circuit parameters R_f and L_f) observed after exposure the vapour for QCR 1 crystals (coated with *Zn-tb-pc* film) with various concentration of Benzene, Toluene, Ethanol and Hexane.

QCR1	$Frequency$ (Hz)	$Consentration$ (ppm)	$Consentration$ $(p/p_{s)}$	Δf (Hz)	Y_{max} (S)	ΔR (Ω)
Air	9985500	-	-	-	0.01751814	-
Benzene	9984600	39533	0.40131	900	0.011837689	-27.3
	9983900	63253	0.64209	1600	0.007587012	-74.7
	9983600	79067	0.80261	1900	0.006033844	-108.6

Hexane	9981400	53493	0.31884	4100	0.002664425	318.2
	9980700	80240	0.47826	4800	0.002373514	364.2
	9980900	133734	0.7971	4600	0.002509545	341.3
Ethanol	9981500	24148	0.41426	4000	0.002681304	315.8
	9980500	36222	0.82852	5000	0.002330993	371.9
	9980500	48296	1.03565	5000	0.002311849	375.4
Toluene	9981600	6626	0.23163	3900	0.002972418	-279.3
	9981000	16565	0.57907	4500	0.002681839	-315.7
	9980500	29818	1.04233	5000	0.002408099	-358.1

Table (6-4) Example of changes in frequency and admittance magnitude observed after exposure to a range vapour concentrations for one crystal.

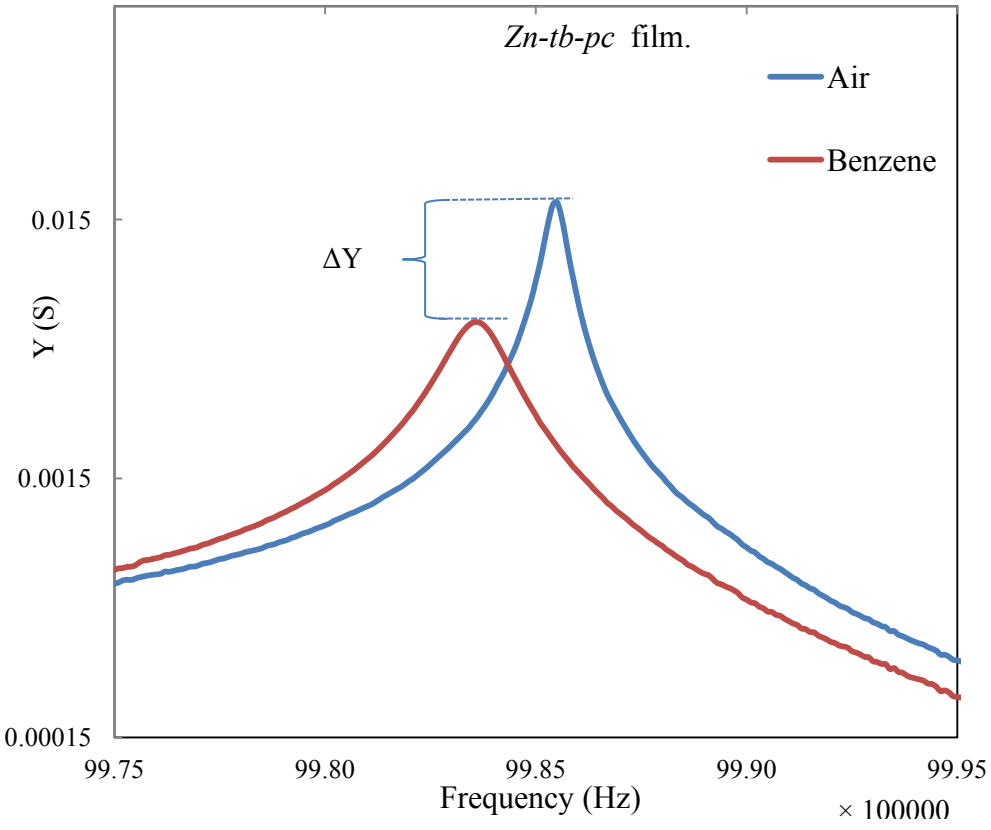

Figure (6-9) Extracting ΔY for QCR (*Zn-tb-pc* film)**.**

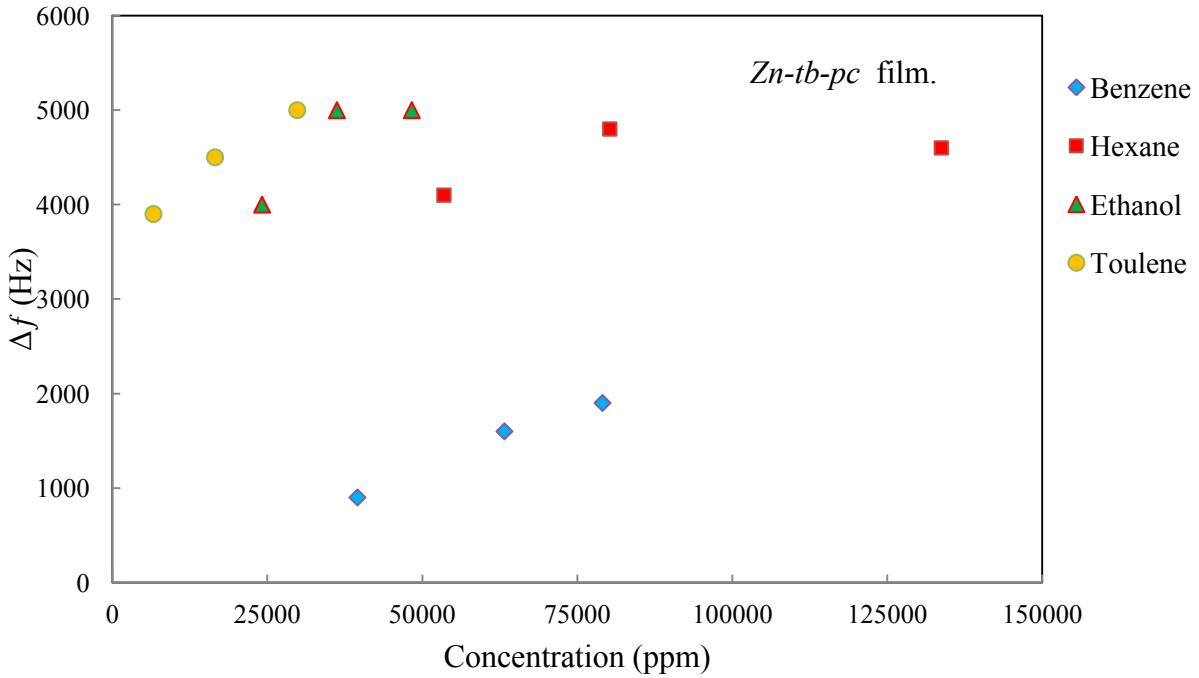

Figure (6-10) Δf Hz against concentration in ppm for *Zn-tb-pc* film..

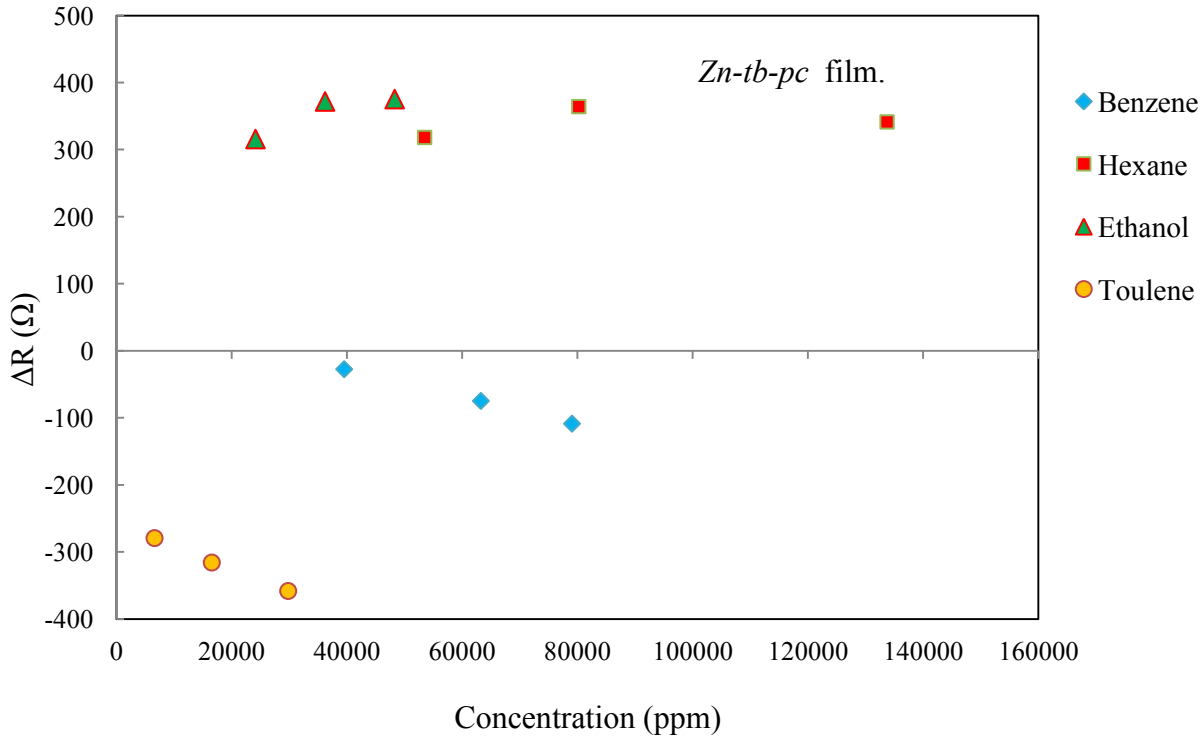

Figure (6-11) ΔR against concentration in ppm for *Zn-tb-pc* film.

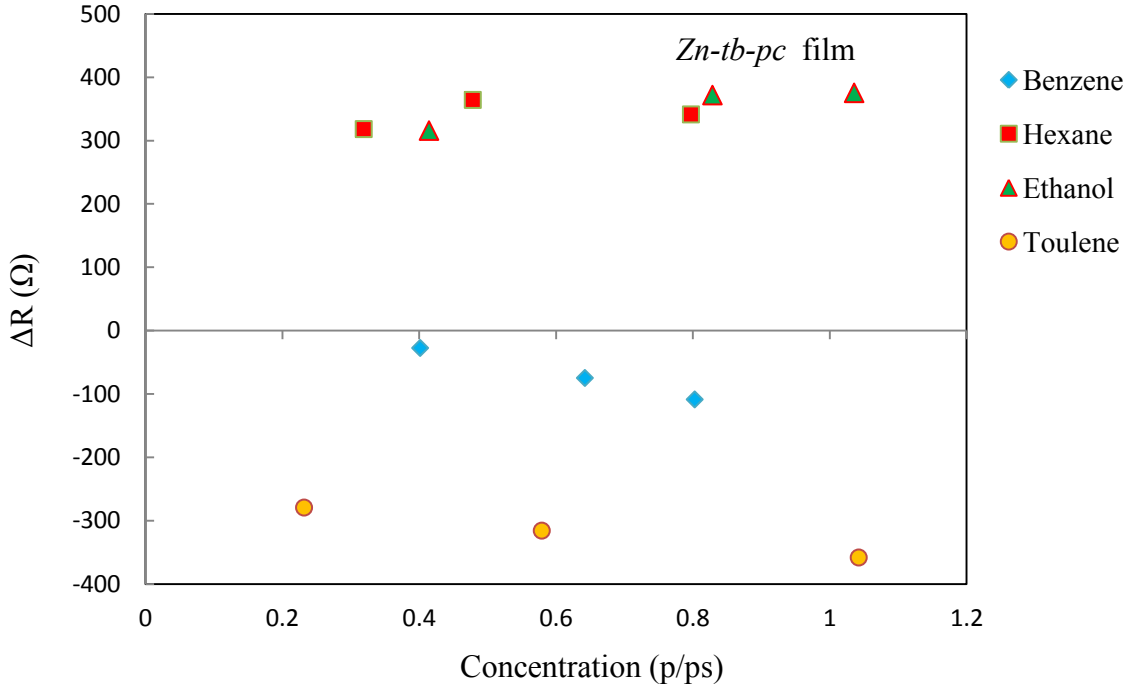

Figure (6-12) Δ*R* against p/ps for *Zn-tb-pc* film.

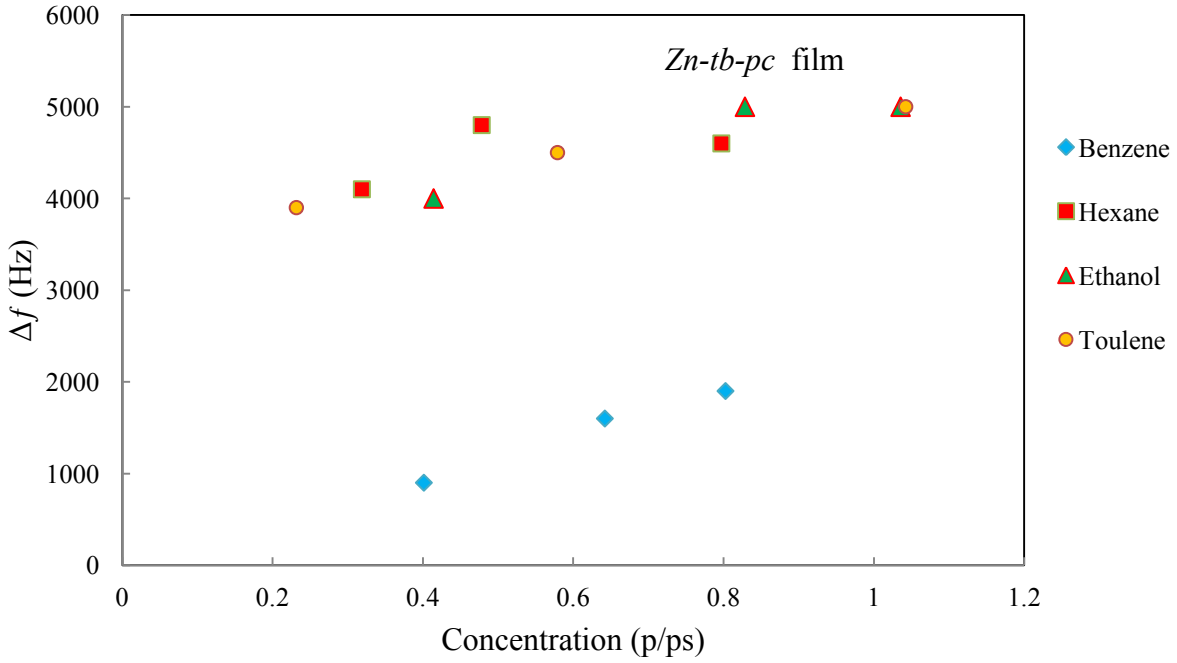

Figure (6-13) Δ*f* Hz against p/ps for *Zn-tb-pc* film..

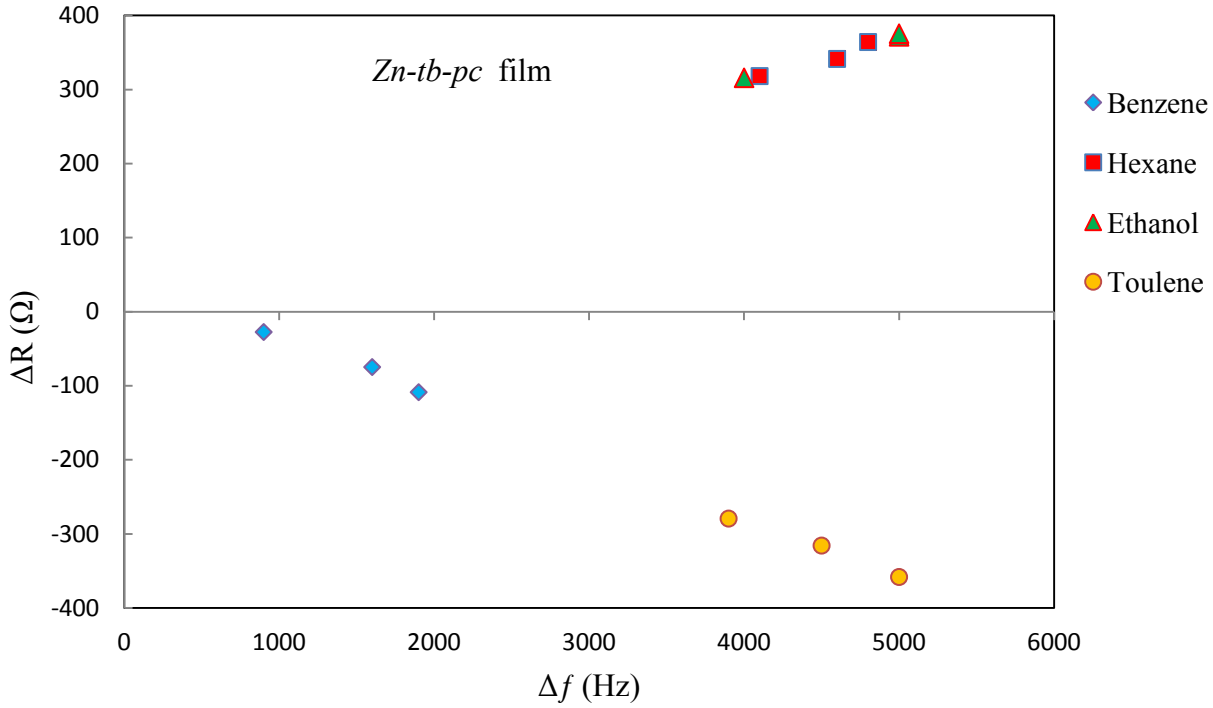

Figure (6-14) ΔR against Δf Hz for *Zn-tb-pc* film.

6.5 Film Properties:

The important information about the coating film: its properties and morphology can be investigated by a range of different techniques as described in chapter two.

In this stage of the project, both ellipsometry and UV-visible spectrometer have been used to determine film thickness and to provide further information about the film.

6.5.1 Ellipsometry Measurements:

We have measured the samples for both kind of the film using Ellipsometry to obtain the film thickness value.

The experimental values of Δ and ψ have been obtained for each film and the optical model commensurate with samples was used as described in figure(3-1) in chapter three. Where the

square fit was used to obtain the best result of film thickness, also optical constant n, k can be extracted.

The thickness' obtained from ellipsometry fitting are listed in Table (6-5).

Combined	Calculated Film *thickness nm*	Measured film *thickness nm*	ΔT_f
$Zn-tb-pc$	29.66	56.8	27.14
$Zn-nph-pc$	16	56.6	40.6

Table (6-5) Thickness obtained in accordance with Ellipsometry fitting procedures for phthalocyanine films deposited at $2000rpm$.

Film thickness were calculate for both Zn-tb-ph and Zn-nph-pc films and compared with measured values figure (6-15) and (6-16). The foreground plot shows the measured thickness from the films deposited on a silicon substrate the rear plot are the calculate thickness values from the QCR measurements.

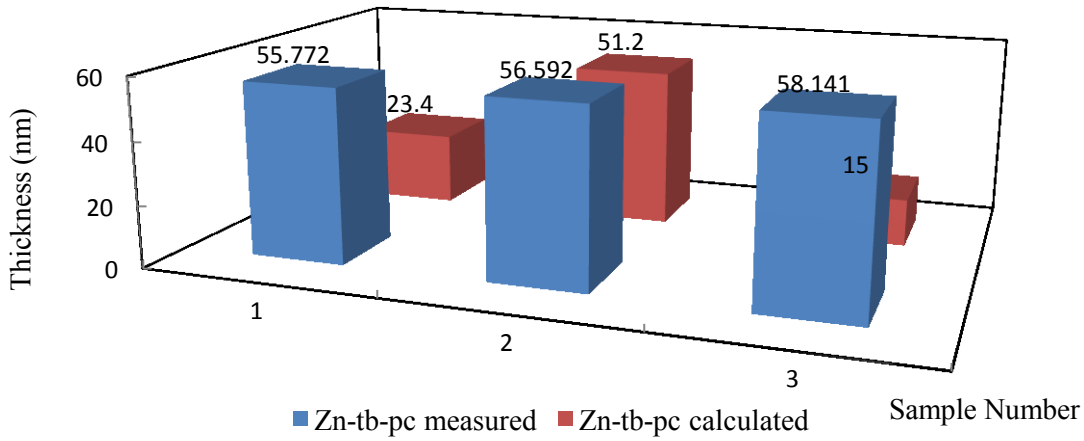

Figure (6-15) Comparison between the measured and calculated thickness values for Zn-tb-pc film, the thickness in nm is shown above each plot.

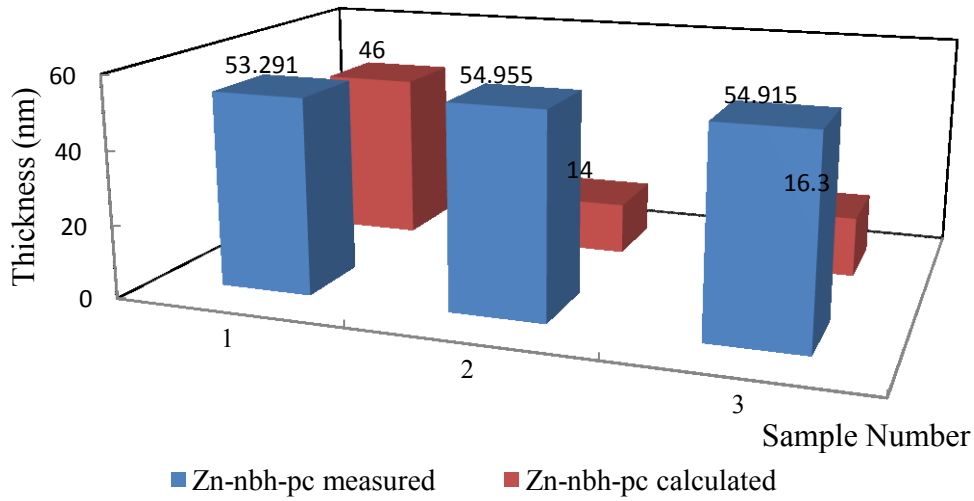

Figure (6-16) Comparison between the measured and calculated thickness values for Zn-nph-pc film, the thickness in nm is shown above each plot**.**

6.5.2 UV-Visible Absorption Spectra:

UV- Visible spectra were recorded on Varian 50 scan UV- visible spectrophotometer.

It was shown earlier that spin coating method provides a simple and convenient procedure for formulating thin films of the phthalocyanines. The electronic absorption spectra of the film of are presented in figure (4-19).It has two intensive bands in the UV-visible spectra.

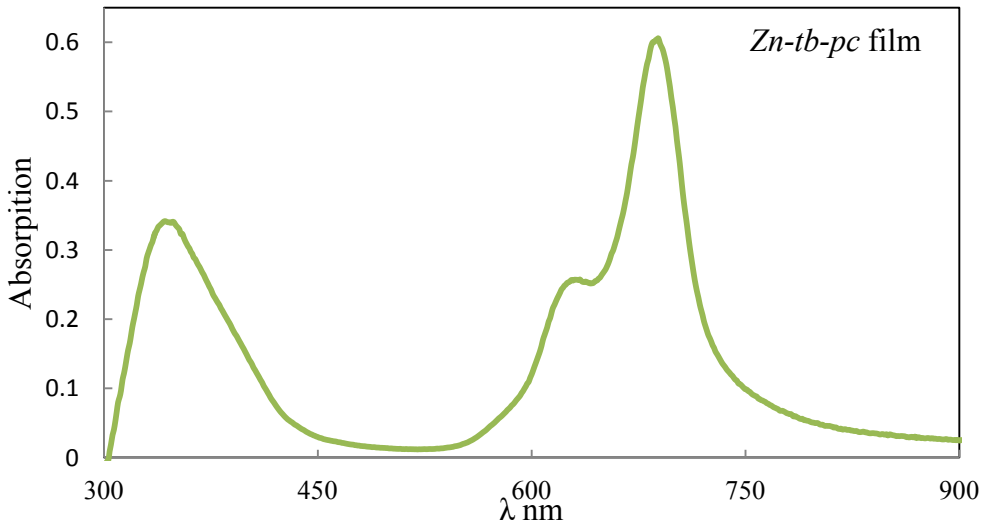

Figure (6-17) the UV-visible spectra for Zn-tb-pc film.

6.6 Main Results:

After preliminary measurements it was established that the tested films gave satisfactory responses and suitable potential to work as a gas/vapour sensors and the coating process produced similar films exhibiting a definite shift in resonance. Therefore, a further range of metallophthalocyanine materials were selected prepared and characterized in order to study their performance as a gas sensor.

In this part, eight substituted metallophthalocyanines were selected to study their response as a gas sensor for specific target analytes (Hexane, Benzene, Ethanol, and Toluene). To achieve this target, three crystals for each compound were utilized as the substrate element all with 10 MHz fundamental resonance frequency. In total 24 crystals were used.

6.6.1 Impedance analysis:

The impedance analysis technique was used to record the admittance spectra and determine the resonance frequency of quartz crystal in intervals of 9.96 MHz to 10.02 MHz. Although initial measurements were taken using the Solatron 1260a limitations in the acquisition speed imposed a significant bottle neck in the measurement process. Therefore, a faster and high specification impedance analyzer was purchased.

Subsequence measurements were taken using a Keysight E4990A impedance analyser controlled via PC running LabVIEW software to record the spectra. Each sweep was divided into 500 points and took approximately 15 seconds (to improve accuracy the measurement time setting was set to increased resolution (state3) on the impedance analyser resolution). The maximum admittance frequency was centred in each sweep as shown in figure (6-18) and the example of magnitude and phase spectra for all crystals are given in figure (6-19).

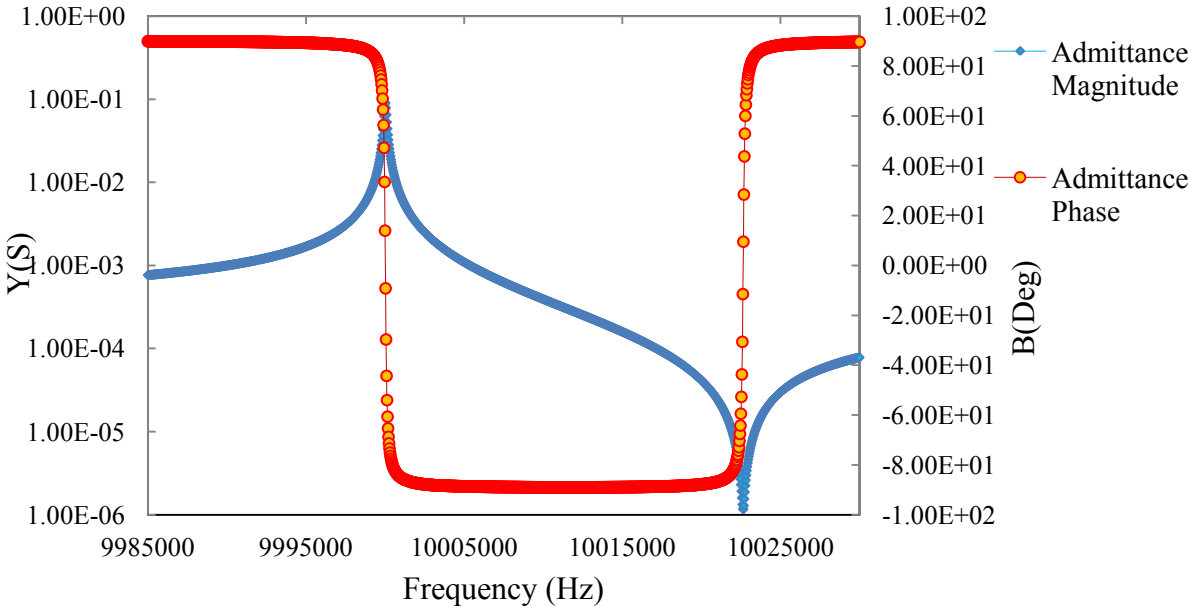

Figure (6-18) Zero phase crosses with maximum/minimum admittance spectra at series/parallel resonance.

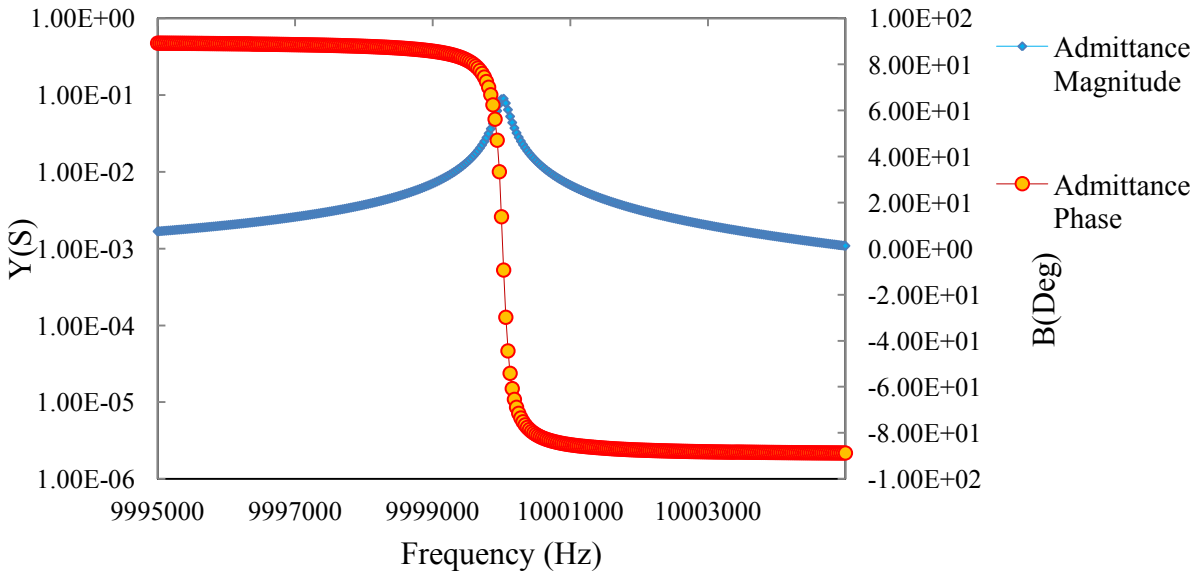

Figure (6-19) Zero phase point cross with series resonance.

The motional equivalent circuit elements and resonance frequency were recorded for each crystal. The crystals parameters are listed in table (6-6). As the table shows there are a slight differences between admittance spectra of all uncoated crystals where the maximum resonance frequency and maximum resistance are 10000063 Hz , 18.68 Ω respectively

And the minimum resonance frequency and minimum resistance are 9999250 Hz, 9.55 Ω respectively.

Crystal	C0 (F)	C1(F)	L1(h)	R1(Ω)	Ƒ(Hz)
1	4.8793e-12	2.2100498e-14	1.146e-2	10.97	10000031
2	4.7228e-12	2.1984793e-14	1.152e-2	11.12	9999250
3	4.7792e-12	2.1954693e-14	1.153e-2	11.51	10000031
4	4.7458e-12	2.2757404e-14	1.113e-2	12.31	10000031
5	4.7808e-12	2.2590587e-14	1.121e-2	11.65	10000000
6	4.7534e-12	2.2066439e-14	1.147e-2	9.63	10000031
7	4.9939e-12	2.2185625e-14	1.141e-2	9.99	10000031
9	4.7700e-12	2.195934792e-14	1.153e-2	13.09	10000031
10	4.8801e-12	2.2129017e-14	1.144e-2	10.28	10000031
12	4.7967e-12	2.26695713e-014	1.117e-2	10.35	10000063
13	4.7579e-12	2.30446974e-14	1.099e-2	11.81	10000031
14	4.7901e-12	2.2769453e-14	1.112e-2	10.77	10000063
15	4.8566e-12	2.24635133e-14	1.127e-2	9.92	10000031
16	4.85901e-12	2.1977584e-14	1.152e-2	12.32	10000031
17	4.9253e-12	2.18707996e-014	1.158e-2	11.03	10000031
18	4.7269e-12	2.24804940e-14	1.126e-2	9.82	10000031
19	4.95075e-12	2.20068429e-14	1.151e-2	11.58	10000031
20	4.7207e-12	2.23181506e-14	1.134e-2	9.55	10000063
21	4.8000e-12	2.3338191e-14	1.085e-2	18.68	10000031
22	4.7404e-12	2.21093343e-14	1.145e-2	13.59	10000031
23	5.5658e-12	2.49899396e-14	1.013e-2	12.62	9999938
24	4.9325e-12	2.24862389e-14	1.126e-2	11.13	10000031
25	4.79402e-12	2.22891299e-14	1.136e-2	11.32	9999844

Table (6-6) The equivalent circuit elements and resonance frequency for crystals.

	Mean	Standard Deviation (SD)
Frequency (Hz)	9999987.69	167.12
Resistance (Ω)	11.52	1.909

Table (6-7): Statistics of the *f* and R parameters using in this study.

6.7 Crystal coating:

A spin coating set up described in chapter four was utilized to produce a suitably thin film. The coating processes of crystal with selected compound produce a definite shift in resonance peak changes in both frequency and magnitude (mass loading and film damping) are observed. The changes in resonant frequencies and resistances of a selected crystal after coating process are depicted in figure (6-20) and (6-21) respectively.

Moreover, change in the resistances obtained by coating crystal (ΔR) indicating a non-gravimetric response. This can be attributed to differences in one or more of film parameters such as film thickness, surface roughness, homogeneity, film coverage and viscosity.

Results for all crystals with selected Pcs compound are reported in table (6-8).

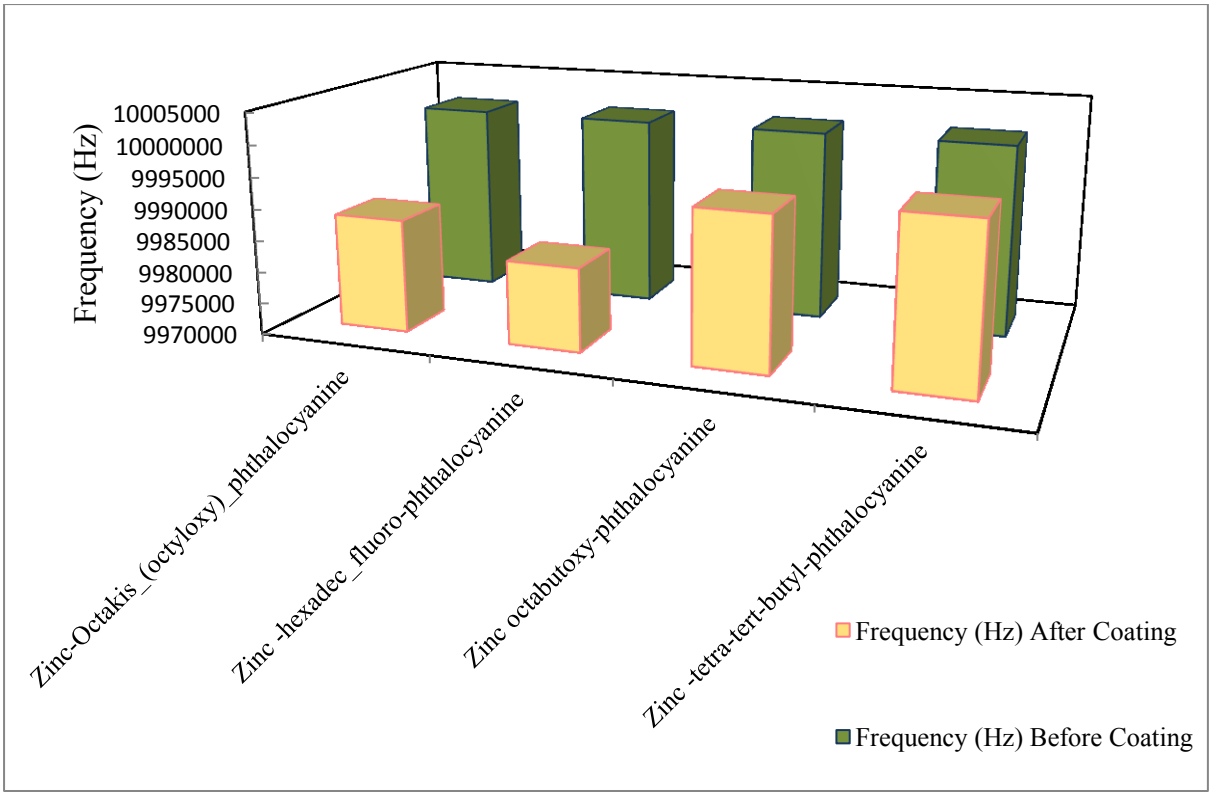

Figure (6-20) The changes in resonant frequencies of a selected crystal after coating process.

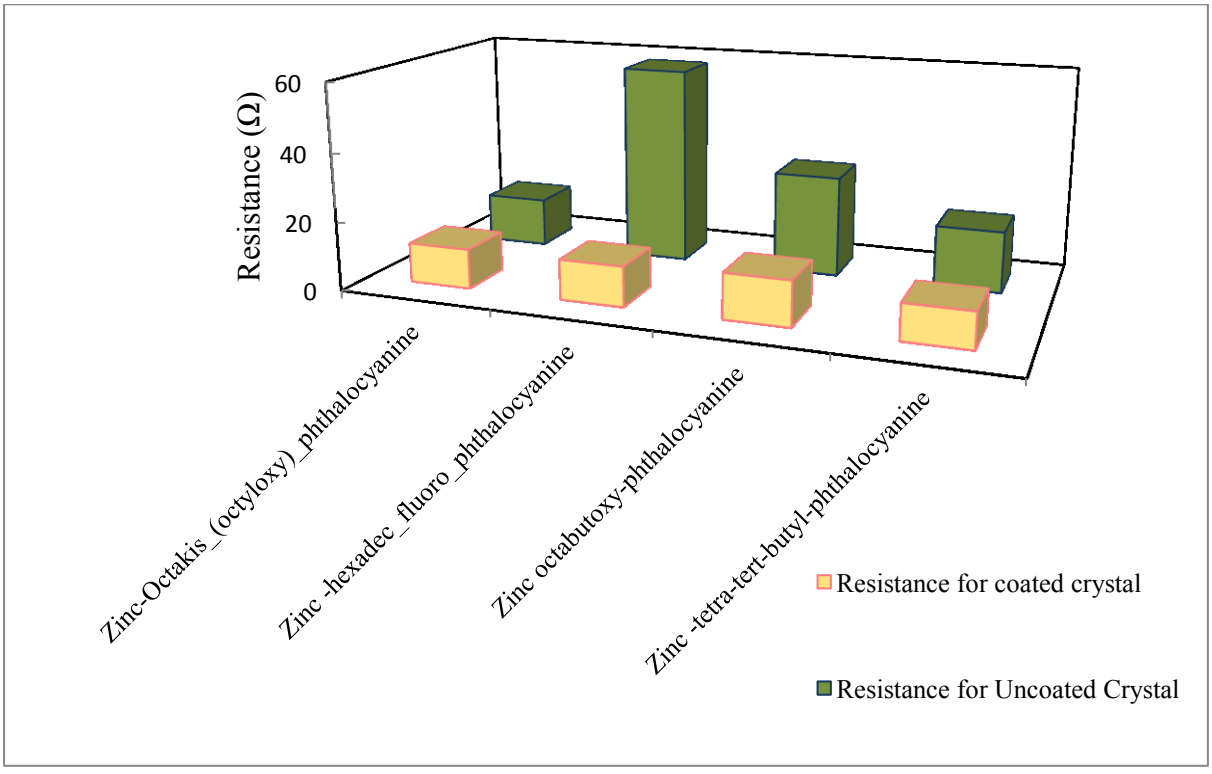

Figure (6-21) The changes in resistances of a selected crystals after the coating process.

$Film$	Sample Number	$f\ (Hz)$ before coating	$f\ (Hz)$ after coating	$\Delta f\ (Hz)$	Y_{max} (s) before coating	Y_{max} (s) after coating	ΔY_{max} (s)	T_f nm $film$ $thickness$
Zinc-Octakis(octyloxy) phthalocyanine	1	10000031	9992375	7656	0.08982	0.079526	0.010294	33.8
	2	9999250	9991250	8000	0.089684	1.340185	-1.250501	35.4
	3	10000031	9987844	12187	0.08673	0.070148	0.019536	53.92
Zinc - hexadecafluoro-phthalocyanine	4	10000031	9986331	13700	0.080337	0.009793	0.070544	60.6
	5	10000000	9983121.9	16878.1	0.08522	0.01731	0.06791	74.68
	6	10000031	9984138	15893	0.102656	0.361995	-0.25933	70.32
Zinc octabutoxy-phthalocyanine	7	10000031	9994718.75	5312.55	0.099635	0.094617	0.005018	23.5
	9	10000031	9993888	6143	0.075534	0.034114	0.04142	27.18
	10	10000031	9997156	2875	0.096652	0.090129	0.006523	12.72
Zinc -tetra-tert-butyl-phthalocyanine	12	10000063	9995750	4313	0.09607	0.056168	0.039902	19.08
	13	10000031	9996500	3531	0.084462	0.072252	0.01221	15.62
Nickel(II) - octabutoxy-phthalocyanine	14	10000063	9996281	3782	0.092088	0.084192	0.007896	16.73
	15	10000031	9996688	3343	0.099951	0.102176	-0.002225	14.79
	16	10000031	9996781	3250	0.080869	0.078626	0.002243	14.38
Cobalt (II) phthalocyanine	17	10000031	9999469	562	0.089802	0.015078	0.074724	2.48
	18	10000031	9999719	312	0.101845	0.019268	0.082577	1.38
	19	10000031	9999313	718	0.08552	0.009752	0.075768	3.17
Nickel(II) phthalocyanine	20	10000063	9998969	1094	0.104586	0.035499	0.069087	4.84
	21	10000031	9998188	1843	0.053211	0.010192	0.043019	8.15
	22	10000031	9998313	1718	0.07258	0.016771	0.055809	7.60
Copper (II) phthalocyanine	23	9999938	9997844	2094	0.065977	0.050556	0.116533	9.26
	24	10000031	9999813	218	0.089904	0.01515	0.038394	0.964
	25	9999844	9999625	219	0.087668	0.054998	0.03267	0.969

Table (6-8) Parameter of crystals with selected PCs compound before and after coating.

6.8 Film characterization:

Validation of film characteristics has been established using complementary existing methods such as Ellipsometry, UV- Visible absorption Spectrophotometer and AFM.

This was undertaken as properties of the film play essential role in sensor behaviour.

6.8.1 UV–Vis absorption spectra

To observe the UV absorbance properties of Pc films, UV–Vis spectroscopy was utilized. The samples of Pc films were prepared on pure glass wafers and Varian 50 UV- visible spectrophotometer was used to measure electronic absorption spectra of nine films studied in this thesis.

As figure (6-17) shows, the UV–Vis absorption spectra of Zn_tb_Pc is characterized with two strong absorption regions. One in the wave length range of (600 - 750) nm (Q-band) is assigned to ($a_{2u} \rightarrow e_g$) ($\pi \rightarrow \pi^*$) transitions and another in the range of (300 - 400) nm (B- band) are ascribed to transitions. Where a_{1u} and a_{2u} are two highest occupied molecular orbital (HOMO) and e_g is the lowest unoccupied molecular orbital (LUMO).

Furthermore, it can be seen that the Q-band absorption is split into peaks with different intensity. This separation can be interpreted to aggregation in chloroform solution, where the aggregation in phthalocyanine molecules occurs via intermolecular ($\pi \rightarrow \pi^*$) interaction.

The electronic absorption spectra of all films in this study are presented in figure (6-22)

The absorption spectrums of Pc compounds are reported elsewhere [12, 13].

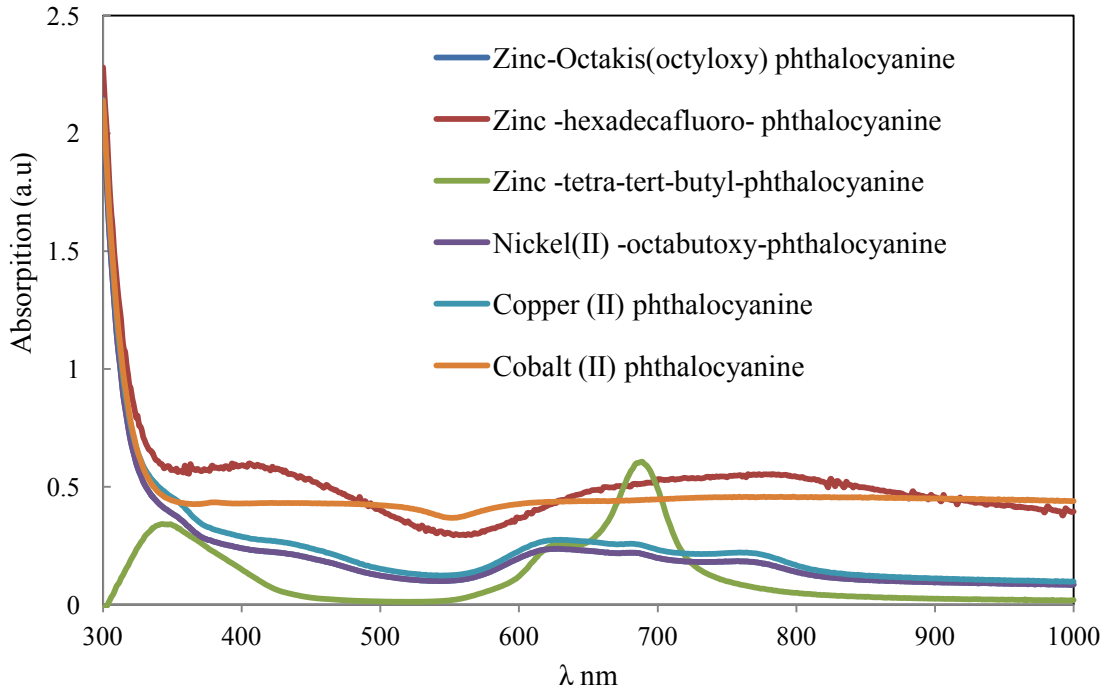

Figure (6-22). the UV-visible spectra for studied film.

6.8.2 Ellipsometry measurements:

Ellipsometry measurements described in chapter four were used to obtained films thicknesses of the same sample were used for AFM measurements. Additionally, the thickness for all coated films was calculated directly from the frequency shift using the Sauerbrey equation. Comparisons between calculated and measured film thickness value are reported in table (6-9)

Notable differences were obtained in the calculation of film thickness as compared to film thickness obtained from the Ellipsometry. This can be attributed to the effects of the viscoelastic film.

crystal	$Comboned$	Calculated Film $thickness\ nm$	Measured film $thickness\ nm$	ΔT_f
1	Zn-oct-oct-Pc	33.8	116.2	82.4
2	Zn-oct-oct-Pc	35.4		80.8
3	Zn-oct-oct-Pc	53.92		62.28
4	Zn-hexa-Pc	60.6	130.64	70.04
5	Zn-hexa-Pc	74.68		55.96
6	Zn-hexa-Pc	70.32		60.32
7	Zn-octa-Pc	23.5	82.13	58.63
9	Zn-octa-Pc	27.18		54.95
10	Zn-octa-Pc	12.72		69.41
12	Zn-tp-tb-Pc	19.08	56.8	37.72
13	Zn-tp-tb-Pc	15.62		41.18
14	Ni(II)-oct-Pc	16.73	73.5	56.77
15	Ni(II)-oct-Pc	14.79		58.71
16	Ni(II)-oct-Pc	14.38		59.12
17	Co(II)-Pc	2.48	154	151
18	Co(II)-Pc	1.38		152.62
19	Co(II)-Pc	3.17		150.83
20	Ni(II)-Pc	4.84	142	137.16
21	Ni(II)-Pc	8.15		133.85
22	Ni(II)-Pc	7.60		134.4
23	Cu(II)-Pc	9.26	56.4	47.14
24	Cu(II)-Pc	0.964		55.44
25	Cu(II)-Pc	0.969		55.43

Table (6-9) Comparisons between values of calculated and measured film thickness.

6.8.3 AFM measurements:

Investigation of Pcs films morphology was carried out using AFM measurements, where AFM measurements in tapping mode have been implemented on all samples in this study. Thin films of selected Pcs were prepared using spin coating of their solutions in chloroform in concentration of 10 *mg/ml* at room temperature, were then spun at 2000rpm onto silicon substrates. Finally vaporization of the chloroform leaves the desired film spread across the substrate.

AFM picture as figures from (6-23) to (6-31) shows typical features and corresponding cross-sections of Pc films deposited onto silicon substrates and the roughness analysis of

AFM images (the main roughness “Ra”, standard deviation “RMs” and maximum height “ Rmax”) are summarised in table (6-10)

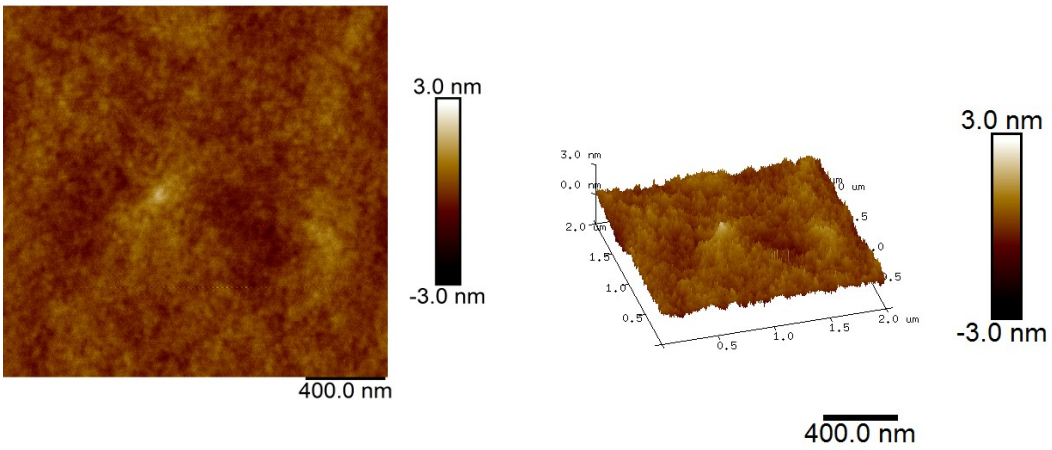

Figure (6-23) AFM image of *Zn-tb-pc* film.

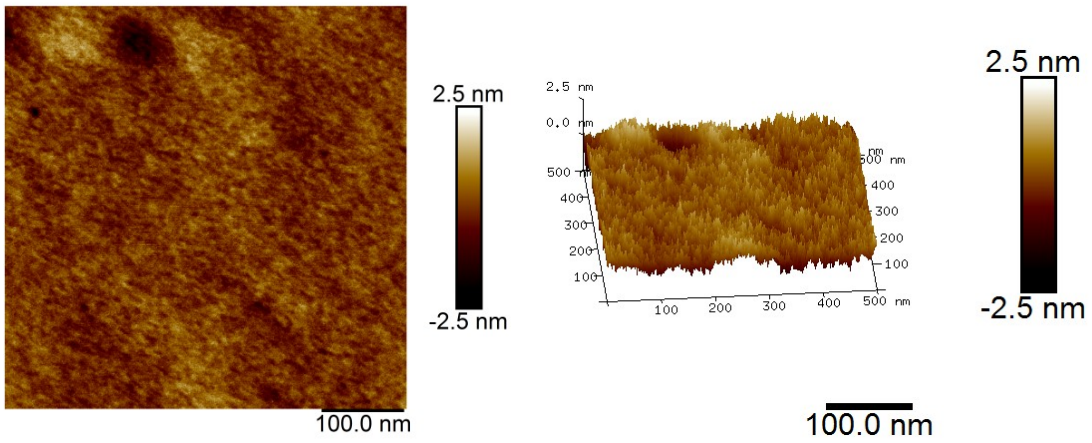

Figure (6-24) AFM image of Zn-hexa-Pc film.

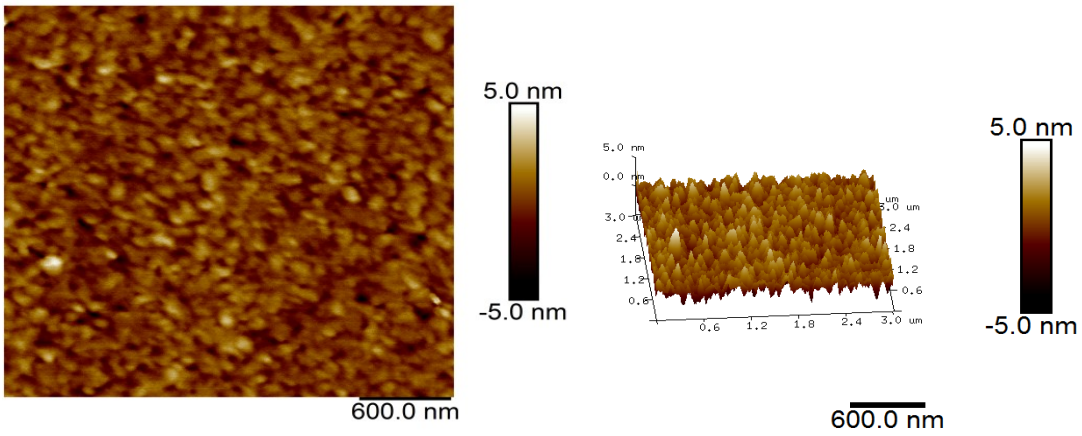

Figure (6-25) AFM image of *Zn-nph-pc* film.

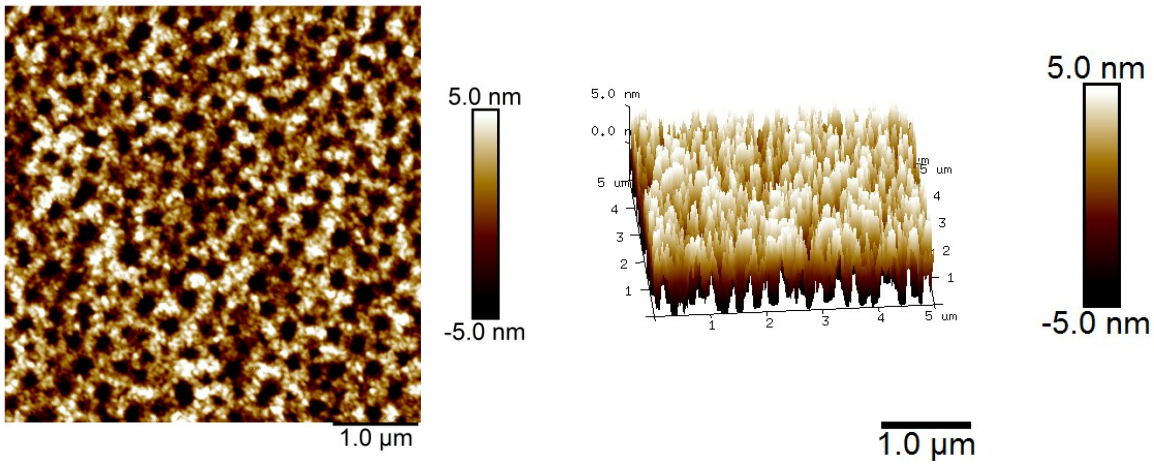

Figure (6-26) AFM image of Zn-oct-oct-Pc film.

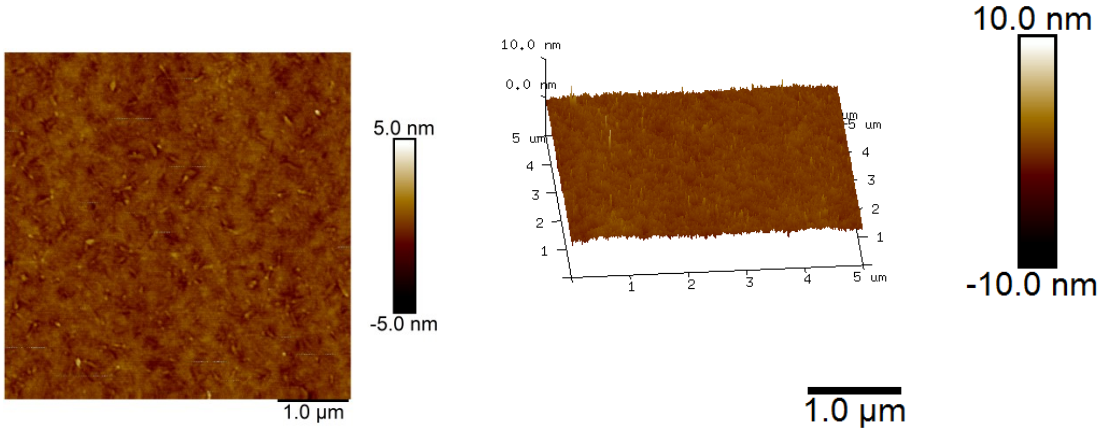

Figure (6-27) AFM image of Zn-octa-Pc film.

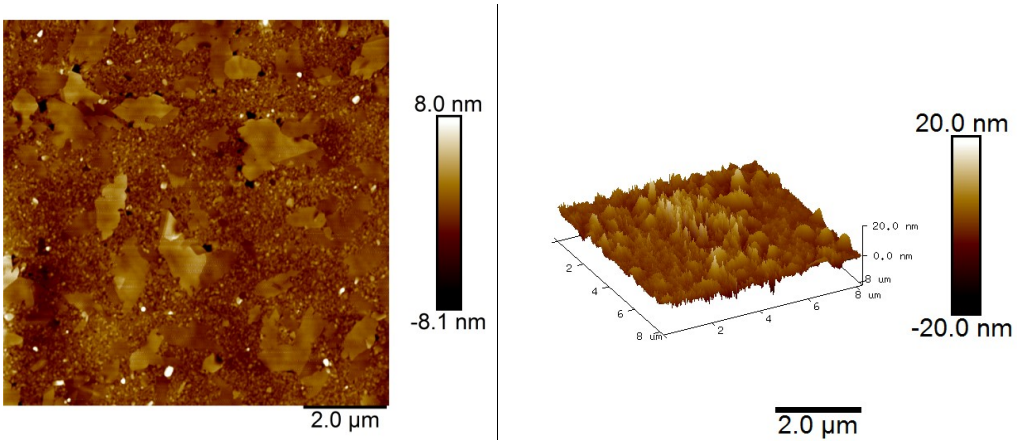

Figure (6-28) AFM image of Ni(II)-oct-Pc film.

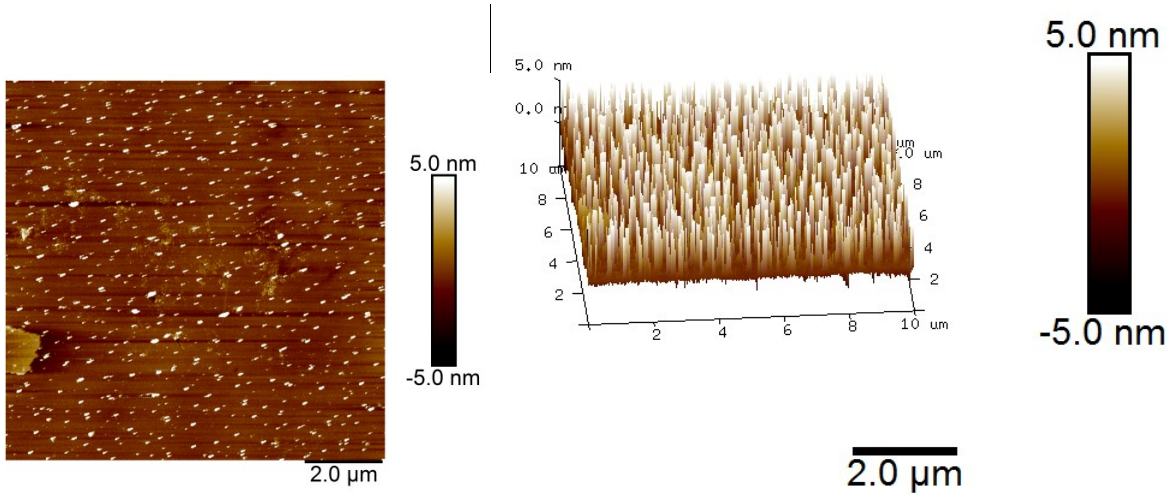

Figure (6-29) AFM image of Co(II)-Pc film.

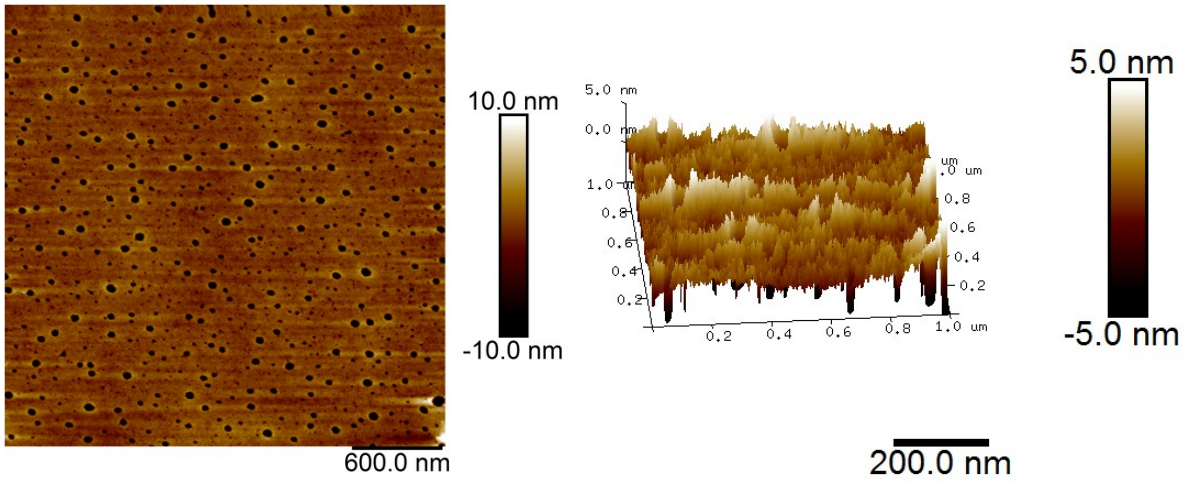

Figure (6-30) AFM image of Zn-oct-oct-Pc film.

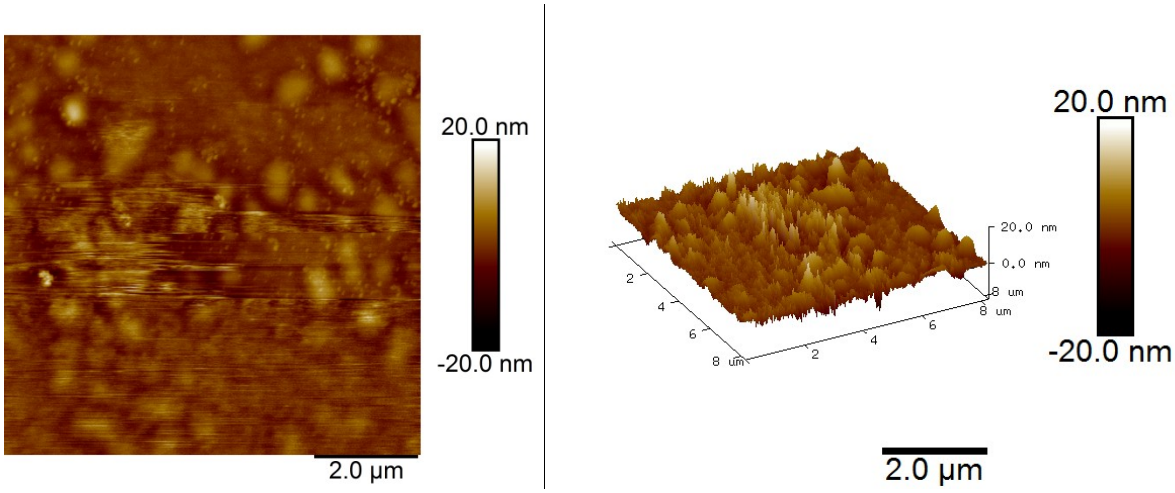

Figure (6-31) AFM image of Cu(II)-Pc film.

Film	R_a nm	RMS, nm	R_{max}, nm
Zn-oct-oct-Pc	0.913	0.285	7.345
Zn-hexa-Pc	0.463	0.562	2.615
Zn-tp-tb-Pc	0.729	0.989	2.325
Zn-octa-Pc	0.514	1.007	3.546
Ni(II)-oct-Pc	0.643	0.172	0.864
Co(II)-Pc	0.155	3.697	7.948
Cu(II)-Pc	1.823	1.624	3.275
Ni(II)-Pc	0.569	1.162	14.475
Zn-tp-tb-nPc	1.262	1.298	3.788

Table (6-10) Roughness parameters of all films.

6.9 Summary

As preliminary measurements, two sensitive members of substituted ZnPcs have been successfully employed associated with QCR measurements techniques (oscillator circuit, impedance analysis) to detect VOC gases.

A thin film of sensitive material has been achieved using spin coating technique which clearly produces a frequency shift.

Three QCR frequency only measurements were tested for all organic solvents and show a good level of discrimination. Moreover, impedance analysis measurement gives additional electrical parameters [R_f,L_f] of target tested material (film) which related with mass loading and change in film viscosity caused by vapour adsorption.

After satisfactory response from preliminary measurements, eight more material have been investigated. Full film characterization was performed to confirm film validation, the film thickness and morphology was carried out using Ellipsometry and AFM measurements respectively.

References:

1- Basova, T., Tsargorodskaya, A., Nabok, A., Hassan, A., Gürek, A., Gümüs, G., & Ahsen, V. (2009). Investigation of gas-sensing properties of copper phthalocyanine films. *Materials Science and Engineering: C, 29*(3), 814-818.

2- Harbeck, M., Erbahar, D. D., Gürol, I., Musluoğlu, E., Ahsen, V., & Öztürk, Z. Z. (2011). Phthalocyanines as sensitive coatings for QCM sensors: Comparison of gas and liquid sensing properties. *Sensors and Actuators B: Chemical, 155*(1), 298-303.

3- Kobayashi, N. (1999). Phthalocyanines. *Current Opinion in Solid State and Materials Science, 4*(4), 345-353.

4- McKeown, N. B. (1998). *Phthalocyanine materials: Synthesis, structure and function* Cambridge University Press.

5- Moser, F. H., & Thomas, A. L. (1964). Phthalocyanine compounds. *Journal of Chemical Education, 41*(5), 245.

6- Mukherjee, D., Manjunatha, R., Sampath, S., & Ray, A. K. (2017). Phthalocyanines as sensitive materials for chemical sensors. *Materials for chemical sensing* (pp. 165-226) Springer.

7- Nalwa, H., Shirk, J., Leznoff, C., & Lever, A. (1996). Phthalocyanines: Properties and applications. *By CC Leznoff and ABP Lever, VCH Publications, New York, 4*

8- Zhou, R., Josse, F., Göpel, W., Öztürk, Z., & Bekaroğlu, Ö. (1996). Phthalocyanines as sensitive materials for chemical sensors. *Applied Organometallic Chemistry, 10*(8), 557-577.

9- Hassan, A., Ray, A., Nabok, A., & Wilkop, T. (2001). Kinetic studies of BTEX vapour adsorption onto surfaces of calix-4-resorcinarene films. *Applied Surface Science, 182*(1-2), 49-54.

10- Kasai, N., Sugimoto, I., Nakamura, M., & Katoh, T. (1999). Odorant detection capability of QCR sensors coated with plasma deposited organic films. *Biosensors and Bioelectronics, 14*(6), 533-539.

11- Kumar, A., Brunet, J., Varenne, C., Ndiaye, A., Pauly, A., Penza, M., & Alvisi, M. (2015). Tetra-tert-butyl copper phthalocyanine-based QCM sensor for toluene detection in air at room temperature. *Sensors and Actuators B: Chemical, 210*, 398-407.

12- Claessens, C. G., Hahn, U., & Torres, T. (2008). Phthalocyanines: From outstanding electronic properties to emerging applications. *The Chemical Record, 8*(2), 75-97.

13- Sakamoto, K., & Ohno-Okumura, E. (2009). Syntheses and functional properties of phthalocyanines. *Materials, 2*(3), 1127-1179.

CHAPTER SEVEN:

RESULT AND EXPERIMENTAL DISCUSSION

This chapter gives an extended analysis of vapour exposure to the selected substituted ZnPcs. The films that demonstrated the highest performance in terms of sensitivity have been further investigated and material evaluated. Moreover, the sensitive material shear modulus results are also discussed.

- **Vapour exposure results:**
- **Results of QCR impedance measurements for the compared materials:**
- **Evaluation and analysis of non gravimetric film responses:**
- **Sensitive materials shear modulus analysis:**

7.0 Chapter overview:

This chapter provides an extended analysis of vapour exposure as related to the proposed work and gives an overview of the sensing performance of the materials that were used.

The first part of this chapter focuses on the frequency response of one coated film to four different analytes used in this study. While the second part gives one typical examples of frequency responses of four coated ZnPc films to toluene analytes over a range of concentrations.

The investigation of the change in resonance frequency of peak of QCR sensors coated with synthesise ZnPc against concentration of tested analytes (Benzene, Hexane, Ethanol and Toluene) are reported. The sensing performance of studied material including response time, sensitivity and selectivity are also discussed. Finally the sensitive material shear modulus has been reviewed.

A typical impedance measurement protocol was carried out as described in chapter four

Exposure of the film coated crystal resonator to varying concentrations of tested analytes vapours was undertaken utilizing the Teflon chamber depicted in section 5.5.2.

Between each concentration as in previous experiments the vapour was allowed to totally desorb from the film by purging the chamber with flush air. For each concentration exposure, resonant frequency of the film coated resonator and elements of equivalent circuit were recorded.

The fitting procedure as described in section 5.6 are used to obtain the measured values of film parameters R_f, L_f during the vapour exposure, where the admittance spectra of uncoated QCR fitted before to BVD circuit model and parameters of both motional arms R, L, C and parallel capacitance C_0 was extracted and recorded. In gas phase, the parameters (C) elasticity of quartz and (C_0) the capacitance between two electrodes applied on quartz should be remains constant during fitting process [1, 2]. Consequently, the film parameters are determined from variation between uncoated and exposure values. As a general trend, definite shifts in the resonance peak of QCR sensors coated with (Zinc- phthalocyanine) exposed to range of vapours concentrations are observed. An example frequency response of Zn-oct-oct-Pc exposure to tested analytes is illustrated in Figure (7-1). Also the change in admittance magnitude in addition to frequency can be interpreted as a viscous film response (film damping and mass loading) (see section 7.1).

The different films have varying levels of sensitivity to the target vapours. The Zn-oct-oct-Pc film show considerable co linearity of the sensor responses with all tested vapours. As depicted in Figure (7-1) the response curve demonstrate clear well defined and consistent response characteristics of the Zn-oct-oct-Pc coated QCR sensors.

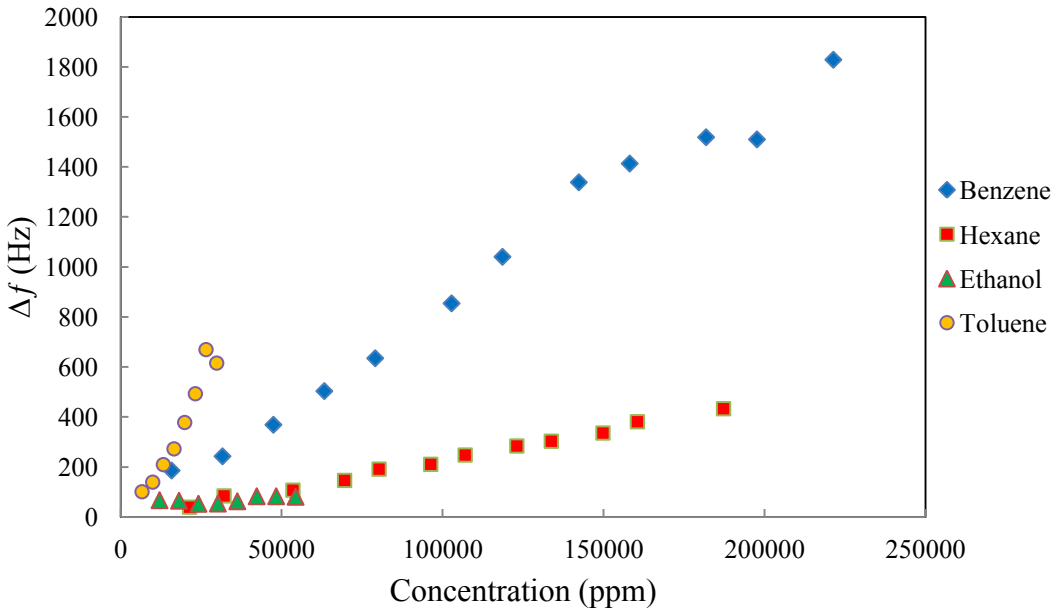

Figure (7-1) Frequency response of Zn-oct-oct-Pc coated QCR exposed to several concentrations of tested vapours.

Also toluene vapour appears to be more sensitive than other analytes vapour, this could be attributed to the relative values of vapour pressure as table (5-1) shows.

Therefore, in the next section toluene was selected as a suitable benchmark to measure and classify the sensitivity relative to each film tested in this study.

All films demonstrated a high response to toluene within the range of concentrations tested. This is shown in absolute units of parts per million and relative vapour pressure, figure (7-2a) and (7-2b) respectively. Additionally both Zn-octa-Pc and Zn-tp-tb-Pc have a similar response and greater sensitivity to Toluene as compared to other synthesised ZnPcs. showing two distinguishably different response trends between the other Pcs as depicted in figures (7-2a, 7-2b).

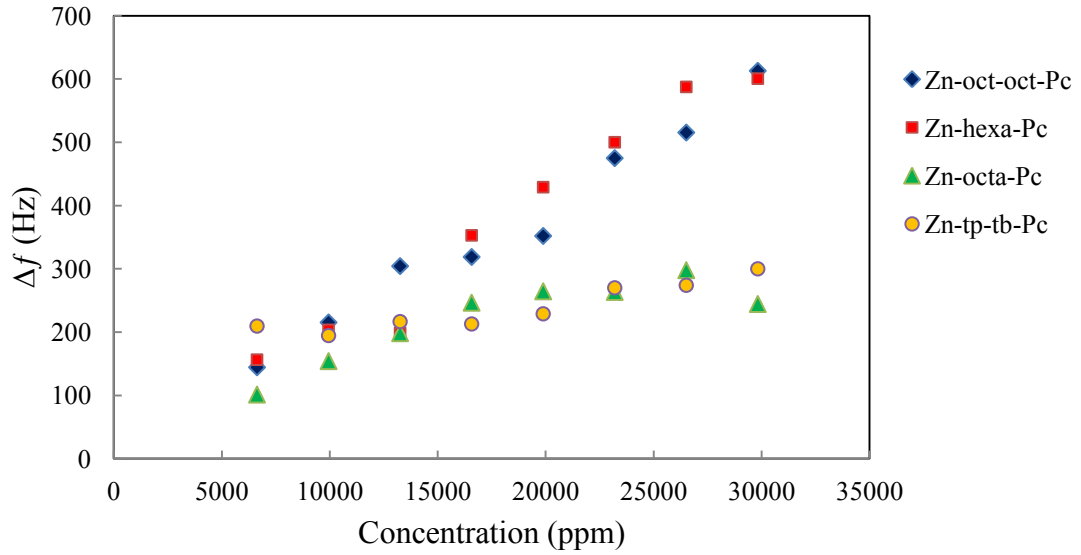

Figure (7-2a) Frequency response of coated QCR exposed to several concentrations of Toluene vapours in absolute units of parts per million.

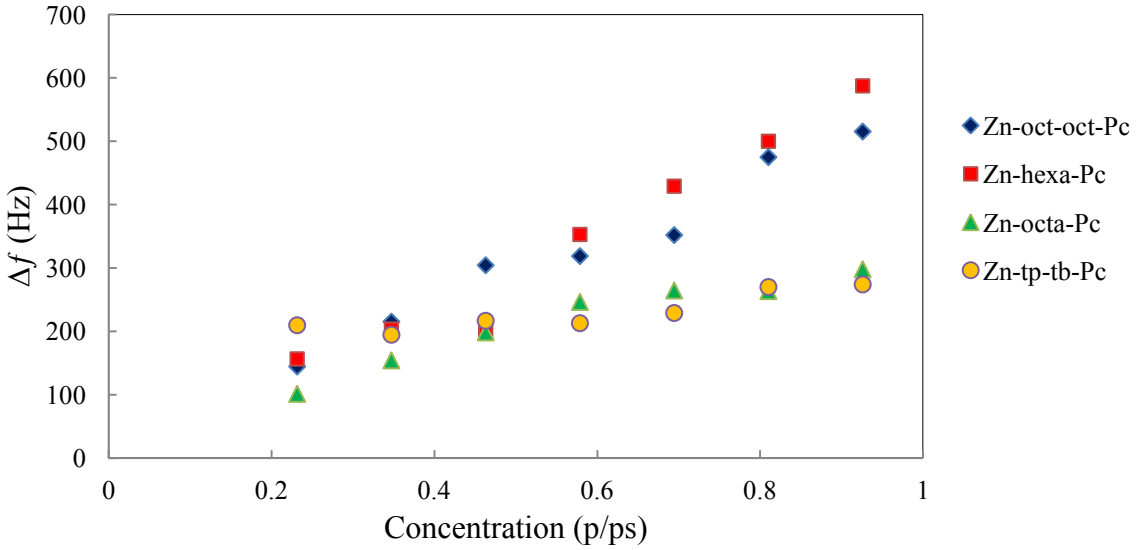

Figure (7-2b) Frequency response of coated QCR exposed to several concentrations of Toluene vapours in units of relative vapour pressure.

The change in series resonance frequency obtained from the peak of the QCR admittance spectra for sensors coated with synthesise ZnPc films against concentration of tested analytes used in this study are illustrated in Figures from (7-3) to (7-10).

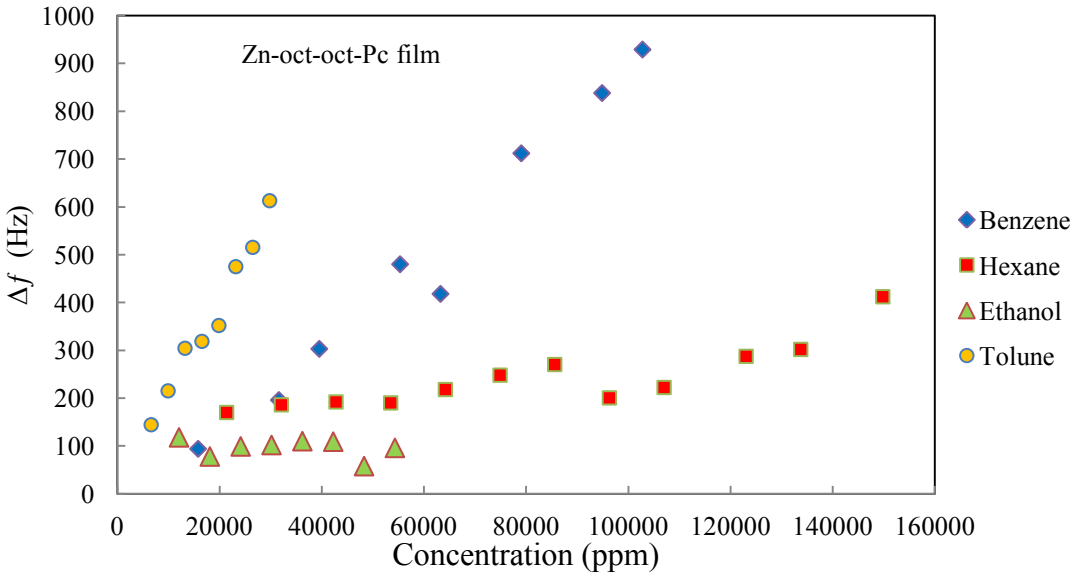

Figure (7-3) Δf Hz against concentration in ppm for Zn-oct-oct-Pc film.

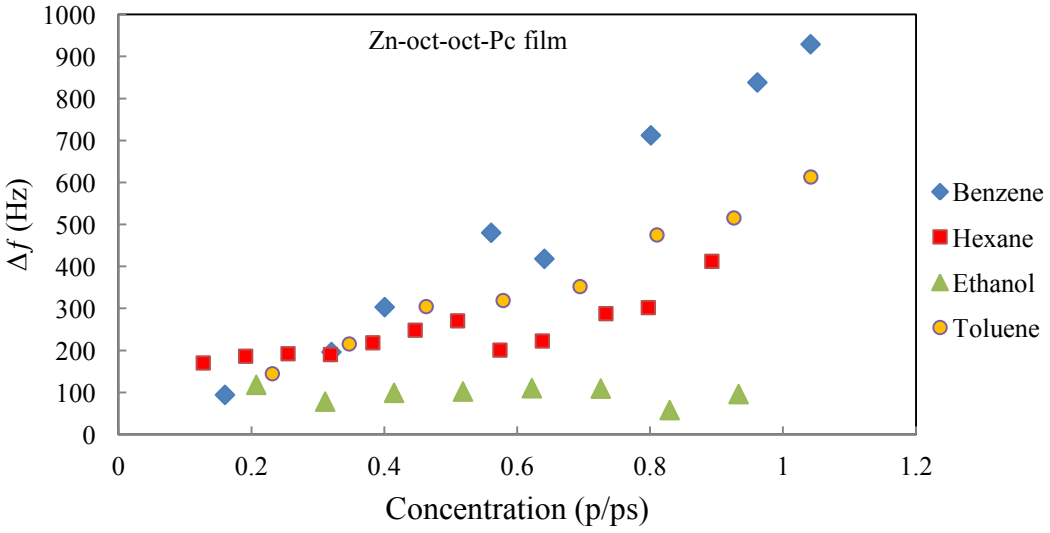

Figure (7-4) Δf Hz against concentration in p/ps for Zn-oct-oct-Pc film.

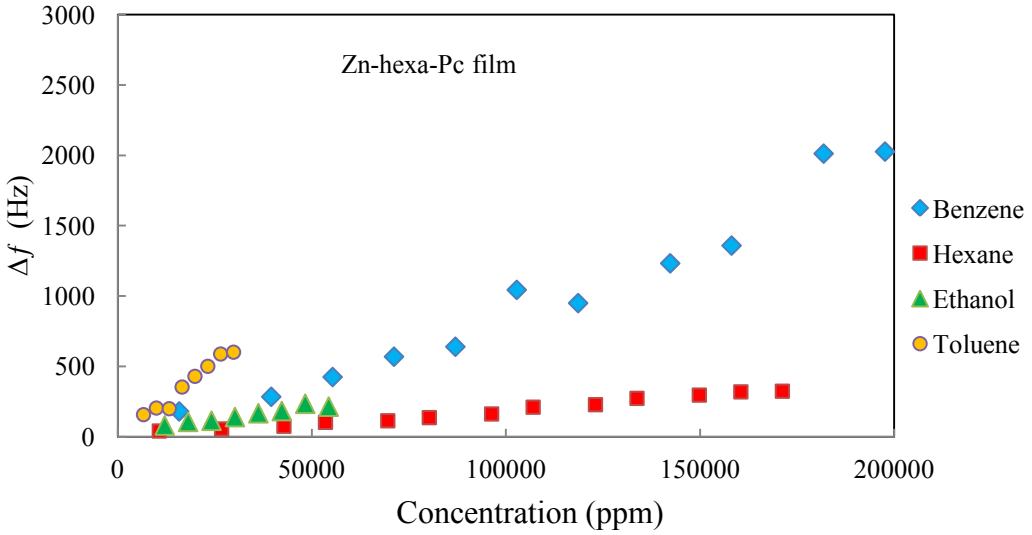

Figure (7-5) Δf Hz against concentration in ppm for Zn-hexa-Pc film.

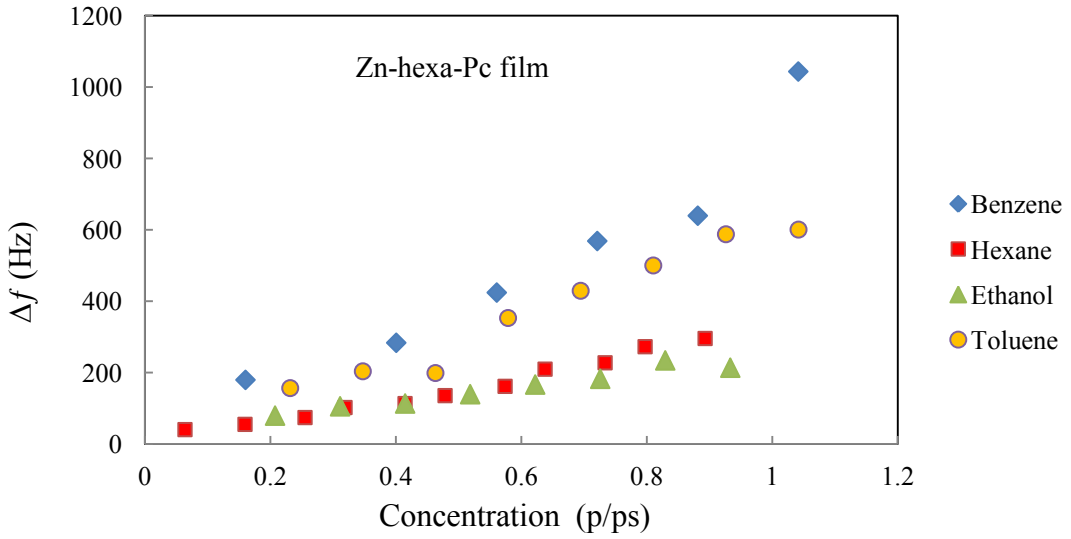

Figure (7-6) Δf Hz against concentration in p/ps for Zn-hexa-Pc film.

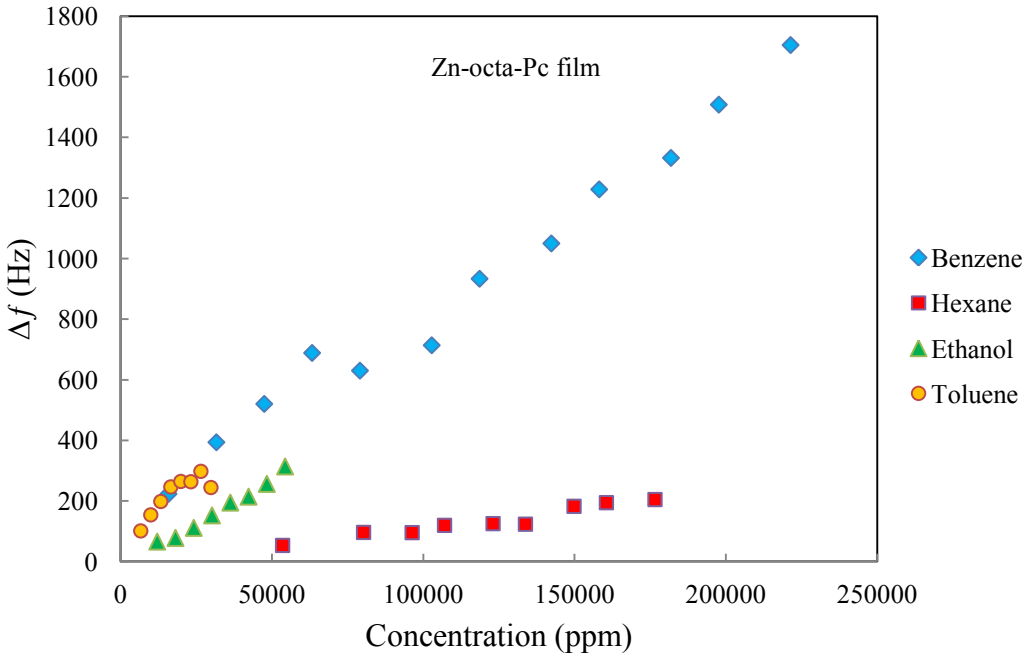

Figure (7-7) Δf Hz against concentration in ppm for Zn-octa-Pc film.

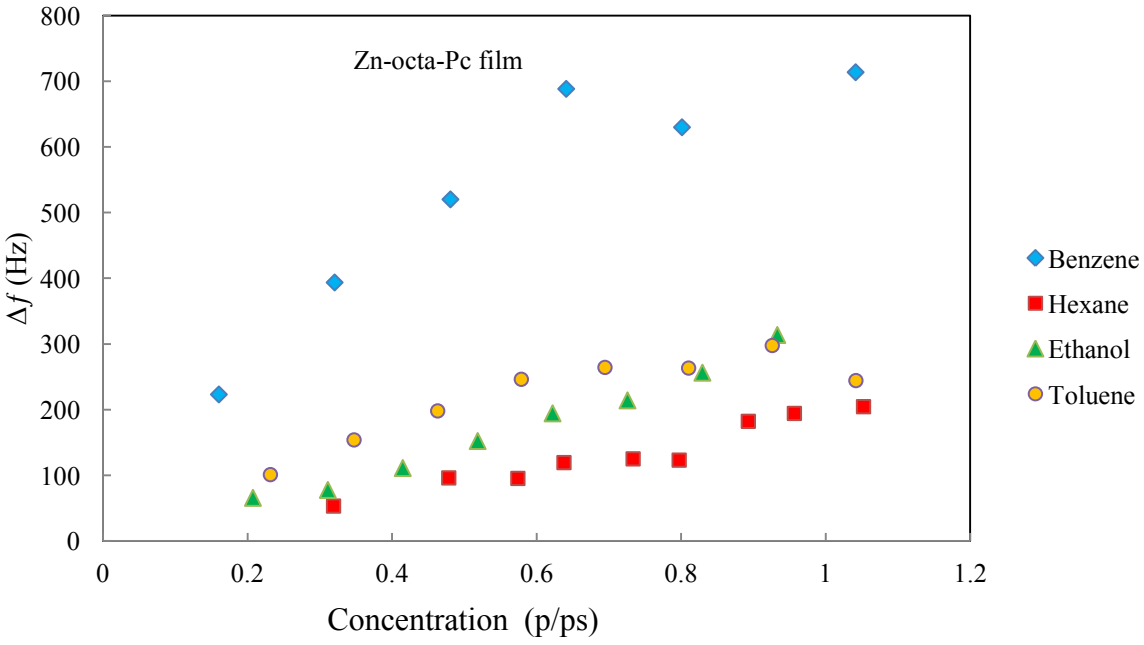

Figure (7- 8) Δf Hz against concentration in p/ps for Zn-octa-Pc film.

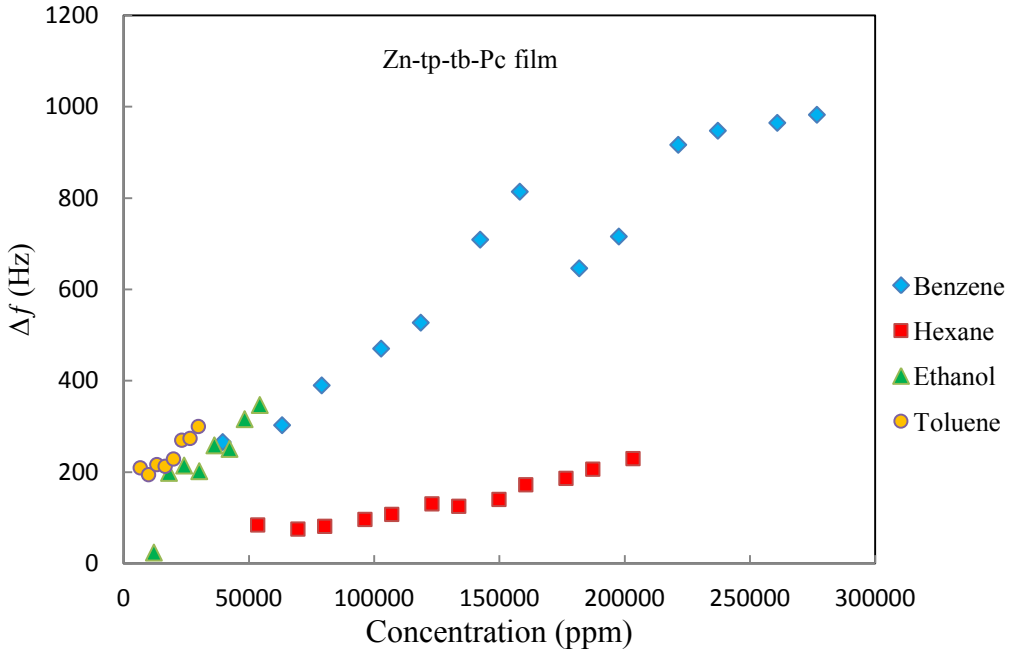

Figure (7-9) Δf Hz against concentration in ppm for Zn-tp-tb-Pc film.

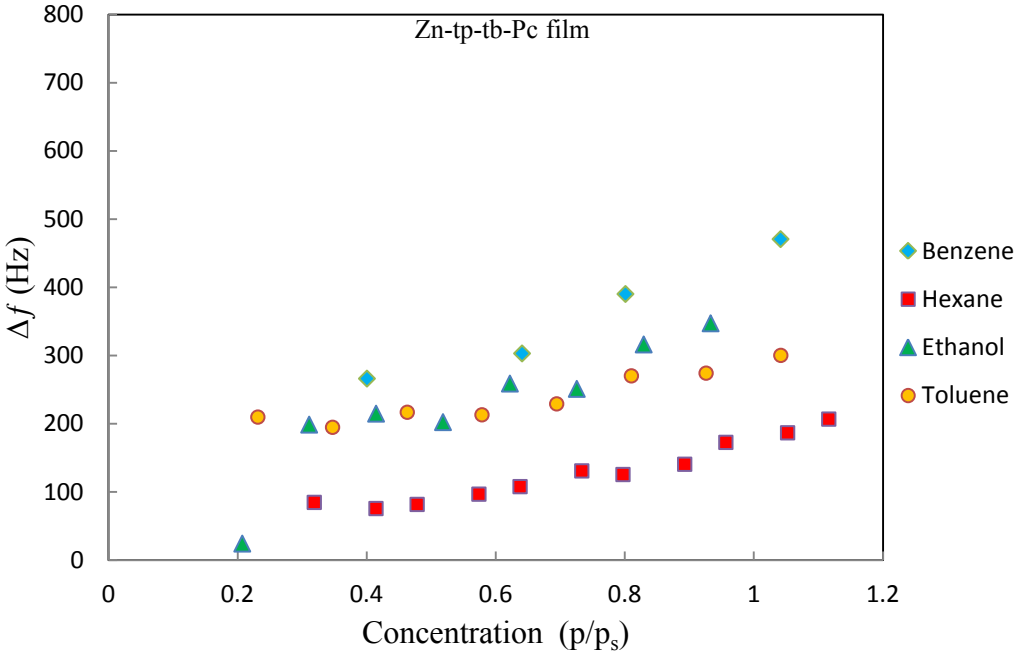

Figure (7-10) Δf Hz against concentration in p/ps for Zn-tp-tb-Pc film.

7.1 Sensing Performance:

In the following section, the attention will be focused on response time, sensitivity and selectivity of analytes exposure on sensitive material was used in this study.

7.1.1 Response time:

As definition of sensor device which is the time to reach a 90% of a signal change. [3, 4] Subsequently, the response and recovery time of exposure measurement was estimated as explained in figure (7-11). In this instance the ad/desorption measurement of 63253.9 ppm of benzene analytes is used; the frequency decreased to reach a steady state after analyte injection, the sensor response time is 7.1 min. Furthermore, the frequency increased back to the baseline after flushing the chamber and it can see that the signal recovered fast and the recovery time estimated approximately at 2.3 min. From the (6-7) and (7-11) figures that the recovery time is faster than the response time; this can be attributed to the time the analytes required to fully evaporate inside the chamber.

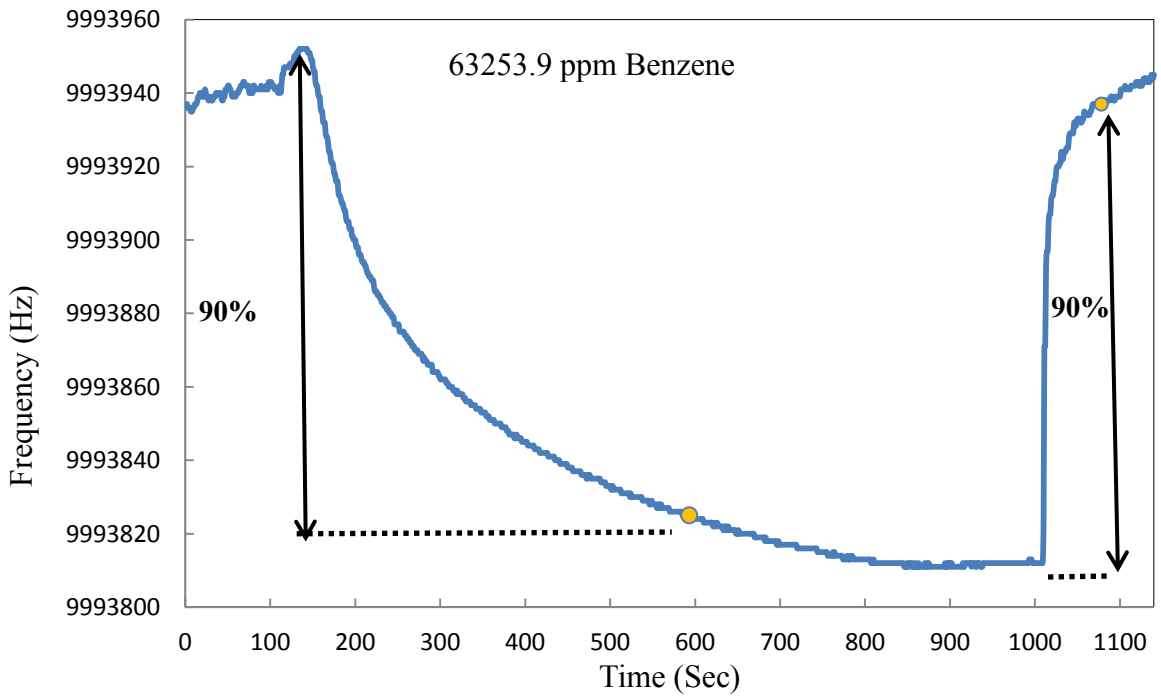

Figure (7-11) Frequency variation for one exposure to concentration of Benzene (63253.9 ppm) and recovery. Response and recovery time are represented respectively.

The response and recovery time of exposure measurements for range of concentration for the different tested analytes are listed in table (7-1).

Table 7-1

Film	Benzene (102787.6 ppm)		Hexane (107013.1 ppm)		Ethanol (36222.63 ppm)		Toluene (19879.11 ppm)	
	Response Time (min)	Recovery Time (min)	Response Time (min)	Recovery Time (min)	Response Time (min)	Recovery Time (min)	Response Time (min)	Recovery Time (min)
Zn-oct-oct-Pc	4	0.75	3.8	0.87	1.5	0.13	5.5	0.38
Zn-hexa-Pc	3.75	1	2.675	0.675	2.8	0.7	5.1	1.13
Zn-octa-Pc	3	0.5	2.17	1.17	1.7	0.43	2.55	0.7
Zn-tp-tb-Pc	3.87	0.63	3.67	0.43	1.63	0.23	3.37	1

7.1.2 Sensitivity and selectivity:

The sensitivity properties of the coated film tested for corresponding gas concentration range are defined as a slope of frequency change divided by tested gas concentration in ppm, the slope was taken from the linear fitting the data see figure (7-12). The experiments performed at room temperature.

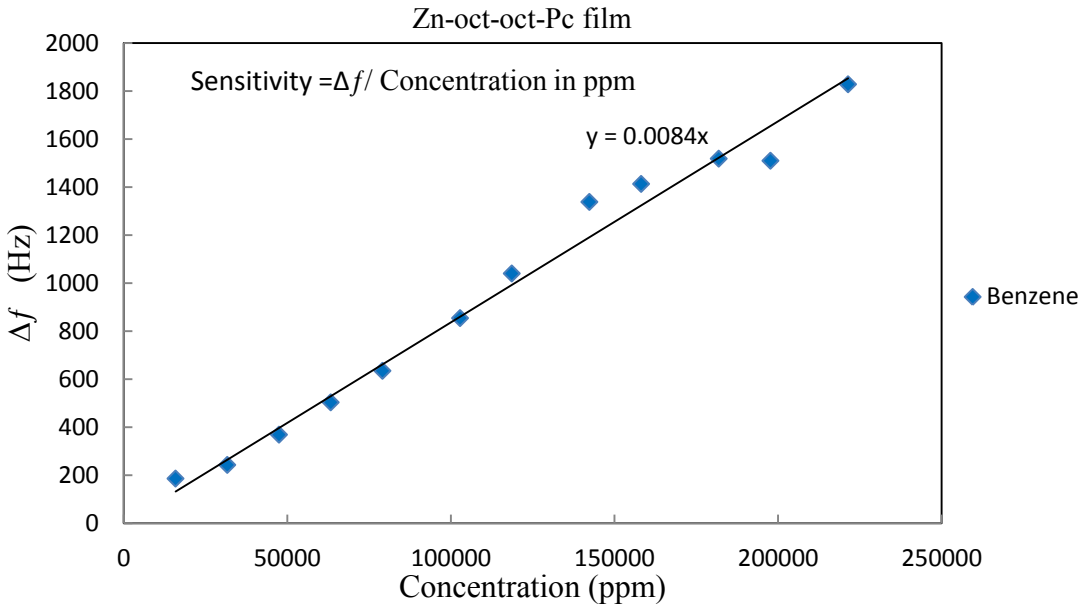

Figure (7-12) Extracting sensitivity of Zn-oct-oct-Pc film exposed to different concentrations of Benzene analytes.

Figure (7-13) shows a typical plot of data collected from vapour exposure measurements of coated QCR with Zn-oct-oct-Pc film. The plot shows how ΔR can be estimated from responses change before and after exposure to vapour. Additionally, in this work to increase measurement accuracy, the values of ΔR were extracted from subsequent fitting of the spectra to the BVD model as shown in figure (7-13), as described in section 5.6.

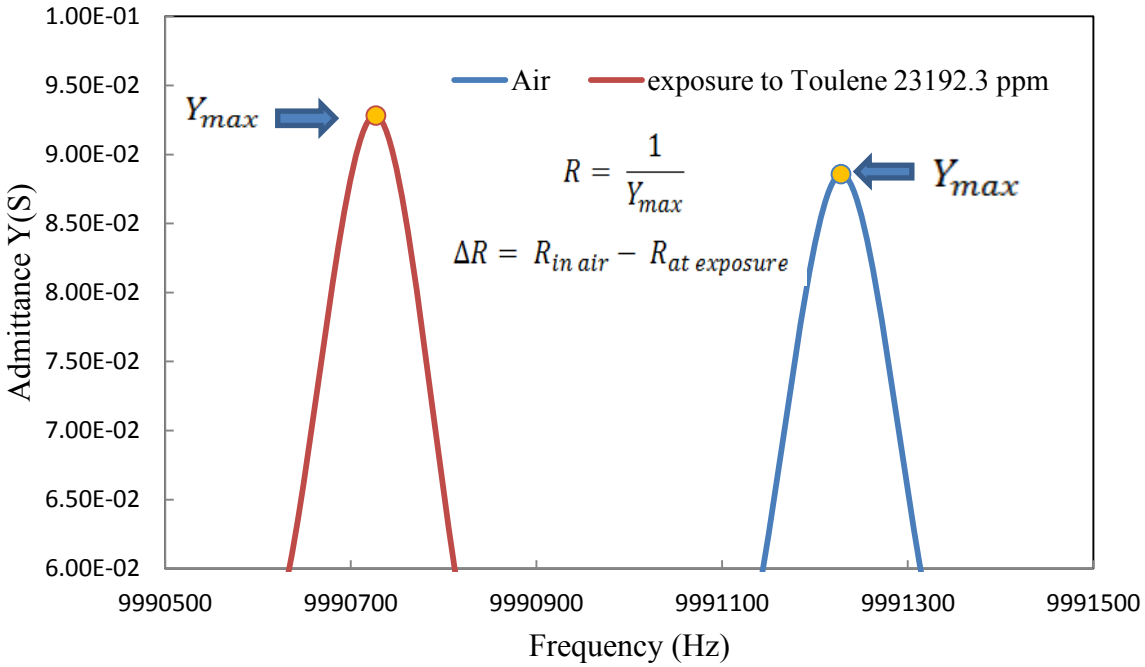

Figure (7-13) The change in admittance during a typical vapour exposure with ΔY indicated.

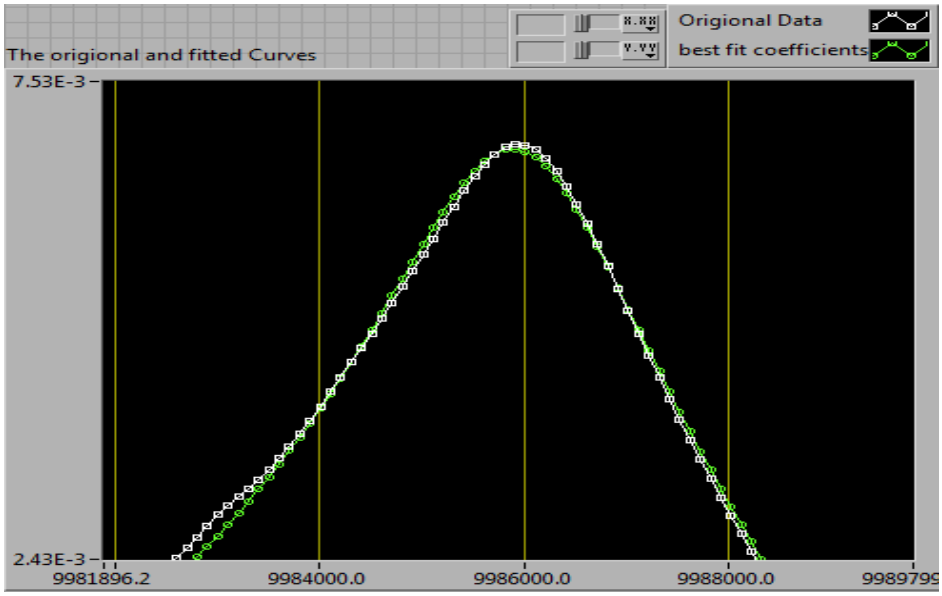

Figure (7-14) original data, of the spectra fitted to the BVD model using 4th order polynomial.

The Δf for the selected concentrations and target analtyes are plotted against concentration in ppm and saturated vapour pressure respectively. Moreover, to provide further detailed the plots are also shows the admittance spectra of exposure films. The frequency shift (Δf) and

change in magnitude (as related to ΔR of the BVD equivalent circuit) indicate changes in the films viscoelastic properties for the increasing concentrations of analytes vapours. The extracted values of Δf and ΔR from subsequent fitting of the spectra to the BVD model are shown in figures (7-14) .

Examples of responses of coated QCR with Zn-oct-oct-Pc film exposure to range of toluene vapours concentration are depicted in figure (7-15). Increases in admittance and decrease in resonant frequency point are presented in vapour adsorptions. As referred too in chapter one only a change in resonance peak indicate to a purely rigid film, in this study result, the change in admittance curve refers to viscoelastic contribution. Significant changes in mass loading and film damping are observed on vapour exposure, with an approximately linear relationship for both parameters as can be seen in figures (7-16) to (7-51).

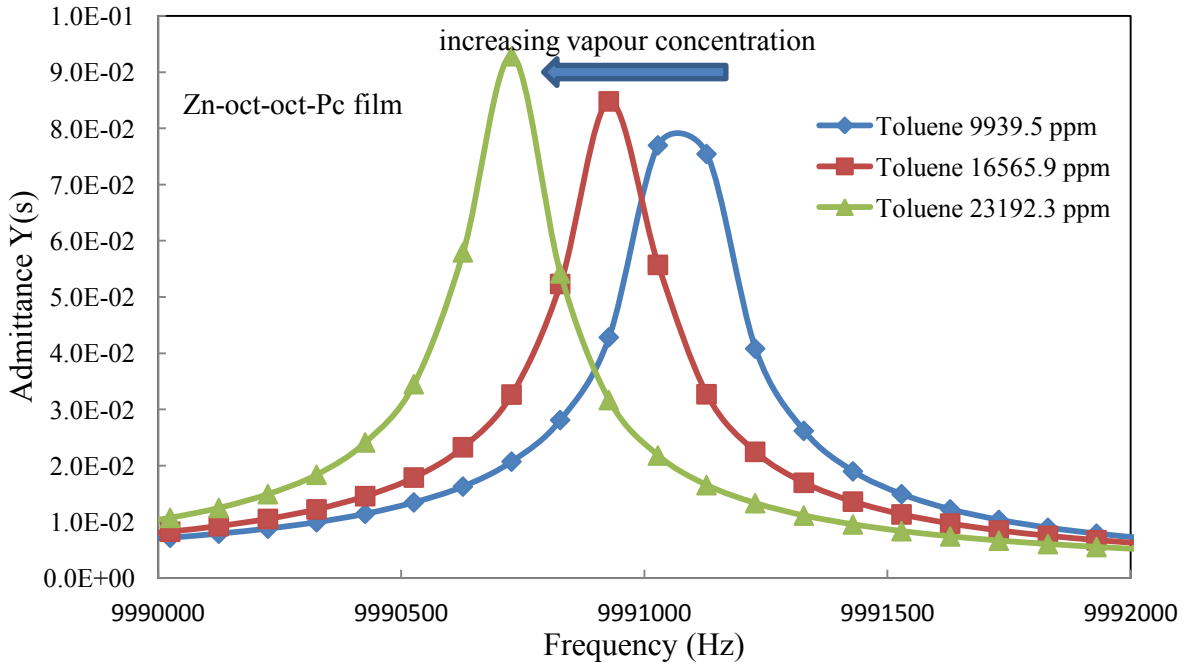

Figure (7-15) Change in admittance spectra measured at different Toluene vapour concentrations.

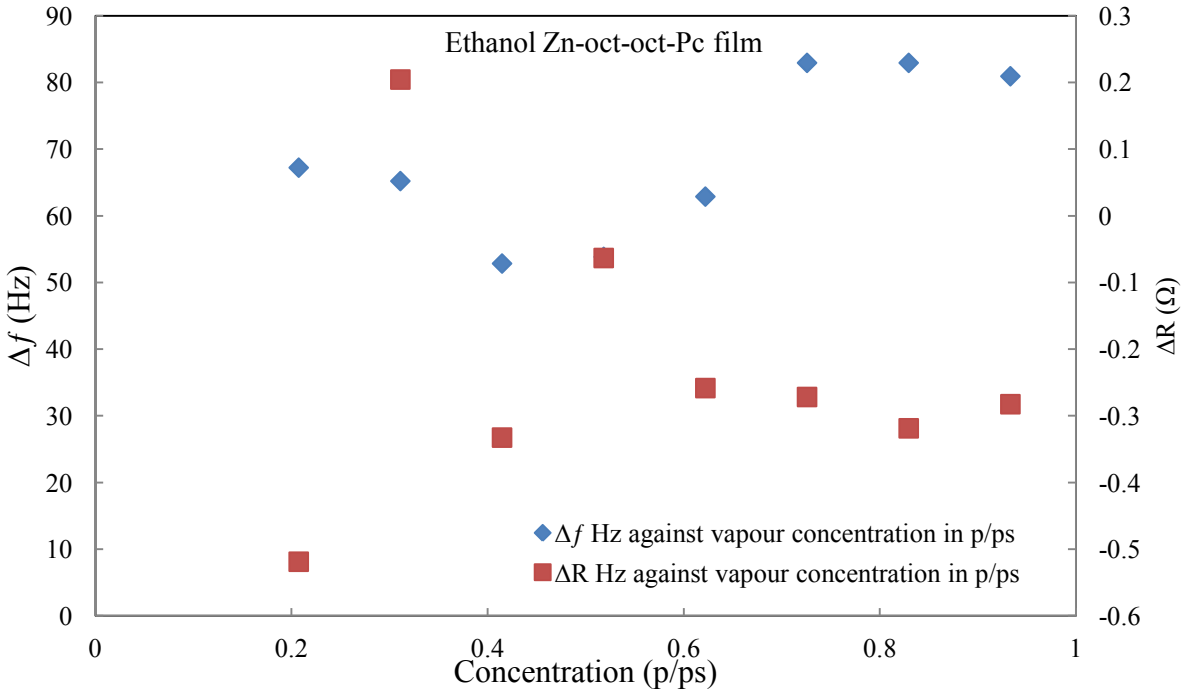

Figure (7-16). Frequency and resistance response of coated QCR (Zn-oct-oct-Pc film)

exposed to several ethanol vapour concentration in p/p_s.

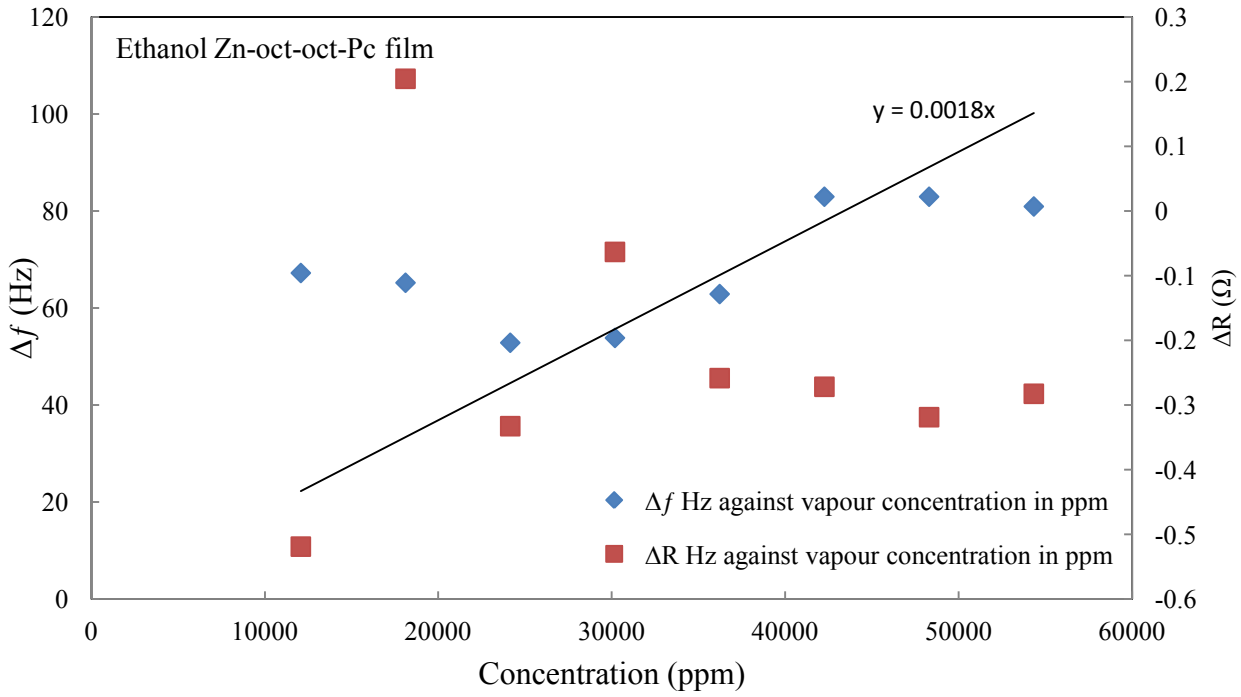

Figure (7-17) Frequency & resistance response of coated QCR (Zn-oct-oct-Pc film)

exposed to several Ethanol vapour concentration in ppm.

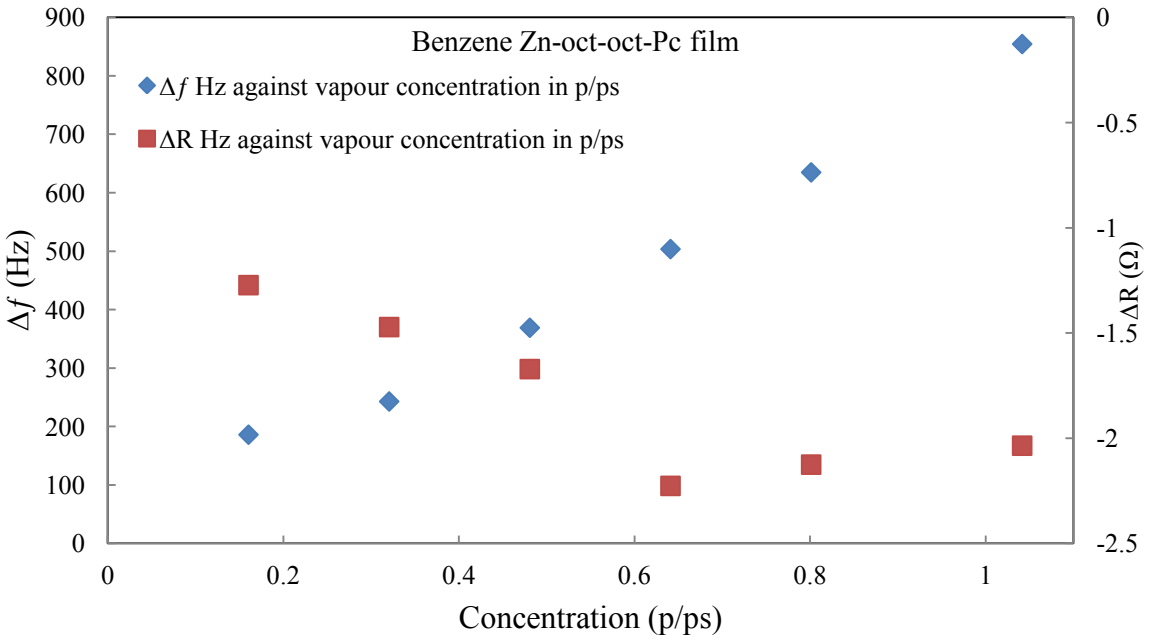

Figure (7-18) . Frequency & resistance response of coated QCR (Zn-oct-oct-Pc film) exposed to several Benzene vapour concentration in p/p_s.

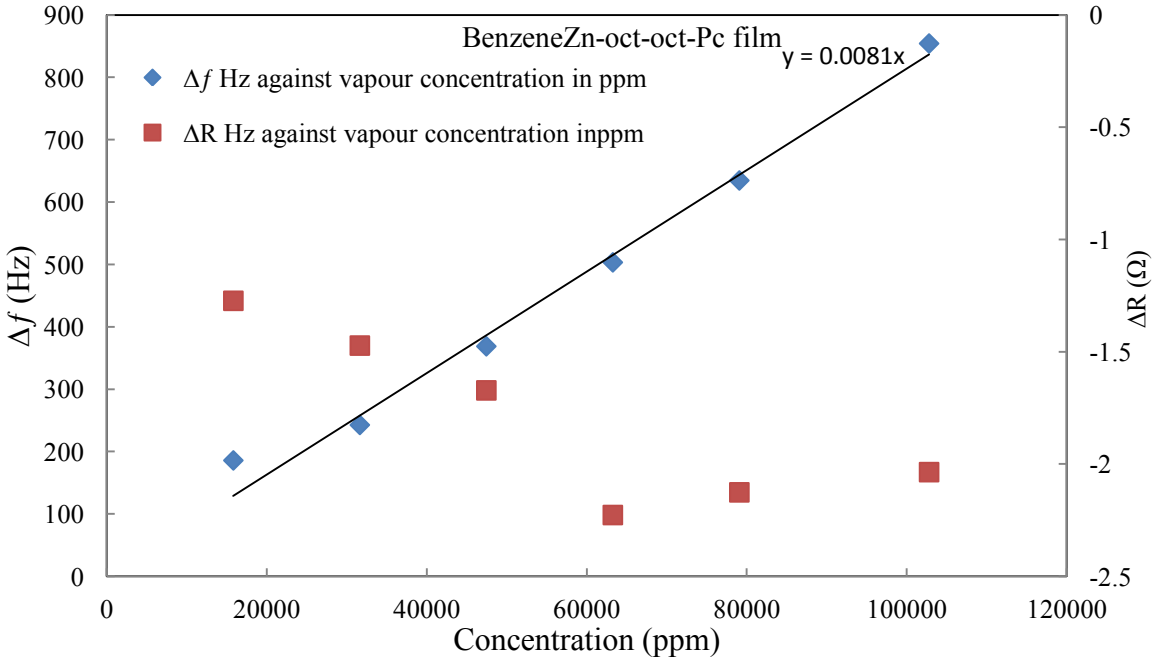

Figure (7-19). Frequency & resistance response of coated QCR (Zn-oct-oct-Pc film) exposed to several Benzene vapour concentration in ppm.

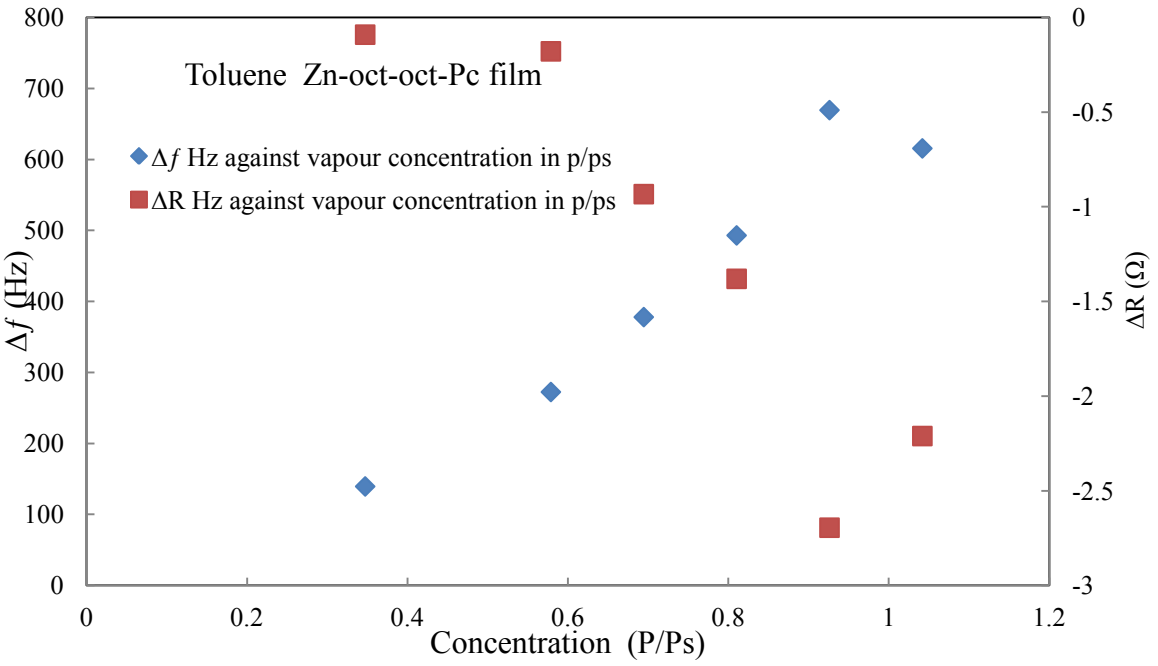

Figure (7-20) . Frequency & resistance response of coated QCR (Zn-oct-oct-Pc film) exposed to several Toluene vapour concentration in p/p_s.

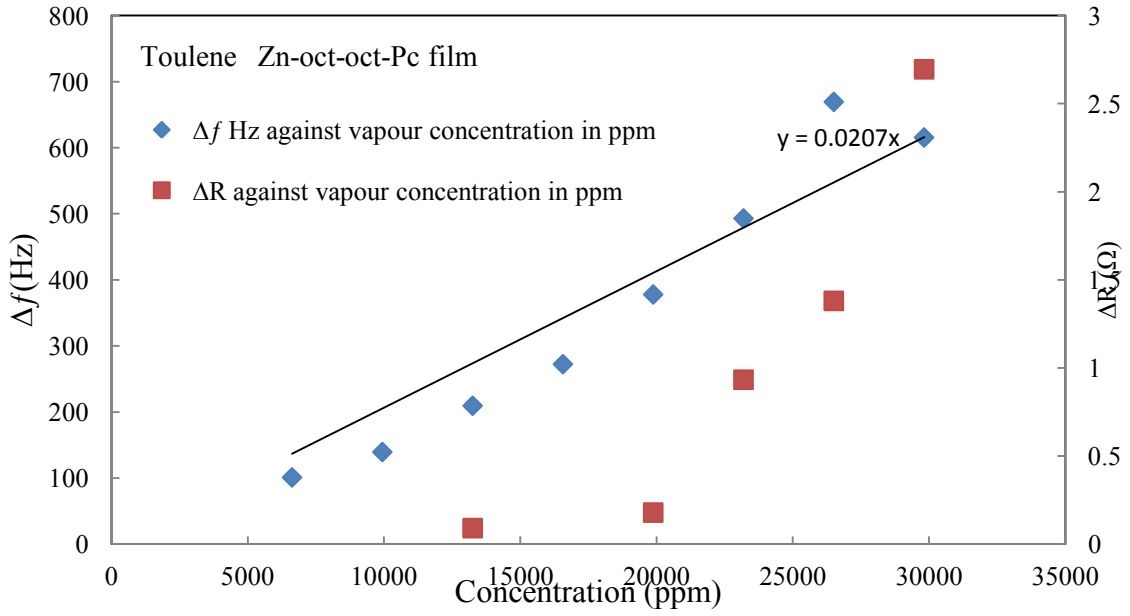

Figure (7-21) Frequency & resistance response of coated QCR (Zn-oct-oct-Pc film) exposed to several Toluene vapour concentration in ppm.

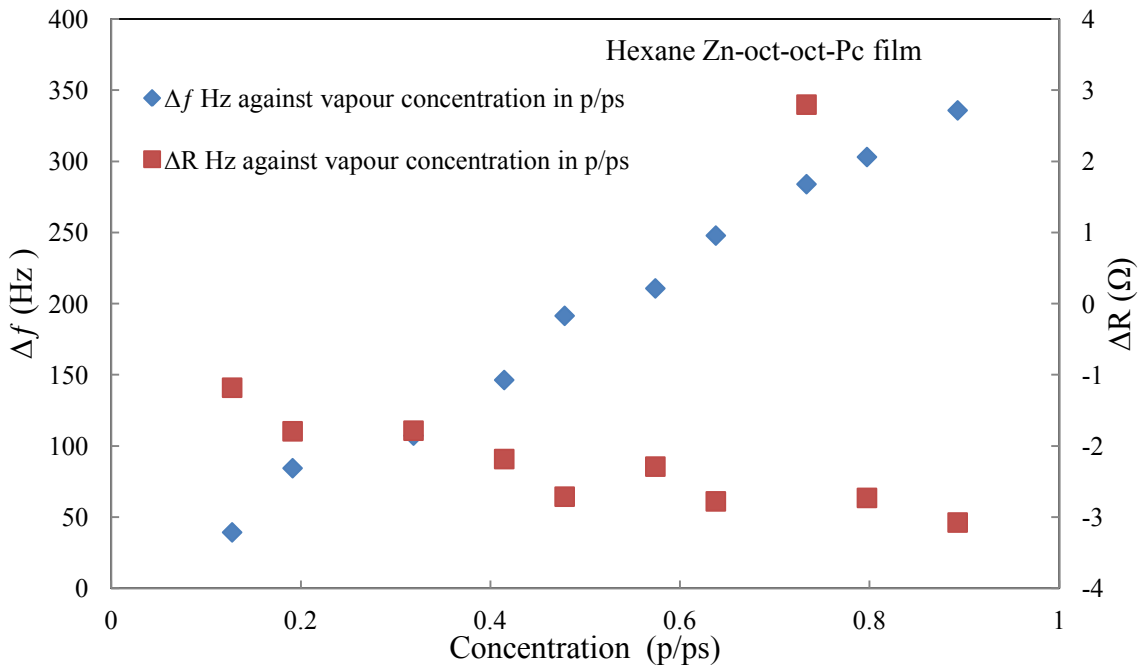

Figure (7-22) Frequency & resistance response of coated QCR (Zn-oct-oct-Pc film) exposed to several Hexane vapour concentration in p/p_s.

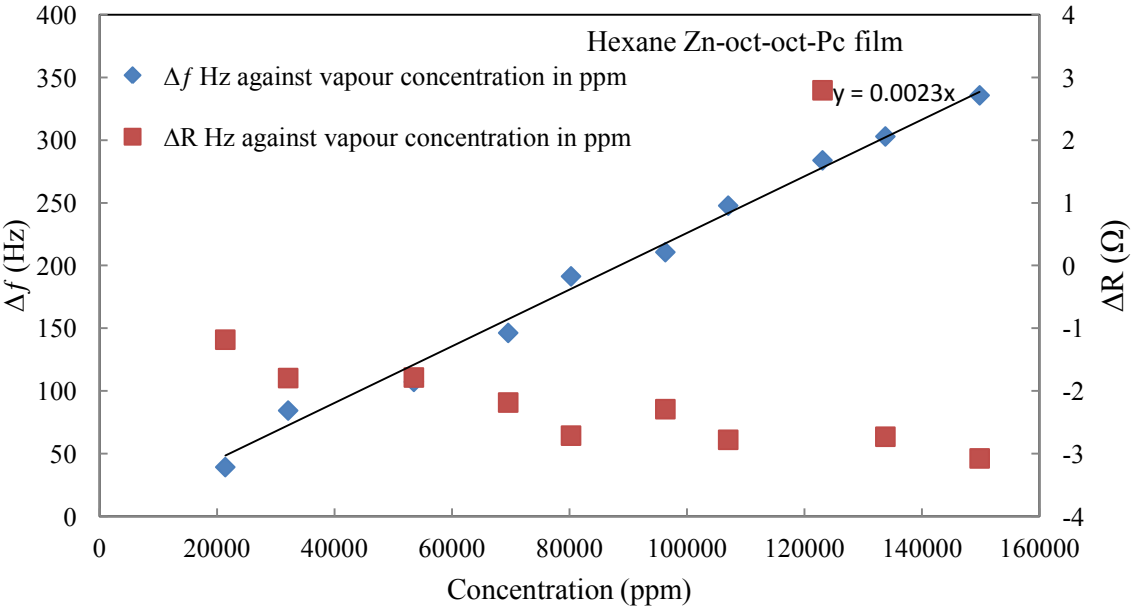

Figure (7-23) Frequency & resistance response of coated QCR (Zn-oct-oct-Pc film) exposed to several Hexane vapour concentration in ppm.

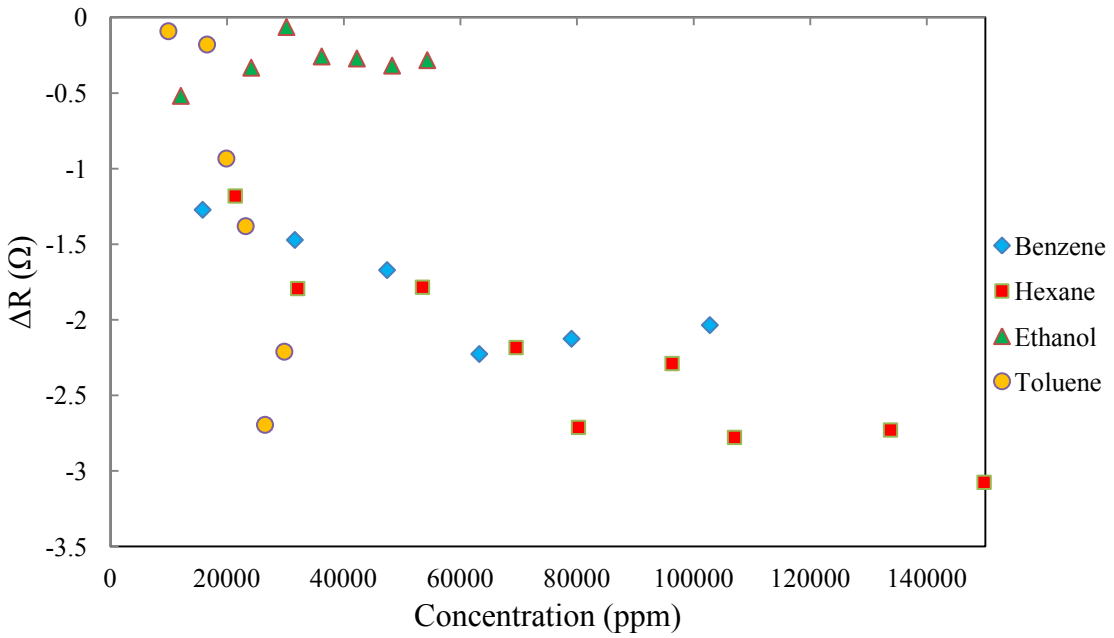

Figure (7-24) Comparison of resistance response of coated QCR (Zn-oct-oct-Pc film) exposed to several vapours concentration.

For Zn-Oct-Oct-Pc film as show in figures (7-16) to (7-24), the film exhibits a good sensitivity to benzene and toluene analytes, additionally, considerable changes in magnitude and frequency which indicate mass loading and film damping are also obtained on vapour exposure. There are changes in the films viscoelastic properties for higher concentrations of benzene, hexane and toluene which can be observed from a negative frequency shift and changes in magnitude (related to ΔR of the BVD equivalent circuit). Moreover, figure (7-53) shows the relation between frequency shift and resistance change which potentially gives information about selectivity, where two analytes with different concentration could have a unique $\Delta f/\Delta R$ combination. In such cases, the resistance response will allows discrimination between analytes. As an example for the plots of Zn-Oct-Oct-Pc film it can be noted that frequency shift of 100Hz obtainable for all tested analytes. However, to distinguish, we need to look to ΔR and Δf relationship as figure (7-53) show.

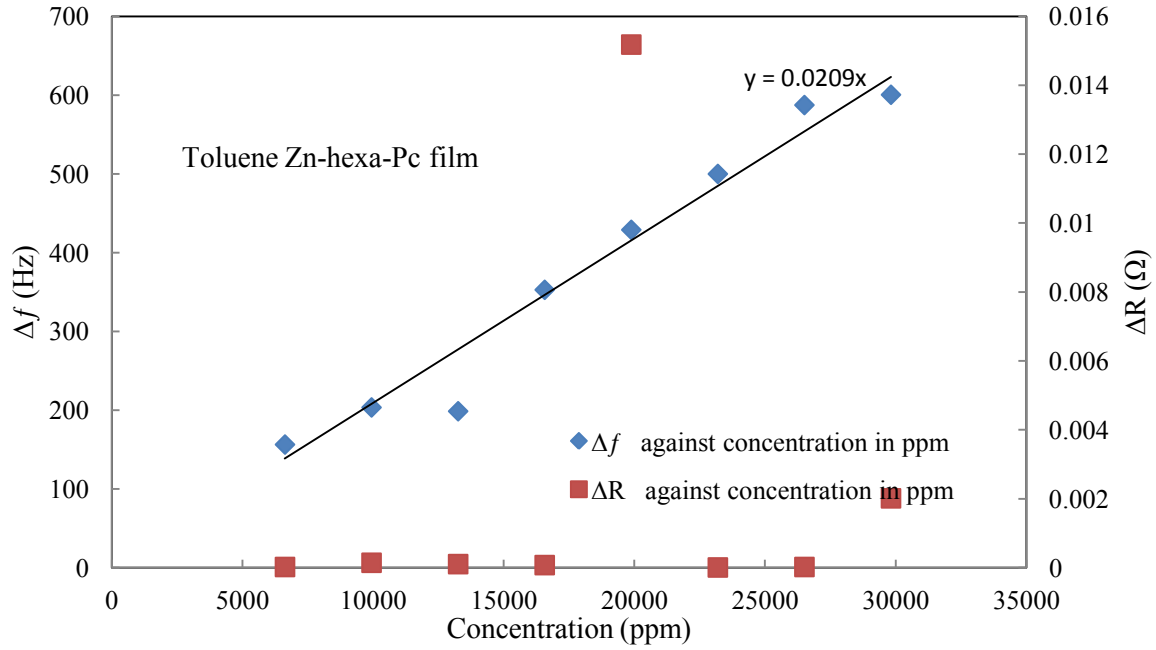

Figure (7-25) Frequency & resistance response of coated QCR (Zn-hexa-Pc film) exposed to several Toluene vapour concentration in ppm.

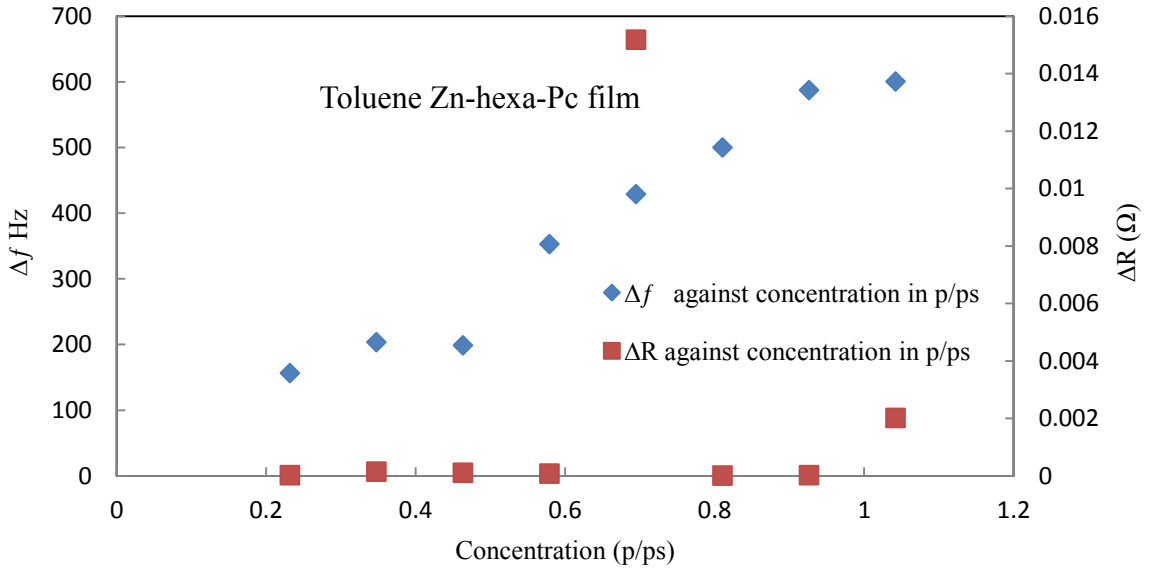

Figure (7-26) Frequency & resistance response of coated QCR (Zn-hexa-Pc film) exposed to several Toluene vapour concentration in p/p_s.

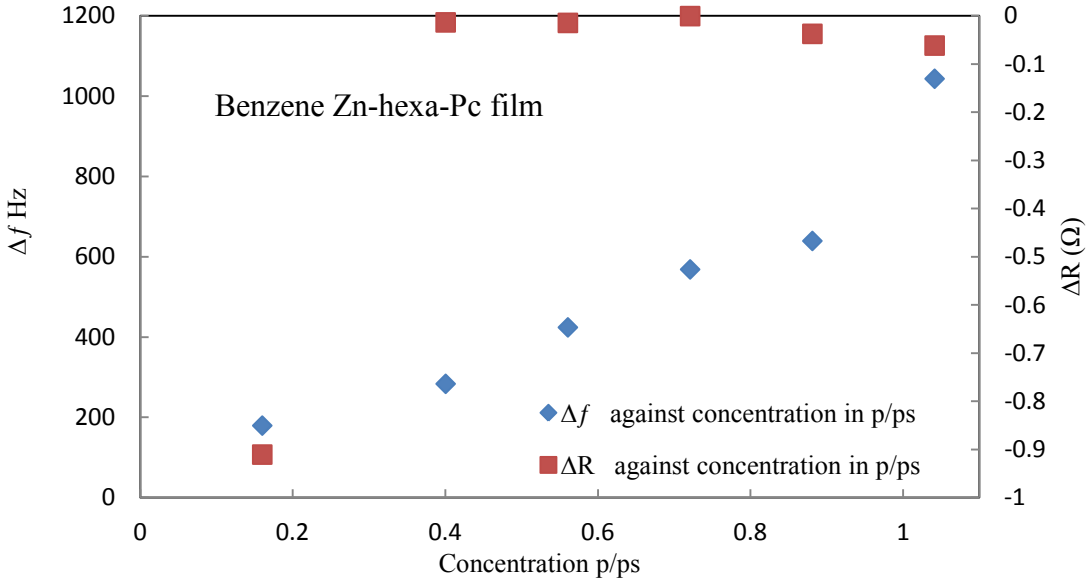

Figure (7-27) Frequency & resistance response of coated QCR (Zn-hexa-Pc film) exposed to several Benzene vapour concentration in p/ps.

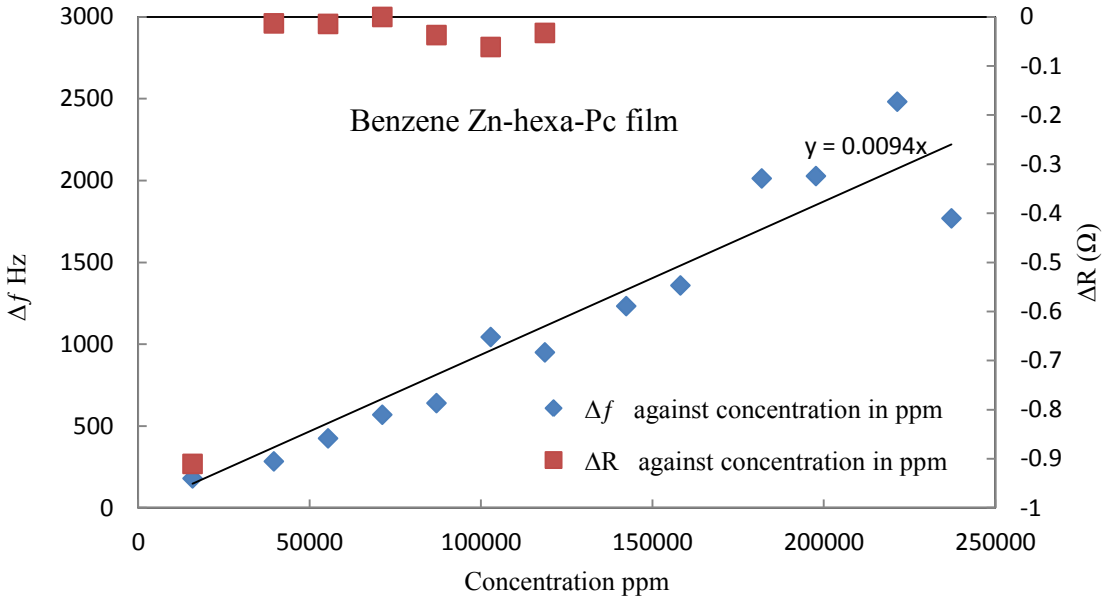

Figure (7-28) Frequency & resistance response of coated QCR (Zn-hexa-Pc film) exposed to several Toluene vapour concentration in ppm.

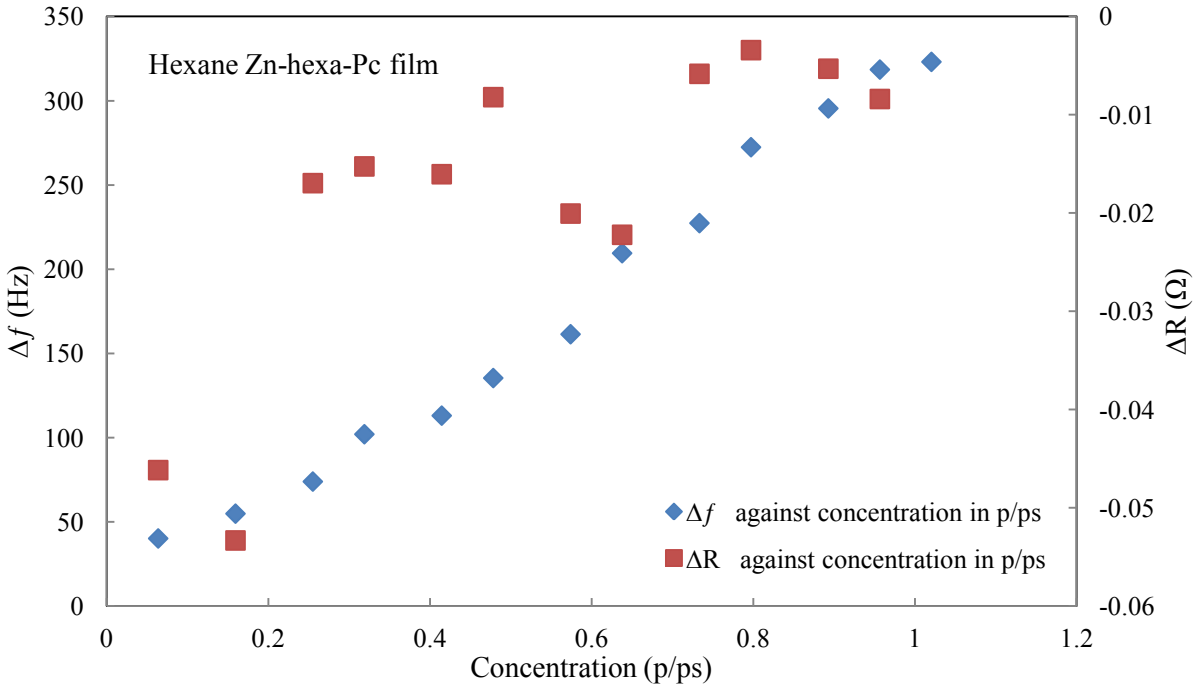

Figure (7-29) Frequency & resistance response of coated QCR (Zn-hexa-Pc film) exposed to several Hexane vapour concentration in p/p_s.

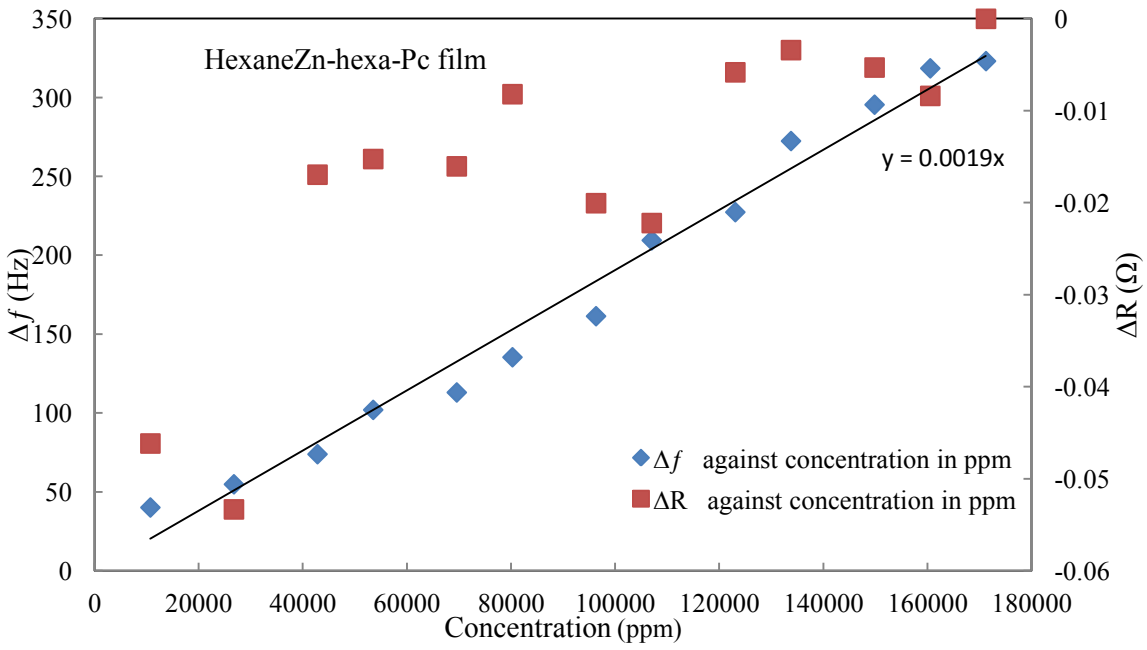

Figure (7-30) Frequency & resistance response of coated QCR (Zn-hexa-Pc film) exposed to several Hexane vapour concentration in ppm.

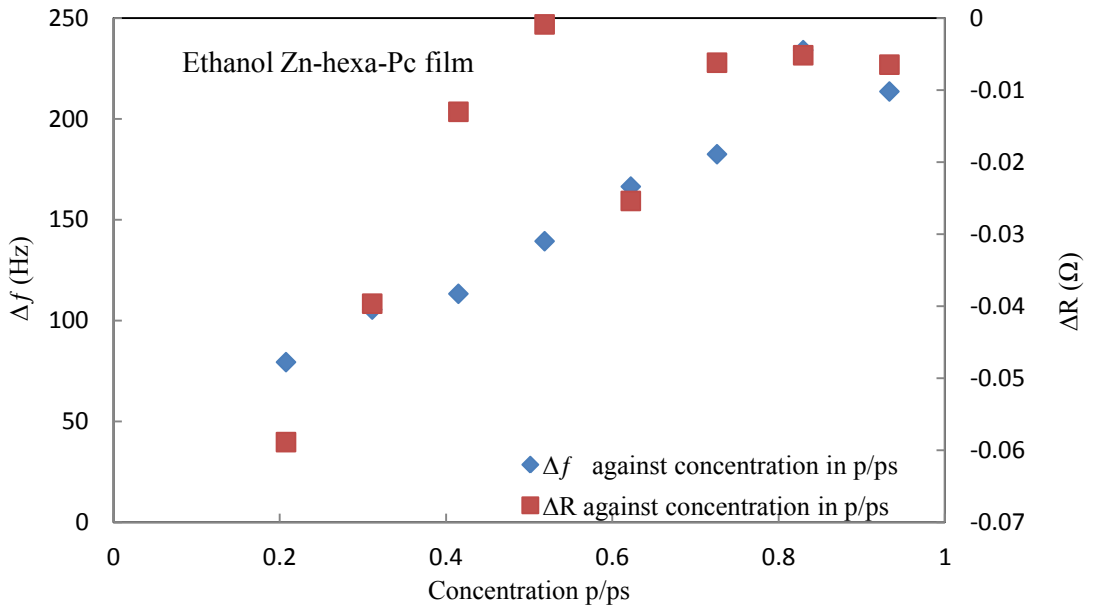

Figure (7-31) Frequency & resistance response of coated QCR (Zn-hexa-Pc film) exposed to several Ethanol vapour concentration p/p_s.

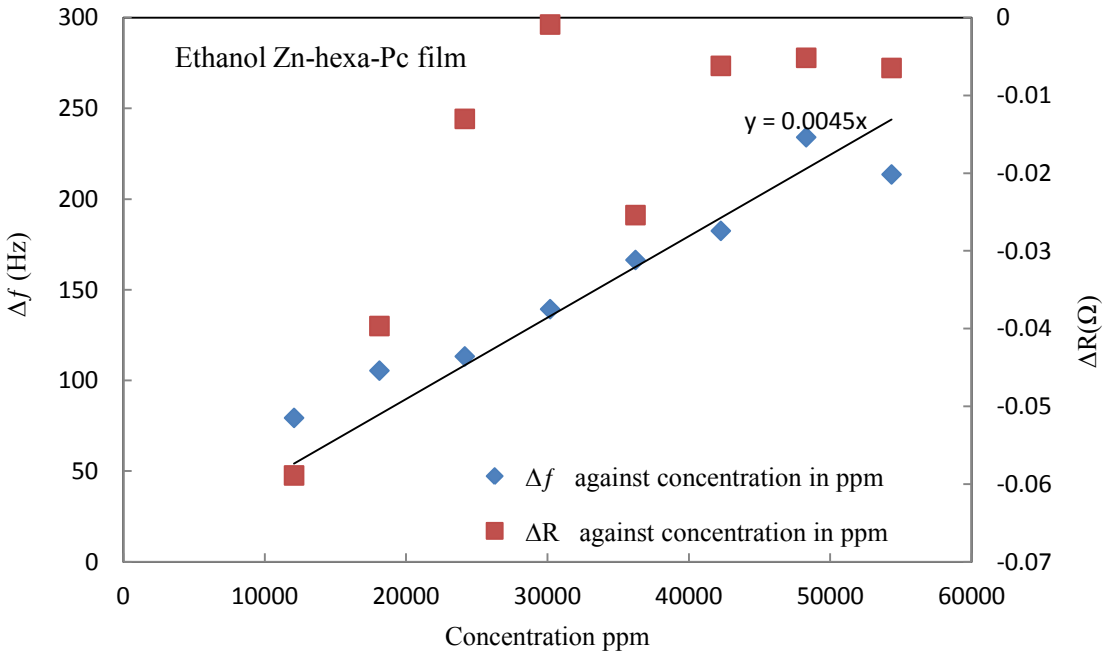

Figure (7-32) Frequency & resistance response of coated QCR (Zn-hexa-Pc film) exposed to several Ethanol vapour concentration in ppm.

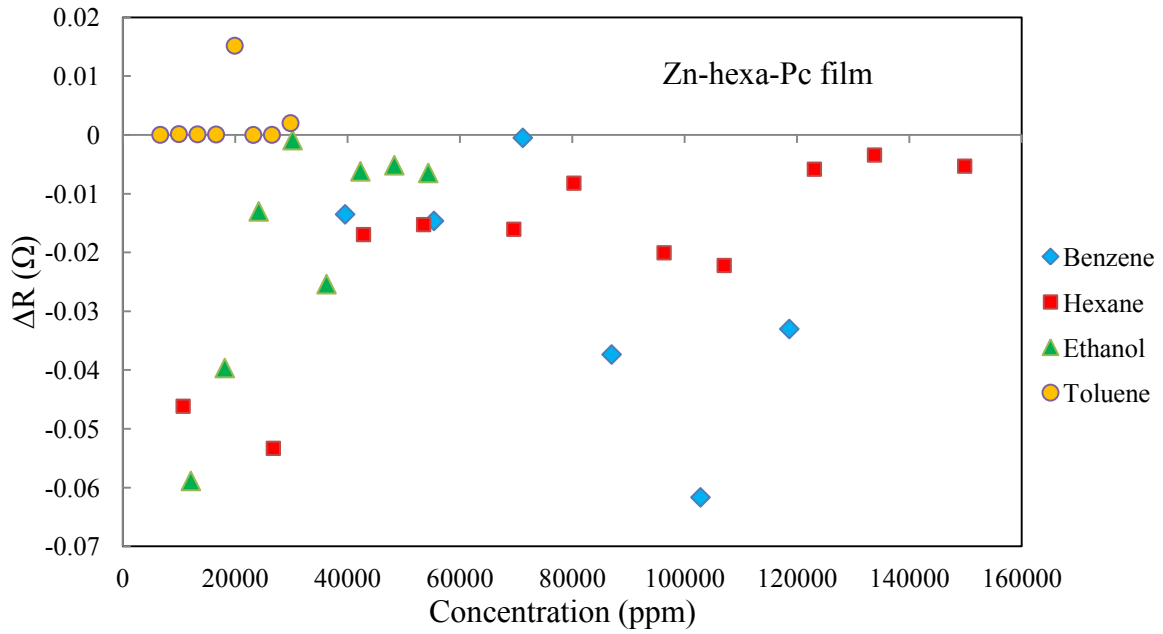

Figure (7-33) Comparison of resistance response of coated QCR (Zn-hexa-Pc film) exposed to several vapours concentration.

For Zn-hexa-Pc film as show in figures (7-25) to (7-33), and figure (7-54) Significant changes in mass loading are observed on vapour exposure, with an approximately linear relationship. The sensitivity of the coating has been estimated from the slope of fitted trend line and gives values of (47, 106, 222, 526) ppm/Hz for toluene, benzene, ethanol and hexane respectively.

A frequency shift (Δf) and change in magnitude (as related to ΔR of the BVD equivalent circuit) indicate negligible changes in the films viscoelastic properties for the increasing concentrations of tested vapour. The extracted values of Δf and ΔR from subsequent fitting of the spectra to the BVD model are show in figure (7-54) which indicate a rigid film properties comparing with other tested film as figure (7-52) show.

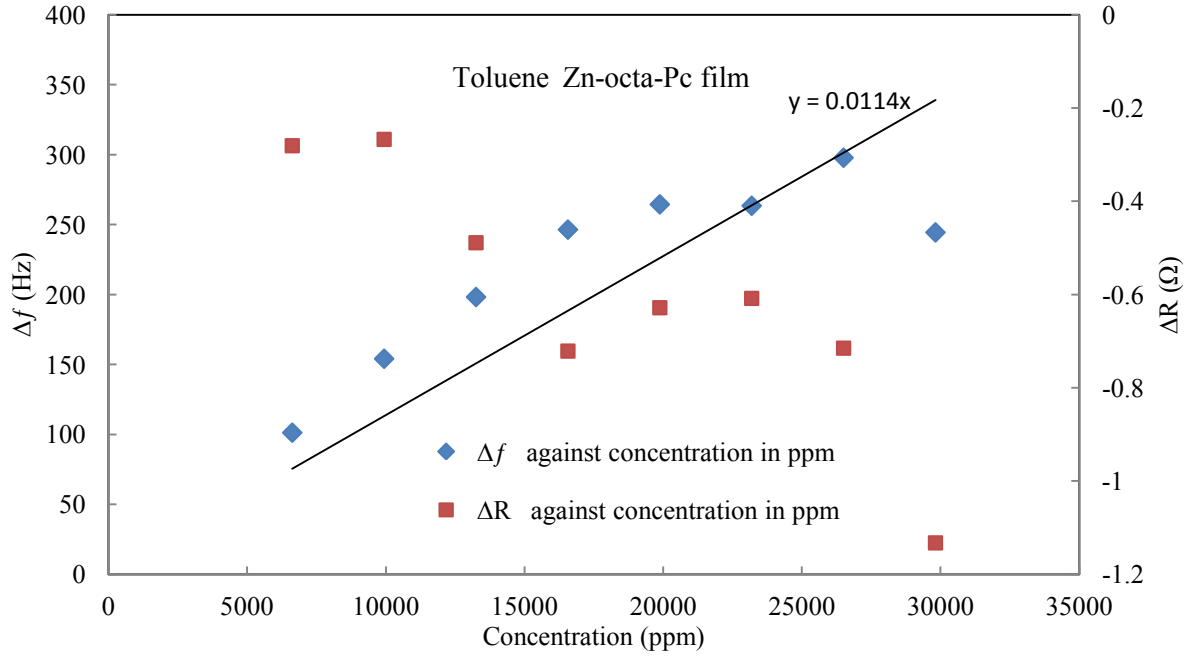

Figure (7-34) Frequency & resistance response of coated QCR (Zn-octa-Pc film) exposed to several Toluene vapour concentration in ppm.

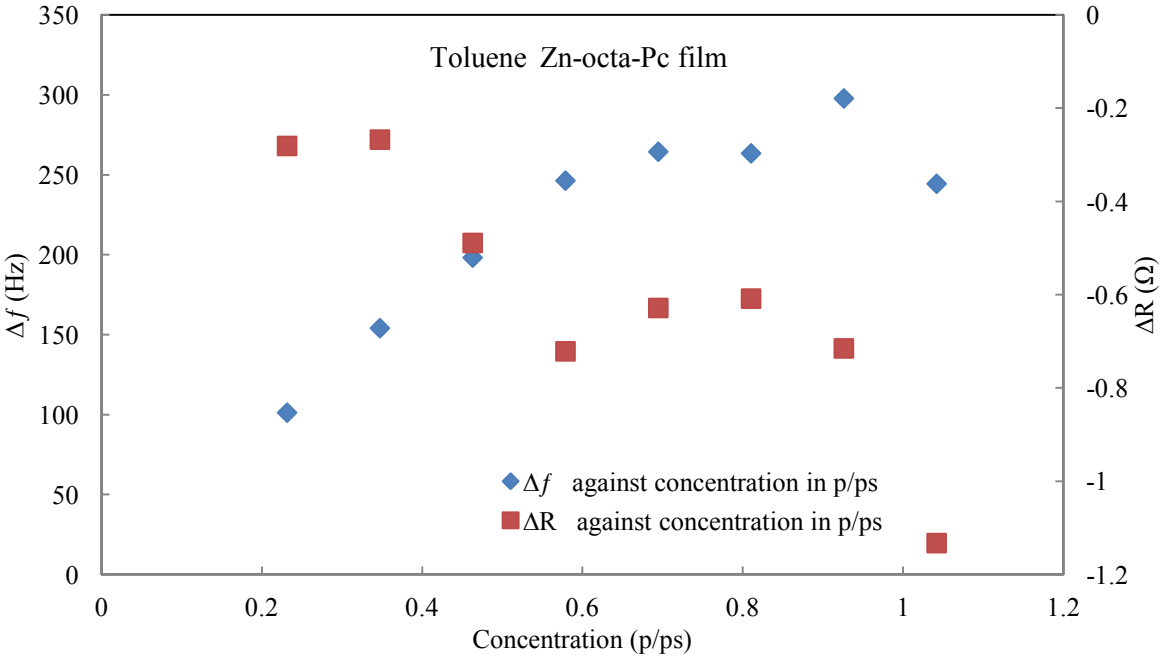

Figure (7-35) Frequency & resistance response of coated QCR (Zn-octa-Pc film) exposed to several Toluene vapour concentration in p/ps.

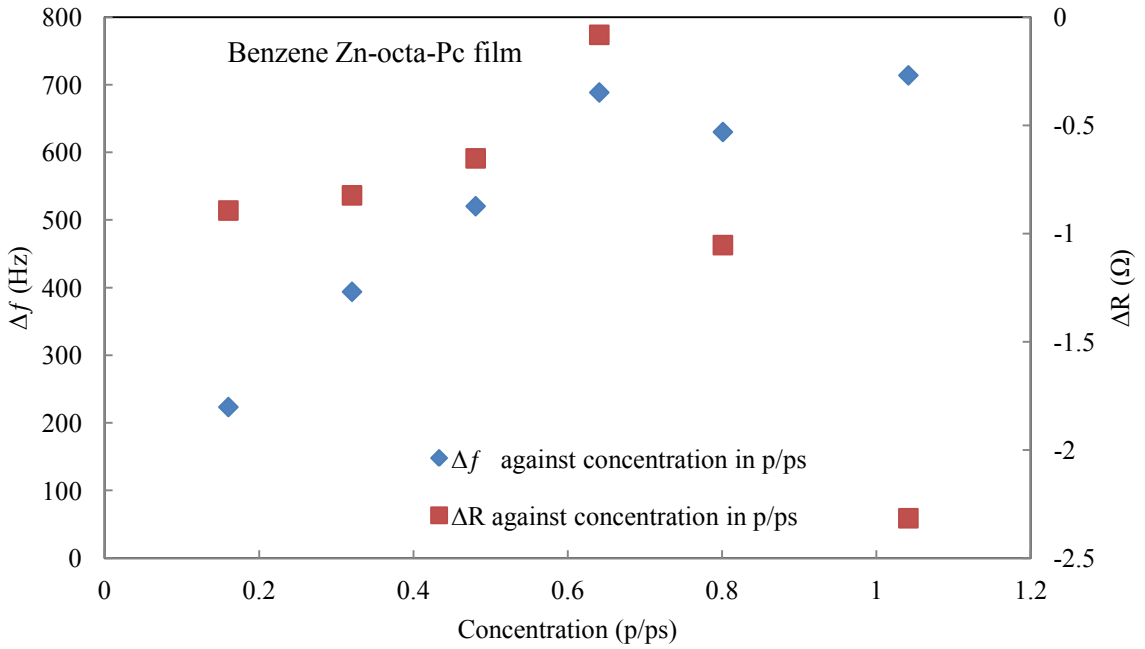

Figure (7-36) Frequency & resistance response of coated QCR (Zn-octa-Pc film) exposed to several Benzene vapour concentration in p/p_s.

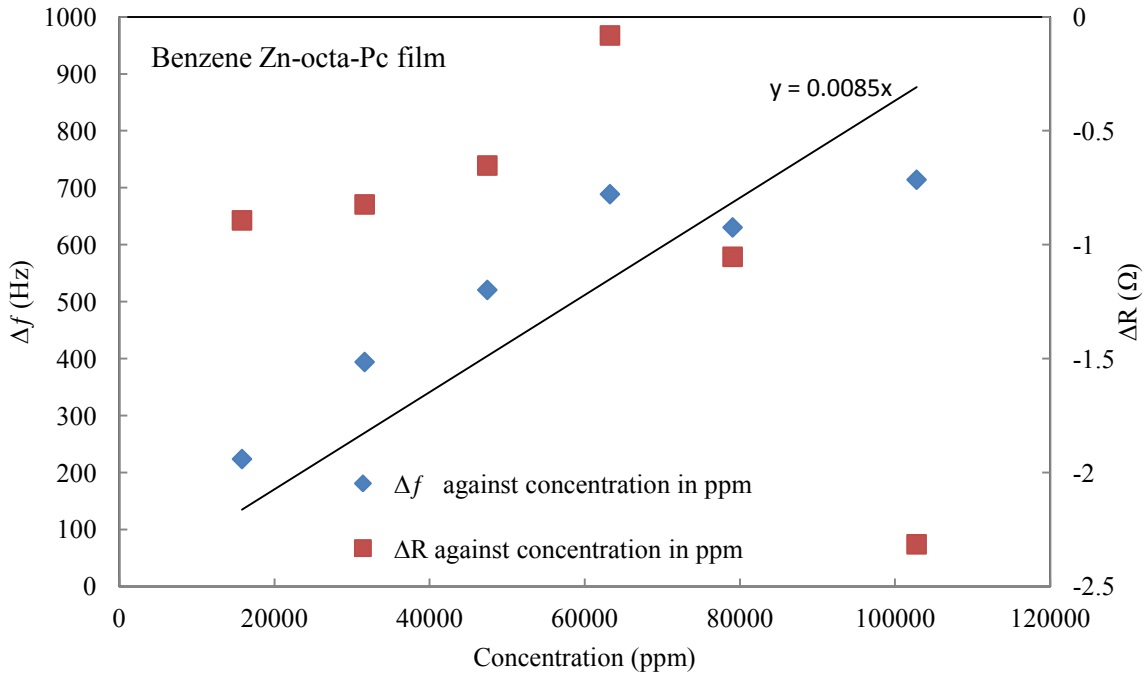

Figure (7-37) Frequency & resistance response of coated QCR (Zn-octa-Pc film) exposed to several Benzene vapour concentration in ppm.

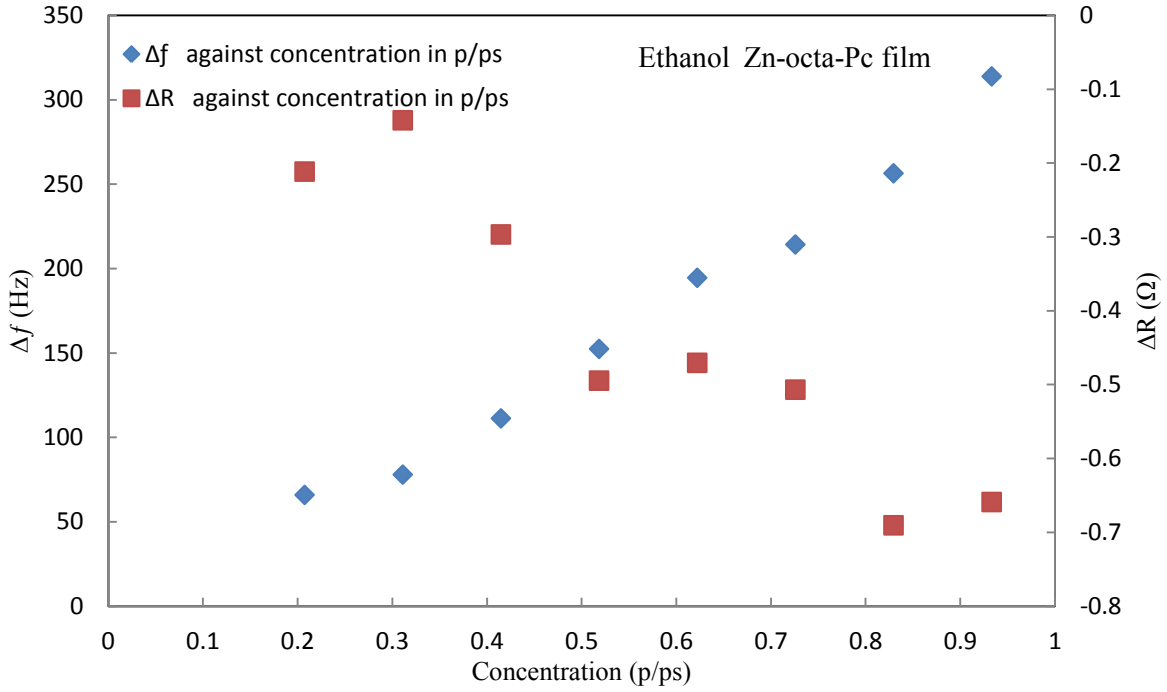

Figure (7-38) Frequency & resistance response of coated QCR (Zn-octa-Pc film) exposed to several Ethanol vapour concentration in p/p_s.

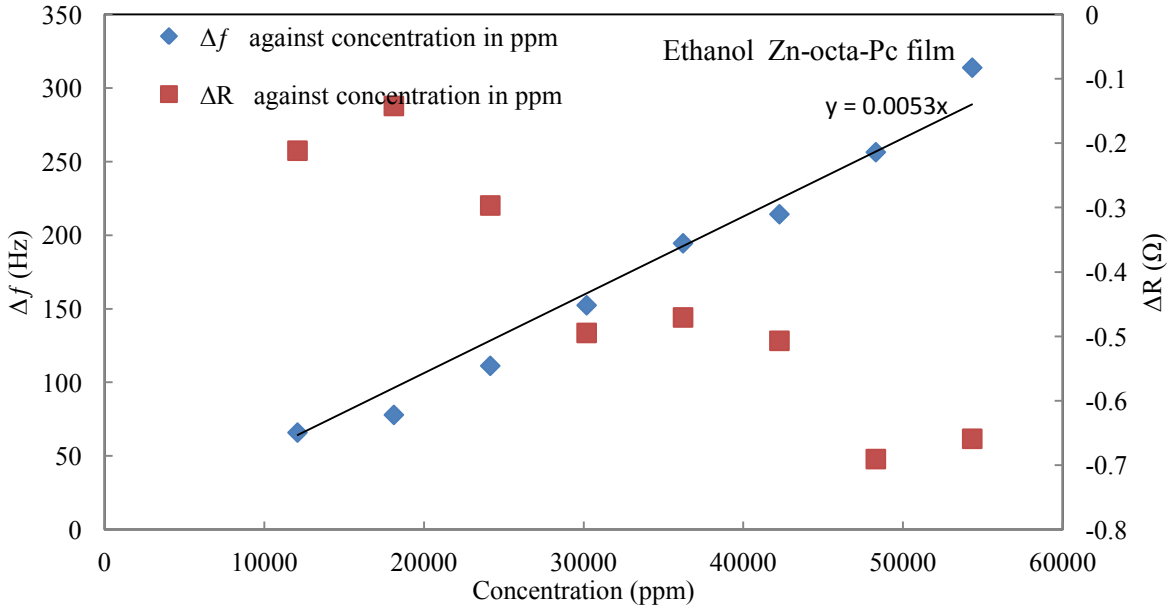

Figure (7-39) Frequency & resistance response of coated QCR (Zn-octa-Pc film) exposed to several Ethanol vapour concentration in ppm.

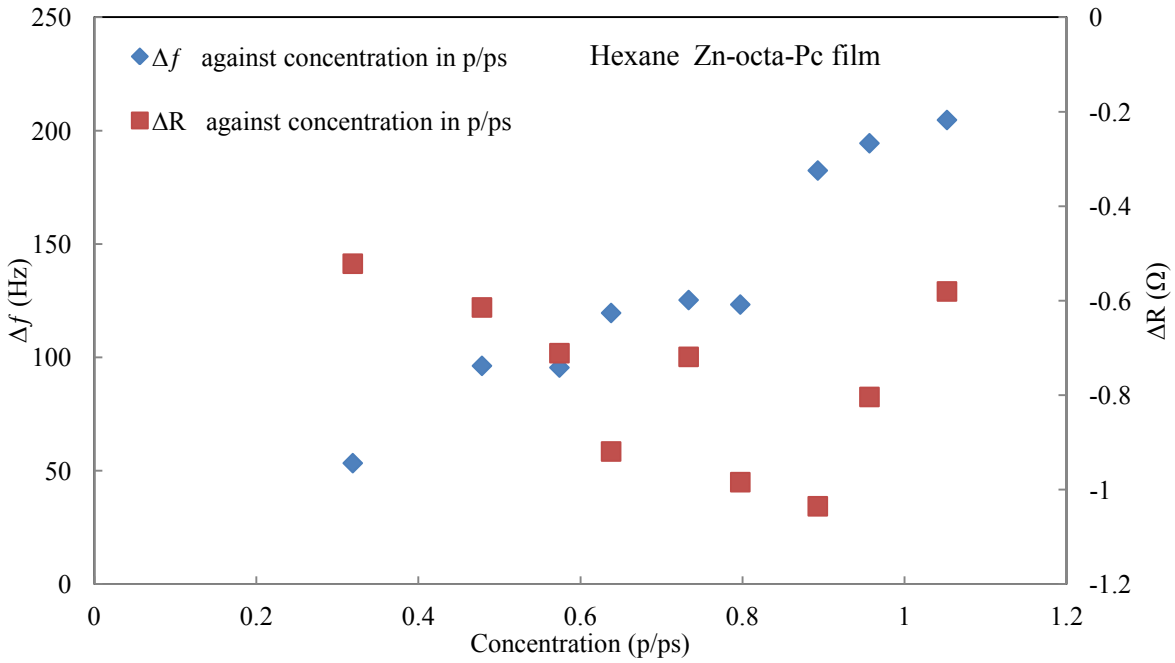

Figure (7-40) Frequency & resistance response of coated QCR (Zn-octa-Pc film) exposed to several Hexane vapour concentration in p/p_s

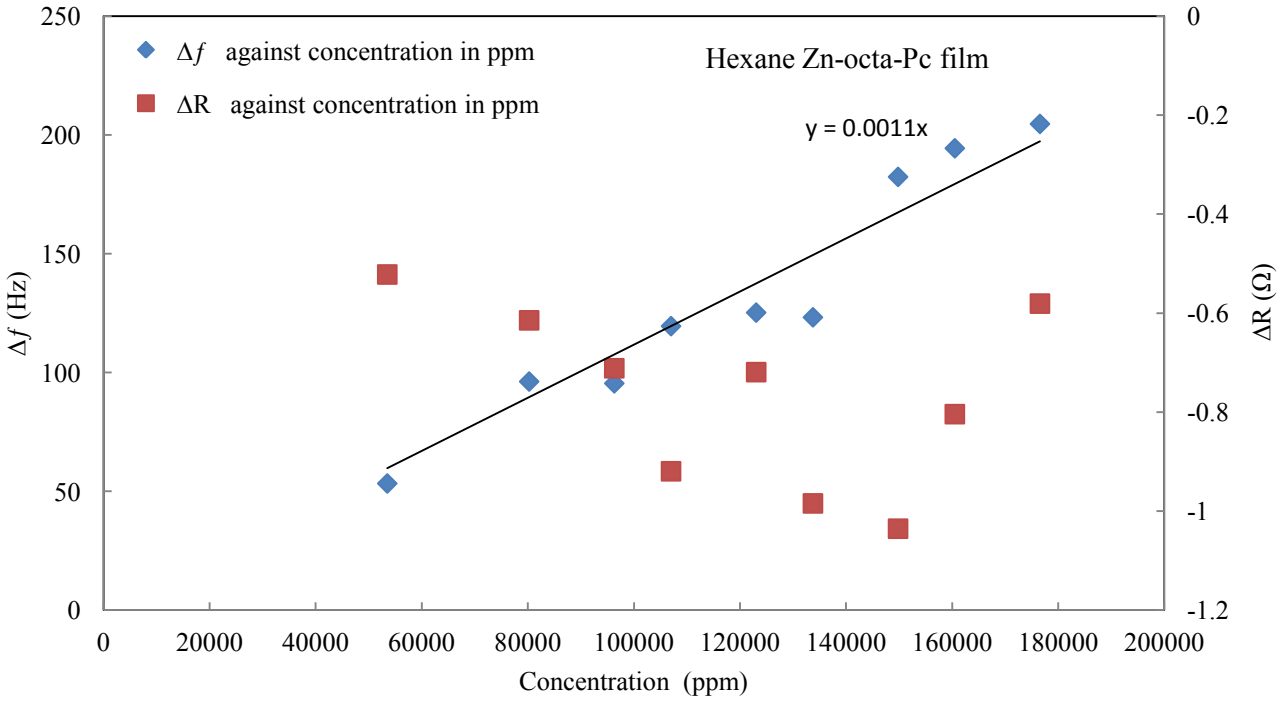

Figure (7-41) Frequency & resistance response of coated QCR (Zn-octa-Pc film) exposed to several Hexane vapour concentration in ppm.

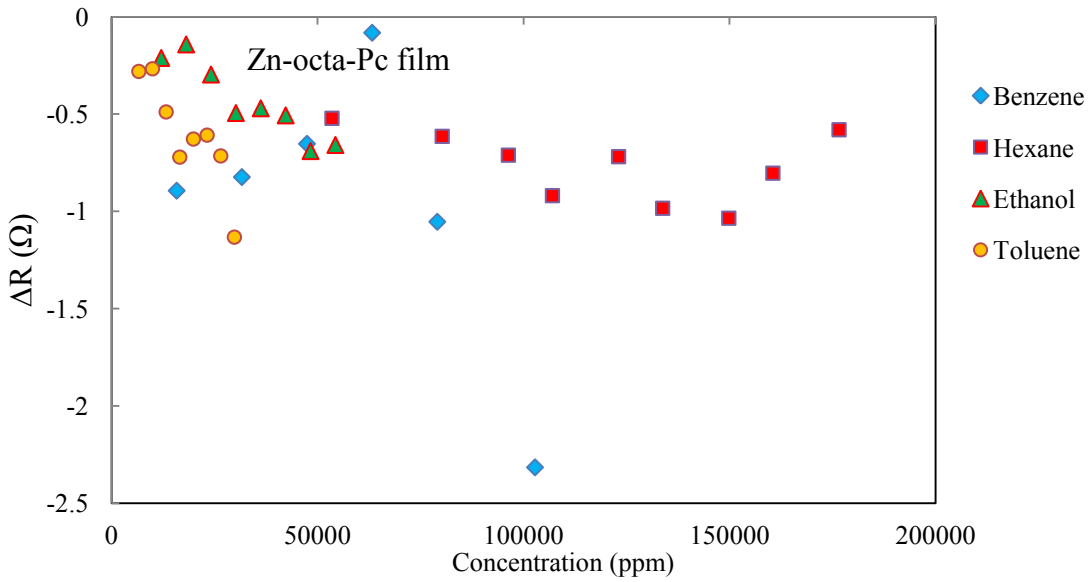

Figure (7-42) Comparison of resistance response of coated QCR (Zn-octa-Pc film) exposed to several vapours concentration.

For Zn-oct-Pc film as show in figures (7-34) to (7-42), and figure (7-55) the film exhibit a good response to all tested analytes with 87ppm/Hz for toluene vapour and 117ppm/Hz to benzene as figures (7-34) and (7-37) show respectively. Moreover, it can see that the sensor response increase with increase analytes concentration as expected. Furthermore, the film shows similar sensitivity characteristics with both concentration in absolute units of parts per million and in relative vapour pressure. Additionally, significant changes in mass loading and film damping are also observed on vapour exposure as can see in figure (7-55) with negative resistance shift, however less distinct separation between responses is noted and overall smaller resistance change as compared to the Zn-oct- oct – Pc film.

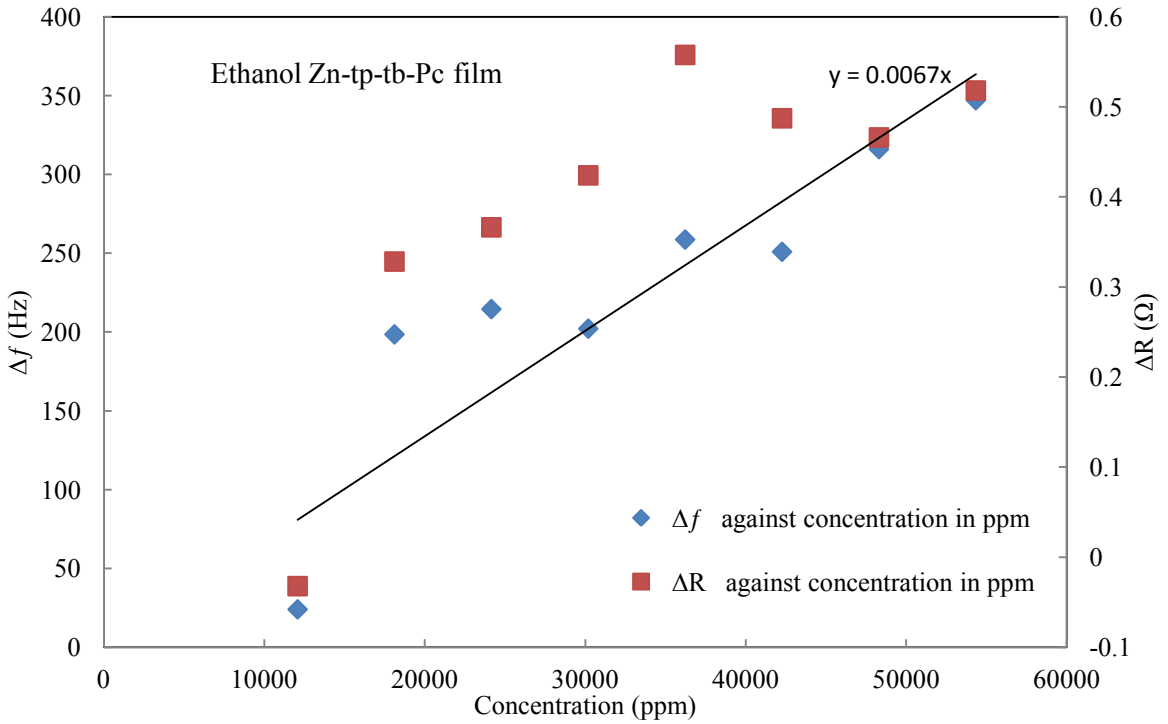

Figure (7-43) Frequency & resistance response of coated QCR (Zn-tp-tb-Pc film) exposed to several Ethanol vapour concentration in ppm.

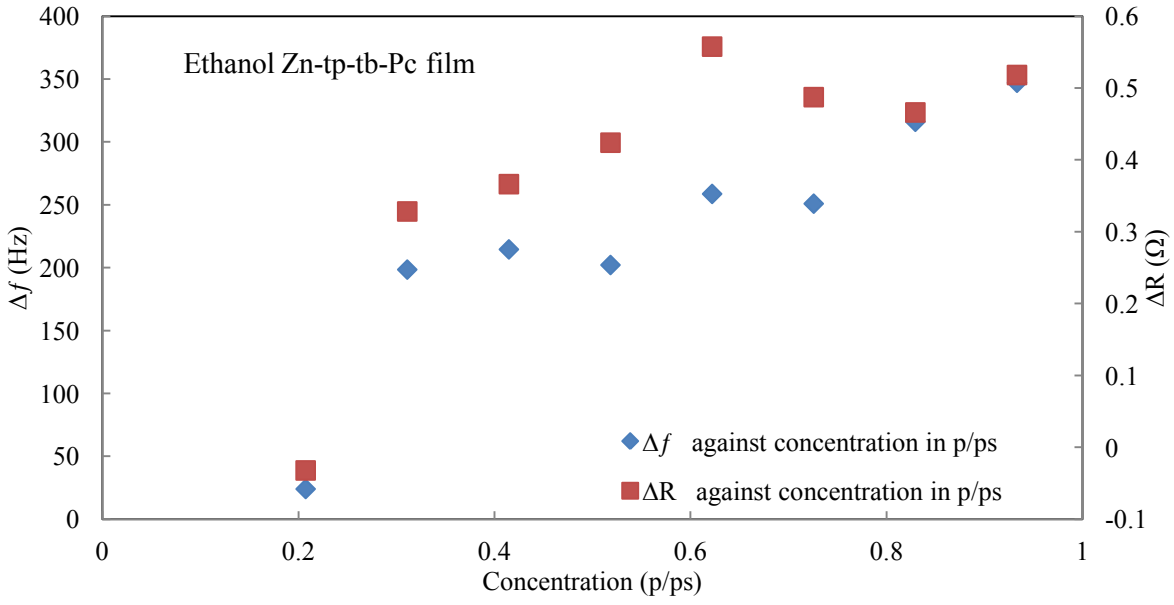

Figure (7-44) Frequency & resistance response of coated QCR (Zn-tp-tb-Pc film) exposed to several Ethanol vapour concentration in p/p_s.

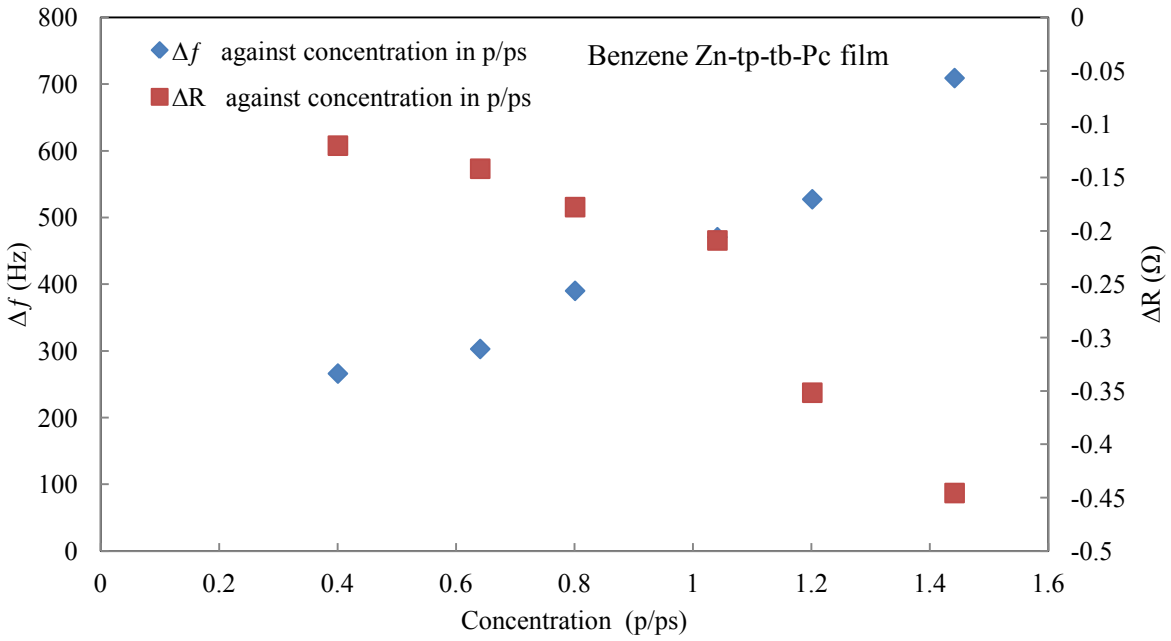

Figure (7-45) Frequency & resistance response of coated QCR (Zn-tp-tb-Pc film) exposed to several Benzene vapour concentration in p/p_s.

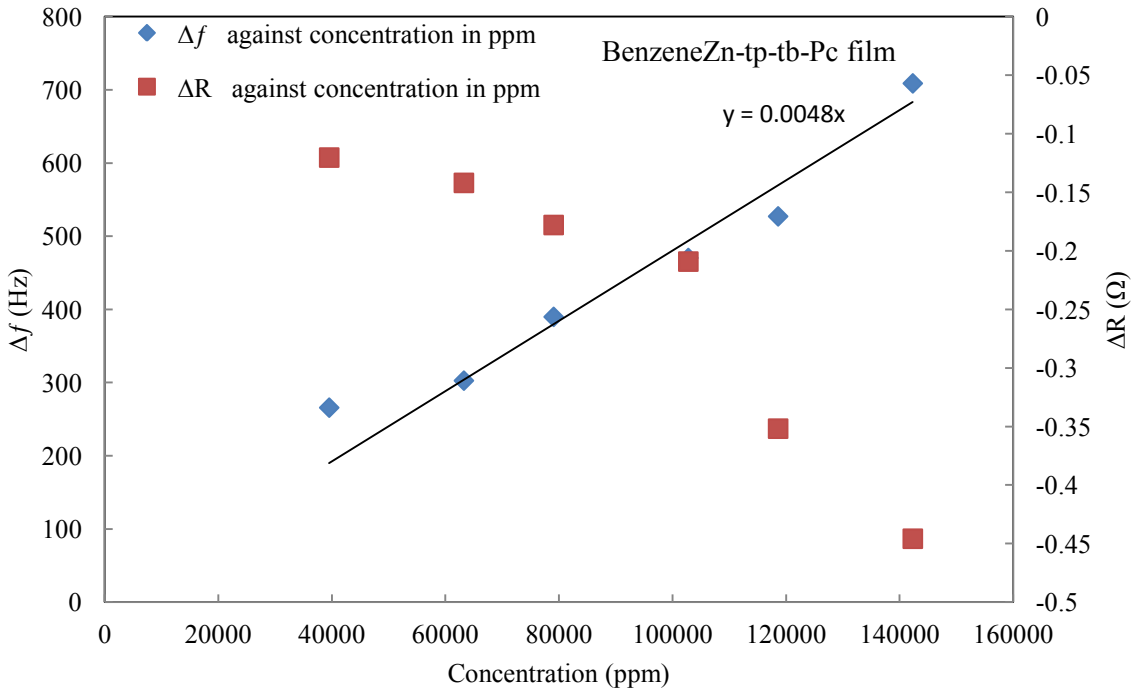

Figure (7-46) Frequency & resistance response of coated QCR (Zn-tp-tb-Pc film) exposed to several Benzene vapour concentration in ppm.

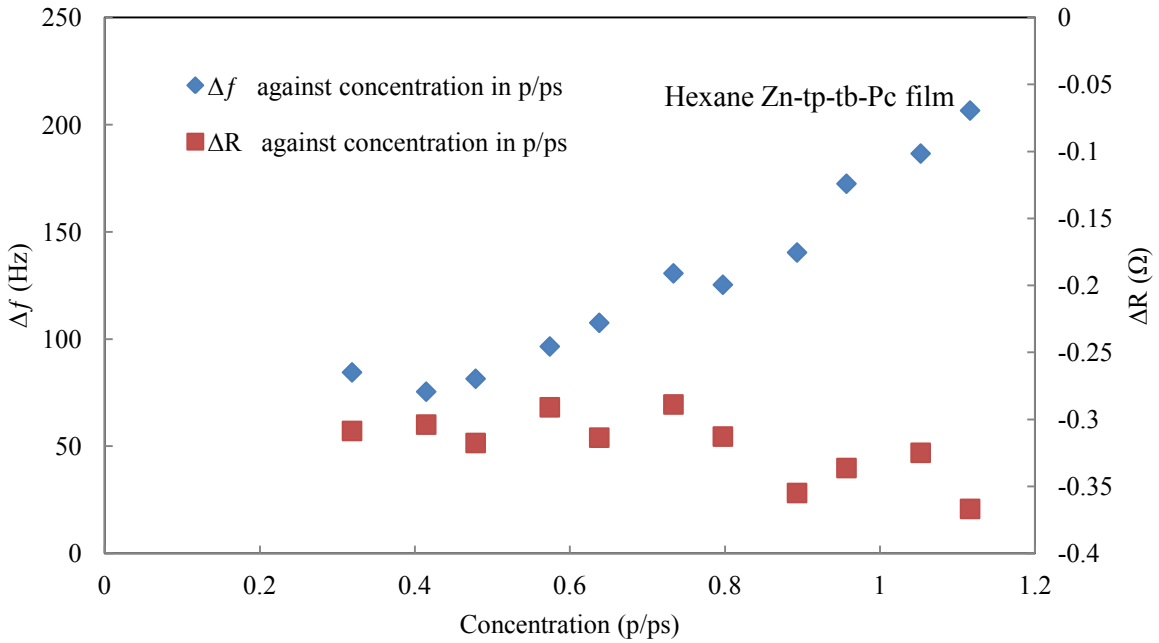

Figure (7-47) Frequency & resistance response of coated QCR (Zn-tp-tb-Pc film) exposed to several Hexane vapour concentration in p/p_s.

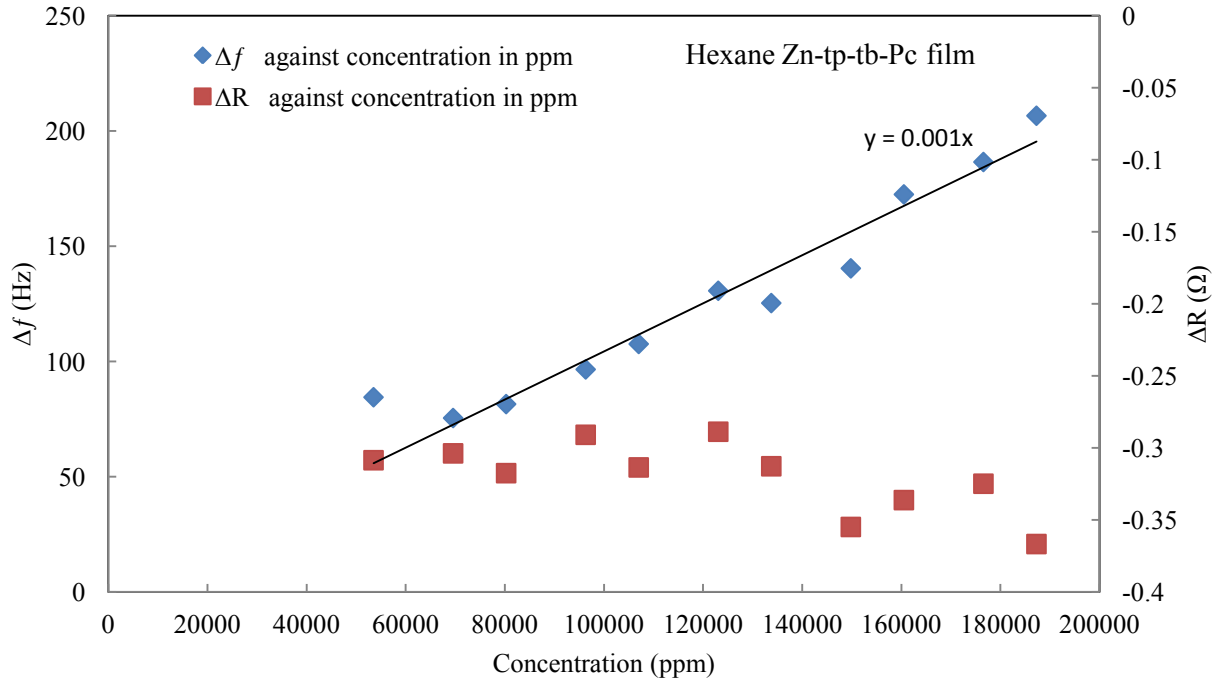

Figure (7-48) Frequency & resistance response of coated QCR (Zn-tp-tb-Pc film) exposed to several Hexane vapour concentration in ppm.

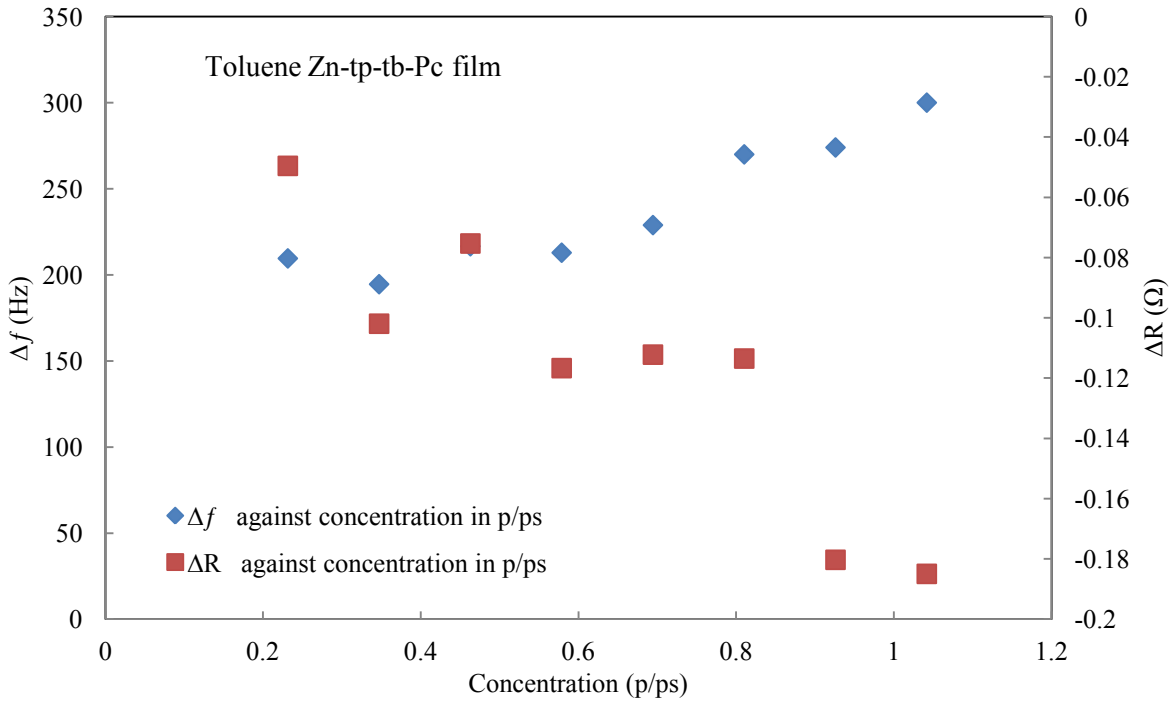

Figure (7-49) Frequency & resistance response of coated QCR (Zn-tp-tb-Pc film) exposed to several Toluene vapour concentration in p/p_s.

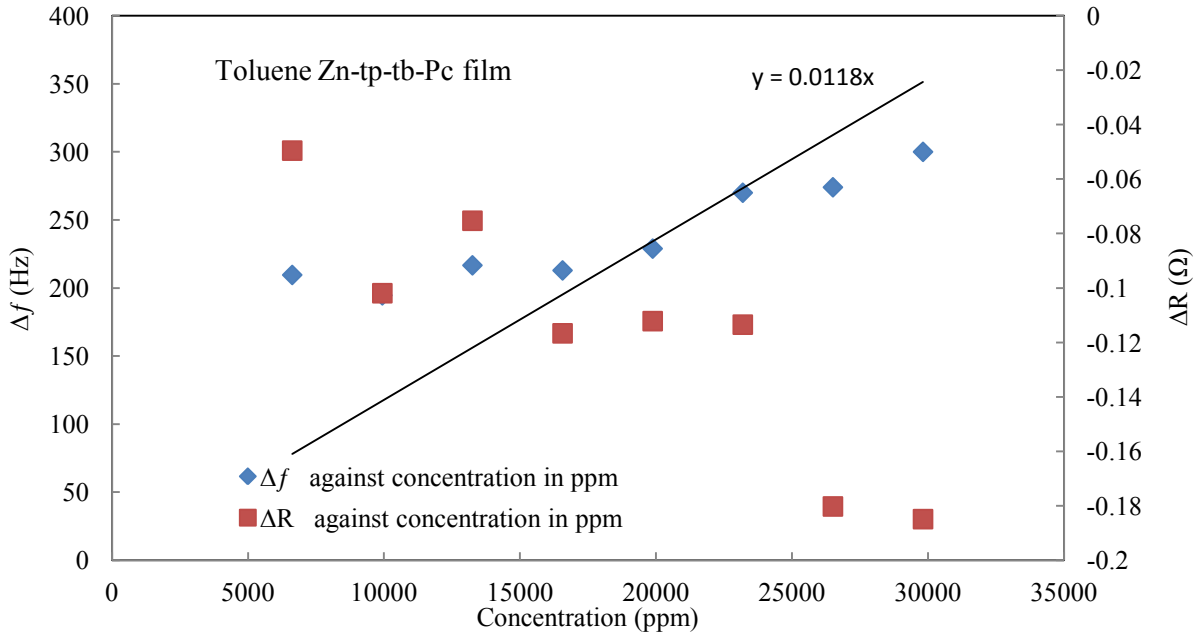

Figure (7-50) Frequency & resistance response of coated QCR (Zn-tp-tb-Pc film) exposed to several Toluene vapour concentration in ppm.

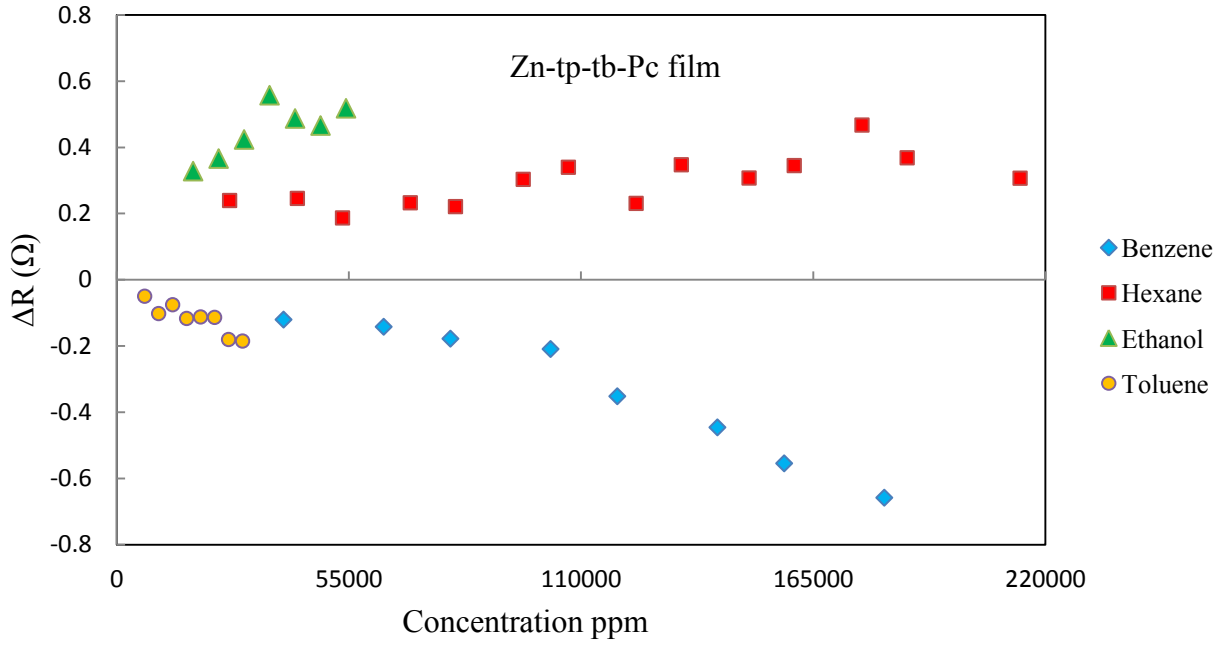

Figure (7-51) Comparison of resistance response of coated QCR (Zn-tp-tb-Pc film) exposed to several vapours concentration.

Comparing to Zn-tp-tb-Pc film as show in figures (7-43) to (7-51), and figure (7-56) the film has varying levels of sensitivity to the target vapours, and the sensor responses show an approximately co linearity relationship with increasing concentration of analyte. Toluene consistently produces the highest response with sensitivity of 84ppm/Hz. While the film appears more rigid as can see from figure (7-52) with minor change in film resistance, there are however a distinct trends. Hexane and Ethanol producing relatively linear positive resistance changes with increasing concentration while toluene and Benzene producing similarly linear but negative resistance changes.

As expected figures (7-17) through (7-51) show the sensor responses typically decreases infrequency with increased analyte concentration. However, the resistance parameter a function of a film viscosity has shown some distinct features for specific analytes. As a specific example (see figure 7-1) and figure (7-19) which show exposure of the Zn-oct-oct-Pc

film to benzene. Both show consistent level of increasing frequency shift in response to increasing vapour concentration. The data sets produce a sensitivity of approximately 0.007-0.008 Hz/ppm (123ppm/Hz) for test one and the sensitivity of 0.0081 for test two, which shows a good level of film reproducibility and experimental repeatability between tests. Additionally, significant changes in film damping are also observed on vapour exposure, with an approximately negative linear relationship for increasing vapour concentration.

Taking the system measurement accuracy and noise into consideration (± 5Hz) this gives a detection limit of approximately ppm below the LEL threshold and IDLH thresholds of 12000ppm and 500ppm respectively [5, 6]. Additionally, for the selected analytes, there are decreases in resistance for increasing concentration as demonstrated in Figures (7-24). The overall trend appears negative, however some variation is observed between analytes.

Vapour	**Sensitivity Hz/ppm**	**Sensitivity ppm/Hz**	**IDLH ppm**	**LEL ppm**	**LEL %Vol**	**HEL %Vol**	**Detection Limit ≅ ppm**
Benzene	0.0081	123.4	500	12000	1.3%	7.9%	1300
Hexane	0.0023	434.7	1100	11000	1.2%	7.4%	4500
Ethanol	0.0018	555.5	U	U	3.3%	19.0%	5500
Toluene	0.0207	478	500	11000	1.2%	7.1%	5000

Table 7-2 Sensitivity levels and detection limits of Zn-oct-octa-Pc film calculated from linear relation of the experimental data in figure (7-17,19, 21,23).

The sensitivity of the coatings has been estimated from the slope of fitted trend line for all analytes (see figure 7-5) as example, the values of sensitivity for the Zn-hexa-Pc film are given in table (7-2).

Of particular interest is if a unique relationship for $\Delta f/\Delta R$ exists for the films tested, which would indicate specific changes in film damping/mass loading relationship for each film. Figure (7-52) shows this relationship for tested films, toluene used a target analytes as example. Zn-octa-Pc and Zn-oct-oct-Pc film shows the same negative linear relationship while the other two films appear more as a rigid film, because the resistance shift is negligible over the concentration range tested for toluene vapour. The decrease in resistance typically indicates a hardening of the film or could be attributed to film resonance as highlighted in a several paper [1, 7, 8,19,10,11].

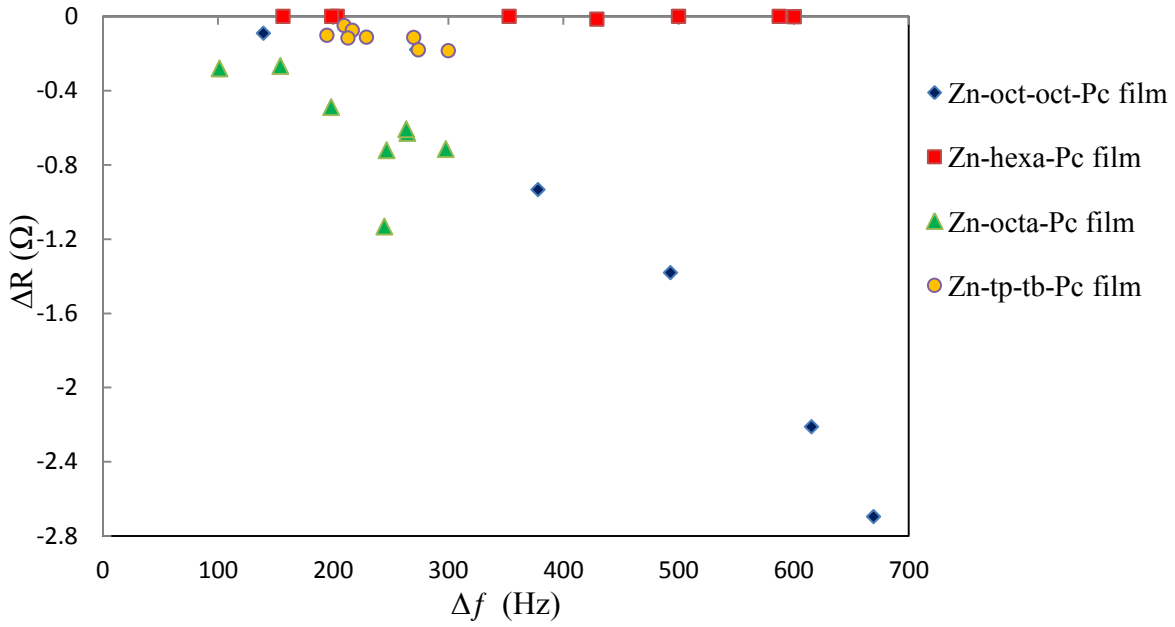

Figure (7-52) the dependence of ΔR against Δf for toluene vapours.

The relationship between Δf and ΔR for all films are plotted in Figures (7-53) to (7-56). Measurement of these parameters provides a unique response on exposure to Hexane, Benzene, Ethanol and Toluene vapours giving the potential for sensor selectivity in several cases.

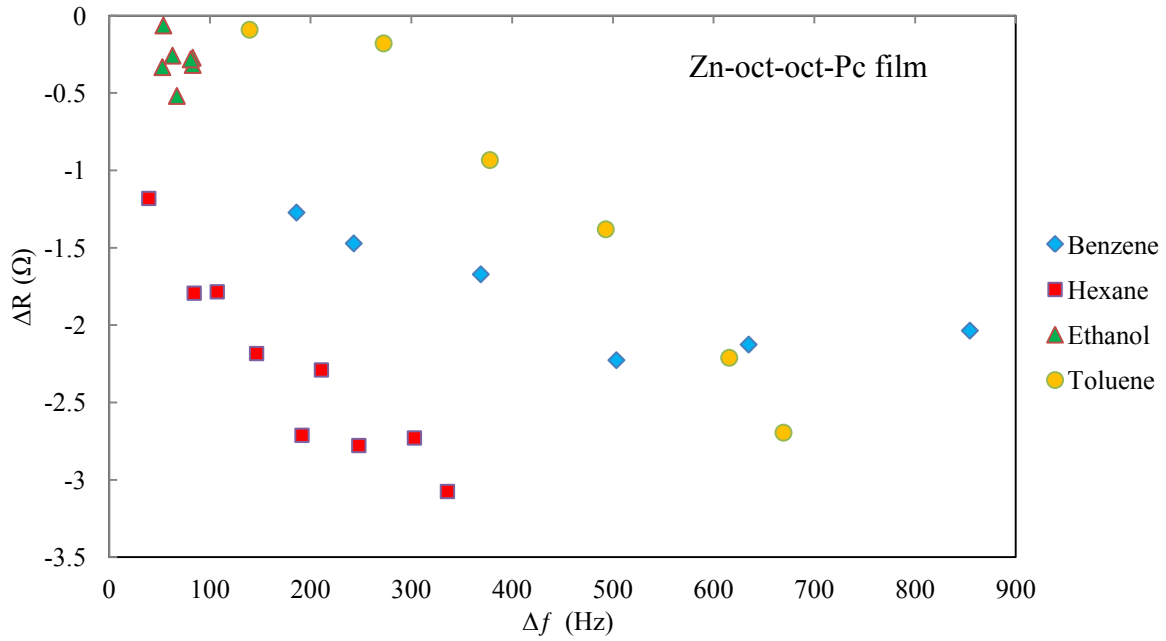

Figure (7-53) Figure ΔR against Δf for Zn-oct-oct-Pc film exposed to several vapours.

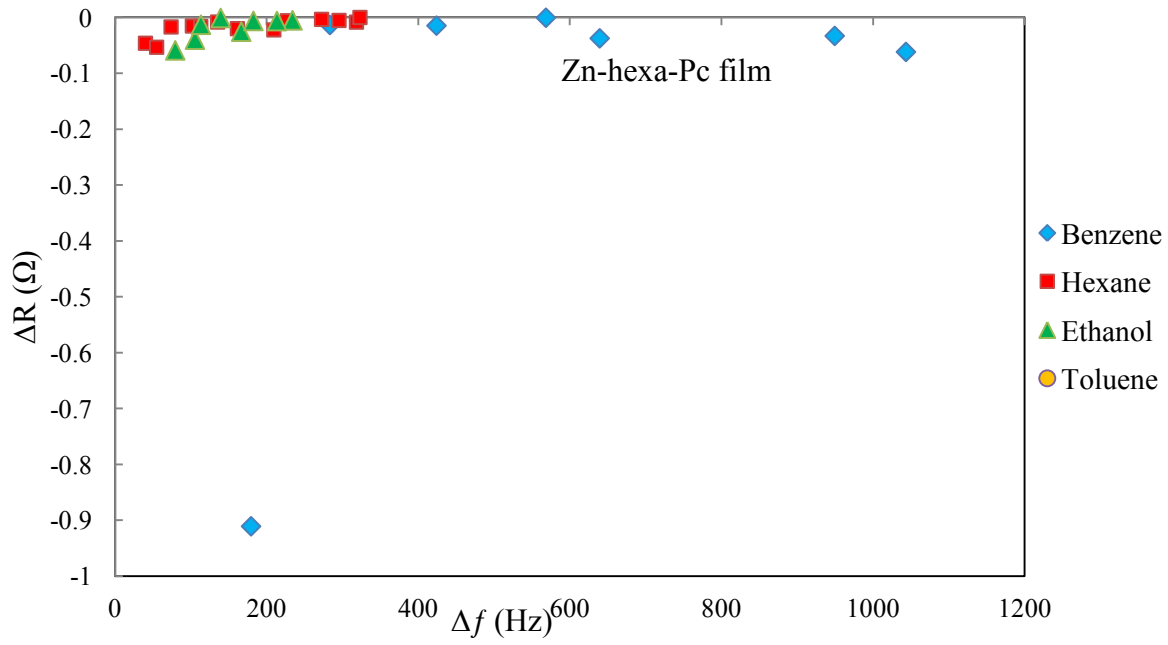

Figure (7-54) Figure ΔR against Δf for Zn-hexa-Pc film exposed to several vapours.

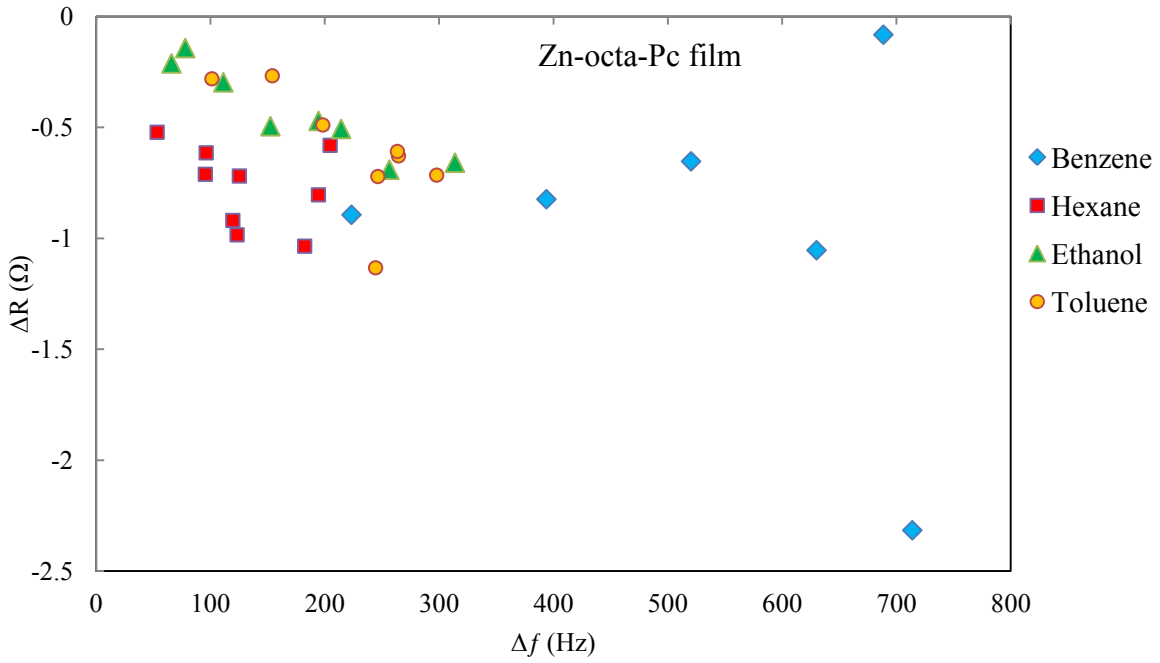

Figure (7-55) Figure ΔR against Δf for Zn-octa-Pc film exposed to several vapours.

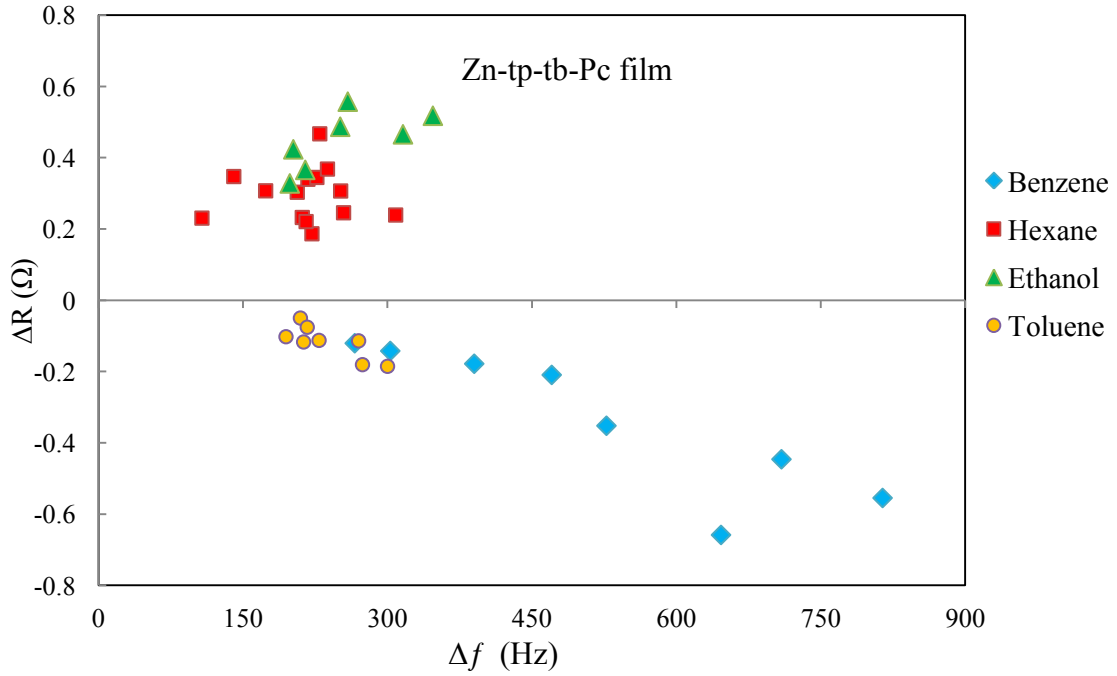

Figure (7-56) Figure ΔR against Δf for Zn-tp-tb-Pc film exposed to several vapours.

as depicted in figure (7-53) and (7-55) both Zn-oct-oct-Pc and Zn-octa-Pc film show a negative linear relationship and the Zn-oct-oct-Pc could give potential of distinguishability between tested analytes, however the other film figure (7-54) appear to have a small/ negligible change in resistance making a comparison almost impossible as the measure changes are of similar magnitude to the noise of the system. Additionally, the Zn-tp-tb-Pc film as figure (7-56) gives a two response regions which provide distinguishable between tested analytes.

The organic semiconductors such as phthalocyanine films have gain a high sensitivity to gases like Benzene and Toluene. The interaction between the gases molecules with phthalocyanine films case a high sensitivity, that lead to a noticeable change in electric conductivity of film. The sensing gas plays as a planer [π - electron acceptor] forming as a redox couple during charge transfer interaction [12, 16].

Where the negative charge resulted from redox couple leave its right place over the Pc rings which in turn increase the conductivity. More information about a conductivity change and interaction mechanism in phthalocyanine materials are reported elsewhere. [11, 13, 14, 15]

7.2 Results of QCR Impedance measurements for the compared materials:

During the process of film selection and evaluation, a range of other phthalocyanine has been considered. The materials used in this section were initially selected for impedance measurements'. These materials were considered to be potential sensor coating and have consequently been compared to Zinc Pc's which already used in previous section in this study.

In total four different metal phthalocyanines were prepared and characterized in order to study their performance as a gas sensor. Namely, Nickel(II) 1,4,8,11,15,18,22,25-octabutoxy-

29*H*,31*H*-phthalocyanine (Ni(II)-oct-Pc), Nickel(II) phthalocyanine (Ni(II)-Pc), Cobalt(II) phthalocyanine (Co(II)-Pc) and Copper(II) phthalocyanine (Cu(II)-Pc). The films were produced by spin coating as described in section 5.1.

An example of sensor response to tested analytes for compared material in both concentration in absolute units of part per million and relative vapour pressure are shown in figure (7-57) and (7-58).

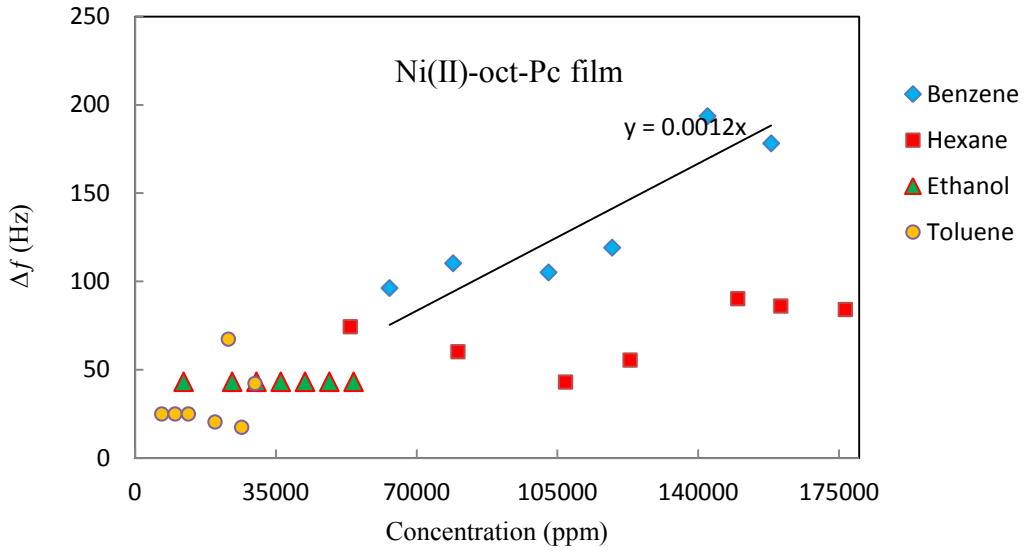

Figure (7-57) Frequency response of Ni(II)-oct-Pc coated QCR exposed to several concentrations of tested vapours in absolute units of parts per million.

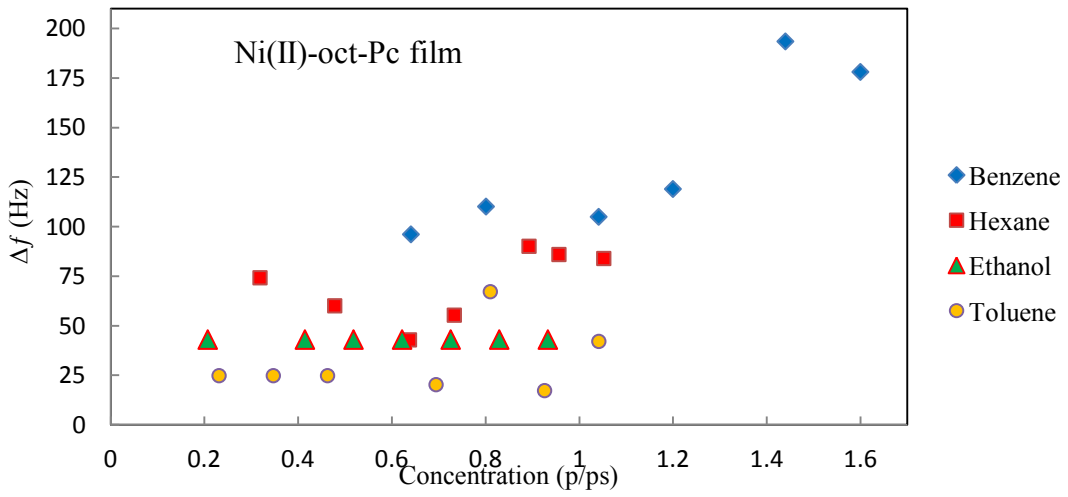

Figure (7-58) Frequency response of Ni(II)-oct-Pc coated QCR exposed to several concentrations of tested vapours in relative vapour pressure.

As can see from (7-57) figures, the shift in frequency peak of QCR coated with Ni(II)-oct-Pc film appear to be a small compared to ZnPc's materials. Where the maximum frequency shift was about 200 Hz for a concentration of 158134 ppm of benzene analyte, and not exceeding 50 Hz for 54000 ppm of ethanol concentration.

By calculating the sensitivity for the Ni(II)-oct-Pc film when expose to benzene gas, it was found to be around 0.0012 Hz/ppm , 833 ppm/Hz which is higher than the IDLH of benzene (500 ppm). Overall, the films appear unresponsive giving a flat undistinguishable behaviour.

A corresponding result was also exhibited by the other three films all giving inconsistency in frequency change when analytes concentration increased. The inconsistency in compared material response during exposure measurements can be interpreted as a result from non-homogenous film surface, the film material was unable to dissolve in chloroform and consequently not synthesise suitable film.

7.3 Sensitive Material Shear Modulus:

In this section the Thickness Shear Mode (TSM) quartz resonators will be used to characterize the thin film layers of sensitive material used in this work, in particular to investigate the viscoelastic properties of the studied films in contact with quartz crystal resonator (QCR).

The (TSM) approach is based on impedance spectrum measurements around the resonant frequencies of the transducer elements (QCR). The shear modulus of thin films can be calculated from both measurements of the impedance spectrum and layer properties

(thickness and density). The technique has been described in several research works [1, 2, 7, 8, 9, 10, 16, 17, 18].

As defined in section 4.2 the shear modulus is the ratio between stress and strain, and in case of viscoelastic film, part of energy is stored when shear stress is applied, while the other energy part dissipated. Accordingly, the shear modulus is described by equation;

$$G = G' + jG'' \qquad (4-23)$$

Where

G' is the elastic term, G'' is the viscous term, and the ratio between G', G'' defined as the loss tangent.

$$\frac{G''}{G'} = \tan\delta$$

If $tan\delta \ll 1$ The layer behaves as a glassy material

If $tan\delta$ close to unity the film layer is rubbery state. [7, 9, 16, 18, 19]

In this study, an identical method of impedance analysis was used described previously in section 5.4.

The values of R_f and L_f for the films (layers) were obtained by subtracting the loaded value from the unloaded values.

The shear modulus of the layer could then be extracted by modelling the impedance response using equations $(4-29a)$ and $(4-29b)$

In order to calculate shear modulus of the studied films a Matlab program was implemented using the equations from section 4.2 and film properties (thickness and density) established earlier. See appendix [A].

To validate the method; the procedure was used to calculate a shear modulus, of two independent data sets.

Firstly, the Matlab program (1) as shown in appendix [A] has been applied to the data obtained from published results [10, 16, 17, 18, 19] in order to confirm that the method works and gives resultant values of shear modulus in agreement with published data.

Secondly, from the experimental work of this study, The resultant data was used to calculate the shear modulus using program (1) in appendix [A] Initially the value of resistance and inductance which have been extracted from the fitted impedance spectra of the tested film are entered along with several of the known film parameters such as thickness and density. The values of shear modulus G', G'' are subsequently determined.

The obtained values of shear modulus G', G'' are then substituted into program (2) from appendix [B] which in turn generates an admittance spectra based on theoretical background explained in chapter 4.

By visually examining both generated and experimental spectra and direct comparison of key parameters (resonance and values and fitted equivalent circuit parameters) excellent agreement was obtained, giving almost negligible difference between the critical values of film properties [R_f , L_f].

Figure (7-59) shows experimental and generated spectra from extracted values of shear modulus.

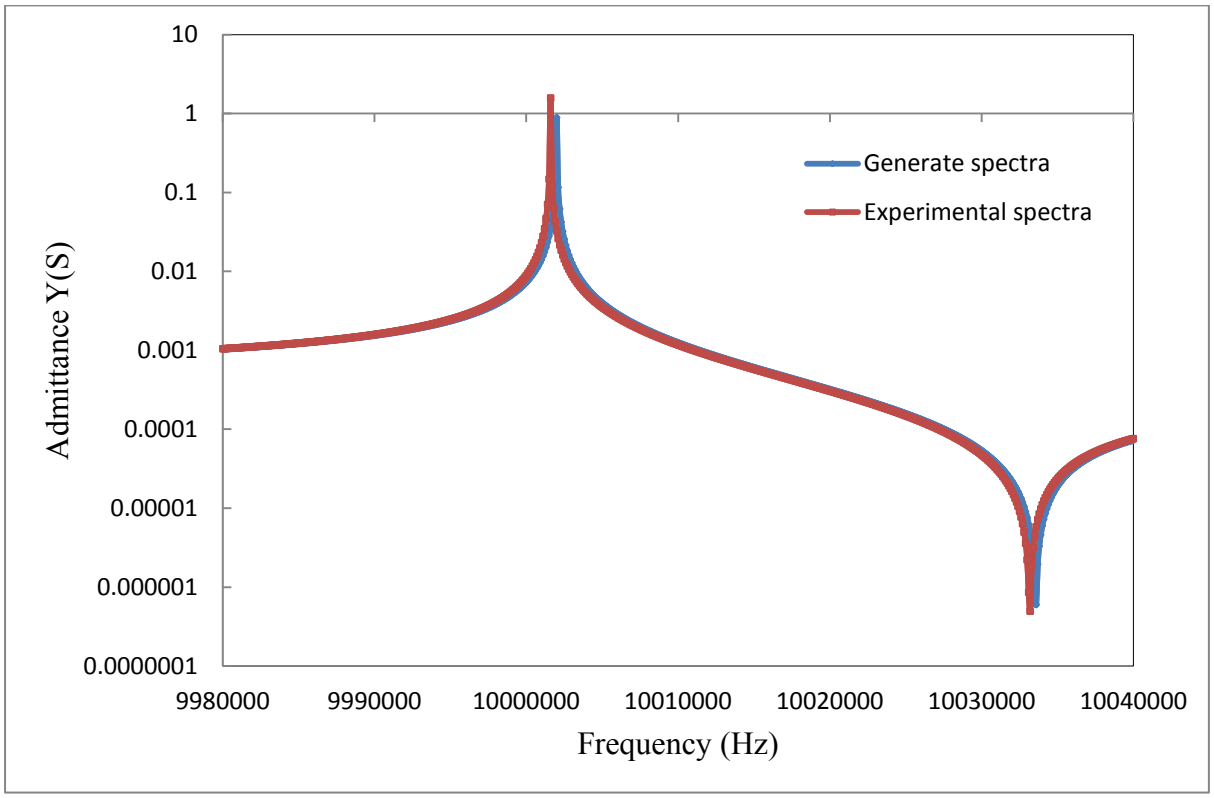

Figure (7-59) experimental and generated spectra from extracted values of shear modulus for Zn-oct-oct-Pc film.

The calculations of the shear modulus of the films from this study are listed in table (7-3)

Sensitive materials (Film)	**storage shear modulus** G' (N/m^2)	**loss shear modulus** G'' (N/m^2)	**The loss tangent tan δ** $\frac{G''}{G'} = \tan\delta$
Zn-oct-oct-Pc	2.376e+02	3.1711e+3	13.34
Zn-hexa-Pc	61.51244	2.4431e+03	39.71
Zn-octa-Pc	62.85444	9.3919e+02	14.94

Zn-tp-tb-Pc	2.6970e+02	3.1733e+03	11.76

Sensitive materials (Film)	**storage shear modulus** $log\ G'/P_a$	**loss shear modulus** $log\ G''/P_a$	**The loss factor** $\frac{(log\ G''/P_a)}{(log\ G'/P_a)}$
Zn-oct-oct-Pc	2.37	3.5	1.47
Zn-hexa-Pc	1.78	3.38	1.89
Zn-octa-Pc	1.79	2.97	1.65
Zn-tp-tb-Pc	2.43	3.5	1.45

Table 7-3 Shear modulus value of studied films.

The results of the loss factor of tested film are approximately between for 1.4 and 2.

The results indicate to the rubbery regime, where there the tested films are deformed on a time scale more than relaxation time [7, 18, 19]. This can be concluded from the loss factor and (film damping) increasing the resistance which are an indicator of viscoelastic contribution. Nevertheless, the co-linearity of frequency change is not a sufficient explanation of Mass accumulation only (gravimetric regime).

Using program (3) listed in appendix [C] from plotting the comparison between the frequency shift using a Sauerbrey equation (1-1) and the frequency shift extracted using a shear modulus for selected material obtained from experimental admittance spectra as figure (7-60) shows, the frequency shift is more than 10000Hz for estimated Zn-oct-oct-Pc film thickness of (116.2 nm) which is in good agreement with expermintal data listed in table (6-7). In general, this figure confirm earlier discussion and gives a significant proof of a

viscooelastic film behaive and non gravimetric regime. Moreover, the expermintal process based on theoratical background has proven to be an effective tool in film characterization in gas sensor application and gives a satisfactory result of film shear modulus.

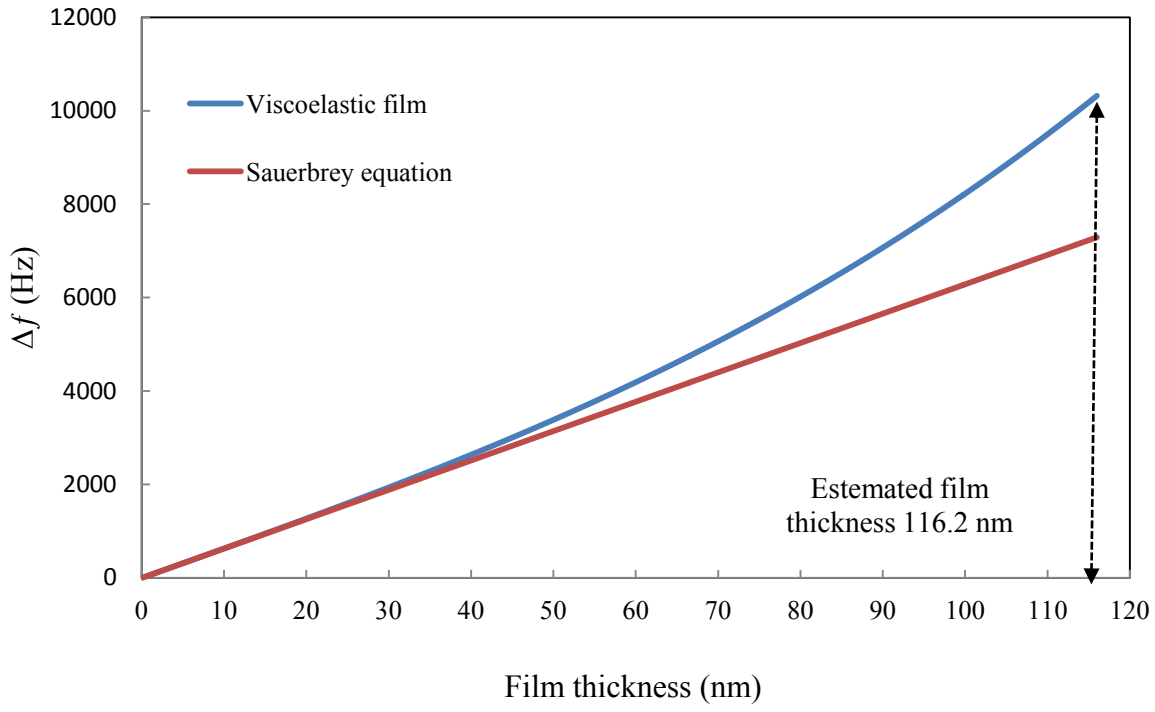

Figure (7-60) Comparison between the Δf from Sauerbrey equation and Δf extracted using a shear modulus.

7.4 Summary

Due to the high sensitivity, repeatability, relatively simple measurement system and experimental procedure, the quartz Thickness Shear Mode (TSM) resonator was adopted to characterize the properties of synthesise zinc phthalocyanine films and studying their performance as a VOC sensors. In order to achieve this goal, admittance spectrums of uncoated and coated quartz TSM resonator with 10MHz were measured by Keysight E49990A impedance analyzer controlled via PC running LabVIEW software.

Where, the impedance analysis technique was chosen to provide comprehensive information about film parameter before and during exposure to target analytes. Additionally, a fitting procedure was also used. Moreover, the TSM resonator is adopted to extract the complex shear modulus of tested films in this study.

The impedance analysis technique has exhibited good accuracy and gives important information about ad/desorption analytes in film. Accordingly, a number of selected films give a good sensitivity results when exposed to VOC vapour used in this study and shows an approximately linear response over a typical target range of concentration. Additionally, short response times and full recovery has been observed which indicate to high capability of being a good sensing membrane for gas sensor application.

Glassy and rubbery regimes were investigated and both storage shear modulus G' and loss shear modulus G'' were estimated from the parameters' of film which obtained from used measurements for each crystal. The reported results of impedance analysis and shear modulus calculation indicate film damping and non-gravimetric (viscoelasticity) contribution which explanation as a non gravimetric regime or (rubbery regime).

The obtained values of film modulus provide an indicative classification of the films properties and confirm a rubbery (viscoelastic) effect is in operation. The calculated modulus values are however susceptible to error due to influence from a number of experimentally obtained parameters. For instance, an inconsistent film thickness produced a coating which varied by (40% to 60%), additionally attributes such as non-uniformity, non-homogeneity add to the experimental error.

References

1- Bandey, H. L., Martin, S. J., Cernosek, R. W., & Hillman, A. R. (1999). Modeling the responses of thickness-shear mode resonators under various loading conditions. *Analytical Chemistry, 71*(11), 2205-2214.

2- Holloway, A., Nabok, A., Thompson, M., Ray, A., & Wilkop, T. (2004). Impedance analysis of the thickness shear mode resonator for organic vapour sensing. *Sensors and Actuators B: Chemical, 99*(2-3), 355-360.

3- Sberveglieri, G. (2012). *Gas sensors: Principles, operation and developments* Springer Science & Business Media.

4- Steinem, C., & Janshoff, A. (2007). *Piezoelectric sensors* Springer Science & Business Media.

5- ***Combustible Gas Chart***. [online]. Last accessed 9/8 2017 at: http://www.afcintl.com/pdfs/applications/combustibles.pdf

6- Gas, L. (2013). Lower and upper explosive limits for flammable gases and vapors (LEL/UEL). *Matheson Gas Products,* , 22.

7- Behling, C., Lucklum, R., & Hauptmann, P. (1998). Response of quartz-crystal resonators to gas and liquid analyte exposure. *Sensors and Actuators A: Physical, 68*(1-3), 388-398.

8- Cernosek, R. W., Martin, S. J., Hillman, A. R., & Bandey, H. L. (1998). Comparison of lumped-element and transmission-line models for thickness-shear-mode quartz resonator sensors. *IEEE Transactions on Ultrasonics, Ferroelectrics, and Frequency Control, 45*(5), 1399-1407.

9- Lucklum, R., & Hauptmann, P. (1997). Determination of polymer shear modulus with quartz crystal resonators. *Faraday Discussions, 107*, 123-140.

10- Lucklum, R., & Hauptmann, P. (2000). The Δf–ΔR QCM technique: An approach to an advanced sensor signal interpretation. *Electrochimica Acta, 45*(22-23), 3907-3916.

11- Mukherjee, D., Manjunatha, R., Sampath, S., & Ray, A. K. (2017). Phthalocyanines as sensitive materials for chemical sensors. *Materials for chemical sensing* (pp. 165-226) Springer.

12- 12- Claessens, C. G., Hahn, U., & Torres, T. (2008). Phthalocyanines: From outstanding electronic properties to emerging applications. *The Chemical Record, 8*(2), 75-97.

13- Moser, F. H., & Thomas, A. L. (1964). Phthalocyanine compounds. *Journal of Chemical Education, 41*(5), 245.

14- Wróbel, D., & Boguta, A. (2002). Study of the influence of substituents on spectroscopic and photoelectric properties of zinc phthalocyanines. *Journal of Photochemistry and Photobiology A: Chemistry, 150*(1-3), 67-76.

15- Zhou, R., Josse, F., Göpel, W., Öztürk, Z., & Bekaroğlu, Ö. (1996). Phthalocyanines as sensitive materials for chemical sensors. *Applied Organometallic Chemistry, 10*(8), 557-577.

16- Holt, R. C., Gouws, G. J., & Zhen, J. Z. (2006). Measurement of polymer shear modulus using thickness shear acoustic waves. *Current Applied Physics, 6*(3), 334-339.

17- Jiang, L., Hossenlopp, J., Cernosek, R., & Josse, F. (2003). Characterization of epoxy resin su-8 film using thickness-shear mode (tsm) resonator. *Frequency Control Symposium and PDA Exhibition Jointly with the 17th European Frequency and Time Forum, 2003. Proceedings of the 2003 IEEE International,* 986-992.

18- Lucklum, R., Behling, C., & Hauptmann, P. (2000). Gravimetric and non-gravimetric chemical quartz crystal resonators. *Sensors and Actuators B: Chemical, 65*(1-3), 277-283.

19- Lucklum, R., & Hauptmann, P. (2001). Thin film shear modulus determination with quartz crystal resonators: A review. *Frequency Control Symposium and PDA Exhibition, 2001. Proceedings of the 2001 IEEE International,* 408-418.

20- Kobayashi, N. (1999). Phthalocyanines. *Current Opinion in Solid State and Materials Science, 4*(4), 345-353.

CHPTER EIGHT

CONCLUDING REMARKS AND FUTUTRE WORK

- **Conclusion**
- **Future work**
- **References**

8.1 Conclusion:

The QCR has become an important tool in a range of sensing and film characterization applications with the continued development and synthesis of new sensing membranes only increasing its versatility

In this research, a range of synthesised phthalocyanine films have been investigated for the application of gas sensing devices. It has prepared as a thin film using the spin coating technique and examined as a sensing membrane to detect different target analytes (toxic chemicals) in gas phases using advanced QCR measurement techniques.

The standard oscillator circuit and impedance analysis technique have been exploited to give an enhanced analysis of the sensor behaviour.

The parameters' of the film can also be obtained from measurements for each crystal.
Where the characteristics of the film properties from parameters obtained from QCR measurements in conjunction with suitable data analysis and modelling techniques were observed. Moreover, validation of film properties (thickness and structure) using complementary existing methods such as AFM, and Ellipsometry has also been confirmed – results in the same order of magnitude. . For completeness UV spectra also measured.

Furthermore, the film parameters extracted from this work are used to estimate the shear modules parameters are monitor any changes in attributed to analyte exposure.

Both methods (the standard oscillator circuits and impedance analysis) have exhibited good accuracy and give important information about ad/desorption analytes in film. However with certain combinations of senor coating and loading conditions anomalous frequency shifts

have been observed; in these instances the film dissipation/viscosity must also considered to establish a full understanding of the effects observed.

In general analytes adsorption in most films used in this study follow an approximately linear response over a typical target range of concentration (see chapter 7 and chapter 8).

Oscillator measurements were used to obtain frequency shifts and the system allows the simultaneous measurement of more multiple crystals (sensor array) [1]. Moreover, the technique has the primary advantages of fast measurement time, relatively low cost and physically small hardware; which makes the potential application in a portable sensor device possible assuming the target film is suitably rigid over the desired concentration range. However, the accuracy decreases or can become invalid in the case when viscosity contributions are involved (viscous film) in particular for thick films.

The impedance measurement set up (impedance analyser) is bulky, complex and expensive. However, it gives extended and detailed information about QCR analysis.

The impedance measurements were performed by a commercially available impedance analyser device, the measurement process was controlled by a specific designed LabVIEW program. The admittance (inverse of impedance) spectra obtained by measurement of frequencies were then fitted to the BVD equivalent circuit by using LabVIEW program and parameters related to the film properties (Δf and ΔR related to L_f and R_f) were extracted.

A range of phthalocyanine film materials (the tested films) have been used in this work with many giving good results in terms of sensitivity and reproducibility when exposed to organic vapours such as (benzene, hexane, ethanol and toluene). Additionally short response time and full recovery were observed making them suited for sensor applications.

The coating process did however appear to produce an inconsistent film thickness. A definite shift in resonance is observed, however the calculated thickness varied by (40% to 60%) when based directly on mass loading calculation using the Sauerbrey relationship.

The changes in film parameters are also observed using impedance analysis, in some instances significant variation in admittance magnitude has been noted. Changes in Δf and ΔR are also detected on exposure which indicates mass loading, additionally changes in ΔR were visible which implies film viscosity is affected by ad/absorption of the vapour. Also changes in both Δf and ΔR gave the potential basis for discrimination between different organic vapour.

Film thickness parameters have been confirmed using complementary techniques - Ellipsometry – where results are in the same order of magnitude. For completeness UV spectra also measured.

In this work, a resistance increases in the range of ×10-15 were observed (from 27Ω to 360Ω) during exposure process. The significant resistance change is an indicator for the presence of potentially large viscoelastic contributions' which in turn will form part of sensor response. Also as predicted in literature [2,3,4,5,6,7,8], the non gravimetric contributions can be used as acoustic amplification to increase sensor sensitivity. Although the co linearity between frequency shift and target analytes concentration as it has been illustrate in our result chapters, it is insufficient for gravimetric assumption. However, a positive frequency shift was found in some cases during the exposure processes when using the TSM based structure; this is considered in agreement with several specific cases in the reviewed literatures [8,9] where the effects of film resonance have been established . This again can be considered as a reason to believe that the frequency shift is not exclusively a result of pure mass effect from vapour molecules mass loading.

Consequently, the QCR sensor can act as a gravimetric and non gravimetric sensitive device for thin film depending on load and adsorption characteristics .

The increase in resistance for the coating film at series resonant frequency typically indicate that film behaviour is at rubbery regime which means the calculation of change in film mass from frequency shift (Sauerbrey equation) is inaccurate except for suitably thin rigid films[2,3,5,6,7,8,10]. Therefore, shear modulus calculation directly from one QCR measurement are not accurate.

Moreover, it could explain the sensitivity at molecular level In terms of absorption of gases by interactions between film and gas molecules. Where, there is two possible gas adsorption sites for metallophthalocyanine , the central metal atom and the conjugated electron system also the substituent in microcycle is the one more site added in case of substituted phthalocyanine [11].

From investigation of phthalocyanine film exposure to VOCs gas by UV-Vis, FT-IR spectroscopic and Raman spectra. The studies reported that in case of exposure to aromatic compounds (benzene, toluene), there is change of C – H stretching vibrations and microcycle vibrations which resulted from π - π interaction between aromatic vapour molecule and phthalocyanine ring. While phthalocyanine film interact with molecules with saturated C – C bonds of alkyl compounds (hexane, ethanol) mostly by forming a strong hydrogen bond between donor atom of gas molecules and alkyl chins of the phthalocyanine substituent [11]. In addition, the film parameters extracted from this work are used to estimate the shear modulus parameters. Where the shear modulus calculation requires knowledge of film thickness which has an important influence on electric coating behaviour, where we found the shear modulus of viscous material (coating film) are dependent on film properties and extracted electrical equivalent circuit parameters.

Reviewing the sensor responses and results from this work against the metrics discussed for the state of the art sensors reviewed in chapter 1 figure (1-1) and table 1, the sensitivity of

ZnPc films in combination with the QCR technique used this study leads to a detection limit of around 100 – 1000 ppm (depending on target analyte), this comparable to several of the commercial types of sensor listed. While PID based devices demonstrate much higher sensitivity (ppb range) and lower limits of detection, they are to a restricted a range of analyets, provide no sensor discrimination within the VOC group, have a small range and require extensive calibration. Portable gas chromatographs and mass spectrometers provide excellent levels of sensitivity and selectivity but are still restrictive in cost and complexity. Moreover, electrochemical sensors (OEM) has the advantage of low cost and small size, nevertheless display a lack to sensitivity and sensor range.

Generally, all type of sensor including the QCR this research, gives convergent response time in some cases. Furthermore, benefit of low cost of crystal was used in this study.

The QCR approach used in this work does not offer a particularly superior solution over any of the other sensor techniques available in terms of selectivity/sensitivity or range; however it does provide a good combination of useable response characteristics. These include large range and medium levels of sensitivity, selectivity - through coating/membrane selection and or advanced QCR analysis techniques, fast and recoverable responses, relatively limited complexity and low cost of the sensing element. These collective attributes therefore make CR based sensors a valid and interesting area for further research and potential commercialisation.

8.2 Future Work:

While this thesis has demonstrated the potential of identify a suitable range of membranes for gas sensing applications by advanced QCR measurement techniques, many opportunities for extending the scope of this thesis remain. This section presents some of these directions.

Clearly, the use of other types of substituted Phthalocyanine could be investigated since they have an important influence on the results obtained at the end.

The results indicate that the QCR is viable and can be used to detect (VOC's). However, a wide range of gases can be considered to investigate.

Other coating methods could be also tested, as sometimes a spin coating could give a non-homogeneous surface, further research should investigate different coating methods and gives comparison between resulted films.

Extensions of viscoelastic film behaviour are required to implement a final prototype sensor.

Extended analysis of viscoelastic film behaviour and its contribution to the sensor responses are required to implement a final prototype sensor. Although QCR resonance frequency/ impedance measurements have been successfully used to detect (VOC's), improvements are possible .

The interpretation and performance evaluation of all the phthalocyanine described in Section 7.3 should also be re tested and validated; as the preliminary results of these experiments show some inconsistencies and further study is still required in order to fully understand the behaviour of these films.

References:

1- Holloway, A., Nabok, A., Thompson, M., Ray, A., & Wilkop, T. (2004). Impedance analysis of the thickness shear mode resonator for organic vapour sensing. *Sensors and Actuators B: Chemical, 99*(2), 355-360.

2- Behling, C., Lucklum, R., & Hauptmann, P. (1998). Response of quartz-crystal resonators to gas and liquid analyte exposure. *Sensors and Actuators A: Physical, 68*(1), 388-398.

3- Holt, R. C., Gouws, G. J., & Zhen, J. Z. (2006). Measurement of polymer shear modulus using thickness shear acoustic waves. *Current Applied Physics, 6*(3), 334-339.

4- Jiang, L., Hossenlopp, J., Cernosek, R., & Josse, F. (2003). Characterization of epoxy resin SU-8 film using thickness-shear mode (TSM) resonator. *Frequency Control Symposium and PDA Exhibition Jointly with the 17th European Frequency and Time Forum, 2003. Proceedings of the 2003 IEEE International,* 986-992.

5- Lucklum, R., Behling, C., & Hauptmann, P. (2000). Gravimetric and non-gravimetric chemical quartz crystal resonators. *Sensors and Actuators B: Chemical, 65*(1), 277-283.

6- Lucklum, R., & Hauptmann, P. (1997). Determination of polymer shear modulus with quartz crystal resonators. *Faraday Discussions, 107*, 123-140.

7- Lucklum, R., & Hauptmann, P. (2000). The Δf–ΔR QCM technique: An approach to an advanced sensor signal interpretation. *Electrochimica Acta, 45*(22), 3907-3916.

8- Lucklum, R., & Hauptmann, P. (2001). Thin film shear modulus determination with quartz crystal resonators: A review. *Frequency Control Symposium and PDA Exhibition, 2001. Proceedings of the 2001 IEEE International,* 408-418.

9- Bandey, H. L., Martin, S. J., Cernosek, R. W., & Hillman, A. R. (1999). Modeling the responses of thickness-shear mode resonators under various loading conditions. *Analytical Chemistry, 71*(11), 2205-2214.

10- Cernosek, R. W., Martin, S. J., Hillman, A. R., & Bandey, H. L. (1998). Comparison of lumped-element and transmission-line models for thickness-shear-mode quartz resonator sensors. *IEEE Transactions on Ultrasonics, Ferroelectrics, and Frequency Control, 45*(5), 1399-1407.

11- Basova, T., Taşaltin, C., Gürek, A., Ebeoğlu, M., Öztürk, Z., & Ahsen, V. (2003). Mesomorphic phthalocyanine as chemically sensitive coatings for chemical sensors. *Sensors and Actuators B: Chemical, 96*(1-2), 70-75.

Appendix [A]

Program1:

Program to calculate shear modulus of the studied films using values of R_f and L_f for the films (layers).

```
clear all
format long
size = 1000

p_q = 2.651e3; %density
p_film = 1000 %film density kg m3
%p_film = 1000; %film density kg m3
ep_q = 3.982e-11; %permitivity
c_q = 2.947e10; %piezo electric stiffened elastic constant
e_q = 9.53e-2; %piezoelkectric constsnt
ko2 = e_q^2/(ep_q*c_q); %electromechanical coupling factor
n_q = 3.5e-4; %viscosity
f_q = 10.00e6; %resonant freq of my qcm
AA = 28.3e-6; %area of my qcm in m2
vs = (c_q/p_q)^0.5; %velocity
%h_q = vs/(2*f_q); %quartz thickness
h_q = 1.6615e-04;
Co = (ep_q*AA)/h_q; %static capacitance
hs =0.0;     % film thickness from ellipsometry in m
w = 2*pi*f_q;
R2=0.00; % from expermintal work
L2=0.00; %  from expermintal work

c=(c_q*p_q)^0.5;

Ao=(1*pi)/(4*ko2*w*Co*c);
a1=(19/24)*p_film*hs;
a2=L2/Ao;

a3=R2^2/(w^2*Ao^2);
A1=a1-a2;
A2=(a2-a1)^2;
A3=(A2+a3)^0.5;
a4=(4/15)*w^4*p_film^3*hs^5;
A4=A1+A3;
A=(A4/a4)^0.5;

b1=(4*w^5*p_film^3*hs^5*Ao*A);
b2=(15*R2/b1);
b3=(4*w^2*hs^2*p_film);
b4=5/b3;
B=b2-b4;

Gf_d=B/(A^2+B^2)
Gf_dd=A/(A^2+B^2)
```

Appendix [B]

Program2:

Program to generate sample admittance spectra from the TLM and values of known shear modulus

```
clear all
format long
p_q = 2.651e3;          %density
ep_q = 3.982e-11;       %permitivity
e_q = 9.53e-2;          %piezoelkectric constsnt
n_q = 3.5e-4;           %viscosity
c_q = 2.947e10;         %piezo electric stiffened elastic constant
f_q = 10.00e6;             %resonant freq of my qcm
A = 28.3e-6;            %area of my qcm in m2

vs = (c_q/p_q)^0.5;              %velocity
ko2 = e_q^2/(ep_q*c_q);          %electromechanical coupling factor
%h_q = vs/(2*f_q);              %calculate quartz thickness from resonant
fequnecy
h_q = 1.6615e-04;                %comment this in to specify a QCM
thickness directly
Co = (ep_q*A)/h_q;               %static capacitance
%al_q = (w*h_q)/vs;                %wave phase shift im quartz from luclum
behling j phys d
%al_q = (w*h_q)*((p_q/c_q)^0.5) ;
zc_q = (p_q*c_q)^0.5;
i=1;

%calculate BVD parameters
Co_BVD = ep_q *A/h_q;
R_BVD = ((pi^2)/(8*ko2*Co_BVD)) * (n_q/c_q);
C_BVD = (8*ko2*Co_BVD)/(pi^2);
L_BVD = 1/((2*pi*f_q)^2*C_BVD);

%calculate viscoelastic load
p_film = 1000;             %film density kg m3
hs = 116.2e-9;                %from ellipsometry - 0.5e-6;
w = 2*pi*f_q;

%for a single film with a stree free upper surface  = viscoeleastic film
%coated on one QCM face

      Gf_d= 4.029087293903446e+03;
      Gf_dd= 1.034850954272050;
      Gf = complex(Gf_d,Gf_dd);
      ZLA = (((p_film*Gf)^0.5)*1i);
      ZLB = tan(w * (((p_film/Gf)^0.5)*hs));
      ZL=ZLA*ZLB;

%calculate R_load & L _load of BVD
BVD_load_calculated = (pi/(4*ko2*w*Co))*((ZL)/zc_q);

R_load_BVD = real(BVD_load_calculated)
L_load_BVD = imag(BVD_load_calculated)/w
```

```
for f=9.98e6:100:10.04e6
w=2*pi*f;
al_q = (w*h_q)*((p_q/c_q)^0.5) ;
load=ZL/zc_q;
%Z split into two parts of motional branch
% Impedance of the motional branch
Zmq = (1/((w*Co)*1i)) *(((al_q/ko2)/(2*tan(al_q/2)))-1);
% Additional Impedance of the load in the motional branch
ZmL_front = (1/((w*Co))) *(al_q/(4*ko2))*(ZL/zc_q);
%ZmL_front = ((al_q*(ZL/zc_q))/(4*ko2*w*Co));
ZmL_back = (1/(1-(((ZL/zc_q)*1i)/(2*tan(al_q/2)))));

ZmL = ZmL_front*ZmL_back;
%zm_tot_seperated_loads_only(i)=ZmL+Zmq;
%impedance of the motional branch + parrallel cap Co
%IEEE transactions on ultrasonics .... Vol 45, No 5 1998 R, W Cernosek

Admittance_no_load(i)= (1/(Zmq))+ (w*(Co)*1i);
Admittance_seperated_load(i)= (1/(Zmq+ZmL))+ (w*(Co)*1i);

freq(i)=f;
i=i+1;
end
%plot the data

[Gmax,ind]=max(abs(Admittance_no_load));
R_no_load=1/Gmax;
fs__no_load_approx=freq(ind)

[Gmax,ind]=max(abs(Admittance_seperated_load));
R_loaded=1/Gmax;
fs__loaded_approx=freq(ind)

%get the magnitude only
real_Admittance_no_load = abs(Admittance_no_load);
real_Admittance_seperated_load = abs(Admittance_seperated_load);

semilogy(freq,abs(Admittance_no_load),'b--
o',freq,abs(Admittance_seperated_load),'gx')
%semilogy(freq,abs(Zmotional_full_TLM_only),freq,abs(Ztotal))

xlabel({' f(Hz)';})
ylabel({' Admittance/Impedance';})

%create a folder on the E drive called-  QCM_simulated_matlab_data

%xlswrite1('New a.xls',b,1,'D1')
xlswrite('E:\QCM_simulated_matlab_data\test_alan8.xlsx',freq,1,'A1')
xlswrite('E:\QCM_simulated_matlab_data\test_alan8.xlsx',real_Admittance_no_
load,1,'A2')
xlswrite('E:\QCM_simulated_matlab_data\test_alan8.xlsx',real_Admittance_sep
erated_load,1,'A3')
```

Appendix [C]

Program3:

Program to calculate Δf and ΔR for known shear parameters over defined thickness range and known shear parameters.

```
clear all
p_film = 1000 ;          %film density kg m3
Gf_d =2.376e2;               %Gf_d =0.5e8;
Gf_dd = 3.1711e3;               %Gf_dd = 2e6;
w = 2*pi*10.0e6;

j=1;

for hf = 0.1e-9:0.05E-9:116E-9;


 Gf = complex(Gf_d,Gf_dd);
 ZLA = (((p_film*Gf)^0.5)*1i);
 ZLB = tan(w * (((p_film/Gf)^0.5)*hf));
 ZL=ZLA*ZLB;
 theta=(w *hf*(((p_film/Gf)^0.5)));
 M=w*p_film*hf;  %gravemetric resposne
 V=(tan(theta))/theta;  %acoustic factor

 df_visco(j)=M*(1+((1/3)*(Gf_d/(p_film*(abs(Gf))^2)))*M^2);
 dr_visco(j)=M*(((1/3)*(Gf_dd/(p_film*(abs(Gf))^2)))*M^2);

 hf_p(j)=hf;
 M_p(j)=M;
diff_freq(j)=df_visco(j)-M_p(j);
j=j+1;

end

df_visco_final = df_visco(j-1)
M_p_final = M_p(j-1)
diff_freq_final=df_visco(j-1)-M_p(j-1)

%plot(hf_p,df_visco)
plot(hf_p,df_visco,hf_p,M_p,'x')
%plot(hf_p,diff_freq)
xlabel({' hf (m)';})
ylabel({' \Delta f (Hz)';})
%ylabel({' \Delta R (\Omega)';})

%xlswrite('E:\Matlab_1\test_amani.xlsx',hf_p,1,'A1')
%xlswrite('E:\Matlab_1\test_amani.xlsx', df_visco,1,'A2')
%xlswrite('E:\Matlab_1\test_amani.xlsx', M_p,1,'A3')
```